

Final Report

SALT - Synthetic Aperture Lunar Telescope

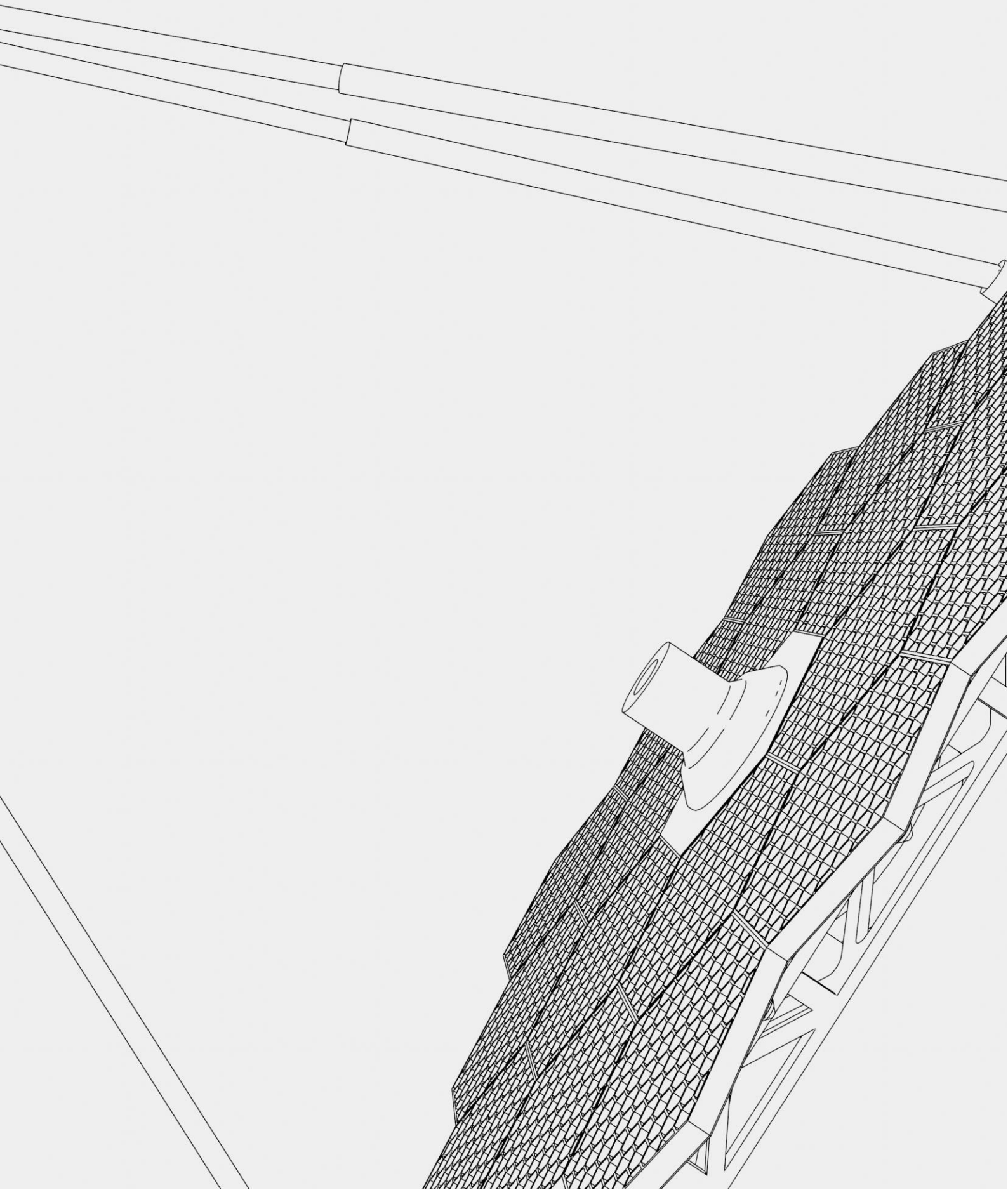
AE3200: Design Synthesis

DSE Group 4 - Very Large Moon Telescope

Delft University of Technology



This page was intentionally left *blank*



Final Report

SALT - Synthetic Aperture Lunar Telescope

by

DSE Group 4 - Very Large Moon Telescope

Student Name	Student Number
Johannes Algera	4856309
Nout Buijs	4771958
Tristan Dijkstra	4798139
Stijn Handgraaf	4794214
Nick Frances Hoeben	4659554
Marnix Meersman	4650808
Keval Sakhida	4646916
Tim Smit	4785630
Daniel Stutman	4873610
Jesse Voskuilen	4795768



Cover Image: Made in-house, by Tristan Dijkstra and Marnix Meersman

Tutor: Jasper Bouwmeester
Coaches: Sagar Adatrao and Anton Tuluk
Teaching Assistant: Lorenza Mottinelli
Institution: Delft University of Technology
Place: Faculty of Aerospace Engineering, Delft
Project Duration: April - June, 2021

Contents

List of Symbols	2
Executive summary	4
1 Introduction	6
2 Market Analysis	7
2.1 Target Market	7
2.2 Competitors: Existing and Planned	7
2.3 Planned Moon Missions	9
2.4 SWOT Analysis	9
2.5 Conclusion of Market Analysis	10
3 Functional Flow and Breakdown Structure	11
3.1 Functional Flow Diagram	11
3.2 Functional Breakdown	11
4 Risk Assessment	12
4.1 Risk Identification and Analysis	12
4.2 Risk Map	12
4.3 Contingency Scenarios	13
5 Requirements	16
5.1 Requirement Coding Scheme	16
5.2 Stakeholders	16
5.3 System Requirements	17
5.4 Change Log	20
5.4.1 Removed Requirements	20
5.4.2 Rephrased	20
6 Operation Location	22
6.1 Temperature	22
6.2 Availability of Solar Energy	22
6.3 Contact with Earth	23
6.4 Potential Presence of Lunar Installations	23
6.5 Lunar Terrain	23
6.6 Observable Region	24
6.7 Final Location	26
7 Mobility Concept Trade-off	27
7.1 Concepts	27
7.1.1 Rails Concept	27
7.1.2 MagLev Concept	28
7.1.3 Rover Concept	28
7.2 Trade-off Method	28
7.3 Trade-off Result	29
7.3.1 Criteria Determination and Weighting	29
7.3.2 Concept Selection	30
7.4 Trade-off Sensitivity	30

8	V&V Procedures	32
8.1	Model Type V&V	32
8.2	System Type V&V	32
9	Optical System and Sensing Design	34
9.1	Principle of Operation	34
9.2	Noise Sources	35
9.3	Optical Model.	37
9.3.1	Method	37
9.3.2	Results	39
9.3.3	Verification	40
9.4	Telescope Architecture	41
9.4.1	Rover Ground Configuration	41
9.4.2	Unit Telescope Architecture	41
9.4.3	Collector Architecture	46
9.4.4	Beam Conditioning	46
9.4.5	Processing and Detection	49
9.5	Upgrades	50
9.6	Compliance Assessment	51
10	Pointing System Design	52
10.1	Pointing Determination	52
10.2	Large Range of Motion Architecture	53
10.3	Fine Pointing Mechanism.	55
10.4	Beam Combiner Rotation.	57
10.5	Verification and Validation	57
10.5.1	Large Range of Motion Architecture	58
10.5.2	Fine Pointing Mechanism	58
11	Thermal Control System Design	59
11.1	Thermal Control Options	59
11.2	Rover and Mirror Design	59
11.3	Combiner Optical Elements Design.	61
11.4	Combiner Bus Design.	62
11.5	Verification and Validation	63
12	Power System Design	64
12.1	Rover	64
12.1.1	Required power	64
12.1.2	Battery sizing	65
12.2	Charging station	66
12.3	Combiner	66
12.3.1	Batteries for Peak Power	67
12.4	Transmission Line	68
12.5	Solar arrays.	68
12.6	Verification & Validation.	69
12.7	Extensibility and Alternative	70
13	Communication System Design	71
13.1	Design Options and Trade-off	71
13.2	System Topology	72
13.3	Data Volumes	73
13.4	Malapert and Earth Link Budget.	75
13.5	Lunar Segment Link Budget	76

13.6 Verification and Validation	78
14 Remote Sensing	79
14.1 Seismic Sensing	79
14.1.1 Seismic Sensing Model	80
14.1.2 Model Results	82
14.1.3 Model Verification and Validation	83
14.1.4 Sensor Design Considerations	83
14.2 Autonomous Vehicle Sensing	84
14.2.1 Light Detection and Ranging (LiDAR)	85
14.2.2 Inertial Navigation System (INS)	86
14.2.3 Radio Detection and Ranging (RADAR).	86
14.2.4 Cameras	87
14.2.5 Sensor Fusion	87
15 Structural Design	88
15.1 Rover Suspension Design	88
15.1.1 Suspension Geometry	88
15.2 Stress Analysis.	89
15.3 Vibrational Analysis	90
15.3.1 The Vibrational Model	90
15.3.2 Verification of the Vibrational Model	91
15.3.3 Design Constraints: Mirror segments	92
15.3.4 Results of Vibrational Analysis	93
15.4 Wheel Design	95
15.4.1 Wheel Configuration and Driving Modes	95
15.4.2 Sinkage.	96
15.4.3 Traction.	96
15.4.4 Soil Compaction Resistance	97
15.4.5 Bulldozing Resistance	97
15.4.6 Rolling Resistance	97
15.4.7 Gravitational Resistance	98
15.4.8 Wheel and Drive-train Design	98
15.4.9 Verification and Validation	99
15.5 Dust-proofing.	99
16 System Characteristics	101
16.1 Communication Flow Diagram.	101
16.2 Hardware Diagram	101
16.3 Data Flow and Software Diagram	102
16.4 Electrical Characteristics	103
17 Project Characteristics	105
17.1 Manufacturing, Assembly, Integration and Testing plan	105
17.2 Operations Site Characteristics	105
17.3 Surface Installation Plan	106
17.4 Operations and Logistics Diagram	108
17.4.1 Maintenance	108
17.5 Subsystem Relations in N ² Chart	110
17.6 Project Design and Development Logic	110
17.7 Project Gantt Chart	112

18 Sustainable development strategy	113
18.1 Environmental Sustainability	113
18.1.1 Lean Manufacturing	113
18.2 Economic Sustainability	114
18.3 Social Sustainability	114
19 Sensitivity Analysis	115
19.1 Operation Location	115
19.2 Optics	115
19.3 Pointing	115
19.4 Thermal	116
19.5 Power	116
19.6 Communication	117
19.7 Structures	117
20 Resource Allocation, Contingencies and Budgets Analysis	118
20.1 Cost Budget	118
20.2 Cost Breakdown Structure	119
20.3 Cost Contingency	120
20.4 Mass Breakdown	120
20.4.1 Mass Contingencies	121
20.4.2 Total Mass	121
21 Reliability, Availability, Maintainability, Safety Analysis and Compliance Matrix	123
21.1 Reliability, Availability, Maintainability and Safety Analysis	123
21.1.1 Component Contribution to System Downtime	123
21.1.2 Redundancy Philosophy	123
21.1.3 Optimisation of Maintenance Procedures	124
21.1.4 Safety	125
21.2 Compliance Matrix.	125
22 Conclusion	128
References	133
A Appendix	134
A.1 Hardware Diagram	134
A.2 Requirements Discovery Tree	135
A.3 Fault tree analysis	136
A.4 Design Option Trees	137
A.5 Link Budgets	138

Acknowledgments

The team has received a great amount of invaluable support during this DSE project. This project wouldn't have been possible without them, and they deserve our mention and our thanks.

First, we would like to thank our project tutor and supervisor Jasper Bouwmeester, as well as our coaches, Sagar Adatrao and Anton Tuluk, and our teaching assistant, Lorenza Mottinelli, for sharing their knowledge on various subjects and their overall assistance to the project.

We would also like to express our most sincere appreciation to Jérôme Loicq, for his key insights and invaluable support in the optical subsystem design of the mission, and to Peter Batenburg, for his continued advice and great expertise. We would also like to thank Stefano Speretta for his assistance in designing the communications subsystem, and his many helpful comments throughout the project. And lastly, we would like to thank Ron Noomen for his extensive knowledge on orbital mechanics that he so readily shared with us.

Furthermore, we would like to express our gratitude to Alessandra Menicucci, Alistair Glasse, Daphne Stam, Deyan Draganov and Sergio R. Turteltaub, for their answers to our burning questions about radiation, optics, lunar motion, seismic sensing, and vibrational analysis, respectively.

We would also like to extend our gratitude to Chayenne Sky Lujan, for her continued and relentless efforts in editing our report.

Finally, we would like to thank the organisation committee and the OSSA members for making this project possible despite the challenges of our times, and granting us the opportunity to participate in a large engineering team.

List of Symbols

Symbol	Definition	Units
A_s	Solar cell area	$[m^2]$
b_w	wheel width	$[m]$
C_{actual}	Actual battery capacity	$[Ah]$
c	Cohesion coefficient of lunar regolith	$[-]$
$d_w h$	wheel diameter	$[m]$
H	soil thrust	$[N]$
I	Current	$[A]$
I_{Actual}	Actual current	$[A]$
I_{mp0}	Current maximum power	$[A]$
i	Solar incidence angle	$[^\circ]$
J_s	Solar incidence	$[W/m^2]$
K	Slip coefficient	$[m]$
k_c	Cohesiveness coefficient of soil	$[-]$
k_p	Peukert's constant	$[-]$
k_Φ	Frictional modulus of soil	$[-]$
l_w	Loading area length	$[m]$
M	Moment	$[Nm]$
n	Exponent of soil deformation	$[-]$
P_d	Power delivered by power line	$[W]$
P_l	Cable power loss	$[W]$
P_{req}	Required power from solar array	$[A]$
p	ground pressure	$[Pa]$
R_C	Resistance of the power line	$[\Omega]$
T	Torque	$[Nm]$
T_d	Discharge time	$[s]$
T_s	Temperature of the solar cells	$[K]$
V_{mp0}	Voltage maximum power	$[V]$
z_w	Sinkage of the wheel	$[m]$
α_s	Absorptivity of solar cells	$[-]$
ε_s	Emissivity of solar cells	$[-]$
η_a	Packing efficiency	$[-]$
η_{PL}	Power line efficiency	$[-]$
σ	Stefan–Boltzmann constant	$[m^2 s^{-2} K^{-1} kg]$
Φ	Angle of internal friction of lunar regolith	$[^\circ]$

Abbreviation	Definition
AIAA	American Institute of Aeronautics and Astronautics
ASRC	Application-Specific Integrated Circuit
BPSK	Binary Phase-Shift Keying
CRC	Cyclic Redundancy Check
DSN	Deep Space Network
ESA	European Space Agency
FBS	Functional Breakdown Structure
FEC	Forward Error Correction
FFD	Functional Flow Diagram
FTA	Fault Tree Analysis
ISS	International Space Station
JWST	James Webb Space Telescope
LRU	Lunar Replacement Unit
MEMS	Micro Electro-Mechanical Systems
MOI	Moment of Inertia
NASA	National Aeronautics and Space Administration
OBC	On-Board Computer
OPD	Optical Path Distance
OQPSK	Offset Quadrature Phase-Shift Keying
ORU	Orbital Replacement Unit
OSSA	Ontwerp Synthese-oefening Student Assistent
PEL	Peak of Eternal Light
PNG	Portable Network Graphics
PSR	Permanently Shadowed Region
QPSK	Quadrature Phase-Shift Keying
RAMS	Reliability, Availability, Maintainability and Safety
SALT	Synthetic Aperture Lunar Telescope
SWOT	Strengths Weaknesses Opportunities and Threats
TRL	Technology Readiness Level
VLT	Very Large Telescope Interferometer

Executive Overview

Mission Objective

Interest in exoplanets has recently increased considerably, leading to numerous unanswered questions. Questions regarding the atmospheric composition of these celestial bodies, as well as observing the potential presence of bio-markers in these atmospheres, may lead to proof of other forms of life existing outside our familiar solar system. These questions lead to the following mission need statement: ***Astronomers need a greater ability to characterise the atmosphere of exoplanets and search for life on other worlds.*** The project objective is formulated from this need: ***The Synthetic Aperture Lunar Telescope (SALT) mission aims to improve the characterisation of exoplanet atmospheres, within 3 years of the next manned lunar landing.***

This report aims to present a design capable of satisfying the stated needs and objectives, and answering the broader question that underpins them: *"Is there life on other worlds?"*

Market Analysis

The intention of the market analysis is to determine how the SALT mission compares to contemporary space telescopes of a similar profile. The target market was identified to consist of agencies such as NASA and ESA, which routinely sponsor these sorts of missions. Specifically, their large astronomy programs form a suitable market for SALT. The identified market does not include any relevant competition, apart from missions that have been on hold for decades such as ESA's Darwin mission. Other proposed missions such as Luvor or HabEx have similar objectives but simply cannot compete with SALT's synthetic aperture, angular resolution and cost. This market gap creates a demand for a mission like SALT, especially now that there is a growing interest in lunar exploration.

Operation Location

The unique challenges that the SALT mission must overcome require careful location planning. Several criteria are considered when selecting the location. These criteria include temperature, the availability of solar energy, the ease of establishing contact with Earth, the lunar terrain and the region of the universe that is observable from that location. Based on these criteria, a trade-off was performed and the Sverdrup crater on the South Pole of the Moon was selected. This location provides permanent darkness inside the crater and permanent sunlight at the crater rim. This means that telescope can operate continuously inside the crater, while power is being generated continuously at the rim.

Design Trade-off

Four concepts were originally proposed, three of which made it to the trade-off. These three were the rover concept, the rail concept and the maglev concept. All of these have advantages as well as disadvantages over each other when measuring different criteria, but through the use of an Analytical Hierarchy Process method, the rover was determined to be the best approach, and was selected as a consequence. Its main advantage was found in its performance, which was the most valued criteria, but was also found to be much easier to both install and expand, if the need for that should come.

Subsystem Design

The design phase followed the trade-off. Several subsystems were designed during this phase, which include, but are not limited to: the optical system, the pointing system, the thermal and power systems, communications systems and structure.

The optical system is designed to perform nulling interferometry in the infrared spectrum. This means that four rovers, called collectors, also called 'grains', collect light and send that light to a central point, called the combiner. Here the light is combined in such a way that the light from the host star is nulled, such that only the light of the exoplanet of interest reaches the detection equipment. The rovers can move around the crater and tilt their mirrors in order to perform observations. A Ritchey–Chrétien configuration was chosen in combination with a segmented primary mirror because of their excellent performance.

The pointing system is designed to orient the mirror precisely and with high stability. To provide a large range of motion, the rover bus itself is rotated and slid across the connection point for the wheel suspension. However, this positioning is not precise enough. To accomplish this precision, a compliant mechanism is incorporated into the system to perform fine pointing. These systems are used in combination with a star tracker which determines the current position of the mirror.

A combination of solutions was chosen to keep the optical elements at their required temperatures. This combination includes multi-layer insulation, Aerogel, a heatshield, a cryocooler and a radiator. Additionally, louvers were added to the combiner to maintain its temperature almost passively.

The system's power is generated using the permanent source of sunlight at the rim of the crater. The solar panels employed in this Peak of Eternal Light are connected with a cable to the bottom of the crater, where the telescope is located. Power is stored in the combiner, in case the demand for power peaks and an extra supply is needed. One of these peak performance moments is when the rovers are recharging their batteries using charging stations. In total, the rovers can operate on one charge for 30 hours.

A ground relay solution was designed in order to communicate with Earth. The rovers communicate with the combiner, which in turn communicates with a station at the crater rim. That station sends data to a relay at Malapert mountain. From there, the data is sent back to Earth. This relay is needed because Sverdrup does not have line-of-sight with Earth for two weeks each month. A UHF link was designed for the Moon-to-Moon communications. For the connection to Earth, an X-band link was designed, to be used in combination with NASA's Deep Space Network.

The rover was designed to navigate autonomously based on a LiDAR system, and is equipped with an inertial navigation system to aid with this. Additionally, sensors have been designed in order to detect incoming moonquakes as part of an early warning system.

The main structural element is a rocker-bogie suspension, which allows for easy navigation over rough terrain. A stress analysis was performed to ensure that the structure can endure the rigours of the lunar terrain. Several vibrational analyses were performed parallel to these, to ensure that the system can survive the frequent moonquakes it will be subjected to. The final steps of the structural design related to the rover wheels, and how to shield them and the rest of the system from ubiquitous lunar dust.

Conclusion

The design activities that were performed show that SALT is a feasible system and is eligible for further design, development and testing. SALT will provide the ability to observe exoplanets at resolution that were never possible before. The design also has major inherent advantages such as ease of maintenance and accessibility. Its modular and highly upgradeable nature is also a first for a space based telescope. SALT will prove that we can build systems on other bodies, that we should build them, and that humans can play an important role in their construction and operation.

1. Introduction

The past decades have seen the appearance of spacecraft like the Hubble Space Telescope, NASA's Kepler and TESS space telescopes, which have a significant advantage over their Earth-bound counterparts: their observations are not disturbed by atmospheric interference, light pollution or radio noise. This affords the possibility of observing objects that normal telescopes would not be able to detect with relative ease, such as exoplanets - planets orbiting other suns. ¹ ² As of April of 2021, 4716 exoplanets have been found and identified by these telescopes. ³ However, these exoplanets only cover a minor region of the galaxy; this leaves a considerable amount of space left to investigate.⁴ As a means to satisfy the need for this technology, various missions have been proposed that make use of satellites to remove the inconvenient terrestrial atmosphere for the observations. Three of such missions are: LUVIOR⁵, HabEx [1] and Darwin [2]. The latter is a complex constellation concept that was proposed by ESA and currently has no further activities planned after an initial study was completed. With the rapid increase in number of discovered exoplanets throughout the last decades, there is an increasing need for innovative technology, capable of analysing these planets.⁶

The Synthetic Aperture Lunar Telescope (SALT) mission aims to improve the Darwin mission by eliminating the space elements and relocating the equipment to the far side of the Moon, while achieving an equal or greater performance. The mission objective is formulated from this goal: *The Synthetic Aperture Lunar Telescope (SALT) mission aims to improve the characterisation of exoplanet atmospheres, within 3 years of the next manned lunar landing.*

SALT eliminates the need for complex constellation flying, an advantage over the Darwin mission. However, the Moon introduces its own complications. Examples of these are the periodic moonquakes, lunar dust and difficulties in communication, given that the observation equipment will be located on the far side of the Moon, out of sight from planet Earth. This report presents a comprehensive feasibility analysis and preliminary design study on SALT.

The report is structured as follows: Chapters 2 to 4 discuss the market-, functional-, and risk analyses. These analyses lead to the requirements that are discussed in Chapter 5. Chapters 6 and 7 discuss the first major trade-offs regarding location and structural design. The verification and validation procedures used throughout the design are presented in Chapter 8. Chapters 9 to 11 present the optical, pointing and thermal subsystem designs, while Chapters 12 to 15 discuss the design of the power, communications, sensing and structures subsystems. The system and project characteristics are found in Chapters 16 and 17 respectively. Chapters 18 to 20 describe the sustainability approach of this mission, the sensitivity analysis and the budgets. Chapter 21 describes the RAMS analysis and the compliance matrix. Finally, the conclusion can be found in Chapter 22.

¹Michele Johnson. *Kepler Mission overview*. Apr. 2015. - URL: https://www.nasa.gov/mission_pages/kepler/

²Rob Garner. *About TESS*. July 2016. - URL: <https://www.nasa.gov/content/about-tess>.

³Jean Schneider. *Interactive Extra-solar planets catalog*. - URL: <http://exoplanet.eu/catalog/>

⁴Pat Brennan. *What is an Exoplanet?* 2nd apr. 2021 - URL: <https://exoplanets.nasa.gov/what-is-an-exoplanet/overview/>

⁵J.D. Myers. *LUVIOR* 4th sep. 2019 - URL: <https://asd.gsfc.nasa.gov/luvoir/>

⁶NASA *Historic Timeline* 30th apr. 2021 - URL: <https://exoplanets.nasa.gov/alien-worlds/historic-timeline/#keplers-largest-batch-of-planets>

2. Market Analysis

A market analysis provides an overview of the current and planned missions in the field, and would allow stakeholders to see how SALT fits therein. Section 2.1 identifies the Target Market for the mission. Section 2.2 compares SALT to related missions and identifies which of them are competitors. Section 2.4 provides a SWOT analysis of the mission. Lastly, Section 2.5 gives a round up of all facets of the market analysis.

2.1. Target Market

As specified in Chapter 1, SALT aims to characterise the atmosphere of exoplanets and search for life on other worlds. Discoveries in this field would greatly influence humanity's perspective on life and the universe. It is therefore that some of the main stakeholders of the SALT mission are the scientific community and humanity. These stakeholders are identified as the target market; any additional stakeholders are identified in Section 5.2. Since the cost of the programme would lie in the billions, the project would fit well within future extensions of programmes such as ESA's Cosmic Vision ¹ or NASA's Large Strategic Science Missions [3]. The modular nature and location of SALT on the Moon facilitate a collaboration between such agencies.

2.2. Competitors: Existing and Planned

Competitor telescopes must be identified to determine SALT's position in the market. Table 2.1 shows a table of important past, active, planned, on hold, and proposed telescope missions that focus on exoplanets. Even though the focus is on exoplanets, their exact goals differ slightly. For past and active missions, the Kepler and TESS missions focus on identifying exoplanets, whereas CHEOPS attempts to investigate the size of previously discovered exoplanets further ^{2 3 4}. In general, SALT could build on these missions by investigating their discoveries in greater detail. They are not considered competitors to SALT as they do not intend to investigate the atmosphere of the exoplanets for bio-signatures.

The JWST, PLATO, ARIEL and Nancy Grace Roman space telescopes are actively being developed and will be operational within the decade. The primary goals of JWST ⁵ are to study the first light of the universe and the objects that formed after the Big Bang. It will also focus on the formation of galaxies, the birth of stars and planets as well as study the properties of exoplanets. Nancy Grace Roman ⁶ will mainly perform a census of planets in nearby star systems and only aims to do spectral analysis on planets larger than Earth. ARIEL ⁷ will have a focus on spectral analysis, yet is only intended for hot inner star system planets observation. PLATO ⁸ will have a focus on detecting and measuring planets in star systems like our own. It has a specific focus on finding candidates for future atmospheric characterisation. As such, PLATO and SALT could work in tandem. PLATO could identify exoplanets of interest and SALT could perform the actual characterisation of the atmosphere.

¹ESA *Cosmic Vision Overview* Nov. 2020. - URL:<https://sci.esa.int/web/cosmic-vision/-/46510-cosmic-vision>

²NASA, Kepler pres kit - URL: https://www.nasa.gov/pdf/314125main_Kepler_presskit_2-19_smfile.pdf

³NASA, Characteristics of the TESS space telescope - URL: <https://heasarc.gsfc.nasa.gov/docs/tess/the-tess-space-telescope.html>

⁴ESA, CHEOPS Red Book - URL: https://sci.esa.int/documents/34375/36249/1567259940843-CHEOPS_EST_SCI_RP_001_RedBook_i1.0.pdf

⁵ESA *JWST fact sheet* Apr. 2021. URL:<https://sci.esa.int/web/jwst/-/45759-fact-sheet>

⁶NASA *The Nancy Grace Roman Space Telescope* May. 2021. URL:<https://www.jpl.nasa.gov/missions/the-nancy-grace-roman-space-telescope>

⁷ESA *ARIEL Summary* Nov. 2020. URL:<https://sci.esa.int/web/ariel/-/59798-summary>

⁸ESA *The PLATO Mission* May. 2021. URL:<https://www.cosmos.esa.int/web/plato>

The Darwin mission was the main inspiration for the SALT mission. The idea that was first proposed in 1993 consisted of five satellites which would orbit the Sun-Earth L2 point. Four of these satellites would be beam collectors, the fifth satellite would be the beam combiner. The satellites would make observations in the infrared spectrum to characterise the atmospheres of exoplanets. Nulling interferometry would be used to cancel out the light of the star that the exoplanet was orbiting. Two areas that required further research were precision formation flying with multiple spacecraft and the use of nulling interferometry in the infrared spectrum [2]. The final study into this mission was concluded in 2007 and no further activities have been planned since then ⁹. Since the Darwin mission was the inspiration for SALT, there is a large amount of overlap between their mission objectives. However, since the Darwin project has had no activity since 2007, it is not seen as a competitor.

Of the proposed missions, HabEx has a main focus on exoplanets [1]. Its main goals consist of characterising exoplanet atmospheres, map out planetary systems and to enable new explorations of astrophysical systems. The LUVOIR mission has similar goals to HabEx. Namely, studying the orbital parameters, atmospheric compositions and surface properties of rocky exoplanets [4]. Lastly, the Origins mission will focus on the properties of star formation and growing black holes, and determining the availability of water on exoplanets whilst characterising their atmospheres [5]. All three missions are proposed to launch in the mid 2030s, with costs ranging between \$6.7 billion for HabEx and Origins to \$8 to \$35 billion for LUVOIR.

Should any of the three proposed missions, especially HabEx, be accepted, it would prove to be a direct competitor to SALT because of the overlap in mission objectives. However, since SALT will use a synthetic aperture, it has the potential to outperform all the proposed missions since these missions only use single mirrors of limited diameters. Therefore, the only real competitor to SALT would be the Darwin mission. Should Darwin receive a resurgence in interest, SALT could be marketed as an alternative. Comparisons should be made during the project to determine if SALT's performance can compete with Darwin. In any case SALT has an advantage in its simpler upgradeability and serviceability.

Table 2.1: Overview of past, active, planned and proposed missions

Name	Description	Launch	Wavelength [nm]	Location	Note
Past and active missions					
Kepler	Single 0.95m diameter mirror	2009	430-890	Earth trailing	2394 confirmed exoplanet discoveries, including earth sized planets
TESS	4 cameras with 100mm diameter	2018	600-1000	High earth orbit	112 confirmed exoplanet discoveries, finds nearby exoplanets
CHEOPS	Single 32cm mirror	2019	330-1100	Sun Synchronous Earth orbit	Deeper investigation into previously discovered exoplanets
Planned missions					
JWST	Segmented 6.5m mirror	2021	600-28000	Orbit around sun-earth L2	Study physical and chemical properties of planetary systems
PLATO	26 telescopes, each with 120mm diameter mirror	2026	500-1000	Orbit around sun-earth L2	Study rocky, icy or giant planets
ARIEL	Single 1.1m x 0.7m mirror	2029	500-7800	Orbit around sun-earth L2	Study atmospheres of planets hotter than 600K
WFIRST/Nancy Grace	Single 2.4m diameter mirror	mid 2020s	500-2000	Orbit around sun-earth L2	Exoplanet detection
On hold indefinitely					
Darwin	Synthetic aperture, 4 collectors, 170m baseline for nulling, 500m baseline for general astrophysics		600-2000	Orbit around sun-earth L2	Characterise exoplanet atmospheres
Proposed missions					
Habex	Single 4m wide mirror	2030's	200-1800	Orbit around sun-earth L2	Image Earth-like exoplanets, and characterise their atmospheric content (main goal)
LUVOIR	8m or 15m segmented mirror (similar to JWST)	2030's	200-2500	Orbit around sun-earth L2	Study atmosphere of exoplanet and planet itself
Origins	Single 5.9m wide mirror	2035	2800-588000	Orbit around sun-earth L2	Study atmospheres of exoplanets using CO2 and other spectral features

⁹ESA Darwin factsheet 2007 URL:https://www.esa.int/Science_Exploration/Space_Science/Darwin_factsheet

2.3. Planned Moon Missions

SALT may require some assembly and maintenance. A major incentive to consider a lunar telescope is the planned human presence on the Moon. Astronauts could assist in the installation of SALT and perform repairs. SALT then also provides Artemis missions with a major scientific objective. It is therefore important to have a timeline of future manned Moon missions, this is given in Table 2.2.

Table 2.2: Planned manned presence on the Moon

Year	Name	Milestone
2024	Artemis III	First manned moon landing of Artemis
2024	Lunar Gateway	Habitat in lunar orbit
2026	Artemis IV	
2027-	Artemis program	Yearly manned Artemis launches
2028	Lunar Gateway	Planned completion of Gateway
2030s	Surface Outposts	Multiple moonbases planned

Of these missions, only Artemis 3 and the Lunar Gateway are planned and funded; the remainder of the Artemis missions are merely proposals. Some of the later Artemis missions could serve to build surface infrastructure for SALT. Artemis and its support missions will mostly be focused on the south pole of the Moon, which influences the design choice of SALT's operation location. Having SALT near human presence could facilitate its installation and maintenance. However, since these missions are merely proposals, a change in policy significantly affects the feasibility of the project. As such, this is taken into account in the SWOT analysis and Risk assessment.

2.4. SWOT Analysis

The SWOT analysis in Figure 2.1 shows the strengths, weaknesses, opportunities and threats from a technological perspective. This gives a clear overview of the internal and external factors that influence the mission.

The first strength of the mission is the fact that the telescope is located on the far side of the Moon. This means that there is no interference to the observations due to the presence of Earth and its atmosphere. This location is also more accessible than the L2 Lagrange point, which was the intended location of the Darwin mission [2]. Secondly, the fact that certain technical analyses have already been completed for the Darwin mission means that less resources have to be put into initial mission design. An additional strength is the use of a synthetic aperture, which ensures that a large angular resolution can be achieved without building an enormous telescope. As has been mentioned before, this is also advantageous for the market position of SALT. Lastly, the mission will focus on an expandable design for the collectors, meaning that additional collectors can be added during the lifetime of the mission, which is a strength for the mission as a whole.

	Helpful	Harmful
Internal	<p>Strengths</p> <ul style="list-style-type: none"> • Location on far side of the Moon • Existing details from Darwin mission • Synthetic aperture • Inherently expandable design • More accessible than L2 alternatives • No complex formation flying 	<p>Weaknesses</p> <ul style="list-style-type: none"> • Harsh Lunar environment • High accuracy and stability requirements • Difficult communication due to location on far side of the Moon • Limitations in system configuration if system stalls on the Moon
External	<p>Opportunities</p> <ul style="list-style-type: none"> • Renewed interest in the Moon • Astronaut presence • Competitive market with multiple launchers 	<p>Threats</p> <ul style="list-style-type: none"> • First of its kind, both as Moon mission or general space mission • Dependent on continued interest in Moon mission

Figure 2.1: SWOT analysis of the mission from a technical perspective

The harshness of the lunar environment is the first weakness for the mission. Moon quakes, temperature variations, radiation, micrometeorites, moon dust and a rough surface during landing contribute to the difficulty of a lunar mission. The second weakness is the fact that, due to the nature of the observations, extremely high accuracy and stability are required for the sensing subsystems. This

might be difficult to attain on the soft and uneven surface of the Moon. The final weakness is the fact that communication with Earth will be difficult, since the telescope is located on the far side of the Moon.

The renewed interest in Moon missions from both the US and Europe provide an opportunity for this mission^{10 11}. This increase in interest may materialise into an increase in activity and funding. It might also lead to a cost reduction for certain mission phases if the market becomes competitive. The final opportunity is the fact that the presence of astronauts on the Moon provides the possibility of assembly and maintenance for the telescope. This will simplify the design and extend the lifetime of the mission.

The first threat for this mission is its novelty. The fact that no similar missions exist, whether it be on the Moon or in space in general, means that a lot of resources need to be put into mission analysis and design. The final threat is the fact that this mission is dependent on the continued interest in Moon missions. As previously stated, the mission is to start operating three years after humans set foot on the Moon once more. It is important that by that time funding is still available and astronauts are present for assembly and maintenance.

2.5. Conclusion of Market Analysis

The target market for SALT consists of the large space agencies such as NASA or ESA. The SALT mission would fit well within their Large Strategic Science Missions or Cosmic Vision programs. It does not have any major competitors in this market apart from the Darwin mission. However, since Darwin is on hold indefinitely, it is not considered to be active in the market. While many of the competitors have similar mission objectives, none of the other missions compare to SALT's performance due to its synthetic aperture and superior angular resolution. Finally, the renewed interest in spaceflight to the Moon strengthens the market position of SALT — this does not mean, however, that it is guaranteed to succeed. The dependence on human spaceflight and interest in the Moon could be a serious problem for the mission, and has to be taken into account.

¹⁰NASA Office of Inspector General *Office of Audits Report No. IG-21-004 NASA'S MANAGEMENT OF THE GATEWAY PROGRAM FOR ARTEMIS MISSIONS* Nov. 2020. URL:<https://www.oversight.gov/sites/default/files/oig-reports/IG-21-004.pdf>

¹¹ESA *First steps: returning humanity to the Moon* Nov. 2020. URL:https://www.esa.int/Science_Exploration/Human_and_Robotic_Exploration/First_steps_returning_humanity_to_the_Moon

3. Functional Flow and Breakdown Structure

3.1. Functional Flow Diagram

The Functional Flow Diagram (FFD, Figure A.5) shows the sequence of critical tasks completed by the system in order to accomplish the mission. This diagram shows three levels of detail: the first level (in red), the second level (in blue), and the third level (in yellow). The sequence of transitions is shown by the arrows. Multiple arrows branching into or out of a task show a one-to-many or many-to-one dependency, respectively. The pill shaped cells indicate conditional flows or conditions, and the circular cells are tags, used to concretely indicate major flow transitions.

3.2. Functional Breakdown

The Functional Breakdown Structure (FBS, Figure A.6) shows more detailed functions than the FFD, and groups them by category, instead of chronologically. The colour scheme retains the meaning of the FFD colour scheme. The uncoloured bullet points represent notes at the current level of detail if they are below a function, or a lower level of detail if they are to the right of a function. First level tasks are expanded horizontally, and second level tasks are expanded vertically. All functions depend on the function below them in the hierarchy. The FBS is also used to detail out-of-chronology functions, or functions that do not necessarily occur at any given point in time, but over the entire mission. For example, power must be supplied at all stages, and has therefore only been included in the FBS.

4. Risk Assessment

Planning for adverse events is essential to ensure that procedures are in place that reduce their probability of occurring and/or reduce their impact. While it is impossible to predict every possible risk the project may face, this chapter presents the major risks that have been identified and the strategies employed to mitigate them. Each risk has been identified in Section 4.1 and risk maps are presented Section 4.2. Finally, contingency strategies are developed in Section 4.3.

4.1. Risk Identification and Analysis

This section contains a list of events that impact the SALT system. These are quantified according to their probabilities of occurring and their impact on the project. The risks are divided into 5 categories: Launch & Deployment (LD), Operations (OPS), Optics (OPT) and Pre-launch (PL), Thermal and Electrical (TE), shown in Table 4.3. Following the framework for risk analysis set-up in during the project plan [6] and baseline [7] reports, risk events have been labelled with an unique identifier. These will be used in the following sections to present the risks and can be found in these tables as well.

The probabilities of an event occurring during the entire mission duration are divided into 5 groups, as seen in Table 4.1. The exact probability of the event cannot always be calculated and is therefore estimated to fall within the defined ranges. Additionally, the impact of each event is divided into 5 categories as seen in Table 4.2.

Table 4.1: Probabilities of occurrence of each event.

Probability (P)	%
Very Low	$p \leq 10$
Low	$10 < p \leq 30$
Medium	$30 < p \leq 50$
High	$50 < p \leq 70$
Very High	$p > 70$

Table 4.2: Categories of the impact of each event.

Description of Impact on Project (I)	Rating
Does not interfere with the mission objectives, costs or timeline	1
Marginally compromises the mission objectives, costs or timeline	2
Significantly compromises the mission objectives, costs or timeline	3
Severely compromises the mission objectives, costs or timeline	4
Mission fails or cannot continue	5

Each risk is individually analysed and assigned a P and I value. The rationale behind these values stems from the effect of each risk on the system. This allows for the identification of risks that may most commonly occur, and those with the largest impact on the project, along with their potential drivers. Finally, mitigation strategies are applied to each risk scenario to reduce their probabilities and/or impact.

4.2. Risk Map

A technical risk map has been generated in order to visualise the effect of the mitigation strategies, as shown in Figure 4.2. This is to ensure that no risk is present in the unacceptable region of the risk map. This region is defined by the region above and to the right of the yellow cells in the risk map. The identified risks in their unmitigated state are displayed in Figure 4.1.

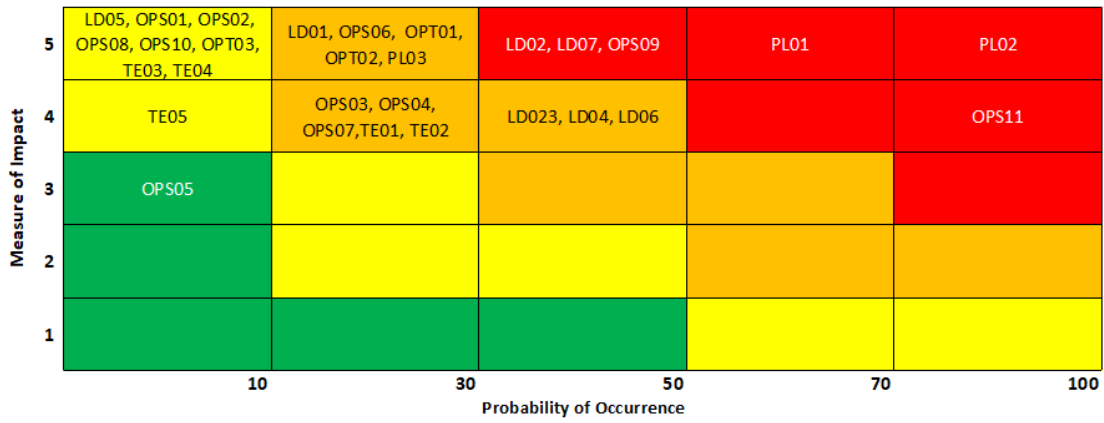


Figure 4.1: Graph displaying the various identified risks in the impact probability space in their unmitigated state.

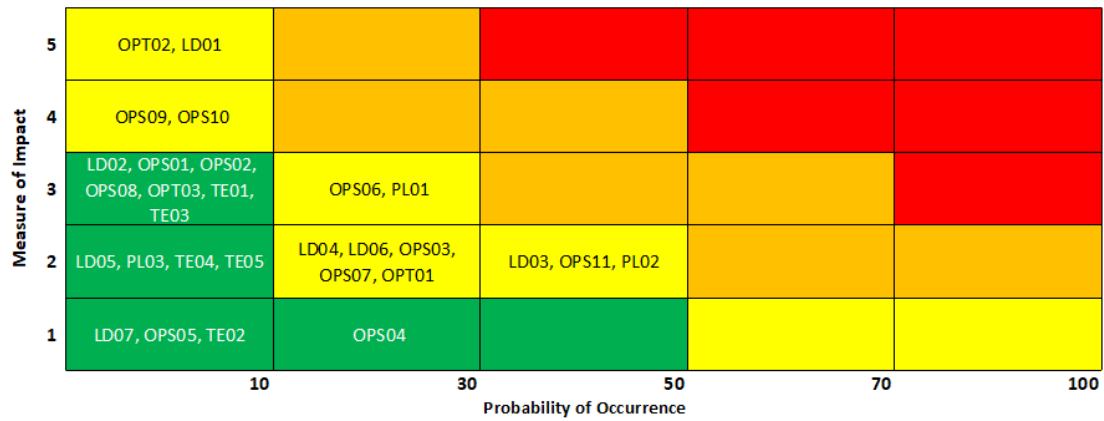


Figure 4.2: Graph displaying the various identified risks in the impact probability space in their mitigated state.

4.3. Contingency Scenarios

Mitigation strategies try to reduce the probabilities and impacts of risk events. If the event still occurs, contingency strategies can be implemented to reduce the damage. Contingency strategies have been put in place for events with an impact of 4 or more after mitigation. These are identified based on the risk map for mitigated risks in Figure 4.2. These contingencies are as follows:

- **LD01C:** Use lander’s return fuel to land in another area, send a mission to refuel the lander after the manoeuvre.
- **OPT02C:** The system must be extendable to increase the effective area and increase signal power, such that the signal to noise ratio is compensated.
- **OPS06C:** Astronauts attempt to diagnose fault and repair. If unsuccessful, a spare rover is sent.

Table 4.3: A table containing all identified risks and mitigation strategies

ID	Description of Risk	Effect of Risk	<i>P</i>	<i>I</i>	Mitigation Strategy	Effect of Mitigation	<i>P_N</i>	<i>I_N</i>
LD01	Lunar lander lands in an inaccessible location	System cannot be assembled	Low	5	Implement guiding system to land and carry extra fuel for course corrections	The moon lander will autonomously avoid inaccessible areas and get out of these areas if needed	Very Low	5
LD02	Astronauts cannot access components to assemble the system	System is not assembled and mission is not performed	Medium	5	Plan for system assembly ensuring accessibility, and an alternative way of unpacking	There is an alternative if the main method of assembly fails	Very Low	3

ID	Description of Risk	Effect of Risk	P	I	Mitigation Strategy	Effect of Mitigation	P_N	I_N
LD03	Launch window is exceeded	System is not launched	Medium	4	Plan multiple launch windows	System can be launched at another time	Medium	2
LD04	Damaged payload upon Moon landing	System may not be able to perform its mission	Medium	4	Incorporate safety margin in structures design. Insure the Spacecraft. Small damages can be fixed with another mission	Insurance will allow the mission to be relaunched or will cover the cost of a repair mission. Safety margin will decrease the likelihood	Low	2
LD05	Launcher fails	System is destroyed and has to be rebuilt. In case it is a maintenance mission it will be delayed	Very Low	5	Pay for insurance of the launch. Prepare backup launcher in maintenance missions	Insurance will cover the financial costs. Back up launcher is launched	Very Low	2
LD06	Damage during launch	System may not be able to perform its mission if launch loads are not withstood	Medium	4	Incorporate safety margin in the structure design. Insurance shall also cover these damages	Insurance will cover the financial costs. Safety margin reduces the probability	Low	2
LD07	Natural frequencies of the system in the launcher resonate with launch vibrations	Rocket can become uncontrollable and system structure may fail	Medium	5	System is designed so natural frequencies are in the range allowed by the launcher and can be validated by structural and shaker tests	System will not resonate	Very Low	1
OPS01	Moonquakes of varying magnitudes	Moonquakes affect telescope measurements and sensing equipment	Very Low	5	Integrate dedicated control systems to stabilise system	Effect of moonquakes on measurements is minimised and reduced risk of component damage	Very Low	3
OPS02	Dangerous particle radiation environment	System fails or data is corrupted due to radiation exposure	Very Low	5	Add a safety margin during radiation design, and reinforce radiation shielding during planned maintenance. Design communication protocols such that corrupted data is not transmitted and perform tests	System will survive the harsh radiation environment and still carry out operations	Very Low	3
OPS03	Delay in scheduled maintenance due to poor accessibility or poor logistics	Might lead to longer downtimes during the operational window	Low	4	Have a safe life system in place for all major components and reschedule maintenance operations	System can continue to remain operational despite longer periods of no maintenance being carried out	Low	2
OPS04	Communication drop/lag	System is unresponsive to inputs or runs out of data storage space	Low	4	Have command acknowledgement protocols in place to assess receipt of commands. System should also be designed to carry out automated subroutines in case of longer periods of no communications	Commands are queued and carried out as intended, with the system operating autonomously to some extent	Low	1
OPS05	Failure to integrate additional beam collectors into the system	System cannot be extended to obtain a larger image	Very Low	3	Astronauts are trained to dismantle the system to accommodate new beam collectors. The CAD drawings of the system layout should be extendable	Mission to extend system to add additional beam collectors proceeds as originally planned	Very Low	1
OPS06	Rover positioning control system loses required precision	Measurements cannot be performed accurately or the system cannot change configuration as required	Low	5	Over-the-air software updates can be performed, or calibration can be performed during planned maintenance missions.	Control system is operable within the required tolerances	Low	3
OPS07	End of life strategy becomes unfeasible	System cannot be decommissioned without leaving an impact or waste on the Moon	Low	4	Use of materials that limit degradation in order to minimise space debris, and develop multi purpose use beyond observation mission	System can be successfully decommissioned perhaps with parts being recycled for future missions	Low	2
OPS08	System is hit by an asteroid	Partial decimation of the system	Very Low	5	A spare combiner and collector will be made on Earth and replacements can be sent while the system operates with lower efficiency if it is partly damaged.	System has increased chances of surviving asteroid impact	Very Low	3
OPS09	Rovers lose traction and get stuck	Rovers can get stranded without the possibility of returning autonomously, leading to limited measurements until they run out of charge	Medium	5	Use data from accurate lunar terrain mapping to generate rover paths encountering minimal resistance. Additionally rovers are designed to be tugged if required	Rovers can continue on their paths uninterrupted and a system is in place to recover the stranded rover.	Low	4

ID	Description of Risk	Effect of Risk	P	I	Mitigation Strategy	Effect of Mitigation	P_N	I_N
OPS10	Large scale control system failure	Telescope elements cannot move as required, thus cannot accurately point and rovers fail to position themselves.	Very Low	5	Implement a system reboot protocol with parameters from the last nominal operations, or force a hard reset.	Control system can be brought back online and the system can resume nominal operations.	Very Low	4
OPS11	Lunar dust affects hinders system operations	Short circuits in electrical systems, reduced optical performance as well as increased degradation and wear of external subsystems.	Very High	4	Subsystems will be designed to protect against lunar via physical barriers and redundancies will be introduced within electrical circuits.	System can operate nominally without extensive degradation due to lunar dust.	Medium	2
OPT01	Mirrors become misaligned due to moonquakes	System makes distorted observations	Low	5	System is designed to be able to achieve correct alignment by astronauts and electronic fine-tuning	Correct alignment can be achieved within a short period of time thus reducing impact on the mission	Low	2
OPT02	Noise power is higher than anticipated	Results in false detection of certain gases in the atmospheres of the planet being observed	Low	5	Design to minimise signal-to-noise ratio, and include a margin of error in estimation of noise power. Design a probabilistic model to verify detection of gases	Observations are clear and conclusions can be drawn from them	Very Low	5
OPT03	Beam collecting rovers fail to reposition due to obstructions in their path	Nulling interferometry fails, thus observations cannot be made	High	5	System is designed to take alternate paths using updated and accurate lunar terrain maps. Additionally, other rovers can reposition if possible, for a coherent configuration.	Rovers can continue moving after a period of downtime and re-enable interferometry capabilities	Very Low	3
PL01	Program gets delayed and/or cancelled	Program does not go ahead resulting in a waste of resources or exceeds budget	High	5	Implement a phased approach to ensure program stays on track, and hire multiple contractors	Probability of the program getting shelved is significantly reduced	Low	3
PL02	Program runs over budget	Funding is cut from sponsors resulting in research and development halting	Very High	5	Ensure proper planning during development and research and implement early testing of new technologies. Further diversify sponsors	Reduced impact of one or more sponsors cutting funding	Medium	2
PL03	Payload size exceeds that which can be transported with the predetermined number of launches	Launch is delayed until payload is within the allowed dimensions	Low	5	Use accurate CAD models to estimate the volume occupied by the payload and increase number of launches with a larger launcher	Reduced impact and probability of payload being oversized	Very Low	2
TE01	Stored energy is not enough	The entire system has a hard shut down. Rovers get stuck	Low	4	Make a safety mode were only essential systems work. Implement a backup battery for the safety mode. Rover batteries can not go under the required energy to return.	Hard shut downs will be less likely to happen.	Very Low	3
TE02	Decay of power generation of solar cells is more than expected	Power generation will not be enough to maintain the mission during the required period	Low	4	Include a safety margin in the decay factor during sizing. Components can be replaced during maintenance	The impact of the problem can be mitigated by astronauts on site. Including the safety margin will diminish the probability	Very Low	1
TE03	Solar flare damages the electronics	All subsystems that have any electronic control may stop working	Very Low	5	Implement circuit breakers to counter power surges and reduce the damage. Manually replace components that are damaged	The impact of the damage is reduced by the circuit breakers	Very Low	3
TE05	Temperature gets outside acceptable range	Parts may be damaged, especially electronics and batteries	Very Low	4	Use a safety factor in the allowable temperature range. Overheat: Shut off all subsystems but thermal control. Too cold: Turning on as many systems as possible, astronauts should be able to add heaters	It is less likely for the temperatures to get outside the range and strategies are in place to reduce the impact	Very Low	2

5. Requirements

This chapter discusses all activities that correspond to the generation and tracking of requirements. A coding scheme has been applied to track and label all requirements in Section 5.1. Possible stakeholders and accompanying stakeholder requirements are presented in Section 5.2, which have been used to derive system and sub-system requirements. Next to the final requirement list in Section 5.3, a change log in Section 5.4 is present that contains all the changes to the requirement list from the baseline up to this report. Furthermore, the requirement discovery tree will be presented in Figure A.2.

5.1. Requirement Coding Scheme

To be able to quickly refer to requirements they have been labelled by a coding scheme. System requirements are the highest level requirements that constrain the mission system and they have been given the following format, in which **[XX]** is the numbering of the requirement:

$$\text{SALT} - \text{SYS} - \text{[XX]} \quad (5.1)$$

The system can be divided into multiple subsystems, among which the lower-level subsystem requirements are distributed. The subsystem requirement coding utilises the following format:

$$\text{SALT} - \text{SSYS} - \text{[Subsystem]} - \text{[XX]} \quad (5.2)$$

[Subsystem] is replaced with the acronym that corresponds to the subsystem the requirement belongs to. The full list of subsystem acronyms is:

- Sensing **[SENS]**
- Mechanical design & installation **[MECH]**
- Thermal **[THM]**
- Communication and Operations **[COM]**
- Operations **[OPE]**
- Power **[POW]**
- Cost **[BUDG]**
- Schedule **[SCH]**
- Project **[PROJ]**
- Reliability **[REL]**

Examples of a system requirement and a subsystem requirement are:

High level system requirement: **SALT-SYS-03: The system shall survive the thermal environment of the Moon.**

Low level sub-system requirement: **SALT-SSYS-THM-01: All optical elements at the collectors shall have a temperature of no more than 40 [K] during observations.**

5.2. Stakeholders

The target audience and additional stakeholders must be identified in order to produce a satisfactory product. The stakeholders are listed in Table 5.1. A comparison was made to previous lunar and telescope missions; the focus of attention being the relatively similar Darwin and Apollo missions. Their needs have been formulated in stakeholder requirements, as displayed in Table 5.1.

Table 5.1: This table contains the identified stakeholders, accompanying stakeholder requirements and codes.

Stakeholder	Requirement Code	Stakeholder Requirement
Customer	STK-TUT-01	The design team shall have a proposal for a Moon telescope after 10 weeks.
Scientific Community	STK-SCI-01	The telescope shall be able to perform highest attainable quality observations in 30 [h].
Scientific Community	STK-SCI-02	The operation of the telescope shall not be affected by other spacecraft fly-overs.
Launcher Provider	STK-LAU-01	The spacecraft shall not damage the launch vehicle.
Investors	STK-INV-01	The mission shall have a probability of success of 0.920 [8] or higher.
Astronauts	STK-AST-01	The telescope shall be accessible for maintenance.
Space Agencies	STK-SPA-01	The telescope shall not interfere with other existing missions.
Humanity	STK-HUM-01	The telescope shall not pollute the surface of the Moon after decommission.
Insurance	STK-INS-01	The selected launcher shall have a reliability greater than 95 percent.

5.3. System Requirements

System and subsystem requirements can be formulated after careful evaluation of the functional flow diagram, risk analysis, experts, user and stakeholder requirements. The focus of this procedure is to limit the design option space to a set that is able to successfully perform the mission without setting unreasonable constraints. The derived list of system and subsystem requirements are displayed in Table 5.2 and 5.3. Additionally, this table also presents the origin of the requirement in the most left column to support traceability. The right-hand side of the table presents the method that can be used to verify the requirement during production.

An example of the procedure that was followed is: *"SALT-SSYS-SENS-01: The angular resolution of the telescope shall be less than 5 milliarcsec at a wavelength of 10 μm ."* This requirement is a concrete statement derived from the following need of the mission: *"SALT-SYS-01: The telescope shall characterise the thermal infrared signature of exoplanets"*. An example requirement generated from a user requirement is: *"SALT-SSYS-THM-01: All optical elements at the collectors shall have a temperature of no more than 40 [K] during observations."* This has been derived in order to comply with user requirement copied from the project guide [9]: *"VLMT-SR-02: The system shall survive the thermal heating during the sunlit period of the Moon-day."* This procedure was followed for all user and stakeholder requirements, and has also been applied to those following from the functional flow diagram, risk assessment and experts' advice. As a means to visually represent the set of requirements and their purpose in the product design, a requirement discovery tree has been made and displayed in Figure A.2.

Lastly, the key requirements, those that are of primary importance to the customer and stakeholders, are listed in Table 5.4 in the second column. The driving requirements - requirements that limit the design more than the average - have been identified and listed in same table in the third column.

Table 5.2: Full list of retrieved subsystem requirements for the SALT mission (1/2).

Origin	Code	Requirement	Verification method
Sensing Subsystem			
VLMT-PER-01	SALT-SYS-01	The telescope shall characterise the thermal infrared signature of exoplanets.	Test
VLMT-PER-05	SALT-SSYS-SENS-01	The angular resolution of the telescope shall be less than 5 milliarcsec at a wavelength of 10 μm .	Test
VLMT-PER-07	SALT-SSYS-SENS-02	The spectral resolution shall be at least 300 [-].	Test
VLMT-PER-06	SALT-SSYS-SENS-03	The spectral range shall cover wavelength of 6 to 20 μm .	Test
VLMT-PER-08	SALT-SSYS-SENS-04	The signal-to-noise ratio shall be equal or greater than 10 for H ₂ O.	Test
VLMT-PER-08	SALT-SSYS-SENS-05	The signal-to-noise ratio shall be equal or greater than 5 for CO ₂ .	Test
VLMT-PER-08	SALT-SSYS-SENS-06	The signal-to-noise ratio shall be equal or greater than 5 for O ₃ .	Test
VLMT-SR-03	SALT-SSYS-SENS-09	The system shall survive the particle radiation environment.	Analysis
Experts	SALT-SSYS-SENS-10	Lunar dust shall not permanently damage the sensing equipment.	Test
Scientific Community	SALT-SSYS-SENS-11	The optical system shall be able to observe exo-planets with a 5.0E-20 [W/m ²] brightness or higher with an SNR of 10 [-] during 10 hours of observation.	Test
VLMT-PER-10	SALT-SSYS-SENS-12	The optical path length shall be able to be corrected.	Demonstrate
VLMT-PER-10	SALT-SSYS-SENS-13	The optical path length shall be kept stable with an accuracy of less than 1.5 [nm] w.r.t. the beam combiner.	Test
VLMT-PER-10	SALT-SSYS-SENS-14	The optical path length shall be controllable with a range of 10 μm .	Demonstrate
Mechanical Subsystem			
VLMT-PER-02	SALT-SYS-02	The telescope shall comprise of 4 beam collectors and 1 beam combiner in an X-configuration.	Inspect
VLMT-PER-03	SALT-SSYS-MECH-01	The beam collectors shall be able to reposition between 50 and 500 meter from the beam combiner.	Inspect
VLMT-PER-04	SALT-SSYS-MECH-02	The telescope shall be extendable to 8 beam collectors (in X-configuration).	Analysis
Experts	SALT-SSYS-MECH-08	Lunar dust shall not permanently damage mechanisms.	Analysis
Humanity	SALT-SSYS-MECH-10	The system shall make use of renewable materials.	Inspect
Functional flow - Landing	SALT-SSYS-MECH-11	The system shall survive the landing phase onto the Moon.	Test
Launcher provider	SALT-SSYS-MECH-12	The payload shall not damage the launch vehicle.	Test
VLMT-SR-01	SALT-SSYS-MECH-13	The system shall survive moon quakes of magnitude 5.	Test
Functional flow	SALT-SSYS-MECH-14	The pointing system shall have a pointing accuracy of 0.5 [arcsec] or less.	Test
Scientific Community	SALT-SSYS-MECH-15	The telescope shall be able to point within an angle of 90 [deg] from the local surface normal vector.	Test
Thermal Subsystem			
VLMT-SR-02	SALT-SYS-03	The system shall survive the thermal environment of the Moon.	Analysis
VLMT-BUDG-03	SALT-SSYS-THM-01	All optical elements at the collectors shall have a temperature of no more than 40 [K] during observations.	Test
VLMT-BUDG-04	SALT-SSYS-THM-02	All optical elements at the beam combiner shall have a temperature of no more than 40 [K] during observations.	Test
VLMT-BUDG-04	SALT-SSYS-THM-03	The detector at the beam combiner shall have a temperature of no more than 10 [K] during observations.	Test
Communication Subsystem			
FFD-Communication	SALT-SYS-04	Communication with the lunar element and the ground station shall be establishable.	Analysis
Risk assessment - OPS04	SALT-SSYS-COM-03	The system shall store commands and information in the event of a loss of communications.	Test
Function flow	SALT-SSYS-COM-04	The lunar segment shall have at least one two-way communication contact between the ground station and all mission elements per terrestrial day.	Analysis

Table 5.3: Full list of retrieved subsystem requirements for the SALT mission (2/2).

Origin	Code	Requirement	Verification method
Operations			
VLMT-TIME-01	SALT-SYS-05	The mission fits within the scope of foreseen (human) spaceflight plans of organisations with experience of launching humans to space.	Analysis
Space agencies	SALT-SSYS-OPE-02	The telescope shall not interfere with other missions.	Analysis
FFD-Installation	SALT-SYS-06	The system shall be deployed and maintained by astronauts and the ground element.	Analysis
Humanity	SALT-SSYS-OPE-03	The telescope shall not pollute the surface of the Moon after decommissioning.	Analysis
VLMT-TIME-02	SALT-SSYS-OPE-04	The telescope shall be operational within 3 years from the next Moon landing by humans.	Analysis
Astronauts	SALT-SSYS-OPE-05	The telescope shall be safe to maintain.	Analysis
Risk assessment - OPS06	SALT-SSYS-OPE-06	The system's software must be update-able.	Test
Functional flow	SALT-SSYS-OPE-07	The lunar element shall be assembled on the Moon surface.	Analysis
Risk assessment	SALT-SSYS-OPE-09	A repair strategy shall be established.	Analysis
Experts	SALT-SSYS-OPE-10	The operations shall not be halted because of the presence of lunar dust.	Analysis
Functional flow	SALT-SSYS-OPE-11	The equipment shall be able to perform 30 [h] operational cycles.	Analysis
VLMT-PER-09	SALT-SSYS-OPE-12	The telescope shall be operational for at least 70 [%] of each Moon night period.	Analysis
Power Subsystem			
FFD-Power	SALT-SYS-07	The power subsystem shall supply continuous power for operation.	Test
VLMT-SUS-01	SALT-SSYS-POW-01	The telescope shall use a renewable energy source.	Inspect
VLMT-SUS-02	SALT-SSYS-POW-02	The telescope shall not use nuclear power.	Inspect
Risk assessment - TE03	SALT-SSYS-POW-04	The power system shall be protected against solar flares up to a magnitude X1.	Analysis
Functional flow	SALT-SSYS-POW-10	The power storage system shall support the power system under peak load.	Test
Functional breakdown - Power	SALT-SSYS-POW-11	The power storage system shall be capable of storing energy to support the equipment for one operational cycle or more.	Test
Functional breakdown - Power	SALT-SSYS-POW-12	The power subsystem shall be able to recharge during one operational cycle or less.	Analysis
Cost			
VLMT-COST-01	SALT-SYS-08	The total cost of the mission for the first five years shall be less than 1000 [M€], excluding cost for already foreseen human Moon exploration missions.	Analysis
Risk assessment	SALT-SSYS-BUDG-01	The cost from failure of the mission shall be mitigated.	Analysis
Risk assessment - OPT02C	SALT-SSYS-BUDG-03	An extra reflector and beam collector shall be manufactured to be sent as replacements if needed.	Inspect
Schedule			
VLMT-PER-11	SALT-SYS-09	The nominal mission shall be 5 years.	Analysis
VLMT-PER-12	SALT-SSYS-SCH-01	The extended mission, including potential upgrades and repairs for less than 20 [%] of the total launch mass, should last for another 10 years.	Analysis
Project			
Stakeholder-Customer	SALT-SYS-10	The design team shall have a proposal for a Moon telescope after 10 weeks.	Analysis
Customer	SALT-SSYS-PROJ-02	The design team shall deliver a final project report before the 22th of June 2021.	Analysis
Customer	SALT-SSYS-PROJ-03	The design team shall deliver a final presentation before the 24th of June 2021.	Analysis
Customer	SALT-SSYS-PROJ-04	The design team shall deliver a presentation at the DSE Symposium 2021 of TU Delft.	Analysis
Reliability			
Investors	SALT-SYS-11	The mission shall have a probability of success of 0.920 [8] or higher.	Analysis
Risk assessment - OPS07	SALT-SSYS-REL-03	The end of life strategy shall not have single points of failure.	Analysis
Investors	SALT-SSYS-REL-06	No single part failure shall cause complete loss of a function.	Test

Table 5.4: Table containing the identified key and driving requirements

Related topic	Key requirements	Driving requirements
User requirements		
Sensing performance	SALT-SYS-01, SALT-SSYS-SENS-01, SALT-SSYS-SENS-02, SALT-SSYS-SENS-03, SALT-SSYS-SENS-04, SALT-SSYS-SENS-05, SALT-SSYS-SENS-12.	SALT-SYS-01, SALT-SSYS-SENS-01, SALT-SSYS-SENS-02, SALT-SSYS-SENS-03.
Stability	SALT-SSYS-MECH-02, SALT-SSYS-SENS-12, SALT-SSYS-SENS-13.	SALT-SYS-02, SALT-SSYS-MECH-01, SALT-SSYS-MECH-02, SALT-SSYS-SENS-13, SALT-SSYS-SENS-14.
Operations	SALT-SYS-05, SALT-SSYS-OPE-02, SALT-SSYS-OPE-04, SALT-SSYS-OPE-12.	-
Thermal		SALT-SSYS-03, SALT-SSYS-THM-03
Power supply	SALT-SSYS-POW-01, SALT-SSYS-POW-02.	SALT-SSYS-07, SALT-SSYS-POW-01, SALT-SSYS-POW-02.
Cost	SALT-SYS-08.	SALT-SYS-08.
Stakeholder - Space agencies		
Operations	SALT-SSYS-OPE-02, SALT-SSYS-OPE-03, SALT-SSYS-OPE-04.	-
Stakeholder - Humanity		
Operations	SALT-SSYS-OPE-03.	-
Stakeholder -Customer		
Schedule	-	SALT-SYS-10, SALT-SSYS-PROJ-02, SALT-SSYS-PROJ-03, SALT-SSYS-PROJ-04.
Risk analysis		
Location	-	SALT-SSYS-REL-03.
End-of-life	-	SALT-SSYS-REL-04.
Functional analysis		
Assembly	-	SALT-SSYS-OPE-07
Communication	SALT-SYS-04.	-

5.4. Change Log

After the Baseline report, where the requirements have been shown last, the list has underwent multiple revisions. This section will go over them and explain the underlying rationale. The change log can be seen in Table 5.5 and contains two categories: Removed and Rephrased. The first column contains the name of the requirement in question, or the change in code name in bold. This is because requirement codes cannot be reused. The middle column states the requirement description and the third column the reason for the action taken.

5.4.1. Removed Requirements

Firstly, it is important to note that requirements have only been removed when in agreement with the user and accompanied by strong factual arguments. An example is "SALT-SSYS-COM-02: All data shall be down-linked to Earth with a minimum average data rate of 1 [Gbit/s]", this requirements was found to be unreasonably and unattainably high due to the low data size produced by the equipment discussed in Chapter 13 and required bandwidth, respectively. Other examples are the latter three requirements: SALT-SSYS-REL-1,2 and 5. All may be omitted due to the usage of the Starship launcher produced by SpaceX, that will provide a launch transport and lander element and is also capable of delivering the equipment in one go, with room to spare.

5.4.2. Rephrased

In the case where a requirement is outdated or not suited for the current design anymore, while relating to a system aspect or parameter that has a need for a constraint rephrasing is opted for. An example of such a case is "SALT-SSYS-SENS-07: The telescope shall be able to perform a highest quality observation in <t.b.d.> [h]", this requirement relates to the final performance of the telescope and needs

to be constrained due to its importance in the mission. The main issue with this phrasing is that it mentions "highest quality". It has been found that there exist no such maximum as a quality limit of the measurement for a spectrometer, as an extended exposure time will always further improve the accuracy. As a means to remove this ambiguity the performance requirement is now related to the minimum brightness an exo-planet must have in order to be visible after one operation cycle under a minimum of an SNR of 10, similar to the formulation of the performance requirement on the JWST¹ [8]. The main part that has driven the action have been highlighted in the table.

Table 5.5: Requirement changelog from Baseline to Final report

Code	(Old) Discription(s)	Reasoning
Action: Removed		
SALT-SSYS-COM-02	All data shall be downlinked to Earth with a minimum average data rate of 1 [Gbit/s].	Overruled by data budget.
SALT-SSYS-POW-03	The power storage system shall have <t.b.d.>[kWh] of reserve energy.	Redundent due to safety margins.
SALT-SSYS-BUDG-02	The system shall be insured.	Insurance is impossible for the TRL of the system.
SALT-SSYS-POW-09	The power storage system shall have enough energy to maintain the telescope in hibernation for 14 days.	Cannot be designed upon rather will be a result of the current system.
SALT-SSYS-OPE-01	All elements shall be launched as cargo in up to three human spaceflight missions plus one dedicated launch or two dedicated launches.	Astronauts will be transported by external party. Furthermore, by using the Starship multiple launches are not necessary.
SALT-SSYS-OPE-08	The system shall be operational after <t.b.d.>[h] from the final landing.	Cannot be designed upon.
SALT-SSYS-PROJ-01	The design team shall deliver a baseline project report before <t.b.d.>.	Accomplished.
SALT-SSYS-REL-01	The system shall be deployed with a launcher that has had at least <t.b.d.>successful launches.	Usage of SpaceX Starship launcher.
SALT-SSYS-REL-02	The selected launcher shall have a reliability greater than <t.b.d> percent.	Usage of SpaceX Starship launcher.
SALT-SSYS-REL-04	The telescope shall be placed on a location of low asteroid impact probability .	Due to a near uniform distribution this requirement did not provide a design constraint.
SALT-SSYS-REL-05	The Moon lander shall have an autonomous guiding system.	Usage of SpaceX Starship launcher.
Action: Rephrased		
SALT-SSYS-SENS-[07->11]	The telescope shall be able to perform a highest quality observation in <t.b.d>[h].	Poorly phrased w.r.t. the current design.
SALT-SSYS-[SENS-08->MECH-14]	The telescope shall be able to point within an angle of <t.b.d>[deg] from the galactic core with respect to the galactic plane .	Poorly phrased w.r.t. the current design.
SALT-SSYS-POW-[07/08->10]	The power subsystem shall have a continuous power output of <t.b.d>[W] during the lunar night . The power subsystem shall have a continuous power output of <t.b.d>[W] during the lunar day .	Lunar day and night are eliminated due to the usage of a PIL and poorly phrased w.r.t. the current design.
SALT-SSYS-POW-[05->11]	The power storage system shall be capable of storing <t.b.d>[kWh] of energy .	Poorly phrased w.r.t. the current design.
SALT-SSYS-POW-[06->12]	The power subsystem shall collect <t.b.d>[kWh] during one lunar cycle.	Poorly phrased w.r.t. the current design.
SALT-SSYS-MECH-[09->12]	The spacecraft shall not damage the launch vehicle.	Poorly phrased w.r.t. the current design.
SALT-SSYS-MECH-[06->13]	The system shall survive moon quakes .	Removed ambiguity.
SALT-SSYS-[COM-01->OPE-12]	The telescope shall be available for at least 70 [%] of each Moon night period .	Removed ambiguity.
SALT-SSYS-[MECH-3,4,5->SENS-12,13,14]	No change in descriptions.	Moved requirements to better suiting engineering department.

¹JWST: James Webb Space Telescope

6. Operation Location

Concepts must be generated before they can be traded off, and the nature of the generated concepts is such that the system's location on the lunar surface has a great influence on the design; aspects such as temperature, available sunlight, and communications line-of-sight with the Earth all have an influence. The location was therefore selected in advance, in order to allow for further design choices. This chapter focuses on this location selection, considering the different aspects that affect the design: temperature, presented in Section 6.1, the availability of solar power, in Section 6.2, communications in Section 6.3, the proximity of other potential lunar installations, shown in Section 6.4, terrain, presented in Section 6.5, and observable exoplanets, as seen in Section 6.6. The final location is presented at the end of the chapter, in Section 6.7.

6.1. Temperature

The Moon's thermal conditions vary wildly—during the day, temperatures can range from 95 to 390 [K].¹ There are a few regions near the poles, however, referred to as Permanently Shadowed Regions (PSR's), that are an exception to this rule. Usually these are found in craters at high latitudes, where the Moon's convenient orbital inclination shields certain areas from solar rays throughout the lunar cycle. PSR's are permanently shadowed, as the name suggests, and allow for temperature ranges between 31 and 100 [K] as a consequence, see Figure 6.1 and 6.2. The two figures present a visual map of the surface temperature of the south pole, centred around the Shackleton crater. Aside from a favourable thermal environment, PSR's allow the sensing apparatus to function throughout the entire lunar cycle due to the absence of sunlight. This makes them an attractive location for the mission.

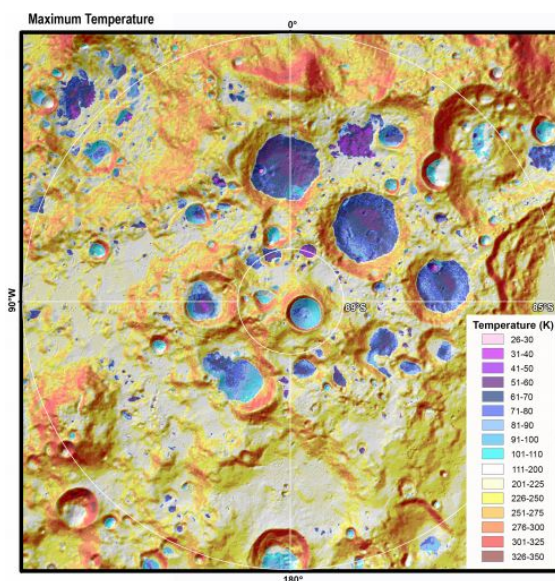


Figure 6.1: Figure displaying the maximum surface temperature of the craters on the south pole of the Moon. [10]

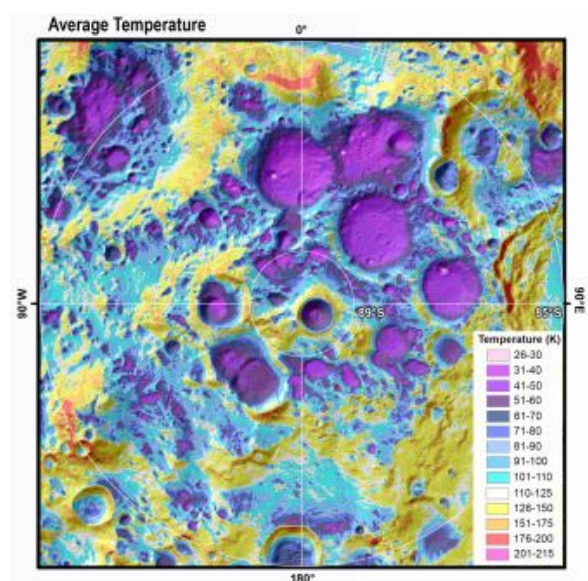


Figure 6.2: Figure displaying the average surface temperature of the craters on the south pole of the Moon. [10]

6.2. Availability of Solar Energy

Similar to PSR's, the lunar surface also hosts PEL's: Peaks of Eternal Light. These are points on celestial bodies that are in (near) constant light from the Sun. The Moon has numerous PEL's, located

¹NASA - Moon Fact Sheet - URL:<https://nssdc.gsfc.nasa.gov/planetary/factsheet/moonfact.html>

on its north and south poles. These peaks are of special interest to this mission because they allow for a continuous energy supply if it uses solar energy, despite the highly oblique angle of incidence of the solar rays. These peaks are particularly useful if they are accompanied by a PSR, as they could present an opportunity for an advantageous operational temperature and power supply.

6.3. Contact with Earth

The Earth has its own emissions, mostly in the infrared. This happens to be the part of the spectrum that the telescope is meant to observe, and as such, emissions of the sort must be avoided to reduce noise. Figure 6.3 displays the South Pole of the Moon, where the highlighted spots show where Earth's radiation reaches the surface [10].

While staying out of the highlighted areas in the figure is desirable for the telescope, this leaves it with no direct line of sight for communication. This means an alternative communication method has to be established, which may require more sophisticated analysis. The choice of location can deeply influence this: a landing on the far side of the Moon would require an orbiter for communication purposes, while being near the terminator or the near side might allow for direct communication, drastically decreasing the complexity of the system. If the telescope is located near the terminator - in the south pole, for instance - it could be placed just out of sight of the Earth, and be paired with an antenna just inside the highlighted area, such that communication can still be established.

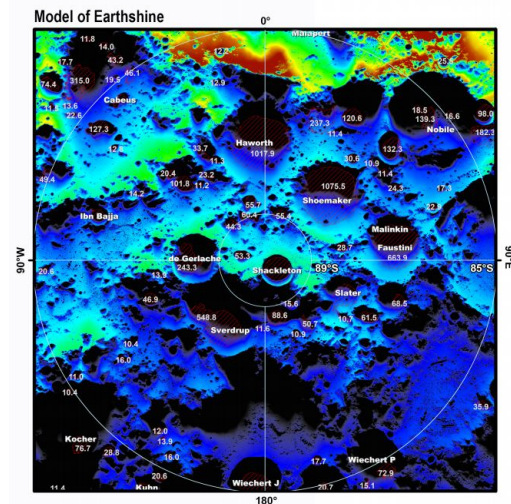


Figure 6.3: The south pole of the Moon with highlighted regions where IR radiation from the Earth reaches the lunar surface. [10]

6.4. Potential Presence of Lunar Installations

Given that multiple space agencies have recently shown interest in exploring the lunar surface, it is a reasonable inference that there might already be operational lunar installations present when SALT is deployed. Naturally, the availability of astronauts is essential to the mission, which would make a location close to any planned landing sites convenient. One example of such a site is the Shackleton Crater, which Artemis is currently considering as a site for a base [11]. Existing lunar surfaces have to be taken into account as well, given that thrusters and/or impact on the Moon's surface could launch lunar dust and debris over several kilometers [12].

6.5. Lunar Terrain

The terrain of the lunar surface has a major influence on both the lander and the translation system of the scientific sensing payload. Certain concepts may not be feasible on hilly terrain or large boulder fields. The LOLA² instrument on the LRO probe has recorded surface elevation maps of outstanding quality that can be used for research on this topic. Figure 6.4 shows a map created using data from LOLA that indicates the slope of the terrain on the South Pole of the Moon.

²Lunar Orbiter Laser Altimeter

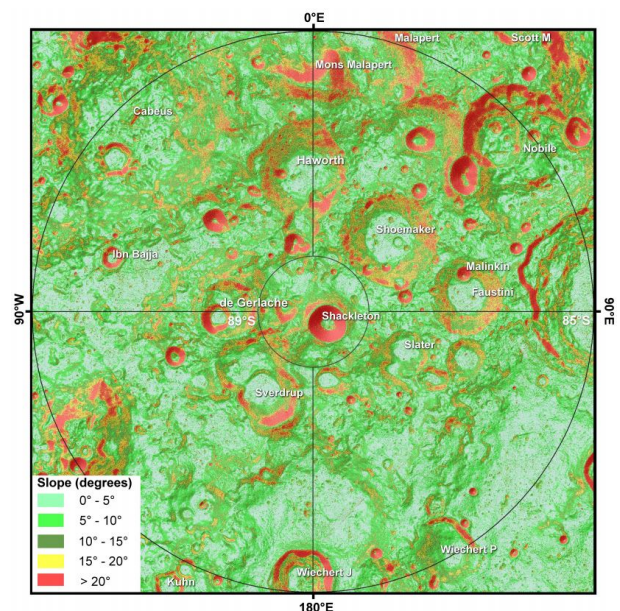


Figure 6.4: Terrain slope of the South Pole of the Moon. [10]

6.6. Observable Region

The goal of this mission is to observe exoplanets; it is therefore important to ensure that the selected location has a reasonable amount of exoplanets in sight. As of this day, 29,398 exoplanet candidates have been registered, with up to 4,383 of these confirmed as such.³

While the list is extensive, a long-term mission could potentially observe each of the exoplanets in its field-of-view. NASA's Exoplanet Archive provides data for each of these exoplanets, including their relative celestial position. These are given in terms of the right ascension and declination of each planetary system. Figure 6.5 shows the coordinate system used. The position of these planetary systems in the night sky can be plotted using this coordinate system, which allows for a detailed analysis of the field-of-view of the telescope on different potential locations on the Moon. Together with a model of the field-of-view of the telescope as a function of time, it is possible to see the path traced by the telescope's field-of-view on the night sky.

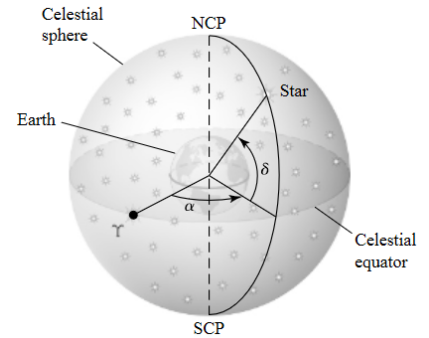


Figure 6.5: The equatorial coordinate system. α , δ and Υ designate right ascension, declination and the position of the vernal equinox, respectively. [13]

A computer model was constructed that allows for a detailed analysis of the exoplanet visibility from different locations on the Moon. This model employs a number of assumptions, listed under Table 6.1.

Assumption	Justification	Result
The Moon's orbit is perfectly circular.	The Moon's orbit has an eccentricity $e = 0.0549$. ¹	A small uncertainty is added to the calculation with every orbit, but the model can be simplified to speed up computations.
The Earth's axial precession is negligible.	A full cycle takes 26,000 years ⁴ , and the mission would take 15 years in the best of cases.	There is a small difference between the coordinate axis used and the one in which the exoplanets are measured, but the model does not need to incorporate the axial precession of the Earth.
The distance covered by the Moon in its orbit is negligible.	The Moon's semi-major axis is $0.3844 \cdot 10^6$ [km], while the distance to the closest exoplanet is 4.25 light-years. The ratio between the two is $9.5536 \cdot 10^{-9}$. The change in the observation angle is therefore minimal.	The observation model can be simplified as a spinning Moon and doesn't need to incorporate motion around the Earth. A small uncertainty is added.
The Moon's surface is perfectly spherical.	The ellipticity of the Moon is 0.0012. ¹	The model doesn't need complex simulations of the Moon's surface features. Some uncertainty is added that needs to be considered after determining a location.

Table 6.1: Assumptions used in the exoplanet visibility model

The model employs a series of coordinate system transformations and trigonometric relations to calculate the path marked across the night sky of a vector perpendicular to the Moon's surface at a given point. From this point, a number of different "pointing angles" are compared to the angle every exoplanet makes with this vector, to see whether the angle is sufficient to see that exoplanet. The model treats the position of the Moon as constant, but not its inclination: it employs several expressions given by the International Astronomical Union to describe the Moon's axial precession - see Figure 6.6.

³NASA Exoplanet Archive - URL: <https://exoplanetarchive.ipac.caltech.edu/cgi-bin/TblView/nph-tblView?app=ExoTbls&config=>

The model takes a given date and mission duration as input, and outputs a number of exoplanets for a given pointing angle, and a plot of the observation path over the night sky. Figure 6.7 shows the observation path for a random latitude of -34° , calculated for a full precession cycle (18.6 years). The thickness of the line shown is due to the multitude of positions being generated and the low variation in angle between them. In truth, a single cycle might vary as little as 0.05° in its declination angle. This difference could matter during operations, but does not significantly influence the estimated number of observable exoplanets by much.

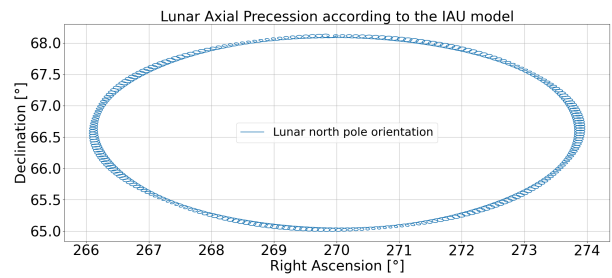


Figure 6.6: Axial precession of the Moon according to the IAU model.

Figure 6.7 shows that the path traced over the night sky could be approximated with a line, and that changes over time are almost negligible when it comes to the number of visible exoplanets. It is worth noting that the line represents only the path traced by the vector perpendicular to the surface of the Moon; the conclusion from Figure 6.7 is that the number of visible exoplanets is more heavily influenced by the achievable pointing angle than by the position on the Moon in itself.

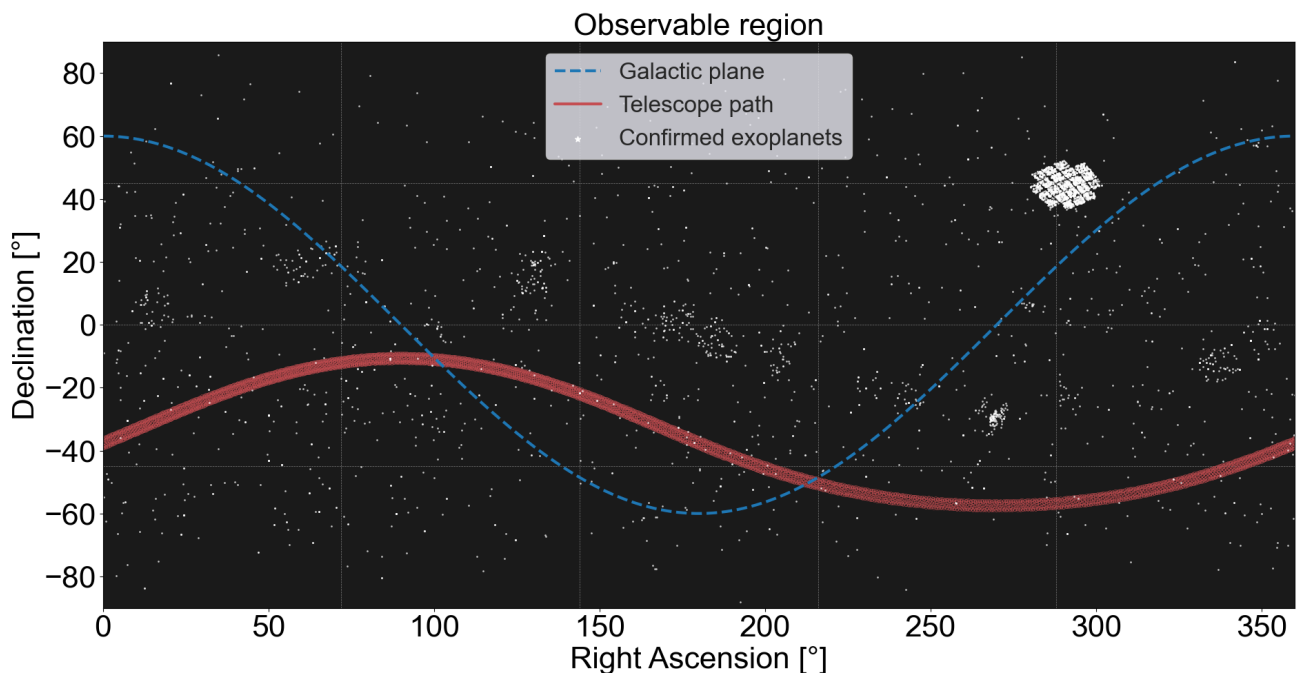


Figure 6.7: Observation path for -34° latitude.

Figure 6.8 shows the estimated number of exoplanets at the Sverdrup crater, near the south pole of the Moon, with a latitude of -88.5° . It is shown for a mission duration of 18.6 years — that specific duration being selected due to it corresponding to the duration of a precession cycle and it not being far off from the longest mission duration required.

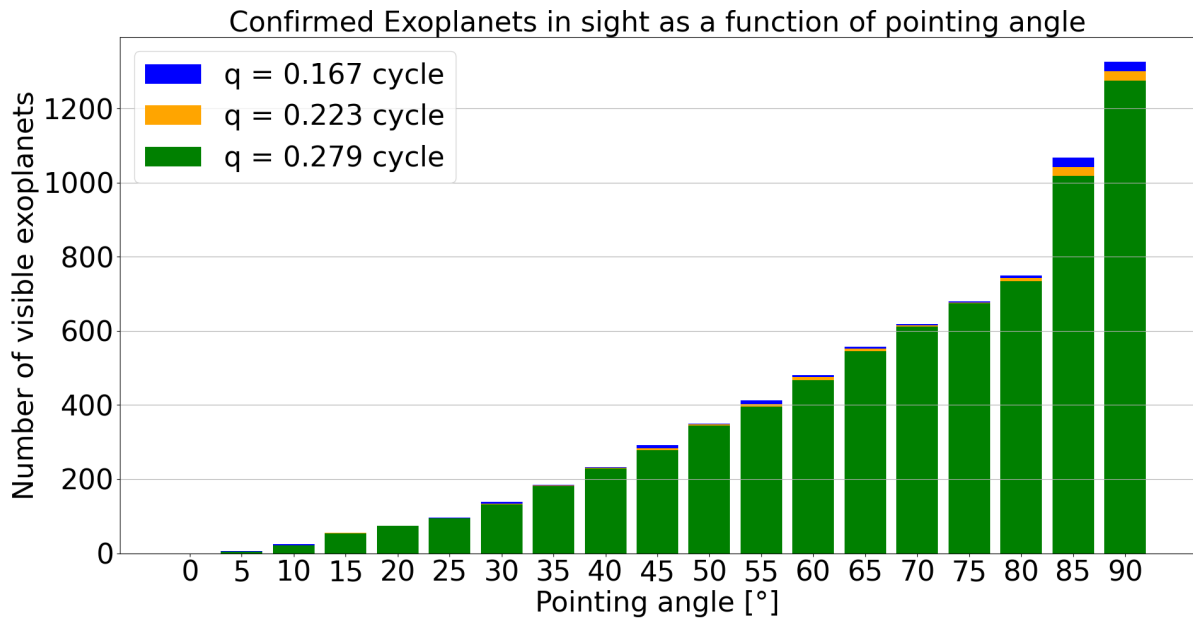


Figure 6.8: Number of observable exoplanets at latitude -88.5° over 18.6 years.

The number of exoplanets shown varies with the pointing angle. Naturally, if this angle is increased, more exoplanets are in sight. The different columns show the visible exoplanets given a certain length of a single observation. A gross estimate of 150 hours was used as average, corresponding to 22.3% of a lunar orbit. The other two values — $q = 0.167$ and $q = 0.279$, or 16.7% and 27.9% — represent 25% less and more than that figure. Clearly, when compared to the Darwin mission’s goal of observing 250 exoplanets [2], and considering that these results apply to the confirmed exoplanets only — allowing for the number to grow in the time leading up to the mission — any location on the Moon would suffice, given a large enough pointing angle.

6.7. Final Location

Table 6.2 shows the different candidate locations and how each ranked in each of the categories. The selected locations cover multiple areas of the Moon, but show a slight bias towards the south pole. This is due to it being more well-understood than most other regions, due to the preexisting interest in the area from space agencies.

Table 6.2: Locations score on trade-off criteria.

Location Trade-off	Temperature	Daylight	Communication	Terrain	Observations	Moon Base
Shackleton Crater	Good: 51-60 [K]	Good: PEL	Good: Relay line-of-sight	Bad: >20° slope	Medium: Up to 1200 planets	Excellent: Artemis base
Sverdrup Crater	Good: 51-60 [K]	Good: PEL	Good: Relay line-of-sight	Good: 0-5° slope	Medium: Up to 1200 planets	Good: 50km from Shackleton
Malapert Mons	Bad: 200 [K]	Good: PEL	Excellent: Direct line-of-sight	Bad: >20° slope	Bad: IR emissions from Earth	Medium: 100km from Shackleton
North Pole	Good: 51-60 [K]	Good: PEL	Medium: Possibility of relay	Medium: Rough terrain	Medium: Up to 1200 exoplanets	Bad: No nearby installations
Equator (terminator)	Bad: 300 [K]	Medium: 14 days sunlight	Medium: Possibility of relay	Medium: Depends on location	Excellent: >4000 planets	Bad: No nearby installations
Equator (180 [°] longitude)	Bad: 300 [K]	Medium: 14 days sunlight	Bad:	Medium: Depends on location	Excellent: >4000 planets	Bad: No nearby installations

The final selected location is the Sverdrup crater, due to its overall good performance: the terrain has a manageable slope, boasts a ridge with perpetual sunlight, is close enough to the terminator to allow for communication without an orbiter, provides plentiful shade - allowing for near-constant operation and low temperatures, permits the observation of a significant number of exoplanets, and is close enough to planned future manned stations that manual assembly and maintenance on the part of astronauts becomes a possibility.

7. Mobility Concept Trade-off

This chapter summarises the conceptual design trade-off for the different mobility concepts. As has been described Chapter 3, the collectors of the telescope will have to move to perform an observation. Since the design of this mobility system impacts the design choices of other subsystems, a trade-off for this system is needed.

7.1. Concepts

In order for the system to operate correctly, the collectors must be able to translate within a range of 50-500 metres from the beam combiner. This makes the mobility of the collectors a driving feature. This section lists the characteristics of the different concepts found in the lead up to the trade-off. The three mobility concepts are the rover, rail and MagLev system, as was previously mentioned in Section A.4. The MagLev system can be seen as the equivalent of the rail system but with magnetic instead of physical translation. Early renderings of the concepts are shown in figures 7.1 and 7.2 respectively.

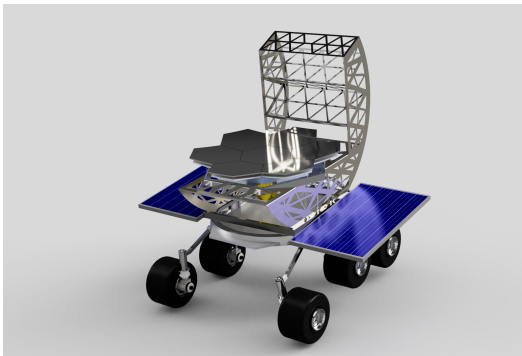


Figure 7.1: Rover based concept.

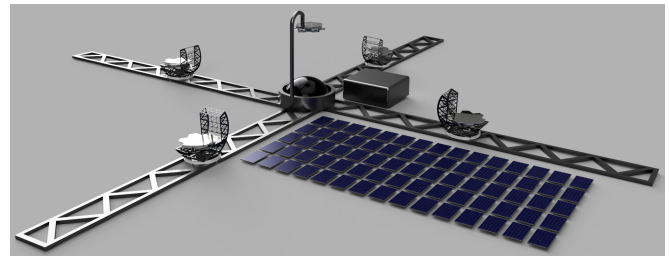


Figure 7.2: Rail system concept; the MagLev concept is similar.

Another concept, the zipline, was dropped early in the design process due to doubts in its feasibility and a low TRL of some of its systems. It should be noted that the considerations in the following sections were made early in the project. Although outdated, they show the views of the team when the trade-off was made. In hindsight, the MagLev concept is inferior to the rail. It was still considered during the trade-off due to its perceived feasibility.

7.1.1. Rails Concept

The rail based concept would use high precision rails as a means to transport the grains radially. Since the Sverdrup crater was chosen as the most suitable location, the rails should be elevated by 0.6 meters to account for the surface roughness inside the crater of 0.4 meter RMS [14]. The characteristics of the rails are as follows:

- The rails allow for precise movement which makes the calibration of the mirrors simpler. This allows for better repeatability.
- The rails allow for a stable base for the telescope. This makes pointing, both to the target and to the combiners easy.
- The rails could resonate with the surface during moonquakes, meaning they would require some form of vibration protection in the rail standoffs.
- Once in place, the system would require very low maintenance.

- The infrastructure for the rails would require an involved installation. This would be a laborious task for the astronauts. Additional equipment would also be needed. Such an installation might take many days to perform. Sverdrup is in permanent darkness complicating the installation further.
- A surface installation is expected to require much more materials to be transported to the moon.
- Extending the system would be as laborious and costly as setting up the original configuration.

7.1.2. MagLev Concept

A MagLev system uses electromagnetism to lift and propel the uppercarriage. The type of magnetic levitation would be either electromagnetic or electrodynamic levitation. In general, a such a MagLev system is similar to the rail concept with some differences:

- The MagLev system has a lower power consumption.
- MagLev would have passive resistance against moonquakes. This is already achieved in Japan's SCMagLev system.
- The guideways of a Maglev would have to be volumetrically larger than for a rail system. The bed of the guideway would have to be wide to allow for lateral stability. This could require a heavier surface installation, although this would have to be investigated further.
- A MagLev system would likely cost much more to develop and manufacture than a rail system.
- A MagLev system theoretically has less wear on its infrastructure than a rail system. A rail system could however be designed to withstand wear for its lifetime, making this advantage void.

7.1.3. Rover Concept

The rover concept would involve a set of 4 Rovers and a static central combiner. The rovers could move around both radially and tangentially to the combiner.

- The platform a rover provides is inherently less stable than that of the rails and MagLev.
- The rover is easier to set up as it does not require infrastructure to be built on the Moon. It is expected that this brings a lower cost compared the rail and MagLev concepts.
- The rovers might still require moonquake protection.
- Since Sverdrup is in permanent darkness, the rovers would have to work purely on battery. Requirement VLMT-SUS-02 prohibits the use of nuclear power. A charging station at the central combiner must be present to provide power to the rovers periodically.
- The rovers are not constrained to a radial line allowing for the rotation of the baseline. This feature greatly enhances the optical performance, by decorrelating the planet's signal from noise sources.
- Rover collectors are more replaceable than the rails or MagLev system. A new rover could be sent up whereas a broken rail would require in-situ rebuilding.

7.2. Trade-off Method

The Analytic Hierarchy Process (AHP) [15] was used to formalise the trade-off process. The AHP breaks decisions down into a series of comparisons between pairs of alternatives. The winner of each comparison can be determined in isolation with a degree of superiority. To illustrate, if one were conducting a trade-off involving 7 criteria and 3 concepts, 21 simultaneous decisions would have to be made. If each criteria was weighted and considered in isolation, only 3 simultaneous decisions would be required. However, with the AHP, only one decision must be made at any moment in time between two alternatives. Furthermore, the AHP subsumes criteria weighting, meaning that the 7 simultaneous decisions required for weighting can also be reduced to a single decision. The particular AHP tool used for this project is AHP-OS¹. This tool implements the AHP method in a digital format, and allows multiple users to independently input their judgements.

¹Goepel, Klaus D., AHP Online System - AHP-OS: <https://bpmg.com/ahp/>

7.3. Trade-off Result

With the method discussed in the previous paragraph the trade-off can be made. This section includes an examination of the weights that have been used and the resulting concept.

7.3.1. Criteria Determination and Weighting

The first step of an AHP trade-off is to select the trade criteria. It is important to select criteria which strongly differentiate between the concepts. It is also desirable to keep knowledge of the specific concepts out of the trade-off setup process, so as not to bias the trade-off structure towards one concept. In the SALT trade-off, total isolation of concept from the trade-off setup was not possible due to project scheduling, but an attempt was made to maintain this mental separation when selecting criteria. The hierarchy of criteria selected for this trade-off are presented here, together with a description of each criteria.

Risk	Operational difficulty	Performance	Extensibility	Cost
- Development risk	- Installation difficulty	- Measurement quality	- Difficulty of converting X to star	- Cost to build
- Intrinsic system risk	- Maintenance difficulty	- Measurement rate	- Difficulty of extending life	- Cost to maintain
		- Observable planets		- Cost to perform EOL

With the criteria defined and entered into AHP-OS, the weight determination was performed. The resulting weights were calculated by the tool. The tool also provides a measure of consensus which indicated very high agreement between the members of the group, even without coordination of choices. This significantly increases confidence in the correctness of the results, which are shown in Figure 7.3.

Risk

The risk criterion encompasses both the developmental risk and the intrinsic system risk. The developmental risk is the probability of the project failing before it has reached an operational status. Examples of developmental risks would be a low Technology Readiness Level (TRL), or proven but extremely complex systems. Intrinsic system risk relates to risks that involve the operation of the system, and would have to be mitigated. One example of this type of risk would be a higher inherent susceptibility to moonquakes.

Operational Difficulty

Operational difficulty was the next criteria considered. It was subdivided into the installation difficulty and the maintenance difficulty. These two subdivisions can be interpreted as the up-front and ongoing operational difficulty respectively. The difficulty of operating the ground element was not included, as it was not believed this would significantly differentiate between alternatives.

Performance

It was clear to the SALT team from the beginning that one of the most important trade-off criteria would be the performance of the system. Each of the three performance sub-criteria above relates to a distinct concern of the SALT team. Measurement quality is largely self-evident. These measures relate to user requirements on signal-to-noise ratios and angular resolution, but also to the quality capability of competitors. Measurement rate relates to the exposure time required for a certain quality observation, and largely determines the number of planets the system will be able to observe over its lifetime. Finally, observable planets relates to the number of planets that will pass within the observable field of the telescope over its lifetime. This depends on a number of factors such as field-of-view, location, and off-axis capability.

Extensibility

The extensibility criterion is a function of the effort required to convert from the four collector X configuration to the eight collector star configuration, and the effort required to extend the mission life. These

are both directly the result of user requirements given to the SALT team. Because the SALT telescope has such a large aperture, and is a complex system, it was believed that different candidate solutions would score very differently.

Cost

The last criteria selected for the trade-off was cost. Early budgeting identified cost as a likely driving requirement for the SALT mission. The program budget of one billion Euros contrasts with the much larger budget allocated to other future missions. Because it was an important requirement, cost was also selected as a trade criterion. It was subdivided in the costs to build, maintain, and EOL the system.

7.3.2. Concept Selection

With the criteria weights determined it was possible to enter the final stage of the AHP process. In this step, the same procedure used for criteria ranking is applied to selection of the best alternative. The only difference between the two steps, other than considering alternatives, is that the results are weighted with the outputs from the previous step. The results of this final trade-off are as shown in Figure 7.3. The table shows that the rover concept was considered the most desirable, accruing a score of 41.2%, compared with 34.5% for the rail concept and 24.3% for the MagLev concept. As the AHP process can be somewhat opaque when viewed at a high level, a qualitative description justifying these results is presented in the following section.

Decision Hierarchy						
Level 0	Level 1	Level 2	Gib Prio.	Rover Concept	Rail Concept	Maglev Concept
SALT	Risk 0.187	Development Risk 0.592	11.1%	0.321	0.495	0.184
		Intrinsic System Risk 0.408	7.6%	0.353	0.472	0.175
	Operational Difficulty 0.158	Installation Difficulty 0.549	8.6%	0.708	0.172	0.121
		Maintenance Difficulty 0.451	7.1%	0.347	0.426	0.227
	Performance 0.474	Measurement Quality 0.641	30.4%	0.443	0.285	0.271
		Measurement Rate 0.100	4.7%	0.246	0.380	0.375
		Observable Planets 0.259	12.3%	0.348	0.326	0.326
	Extensibility 0.070	Difficulty of X to Star 0.378	2.6%	0.780	0.115	0.104
		Difficulty of Extending Life 0.622	4.3%	0.310	0.373	0.317
	Cost 0.112	Cost to Build 0.512	5.7%	0.376	0.419	0.205
		Cost to Maintain 0.385	4.3%	0.297	0.444	0.259
		Cost to Perform EOL 0.103	1.2%	0.542	0.221	0.236
			1.0	41.2%	34.5%	24.3%

Figure 7.3: The results of the concept trade-off determined by AHP-OS, higher numbers are desirable.

7.4. Trade-off Sensitivity

The sensitivity of the concept trade-off was investigated to see what opinion change would have been required to result into a different concept. The sensitivity of the outcome was tested in three different ways: by varying the criteria weights within a previously established confidence interval, by varying the mathematical algorithm that produces an outcome and by varying the performance indicators of each concept within an uncertainty range established by the experts working in their respective department. The performance indicators of the last test can be accessed in the midterm report [16].

By varying the performance indicators, the variance was found to be fairly large and therefore the trade-off was deemed sensitive by this test. The main reason for this is expected to be the high uncertainty in some of the subsystems in the early design phases.

By varying the criteria weights, only very small changes were found in the final trade-off weights. A change in criteria weight larger than 20.6% was needed to drastically impact the results, which is far out of the confidence interval for all criteria weights.

By varying the trade-off solution algorithm, a larger sensitivity was observed both for the Rover and Maglev Concept. However, no algorithm would impact the results such that a different concept would be chosen. After the three aforementioned tests were performed, it became clear that 2 out of 3 tests were not able to impact the results such that it would present a different concept decision. Therefore it can be concluded that the decision to choose the Rover Concept is a robust decision. Figure 7.4, 7.5 and 7.6 showcase the variance and therefore sensitivity of each test as a boxplot.

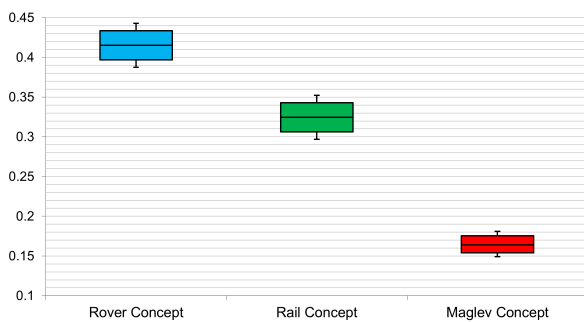


Figure 7.4: Distribution of the trade-off outcome by varying the criteria weights within their confidence interval.

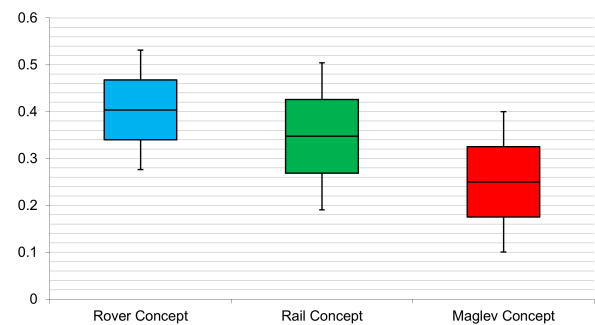


Figure 7.5: Distribution of the trade-off outcomes by varying the performance indicators within their respective uncertainty intervals.

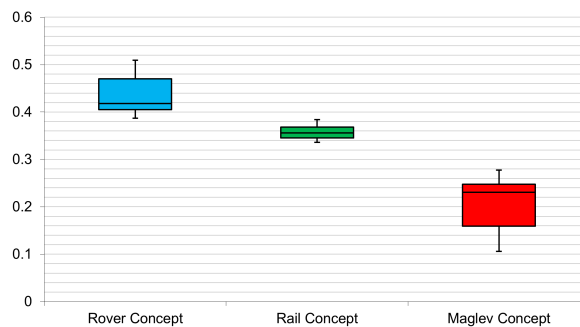


Figure 7.6: Distribution of the trade-off outcome by varying the solution algorithm.

8. V&V Procedures

Verification and validation (V&V) is an important part of any engineering process. V&V procedures increase confidence in the engineering process, allowing for major investment in the design. The SALT project distinguishes between two types of V&V: model type and system type. Section 8.1 describes the model type V&V procedures, while Section 8.2 details the system type V&V procedures.

8.1. Model Type V&V

Several models will be necessary to complete the SALT design process. Because these models strongly influence SALT design decisions they must be trustworthy and accurate. This is ensured with a three-step process comprising pre-validation, verification, and validation.

Model V&V type results will be presented in a dedicated subsection of the relevant subsystem. This subsection will contain an explanation and justification for the verification procedures. The section will also contain a table summarising the tests carried out, the results, and the measured quantities where possible.

Pre-validation

Pre-validation occurs before full development starts, and checks that model assumptions are valid in the context of SALT. SALT is a unique system; its simplifying assumptions are unique. For example, SALT must be isolated from external vibrational disturbances occurring on the Moon. This is unlike previous space telescopes, which were in orbit and experienced time invariant disturbances (over short periods). The validity of all assumptions will be checked by two team members.

Verification

Verification runs in parallel with model development. There are three main classes of verification techniques that can be used for SALT: hand tests, sanity tests and comparative tests. Hand tests are simple test cases performed on paper. These mainly protect against programming errors, but also against subtle modelling mistakes. Sanity tests are also performed on paper, but are much rougher and concerned with orders of magnitude. These identify obvious errors, mostly programming errors. In contrast, comparative tests are performed with another trusted model. An example of a trusted model would be widely used numerical modelling tools. Where possible, tools which have been used in projects similar to SALT will be selected.

Validation

Validation is the final activity before approval of the model. It ensures that the model is valid for the SALT system in particular. Because SALT is a complex and novel system, the validation process has to be flexible and will have to apply its own techniques. An example of a validation test that might be performed is taking input parameters from an existing system and ensuring the model's outputs match the system's design.

8.2. System Type V&V

The goal of the entire engineering process is to reliably produce designs that address customer needs. System V&V is an important part of this process. It follows a similar structure to model V&V. System verification ensures the system fulfils the stated design requirements, while system validation ensures the system addresses the needs of the customer. The results of these activities will be summarised in a "Compliance" subsection with the structure detailed in Section 8.1.

Pre-validation

System pre-validation ensures requirements fulfil customer needs. This activity was already performed in the initial design stages, but will continue as requirements are reviewed and adapted. As system and subsystem requirements arise, they are added to the requirement table. The requirement table includes a field for the source of the requirement. Full traceability to a user requirement is checked when a new requirement is added.

Verification

System verification ensures that the design fulfils all stated requirements, see Table 5.2 and 5.3. This DSE will complete a phase-A design of the system. This means that no actual hardware will exist at its completion. Therefore, verification will generally be performed by analysis or inspection, and not by test or demonstration.

The compliance subsection of a respective chapter details the verification method applicable to that requirement. At the earliest possible opportunity, a (sub)systems design will be verified against all analytical requirements. This can entail applying SALT models, performing hand calculations, inspection, or some other analytical activity. At the end of each subsystem design iteration, verification of all analytical and inspection requirements must be completed and detailed. If any are not satisfied, the design must be iterated. An evaluation of feasibility should be made for any requirements that cannot be verified yet.

Validation

System validation ensures compliance with customer requirements. It will not be possible to fully validate SALT, as the phase-A design does not provide a sufficient level of detail for a complete analysis. However, the various performance analyses of applicable subsystems provide a high level of confidence that the system design is valid. When further SALT development finalises critical subsystems, such as optics, validation can be performed.

9. Optical System and Sensing Design

This chapter describes the optical and sensing system in detail. Section 9.1 discusses the fundamentals behind the SALT system's interferometry based operation. Section 9.2 discusses the various sources of noise and how they impact the optical model, which is describe in Section 9.3. The architecture of the telescope and its comprising optical instruments are described in Section 9.4, and the upgradeability of the SALT system is discussed in Section 9.5. A compliance assessment for the optical system is carried out in Section 9.6, and seismic sensing is discussed in Section 14.1. Finally, Section 14.2 discusses the sensors equipped onboard the SALT system. The SALT sensing subsystem requirements are as follows:

Table 9.1: Optical subsystem requirements

Code	Requirement
SALT-SYS-01	The telescope shall characterise the thermal infrared signature of exoplanets
SALT-SSYS-SENS-01	The angular resolution of the telescope shall be less than 5milliarcsec at a wavelength of 10 μm
SALT-SSYS-SENS-02	The spectral resolution shall be at least 300 [-]
SALT-SSYS-SENS-03	The spectral range shall cover wavelengths of 6 to 20 μm
SALT-SSYS-SENS-04	The signal-to-noise ratio shall be equal or greater than 10 for H ₂ O
SALT-SSYS-SENS-05	The signal-to-noise ratio shall be equal or greater than 5 for CO ₂
SALT-SSYS-SENS-06	The signal-to-noise ratio shall be equal or greater than 5 for O ₃
SALT-SSYS-SENS-09	The system shall survive the particle radiation environment
SALT-SSYS-SENS-10	Lunar dust shall not permanently damage the sensing equipment
SALT-SSYS-SENS-11	The optical system shall be able to observe exoplanets with a 5.0E20 [W/m ²] brightness or higher with an SNR of 10 [-] during 10 hours of observation
SALT-SSYS-SENS-12	The optical path length shall be able to be corrected
SALT-SSYS-SENS-13	The optical path length shall be kept stable with an accuracy of less than 1.5 [nm] w.r.t. the beam combiner
SALT-SSYS-SENS-14	The optical path length shall be controllable with a range of 10 μm

9.1. Principle of Operation

SALT is a nulling interferometer. It uses the phenomenon of wave interference to obviate the need for very wide dynamic range when observing faint emitters around bright stars. If the four beams of light collected by SALT were exactly the same, wave interference to null the star would also eliminate any planetary signal. However, the four collecting telescopes are located at slightly different distance from both the host star and target planet. While the optical system matches the optical path distance (OPD) to the star along each arm, the planet distance generally differs slightly. Although this differential is extremely small relative to the total distance to the target, it is many times the wavelength. The planet is thus not destructively interfered. A four element interferometer such as SALT has a transmission map with intensity variation along two axes. The outer product of these response patterns gives the response pattern or "transmission map" shown in Figure 9.1.

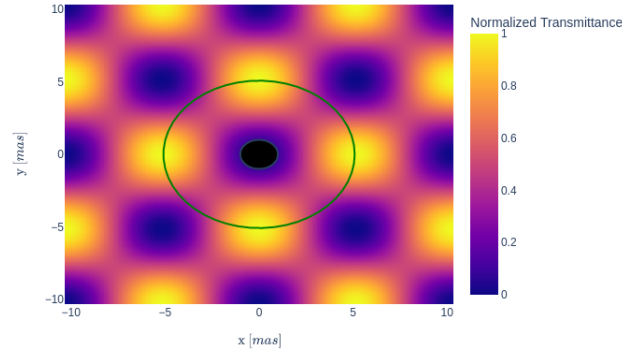


Figure 9.1: Expected transmission map at 10 [μm], x baseline 1000 [m], y baseline 200 [m]

The figure shows the transmissibility of the system over the field of view of the telescope. Yellow regions correspond to high transmissibility, whereas blue regions correspond to nulled regions. Placing the host star (black circle) in a null reduces its impact on observation. It is not completely nulled because it is not a true point source. The transit of the planet (green ring) over nulling and non-nulling regions modulates it with a frequency tied to its radial position. The spatial period of the nulling is set by the ratio $\frac{\lambda}{b}$ where b is the baseline of the telescope. The length of these baselines will be optimized to minimize stellar leakage and maximize the planetary signal for each system.

9.2. Noise Sources

Despite the tremendous noise reduction afforded by an interferometer, there are still a number of noise sources that have a major impact on observation quality. These are primarily the stellar leakage, instrument thermal noise, exo- and local-zodiacal noise, stray light leakage, dark current & readout noise, and shot noise.

Stellar Leakage

As can be seen in Figure 9.1, the telescope transmissibility varies sinusoidally over the field of view. The host star is not a true point source, so this allows some starlight to leak onto the detector. This leakage can be reduced by optimizing the baseline to cover the star with a null to the greatest possible extent. The noise is mostly radially symmetric and can be partially rejected by modulation of the planet signal due to instrument rotation. Despite this it remains a significant contributor to the total system noise [17].

Instrument Thermal Noise

The SALT optical system will be kept at cryogenic temperatures, but it will not be kept at absolute zero. The true temperature of each optical element will be between 10 and 40 Kelvin. This will lead to thermal emissions which are not fully contained near a peak, but are a spread spectrum of energy ($\frac{\text{W}}{\text{m}^2 \cdot \text{m} \cdot \text{sr}}$) described by Planck's law [18]:

$$I(\lambda, T) = \frac{2hc}{\lambda^5} \cdot \frac{1}{\exp \frac{hc}{k\lambda T} - 1} \quad (9.1)$$

where h is Planck's constant ($6.62E-34 [\text{m}^2 \text{kg}/\text{s}]$), and c is the speed of light in vacuum ($3.00E8 [\text{m}/\text{s}]$), and T is the temperature. Figure 9.2 shows the intensity of thermal noise in the SALT band.

It is clear that at 10K emissions in the SALT band of interest are minimal (compared to expected planet fluxes on the order of $0.1 - 10 \left[\frac{ph}{s \cdot m^2} \right]$ (unit ph is photons). However, at 40K the emissions completely swamp the desired signal. This is one of the reasons it is so important to keep the area around the detector at 10K.

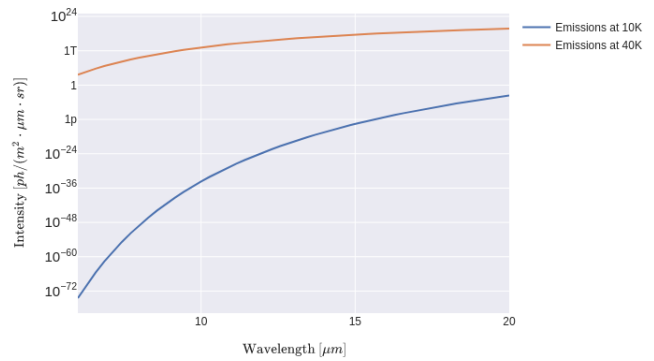


Figure 9.2: Thermal noise in SALT band at 10 and 40 Kelvin

Exo- and Local-zodiacal Noise

The emptiness of space is far from empty. Within our solar system and the target system there are large clouds of dust. These clouds scatter light from the host star, and have their own thermal emissions. These emissions lead to a background noise, which is assumed to be uniform[17]. These emissions can be nearly eliminated by the rotation of the SALT system, which will not modulate uniform emissions. However, exo-zodiacal noise is not yet fully modelled in literature, and the details of the remaining noise depend on precise aspects of the optical design that have not yet been ascertained. As such, this noise source was not included in the current model.

Stray Light

Stray light is light that enters the optical system from the environment. This can be due to reflections off the surround lunar surface, emitters or mechanical components of the collectors or combiner, or a variety of other source. Design provisions have been made for stray light suppression, for example each entry port on the combiner has baffles. However, a sufficiently detailed model of the stray light requires full knowledge of the collector and combiner internal structure, and was left for a later stage.

Readout Noise and Dark Current

Even in an entirely un-illuminated detector there is some current. This movement is known as the detector "dark current", and contributes to system noise. This dark current is significantly reduced in SALT by the operation of the detector at cryogenic temperatures.

Another noise source is the readout noise. Photon impacts on the detector generate electrons. These are collected and amplified by the readout circuitry before being sent for processing. This readout operation inherently introduces some error and noise into the signal.

Due to the absence of a known sensor operating at the correct wavelengths for the SALT mission or a full characterization from DARWIN, this noise source was not included in the model. It should be added once the detector and readout electronics have been selected. The readout electronics in particular may have a non-negligible impact on instrument sensitivity.

Shot Noise

Shot noise results from the discreet (quantum) nature of light. Any series of measurements can be viewed as a Poisson process. The mean of the measurements is the true value (or spectra in SALT's case), but the variance for a single measurement or small number of measurements is very high. Collecting a large number of photons results in a lower variance. The shot noise varies proportionally to $\frac{1}{\sqrt{N}}$. This has a major impact on signal quality for a very sensitive telescope, where less than 10 photons of signal per second are expected from the target in a limiting case.

9.3. Optical Model

The optical design of SALT involves maximizing the number of target planets. This quantity depends on many characteristics of the optical system and the telescope as a whole.

9.3.1. Method

The SALT optical model evaluates the optical subsystem in a space defined by:

1. The number of collector mirrors
2. The average null depth
3. The mirror diameter
4. The instrument throughput
5. The detector quantum efficiency
6. The target shot SNR
7. The maximum phase error
8. The pointing authority
9. The maximum allowable exposure time
10. The minimum allowable contrast SNR between planet and star

Program Flow

The program flow is as follows:

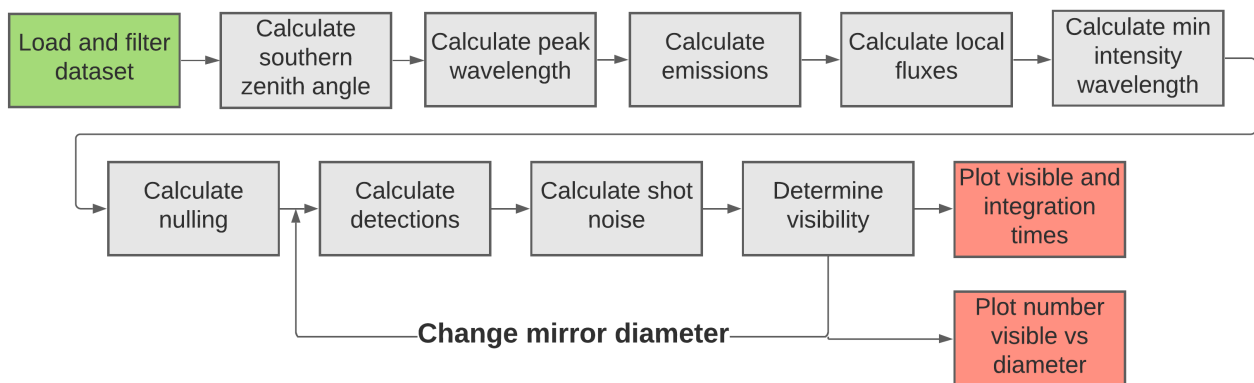


Figure 9.3: Optical model flow

Load and Filter Dataset

At program entry the model loads and filters the ipac NASA Exoplanet Archive¹ to determine observation candidates. The model uses the confirmed planets in the "PS" table, exported on 8 June, 2021. The first filtering stage ensures that all records have the following fields:

- soltype (Solution type)
- pl_controv_flag (Controversial flag)
- sy_snum (System star count)
- sy_pnum (System planet count)
- ra = α (ICRS right ascension)
- dec = δ (ICRS declination)
- sy_dist = D (System distance)
- pl_name (Planet name)
- pl_rade = R_{\oplus} (Planetary radius)
- pl_eqt = T_{\oplus} (Planet equivalent temperature)
- pl_rade = R_{\odot} (Star radius)
- st_teff = T_{\odot} (Star effective temperature)

Then the model filters out records with pl_controv_flag set and those which do not have the "Published Confirmed" solution type. Finally, systems with multiple stars or planets are removed. Planets in such systems could likely still be measured by SALT, but are not considered in the model.

Calculate Southern Zenith Angle

¹ipac: NASA Exoplanet Archive - URL: <https://exoplanetarchive.ipac.caltech.edu/>

An important aspect of the observability of a system is its position on the celestial sphere. SALT will be located near a lunar axis, and will point to roughly the same area of sky over the mission. In the second pipeline step, the model determines the angle between the zenith and the pointing vector to each system. This is accomplished in three stages. First the model rotates a unit X vector by the lunar north α_a around the Z axis, and then by the lunar north δ_{ec} around the rotated Y axis. This vector is negated, giving the lunar south celestial pole. This procedure is repeated for the system α_{as} and δ_{cs} . The dot product of the lunar south vector with system vector gives the cosine of the off-zenith angle.

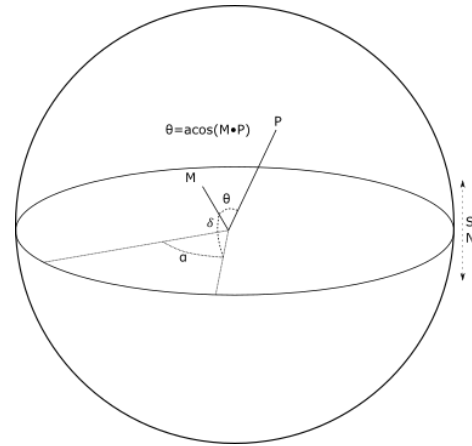


Figure 9.4: Calculation separation depicted on the Celestial Sphere

Calculate Peak Wavelength

The emissions of a black-body are not evenly distributed over some spectral range. They are distributed according to Planck's law as described in Section 9.2. This implies that for any given set of spectral bands there is some lowest intensity spectral range. The model determines the lowest signal spectral band and uses the fluxes in that band for all future calculations.

Calculate Emissions

The model starts the optical calculations by determining the system-local emissions of each candidate. Planet and star fluxes are computed based on their equivalent black-body temperatures. These temperatures already include compensation for emissivity. These fluxes are converted into output power by multiplying by the appropriate surface areas, then divided by the photon energy to give the total photons-per-second emissions of the star and planet.

Calculate Local Fluxes

The system-local emissions are distributed over the area of a sphere centered on the system and tangent to the telescope. This gives the instrument local fluxes.

Calculate Nulling

The telescope nulling depends on one system specific parameter (the angular diameter of the star) and two common parameters (the phase variance and the intensity variance). The optical model has two modes for determining nulling. The first mode computes the nulling according to a model for a two element Bracewell interferometer[17]. The second mode forces the nulling to a known value. The true nulling of a system is very complicated, so the forced mode was used to evaluate performance with a known achievable nulling level ($1E-5$ to $1E-6$) [2, 19].

Calculate detections

In this context, detections mean electrons entering the readout electronics. It depends on the number of incident photons from signal and noise sources, and on the quantum efficiency of the detector. This stage also accounts for modulation of the planet signal by the rotation of the transmission map.

Calculate shot noise

The final performance calculation is the integration time required for a given shot noise, or the shot noise achieved in a given integration time. This is done by applying a shot noise relation that depends on the stellar and planetary detections, the spectral resolution, and the phase variance.

Determine visibility

This stage uses the outputs from the previous stages to determine the set of observable planets. It also tags all non-observable planets with the reason for their exclusion. First it tags planets with a position outside the field of regard of the telescope (requiring more than 60 degrees of off-zenith pointing). Then it tags planets with a star-planet contrast below the set level. Next it tags planets which would require more than 10 [hrs] of integration to achieve shot SNR. The remaining planets are tagged "VISIBLE". It does not account for the effect of stray light from Earth's sun. Because the moon-earth system orbits the sun, one of the model simplifications is the assumption that each planet can be observed when the Sun is out of the target pointing area on the celestial sphere.

Mirror diameter calculations

The observable planets vs mirror diameter plot is generated the same as in other modeling activities, with one exception. Rather than proceeding linearly, the pipeline from "Calculate detections" to "Determine visibility" is repeated for each mirror diameter. The number of visible planets is then tallied and recorded at the end of each iteration.

9.3.2. Results

Figure 9.6 indicates the visibility of planets on the celestial sphere. The results are presented in terms of right ascension and declination. SALT is located on the Moon's south pole, which points in the general direction of celestial south, so most observable planets are near $-\pi$ declination.

Figure 9.7 shows the occurrence of spectral peaks in each indicated range. It is clear that the peak emissions of most exoplanets are outside of the spectral range of SALT, and will not contribute to measurements. This has a strong impact on integration times. The low spectral intensity in the band of interest means that the number of photons impacting the detector is much lower than would be expected from an evenly distributed intensity. This greatly increases the required integration time for a given shot SNR.

Figure 9.5 shows the number of visible planets for a given mirror area. There is a rapid linear increase with mirror area from 0 [m^2] to approximately 4 [m^2]. At this point the incremental gains in detections starts to decrease. It is believed this is due to the capabilities of SALT exceeding the capabilities of the instruments used to create the catalog.

Table 9.2: Optical results

Visibility	Number of Planets
Out of Field of Regard	312
Visible	80
Integration too long	19
Contrast too low	9

Table 9.3: Input optical parameters

Parameter	Value
Number mirrors (-)	4
Average null depth (-)	1E-5
Mirror diameter (m)	2
Instrument throughput (-)	0.5
Detector quantum efficiency (e/ph)	0.2
Target shot SNR (-)	10
Phase error (rad)	9.4E-4
FOR (deg)	60
Maximum exposure (hours)	10
Minimum contrast SNR (-)	10

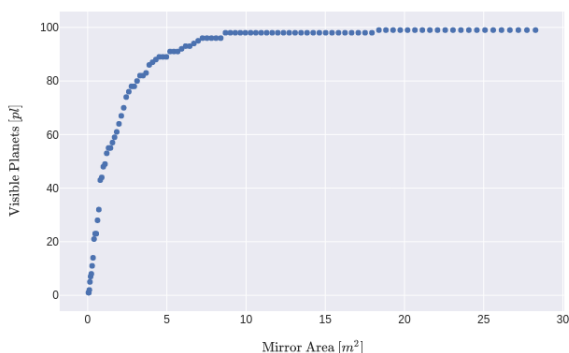


Figure 9.5: Visible planets vs unit mirror area

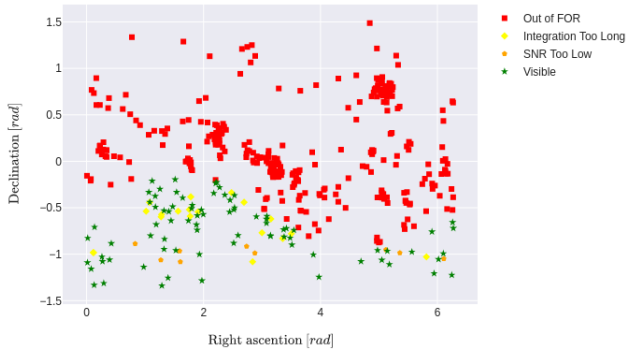


Figure 9.6: Celestial visibility from south pole

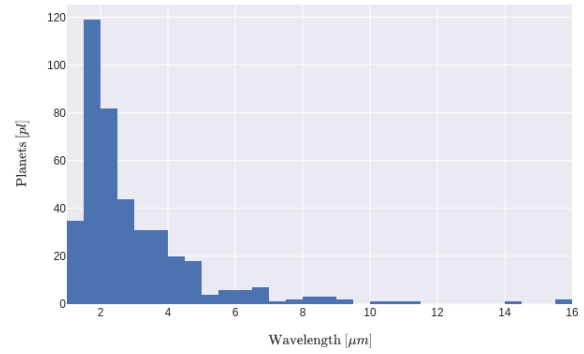


Figure 9.7: Spectral peak histogram

This visibility analysis formed the basis for the selection of the 2 [m] SALT unit telescope diameter. At 2 [m] 80 (74%) of the 108 targets in the field of regard can be observed. Incremental increases in mirror diameter do not lead to significant gains in sensitivity, but they lead to significant additional loads on the cooling, pointing, and structural subsystems. If necessary, the same effect can be achieved by increasing the allowed exposure time. The SALT optical system is also expandable and upgradeable, as will be discussed in section 9.5. With the supported collector doubling SALT will be pushed even further past the capabilities of existing systems.

Based on the results from this model, it is expected the SALT system will be able to observe at least $\frac{80}{420} \cdot 4400 = 838$ [planets]. This is based on a visibility of 80 out of 420 planets in the filtered dataset. This is reduced from the full 4400 planet dataset due to absence of required information for visibility calculations, but it is likely that the distribution of parameters remains similar over the entire dataset.

9.3.3. Verification

The model is almost entirely a pipeline of equations. There are five branches, four of which involve dataset filtering. Only one branch changes the outcome of the measurement and it is only a single statement, involving multiplication by a single factor. Therefore, the model was verified entirely by manually completing equivalent computations by hand for an exemplar planet, or by inspection in the case of very simple subroutines. Where possible, intermediate values were also compared with external references. WASP-96 b was used as the reference planet. The model, manual, and external figures are presented in table 9.4

Table 9.4: Verification results

Property	Model	Manual	External	Agrees?
Pointing Vector	(0.677, 0.0124, -0.736)	(0.677, 0.0124, -0.736)	-	Yes
Lowest Intensity Wavelength [μm]	20	20	20	Yes
Planet Signal [$1E - 3$ e/s]	9.09	9.08	-	Yes
Star Noise [$1E - 5$ e/s]	7.1	6.8	-	Yes
Integration Time [s]	11089	11082	-	Yes (Within rounding error)

The following properties of the model were verified by two-party inspection:

- The system calculates the correct separation angle based on the moon pole vector and system pointing vector.

- The four filtering branches (single statement) are correctly implemented.
- The system correctly labels system visibility conditions.
- The plotted outputs correctly represent the computed data.
- The model correctly forces the null depth to the Darwin reference value.

9.4. Telescope Architecture

With the availability of the mirror diameter, and other performance metrics, the telescope can be sized, and its comprising systems can be designed.

9.4.1. Rover Ground Configuration

In order for the SALT system to perform accurate measurements, the ground configuration of the rovers must be optimised. Prior to the DARWIN mission's proposal, [2] a planar X-configuration was envisioned instead of the non-planar "Emma" architecture. A driving reason for this is the redundancy that this configuration offers, as the SALT system can still operate in the same configuration in case one of the collector rovers fail [20] — albeit at reduced efficiency. Additionally, the configuration allows for a higher planet signal modulation efficiency in comparison to other configurations [21]. For these reasons, the SALT system will adopt a modified X-configuration for primary operations.

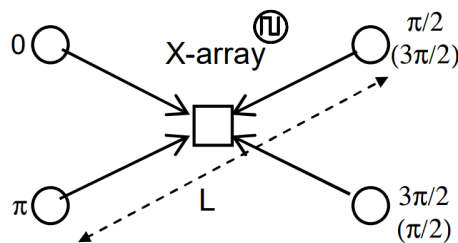


Figure 9.8: The general X-configuration that will be used by the SALT system [21]

The primary adaptation for the SALT mission is that the beam combiner will not be located at the centroid of the four collectors for all measurements. The reasons for this are detailed in Section 9.4.4.

9.4.2. Unit Telescope Architecture

As one of the major optical components, each beam collecting rover is mounted with a primary mirror, and secondary mirror. The results of the trade-off between possible primary mirror configurations [16], can be seen in Table 9.5.

Table 9.5: A table showing the mirror configuration trade-off.

Mirror Configuration	Performance	Complexity	Cost	Manufacturability	Weight	Normalised Score
Rigid Monolithic	5	5	2	3	1	0.720
Solid Actuated Segments	5	2	3	4	4	0.747
Segmented MEMS	3	4	4	3	4	0.627
Bimorph	2	3	3	2	2	0.400
Ferrofluid	1	1	4	5	5	0.693
MEMS	2	3	3	3	4	0.653

The SALT system will make use of a segmented primary mirror due to the replaceability of segments, lower costs associated with production, ease of manufacturing and overall weight savings. Having determined this, the segments can be sized.

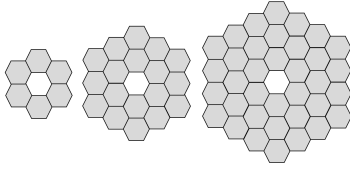


Figure 9.9: Hexagonal configurations with 6, 18 and 36 hexagonal segments

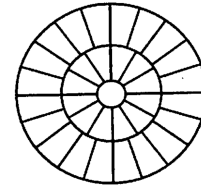


Figure 9.10: Petal configuration [22]

Figure 9.9 shows the possible configurations of the primary mirror in a hexagonal shape. Additional segment configurations included a petal geometry, however implementing uniform active control would be difficult to achieve. Furthermore, the support structure would be complex to design as it would vary per segment type, resulting in increased complexity [22]. For this purpose, hexagonal segments are chosen.

Table 9.6 shows how the sizes of the mirror segments vary with the number of segments used. The segment size is the diameter of a hexagonal plate, measured between the flat edges. The fill factor of the mirror is given by the ratio of its light sensitive area to its total area. For this calculation, it is assumed that the packing of hexagonal segments was gap-less, and the fill factor reduction was largely attributed to the missing central panel. To reduce design complexity, 18 segments are used, as they provide a high fill factor without the need for an increased number of panels which require additional actuators — leading to a reduction in overall mass for the primary mirrors, which scales with the number of segments used. The following equation calculates the length of a segment side and allows the determination of the segment sizes required to achieve an equivalent area circular aperture of $2m$:

$$a = D \sqrt{\frac{\pi}{6\sqrt{3}N}} \quad (9.2)$$

D = Equivalent area circular aperture diameter [m]

N = Number of segments

Table 9.6: Parameters of each configuration

Segment Size [m]	No. of Segments	Fill Factor [%]
0.449	6	85.71
0.259	18	94.74
0.183	36	97.30

The material used by the mirror segment's substrate only marginally affects optical performance as the mirrors can be correctly aligned by the use of actuators and sensors. The primary purpose of the substrate is to maintain structural integrity, it is coated with a reflective surface which minimises the dispersion of incident rays.

Selection of the mirror material warrants a trade-off. The method used to carry out such a trade-off begins by firstly identifying criteria and assigning weights to determine their order of importance in the overall system design. These criteria are used a basis for categories, and each design option is assigned weights, depending on how well they fulfil the criteria within that category. Finally, a normalised score is assigned to each design option which takes into account the weights assigned throughout the trade-off procedure — generating a final numerical value, for a largely qualitative trade-off.

Table 9.7: Weights assigned to the trade-off criteria

Criteria	Weight [%]
Performance	33.33
Cost	25.00
Ease of manufacturing	25.00
Mass	16.67

Using this method, the trade-off is performed and each material is judged based on identified criteria, which are considered with weights as shown in Table 9.7.

The rationale behind the weighting of these criteria stem from the fact that optical performance is of high importance, as this fulfils the primary objective of the SALT mission to the customer's satisfaction. This criteria considers, as an example, the thermal performance of the material. The cost (which include manufacturing and maintenance costs) and ease of manufacturing are weighted the same, as both these criteria stem from requirements which involve a tight budget (**SALT-SSYS-08**), as well as consider the ease of troubleshooting and assembly of the system (**SALT-SSYS-06**). Mass holds a low priority due to the availability of the starship HLS lander.

Available options [23][22] for the mirror substrate materials are as follow:

- Carbon fibre reinforced polymer (CFRP), which provides low contraction ratios at low temperatures, however does not meet the tight surface restrictions required for telescopes. However to accurately determine the extent of the effects of these restrictions, an error budget must be derived.
- Silicon carbide (SiC) is inexpensive to produce, and has a high specific stiffness. However it has a low TRL and its long term stability remains unknown, and polishing its surface is a time-consuming task due to its hardness.
- ZERODUR is a ceramic material with a low CTE and has actively been used in many telescope systems. However, the significantly higher relative density of the material makes it a poor choice for the SALT system.
- Ultra-low expansion (ULE) fused silica with titanium dioxide has been used in multiple telescope systems, such as the Hubble ² and maintains excellent thermal stability.
- Beryllium has a higher CTE than the other available materials, and a much higher specific stiffness in comparison to its density. However, it is costly to produce due to its toxicity and its long term stability will only be tested once the James Webb Space Telescope (JWST) enters service.

The arguments provided for each substrate can be condensed into a trade-off as shown in Table 9.8. For the SALT system, the primary mirror segment substrate chosen is ULE glass due to its thermal stability, i.e. low CTE, relatively lower density, and ease of production.

Table 9.8: Mirror material trade-off. Higher numbers indicate better performance per category.

Mirror Material	Performance	Cost	Ease of Manufacturing	Weight	Normalised Score
Beryllium	5	1	1	5	0.600
CFRP	2	3	3	4	0.567
Silicon Carbide	2	5	2	3	0.583
ULE	4	3	5	4	0.800
ZERODUR	4	3	5	1	0.700

The mirror segments will be coated with a thin reflective aluminium surface as well as an additional layer of silicon dioxide to protect the aluminium from corrosion on the lunar surface. This combination has a high TRL as well as proven long term stability and a reflectance of up to 98% within the desired spectral range ³, making it ideal for the SALT system. Both of these layers will be in applied with an

²Hubble mirror substrate: hubbleoptics.com/UL18.html

³Mirror coatings in the infrared spectrum from Solaris Optics: solarisoptics.eu/products/mirrors/ir-mirrors/

order of thickness measured in nanometers.

The secondary mirror will consist of a single circular segment, and will be constructed and coated with the same materials as that of the primary mirror.

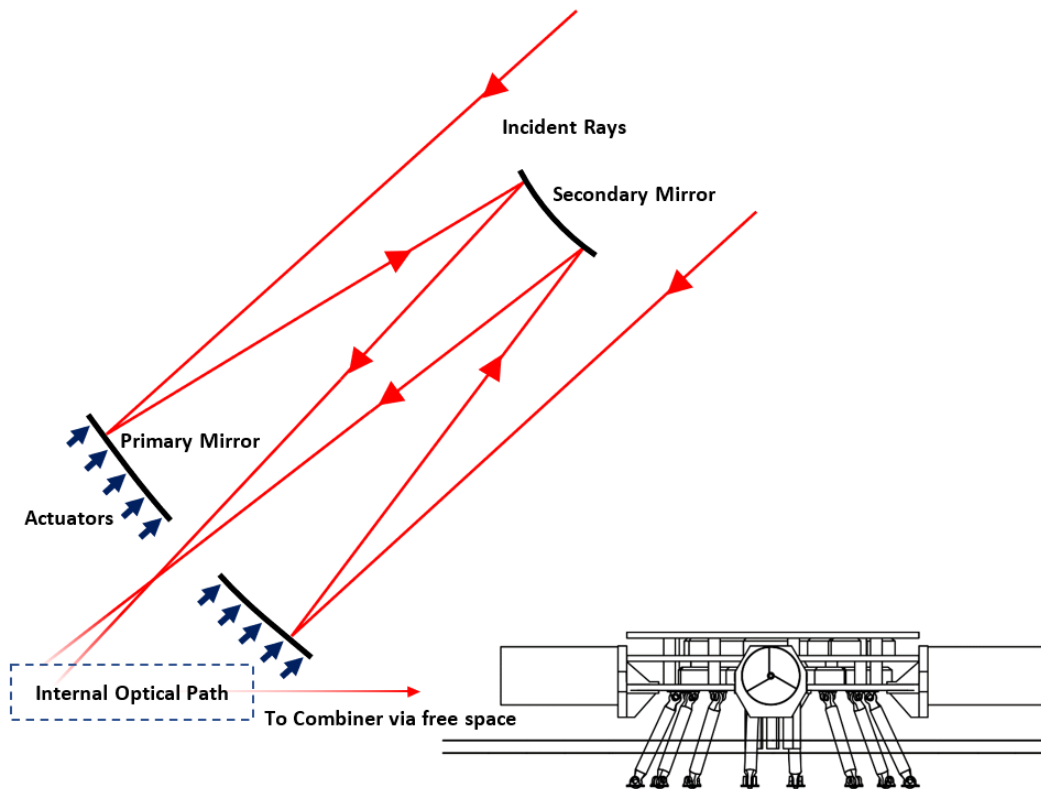


Figure 9.11: Unit telescope optical architecture showing collimated beam travelling to combiner [Not to scale]

The SALT system's beam collectors will use a modified Ritchey–Chrétien telescope configuration due to its ability to eliminate spherical and comatic aberrations [16]. These aberrations are briefly explained as follows:

- Spherical aberrations stem from the geometry of spherical surfaces, which refract incident rays at varying degrees depending on how far they strike off-center. The hyperbolic mirrors used in the Ritchey–Chrétien configuration eliminates this.
- Comatic aberrations arise due to lens imperfections and can distort off-axis incident rays. The hyperbolic mirrors once again eliminate this.

Figure 9.11 shows the unit telescopes architecture making use of this configuration. The entrance columns on the combiner require some sort of actuation as they may need to rotate to accommodate measurements. However the design of this system is beyond the scope of this phase of study. The incident rays are reflected off the segmented primary mirror, and onto the secondary mirror. From here, the beams continue to follow the internal optical path, before being reflected to the combiner.

The unit telescope is sized according to the governing equations of the Ritchey–Chrétien configuration [22]. With the primary mirror diameter fixed at $2m$, the remaining parameters are determined. Using the parameters of the JWST as a reference due to the similarity in instrumentation, the effective f-ratio is determined to be 16.67 and the effective focal length can be calculated by:

$$f = ND_1 \quad (9.3)$$

The optimal f-ratio of the primary mirror is independent of the mirror diameter, and is limited by the sampling capabilities of the detector. The exact detector specifications are undetermined, and thus the

specifications of JWST's Mid-Infrared Instrument (MIRI) will be adapted ⁴ — resulting in a pixel size of $6.2\mu m$ at a wavelength of $10\mu m$. Using these specifications and the equation below, the f-ratio of the primary mirror can be determined.

$$N_1 = \frac{2p}{\lambda} \quad (9.4)$$

The radius of curvature (R) of the primary mirror can be determined by the asphericity and its variation with a d^2D^2/R^3 relation. Once again, the JWST has been used as a reference due to the nature of its segmented mirrors, and its detection capabilities in the infrared domain, which make it the closest comparable design. Using the asphericity parameters of JWST [24], the radius of curvature for the $2m$ primary mirrors of the beam collector telescopes is $72.37m$. The radius of curvature will remain fixed once calibrated for operation, but the segments may need to be realigned if they are replaced during maintenance missions. This process will be similar to that of the JWST, with comparable actuators and wavefront edge sensors being used, to further correct for optical aberrations. The wavefront sensor ensures that all incident rays maintain the same phase, i.e. reflect as intended off the primary mirror. The radius of curvature of the secondary mirror cannot be accurately determined at this stage.

The back focal distance is the point in Figure 9.11 where the two incident rays cross behind the primary mirror. Attempting to quantify the back focal distance (b) and the normalised back focal distance (β) results in an optimisation problem as both of these parameters are interrelated. However, due to impact of these parameters on the primary and secondary mirror separation which have structural and pointing related implications, constraints were added resulting in a value of $0.3m$ for b and 0.121 for β . Additionally, it is to be noted that the radius of curvature will have an impact on these parameters — albeit small, this effect cannot be neglected due to the precision required by the optical system, but cannot be quantified at this stage. The back focal distance and the primary mirror focal length are related as shown in Equation 9.5:

$$b = \beta f_1 \quad (9.5)$$

The magnification of the secondary mirror is simply given by:

$$m = \frac{f}{f_1} \quad (9.6)$$

The separation between the primary and secondary mirrors is given by:

$$s = \frac{f - b}{m + 1} \quad (9.7)$$

The secondary mirror diameter is given by:

$$D_2 = \frac{D_1(f_1 + b)}{f + f_1} \quad (9.8)$$

The optical characteristics of the beam collector telescope can be summarised as in Table 9.9. Additionally, a baffle is considered for the purposes of avoiding stray light from entering the telescope, however further investigation is required at this stage to determine its necessity, and considerations must be made for its large structural implications.

The internal optical path is shown in Figure 9.11. A traditional Ritchey–Chrétien configuration makes use of two hyperbolic mirrors, however, the SALT system will make the use of an additional mirror to direct the collected beams to a fine steering mirror. The fine steering mirror will then reflect the beams to the beam combiner.

Table 9.9: Optical characteristics of the unit telescope

Parameter	Magnitude
Primary mirror diameter (D_1)	2 [m]
Primary mirror f-ratio (N_1)	1.24 [-]
Primary mirror focal length (f_1)	2.48 [m]
Primary mirror radius of curvature (R)	72.37 [m]
Back focal distance (b)	0.3 [m]
Normalised back focal distance (β)	0.121 [-]
Magnification of secondary mirror (m)	13.44 [-]
Primary-secondary separation (s)	2.29 [m]
Secondary mirror diameter (D_2)	0.16 [m]
Effective f-ratio (N)	16.67 [-]
Effective focal length (f)	33.34 [m]

⁴JWST's MIRI instrument properties jwst-docs.stsci.edu/mid-infrared-instrument

9.4.3. Collector Architecture

The first step in the SALT signal acquisition pipeline is the beam collector. This system is responsible for taking celestial emissions and sending a collimated beam of light to the combiner for further processing. The architecture of this system is shown in Figure 9.12.

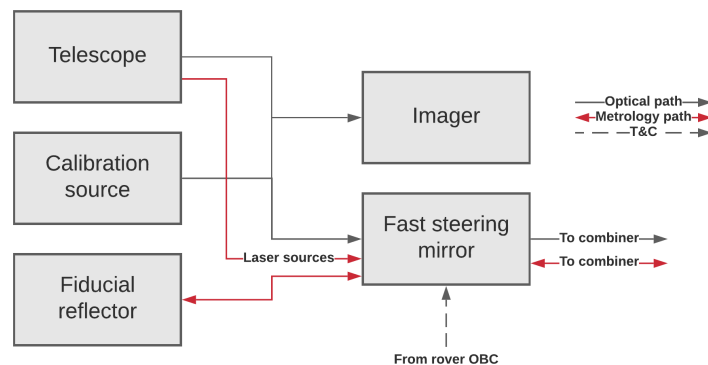


Figure 9.12: Beam collector architecture

Section 9.4.2 describes the collector's unit telescope in detail. Its role is to collect a beam of light from the target. During acquisition, some of this light is sent to the collector imager, where it is used to compute the offset to the system centroid (this forms the first closed loop seek stage). Once initial seeking is complete, the light is redirected to the combiner for further processing. A tip-tilt mirror ensures the light reaches and enters the combiner regardless of the attitude of the collector.

The collector also contains two components central to the laser metrology system, which will be described in further detail in Section 9.4.4. The first of these is the fiducial reflector, which is part of the laser ranging system. These are located near the primary mirror cutout and correspond to a fixed physical location with respect to the primary mirror. The second metrology element is the spider lasers. These are located on the telescope spider (which retains the secondary mirror) and send reference light to the pupil tracking system for lateral deviation correction within the optical paths.

The final component in the collector is the calibration source. This source provides a known spectral emission profile that can be used to identify and correct errors in the system. It contributes to tip-tilt, OPD, and spectrometer calibration. The exact source spatial and spectral profile remains to be determined.

9.4.4. Beam Conditioning

The beams entering the combiner from the unit telescopes will have a variety of errors. Some of these will have been introduced by the attitude of the telescopes with respect to the target, while others will have been introduced along the optical path they have traveled within the system. For example, aberrations will be introduced by the telescope mirrors and the collector fast steering mirror, intensity errors will be induced by differential ageing of mirrors in each telescope, and tip-tilt errors will be introduced by the vibration of the combiner and collectors. The beam conditioning subsystem will eliminate these (and other) errors to the greatest possible extent. The beam conditioning architecture is shown in Figure 9.13.

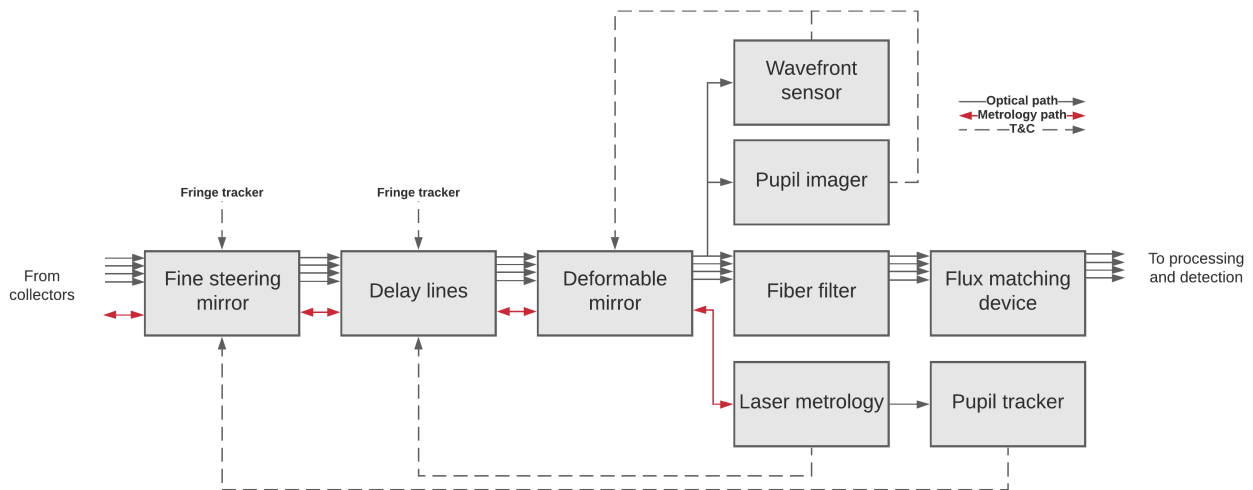


Figure 9.13: Signal conditioning system optical architecture

Internal Metrology

Many of the deviations and errors in the signals entering the combiners will be due to the telescope itself, and not necessarily target pointing errors. For this reason, an internal metrology system is a critical component of any high-precision interferometer. SALT will use a pupil tracker, wavefront sensor, pupil imager and laser ranging system in conjunction with fixed references to detect internal OPD, tip-tilt and wavefront errors. This system is based largely on the design of the various VLT fringe trackers including FINITO [25], PRIMA [25], and GRAVITY [26].

The pupil tracker will detect the location of each pupil centroid and correct tip-tilt/lateral translation errors in conjunction with the fine steering and deformable mirrors. It will do this by detecting the location of the beams from emitters positioned on each unit telescope. The centroid of these beams gives the pupil offset.

The wavefront sensor will detect the errors introduced by the SALT optical system, including those of the primary and secondary mirrors, and the delay lines.

The pupil imager will be used to check system alignment during installation, as in GRAVITY, but will also be used during operation as an additional input to the tip-tilt system to correct for the relative angular position of each collector.

The final component in the metrology system is the laser ranging system, which is used to measure OPDs. A laser pulse is sent from an emitter in the combiner to a fiducial reflector on the collector. The round trip time of this pulse is related to the total path length by the speed of light in vacuum.

Tip-Tilt Correction

Tip-tilt errors are corrected by the fine steering mirrors and deformable mirrors. The fine steering mirror is the first optical surface each beam sees as it enters the combiner. This mirror can correct angular errors along two axes (each parallel to the mirror surface), and is accurate to within tens of $[mas]$. It is partially driven by the pupil tracker, and partially driven by the fringe tracker. Its most important role is to remove bulk errors introduced by the relative motion of the collectors and the rover fast-steering mirrors. This bulk-corrected beam then reflects off the deformable mirror. The deformable mirror is primarily used for wavefront correction, but it also provides a limited range of high precision tip tilt correction with a wide bandwidth. The final tip-tilt correction is provided by the fiber filters, which reject tilted wavefronts.

Optical Path Difference (OPD) Compensation

OPD compensation is accomplished in two stages. The first stage is a larger but slow delay line, while the second is a small but fast one.

The largest OPD variation is introduced by the positioning of the rovers with respect to the target system. This can introduce an OPD difference of up to the baseline length (in the worst case). Such a large delay (up to 1km) is very challenging to introduce efficiently. Accomplishing this with a low number of reflections requires a very long delay line, while doing so in a limited area requires many reflections (with their concomitant losses). An earlier design of the combiner used a folded delay line to overcome this, but it was realized that by relaxing the geometrical relationship between collectors and combiners the need for this delay line can be completely eliminated. Rather than the combiner being located at the center of rotation of the collectors, it will be offset away from the target (see Figure 9.14). The triangle inequality theorem implies there will always be a solution that eliminates the bulk of the OPD errors without any need for a delay line (in Figure 9.14 $a - d \leq b + c$). It should be noted that there is a certain exclusion zone required around the combiner to reduce the risk of a collision with a rover. This does unfortunately lead to a coupling of the minimum baseline and the maximum pointing angle. Reduction of the exclusion zone may be required if very oblique observations at narrow baselines prove necessary.

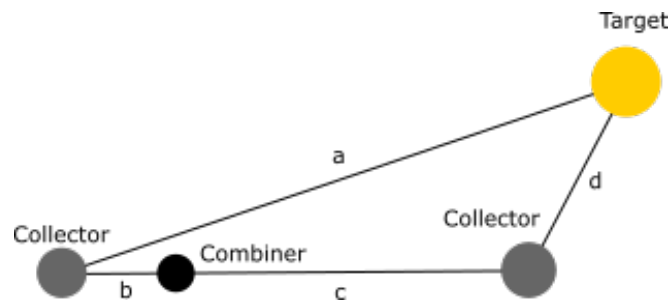


Figure 9.14: Positioning of combiner to eliminate bulk of OPD variation

Some OPD variations will remain, even with this asymmetrical array configuration. This is corrected in the combiner's OPD compensation stage. Light from each collector entering the OPD correction section passes through the first delay line. This system has a travel on the order of tens of centimeters, and corrects for bulk rover positioning errors. However, this delay line's long linear dimension means that it will be limited to near $f = 0$ Hz bandwidth. This means that a second stage of OPD compensation is required to suppress time variations of the path lengths, such as those due to sinkage and vibrations. This second stage will be operated by a voice coil actuator, with a magnetic bearing guide system, which allows the OPD to be controlled with $0.9nm$ precision [27]. This system was developed for the DARWIN mission and can be implemented for long term use due to its wear-free operation. The combiner OPD compensation stages are driven by both the laser metrology system and the fringe tracker. The result of OPD compensation is four beams of cophased light that can be sent into the processing and detection segment of the combiner.

Wavefront Correction

The wavefront of the incoming light beams will be distorted by various aberrations and other errors in the collectors. They will be further impacted by imperfections in the combiner optical path. The deformable mirror will be used to correct these wavefront errors, and the fiber filters will be used to remove any that remain. Each deformable mirror will be driven by the wavefront sensor and the fringe tracker and actuated with piezo elements. The combiner controller will compute the required mirror surface profile to invert the wavefront errors, and will then command the deformable mirror to this profile at a high rate ($>100 [Hz]$). Once the wavefront has been corrected the light will enter the fiber filter. This filter will be either a mono- or multi- mode fiber, depending on the outcome of further investigations and the selected spectrometer configuration (see Section 9.4.5).

Intensity Correction

Because of differential aging of the components in the optical system, and variations in fiber injection efficiencies, the intensity of each light beam will differ. This amplitude difference will reduce or eliminate the desired nulling effect. This will be combatted with flux matching devices. These devices act as a variable attenuator, and will be used to level the relative amplitudes of the beams. This is the last element in the beam conditioning stage as all of the proceeding elements will introduce intensity errors that must be corrected. This can be done at any pre-interference stage with a sufficiently accurate system model, but placing the flux matching devices at the end of the chain simplifies the required control laws. distance between the emitter and the unit telescope.

9.4.5. Processing and Detection

Once the light beams have been fully reconditioned they are sent to the processing and detection segment. This segment of the combiner introduces the necessary phase shifts for nulling, combines the beams, and detects their spectra. It is also where the fringe tracker is located. This system is shown in fig. 9.15.

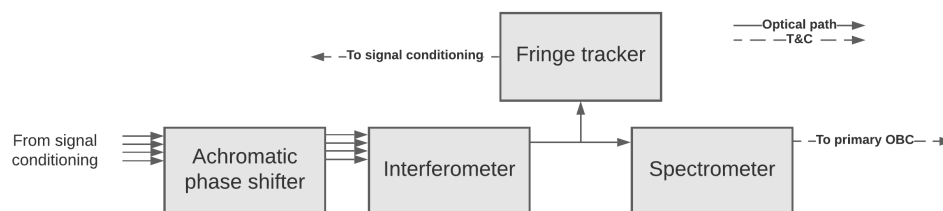


Figure 9.15: Processing and detection system optical architecture

Fringe Tracker

The fringe tracker is among the most important systems on the SALT telescope. Its role is the precise control of the delay lines and tip-tilt mirrors, bringing phase and intensity errors to within the tight tolerances required for effective nulling. It maintains these tolerances over time, providing the stability required for very long integration times. This enables the detection of much fainter planets than otherwise possible. The design of a fringe tracker is complex and will require further work, but existing fringe trackers have demonstrated the level of accuracy required for SALT [28].

Achromatic Phase Shifter

The achromatic phase shifter imparts a fixed relative phase difference on each beam of light across all frequencies. This contrasts with a delay line which imparts a fixed path difference on each beam. Such an achromatic shift is necessary to obviate for OPD scanning. OPD scanning is a technique wherein the path taken by each beam of light is varied to collect a full spectral recording. The downside of such a technique is that the energy in all other wavelengths is lost, meaning exposures are much longer and the system is more sensitive to temporal variations. Elimination of OPD scanning was considered an important feature of the TNO combiner design [29].

Interferometer

The interferometer takes the four fully conditioned, coherently phase delayed beams of light and interferes them to produce several outputs for fringe tracking and observation. There are a number of interferometer designs with complex benefits and drawbacks. SALT will use an adaptation of the latest available Darwin interferometer design by TNO [29]. It should be noted that the TNO design included OPD correction and several other subsystems that are considered part of the combiner subsystem and

not the interferometer in SALT. Additional components detailed in the proceeding sections were also added to incorporate technological developments and the unique operating requirements of the SALT system.

Spectrometer

The spectrometer's role is to determine the intensity of light in each spectral band. The target resolution for the SALT mission is $R = 300$, which corresponds to at least 300 spectral bands. There are two possible designs for the spectrometer, which have very different properties and warrant further investigation in future work.

The first design is a single spaxel detector, with no spatial measurements. This can be efficiently implemented with an echelle grating and diffraction grating. The light enters the spectrometer and bounces off the echelle grating. This spreads the spectrum along one spatial axis. This light then hits a second grating that diffracts each of these beams along a second spatial axis. This encodes one dimensional spectral information in two spatial axes, which allows for efficient use of current- or next-generation 2D sensors. This design allows the use of single mode fibers in the filtering stage, which can provide additional wavefront correction. However, it does not provide a cross sectional view of the target system (this information can be acquired over time with knowledge of the transmission pattern).

The second design is a multi-spaxel detector, giving data with both a spectral axis and a spatial axis. In this system the collimated light entering the spectrometer is compressed along one spatial axis. The diffraction grating then re-spreads it along this axis spectrally, rather than spatially. In this configuration one detector axis is used to measure spectra, and one detector axis is used to measure spatial distributions. This type of spectrometer will provide a linear cross sectional view of the system, but will not allow the use of single-mode fibers. Such a system would need to use multi-mode fibers that preserve spatial information.

9.5. Upgrades

One of the most significant benefits of SALT over competing telescopes is its upgradeability. Historically, launching a space telescope meant its capabilities were fixed. This is not the case with a lunar telescope near a manned human outpost. The flexibility of astronauts enable a variety of improvements. The SALT team has identified two areas where upgrades would have the largest impact, and has made provisions for such upgrades.

The first is an increase in the number of collectors from four to eight. This has the obvious benefit of increasing the collector area. It also increases the number of available baselines drastically (from $\frac{4 \cdot 3}{2} = 6$ to $\frac{8 \cdot 7}{2} = 28$) which allows for more complex transmission maps. This may allow for significantly more structured measurements. This improvement is supported by the ease of adding additional rovers to the configuration, and also by the ease of stacking additional optical tables on the combiner as can be seen in Figure 9.16. Each table can be isolated with a mirror that either deflects the beam, or allows it to bypass the table.

The second upgrade would be of the primary instrument, either to another spectrometer or something totally novel. This would only require the addition of a new optical table. Each table can also be isolated electrically and thermally, which means this upgrade would not necessarily require concomitant upgrades to the power and thermal subsystems (if the original instrument is temporarily or permanently disabled).

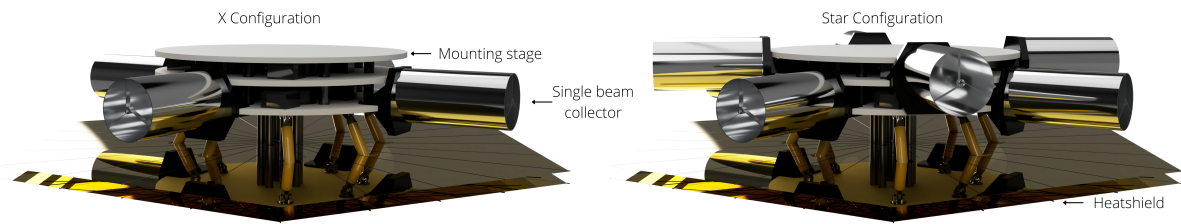


Figure 9.16: Upgrade of the combiner from 4 to 8 collectors (X to star configuration)

9.6. Compliance Assessment

At this stage of the design process a fully detailed verification and validation procedure is not possible. This would require exact numbers of stability, dark current, and many other parameters that cannot be known until exact components (many of which do not yet exist as they will be made just for SALT) are tested in exacting laboratory conditions. However, it is possible to determine whether a design fulfilling the requirements with the described architecture is possible.

The optical model has already proven that **SALT-SYS-01**, **SALT-SSYS-02**, **SALT-SSYS-03**, **SALT-SSYS-04**, **SALT-SSYS-05** and **SALT-SSYS-06** can be met. It evaluated the number of visible planets for a given SNR in the worst SNR band, for a spectral resolution of 300 with 2m mirrors as in Darwin and found a sufficient number of visible planets.

SALT-SSYS-SENS-01 is trivially true for a diffraction limited telescope with the baseline (100-1000m) of SALT. The diffraction limit is given by $\frac{\lambda}{b} = \frac{10E-6}{1000} = 1e-8 [rad] = 2.06 [mas]$. This does assume a diffraction limited telescope, but the systems SALT is based on (VLT and DARWIN) are both diffraction limited, so this level of performance is achievable [30]⁵.

SALT-SSYS-SENS-09 cannot be verified at this stage as it is strongly dependent on sensor selection. All readout electronics and other optical electronics will be design with appropriate HiRel electronics, but further research into the effect of strikes on the detector is required.

SALT-SSYS-SENS-10 is satisfied by environmentally sealing all the optical assemblies. The one optical component that cannot be sealed is the telescope, with its primary and secondary mirrors. A description of lunar dust and strategies to dust proof the system are presented in Section 15.5. If irreversible damage is caused, the damaged segment can be replaced during maintenance missions. The accuracy of the alignment of the replaced segment will be calibrated by the wavefront edge sensors and actuators.

SALT-SSYS-SENS-11 was verified by checking the lowest intensity planet marked as visible by the model. The number of photons per second in the lowest energy band was multiplied by the photon energy of that band. This gave a planet detected at an incident power $4.55E-23 [W/m^2]$.

SALT-SSYS-SENS-12, **SALT-SSYS-SENS-13** and **SALT-SSYS-SENS-12** were verified by comparing performance of the selected delay line architecture with the Darwin mission bread board, which provided the required stability and range. In conjunction with the delay rovers, this will satisfy all OPD correction needs.

⁵ESO: MIDI Overview, URL=<https://www.eso.org/sci/facilities/paranal/decommissioned/midi/overview.html>

10. Pointing System Design

The systems performing the pointing of the telescope are discussed in this section. The design and results of the pointing determination system are presented in Section 10.1. This is followed up with a discussion of the architecture allowing for the large range of motion, in Section 10.2. The fine pointing that accompanies it is found under Section 10.3. The models used to select these design solutions are verified and validated in Section 10.5. The chapter is brought to a close with a compliance check. The design of these systems all depend on a handful of requirements, these are listed in Table 10.1 below.

Table 10.1: Pointing system relevant requirements

Code	Requirement
SALT-SSYS-MECH-08	Lunar dust shall not permanently damage mechanisms.
SALT-SSYS-MECH-14	The telescope shall have a pointing accuracy of 0.5 [<i>arcsec</i>] or less.
SALT-SSYS-mech-15	The telescope shall be able to point within an angle of 60 [<i>deg</i>] from the local surface normal vector.

The purpose of **SALT-SSYS-MECH-14** is to keep the image stable enough for interferometry to be performed on it; the subsystem that ensures this stability is the fine pointing mechanism. **SALT-SSYS-MECH-15** stems from the need to be able to see as many exoplanets as possible. This requirement is limited by other departments and any larger angles would not add any value. The large range of motion architecture is the most affected subsystem. The last requirement, **SALT-SSYS-MECH-08**, affects all three of the subsystems being discussed.

10.1. Pointing Determination

Before the telescope is able to look at the stars, it must first know where to look. For this, a pointing determination system will be put in place to track the stars, which the system will eventually point towards using subsystems later discussed in this chapter.

Finalising requirement **SALT-SSYS-MECH-14** gave more clarity to this subsystem design and it requires a pointing accuracy of 0.5 [*arcsec*]. Getting within 0.5 [*arcsec*] is done in order to get the host star sufficiently within the field of view of the telescope so that the other subsystems can detect it and further increase the accuracy. Additional accuracy will be provided by internal adjustments further explained in Chapter 9.

All that needs to be done is to position the target within the field of view of the telescope, and any further improvements on the pointing will be done by the optics department. In the trade-off on the subsystems in Figure A.4 the most promising concepts were either star trackers or a fine guidance system; the latter, however, is a large and heavy structure that would provide a lot more performance than required. Star sensors have been chosen because they are a lot lighter and can still provide sufficient accuracy. The current level of accuracy of star trackers allows them to point within 0.5 [*arcsec*], which is sufficient to get within our field of view ¹. Although this specific star tracker is expected to have a life expectancy greater than the mission duration, any unexpected failure would result into a large delay, as well as an expensive maintenance mission. For this reason, it has been decided to equip the system with two star trackers. The current pointing accuracy is just within the field of view of the telescope, but in a few years the technology will be more evolved, and a more precise pointing determination system may be equipped [31]. An overview of the subsystem budget allocations can be found Table 10.2.

¹University of Wisconsin-Madison Space Astronomy Laboratory, *ST5000 Specifications*, URL: http://www.sal.wisc.edu/st5000/intro/st5000_final2007.pdf

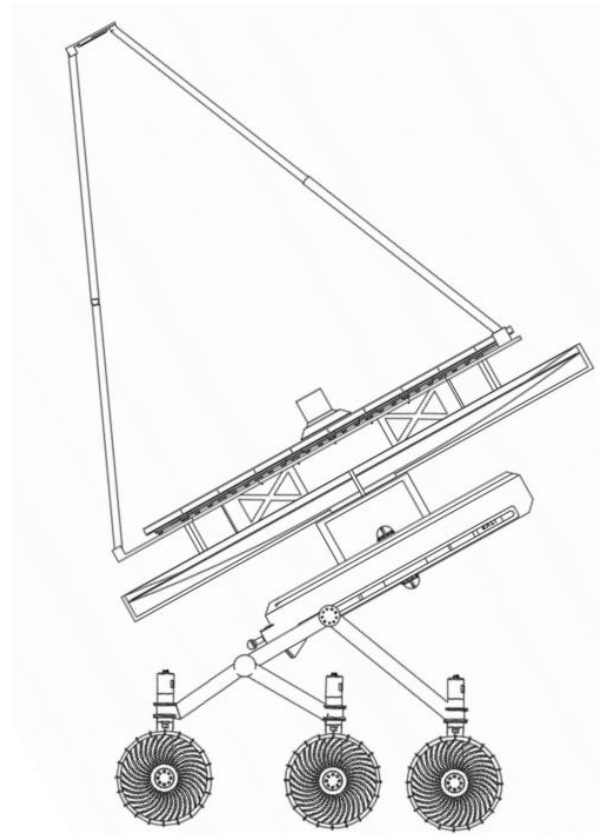
Table 10.2: Pointing determination subsystem parameters

Parameter (for one tracker)	Value	Unit
Type	ST 5000	[-]
Mass	4.08	[kg]
Pointing uncertainty	0.5	[arcsec]
Power	12	[W]
Operating temperature	253 - 313	[k]

10.2. Large Range of Motion Architecture

A system that is capable of performing large rotations needs to be present in order to have a wide field of regard. In order to be able to see a lot of targets, this range of motion is essential. An actuation system has been selected for this, as it came out most referable in a trade-off performed on the subsystem design options found in Figure A.4. Furthermore, a requirement has been set on the capability of this subsystem, more specifically it should be capable of a rotation of minimum 60 [degrees], as per **SALT-SSYS-MECH-15**.

It was made clear during the trade-off that rotating the body around the axle of the wheels is the best way. This is the case for a number of reasons. First, it requires less vertical space, because the system can both rotate and translate. Any piston or bearing system rotating the mirror would need at least a space equal to the mirror radius to rotate it, or even more due to required configurations. For such a system to work, it would require a 90 [cm] piston capable of extending at least 40 percent, considering a 2 [m] diameter mirror. Even this would only work for rotations that go a little over 70 [degrees], and even larger configurations would be required in order to go to larger angles. Taking this into consideration, the design of a rotating body has been selected. The configuration of this body is displayed in Figure 10.1 below. In it, the bus slides relative to the wheels using the slit shown on the side of the bus. The same system also rotates the bus, as well as the mirror that is mounted on top. Using these motions the system can point in the desired orientation whilst keeping its centre of gravity relatively close to the body. It is important to note that these systems will be protected from lunar dust by covers.

**Figure 10.1:** Side view of the pointing system

Apart from the overall geometry of the body, which comes from the structures department, the main variables are: the vertical clearance, translating range, and translating speed. Around these variables a model is constructed in order to find the ideal motion for the system. The focus points lie on the behaviour of the centre of gravity and that of the lowest point with respect to the ground.

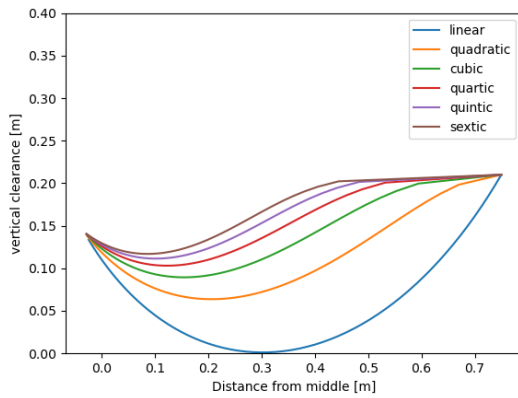


Figure 10.2: Motion of lowest point

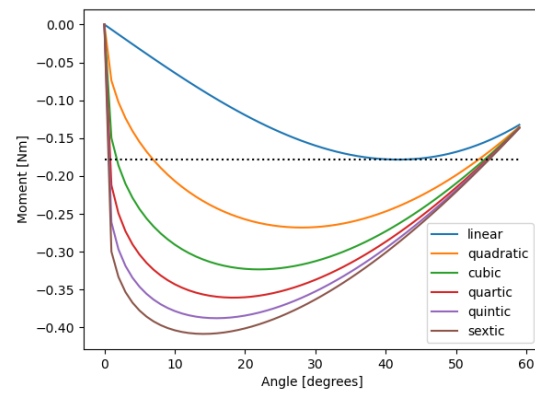


Figure 10.3: Motion of centre of gravity

Figure 10.2 depicts the motion of the lowest part of the bus with respect to the ground. This motion has been analysed for different methods of translating, where the legend refers to the ratio between the percentage it slides and every degree it rotates. As can be seen from the figure a linear motion requires most clearance, roughly $0.209 [m]$. Note that the motion starts at $0.14 [m]$, which occurs when the body is in maximum deflection. The clearance however is measured in horizontal position, which is the final value. Therefore, $0.209 [m]$ is the value that is considered. The least clearance considered is $0.067 [m]$, which is achieved by fully translating almost immediately and rotating afterwards. A penalty induced by this is a high centre of gravity shift, which can be found in Figure 10.3. The centre of gravity offset from the connecting point is depicted in this graph. This is because as the body is translated the c.g. moves accordingly, and so any method of rapid translation induces such a centre of gravity shift. Note that the offsets all end at the same point, given that at an angle of 60° the body will always be in the same position and have the same offset, regardless of the method of translation. Meaning that they all have slid all the way when fully rotated.

An optimisation problem is introduced by Figures 10.2 and 10.3, requiring a small trade-off. This trade-off is between the required clearance of the body and the moment induced by the system. Since there is already redundancy present on the vertical clearance and the induced moment is to be minimised a linear sliding method is preferred. The dotted line in Figure 10.3 indicates the maximum induced c.g. offset.

A vertical clearance of $0.209 [m]$ was found together with a maximum centre of gravity offset of $0.178 [m]$. An overview of all the values used from and resulting off this trade off is given below.

Table 10.3: Model parameters

Inputs	Value	Unit	Outputs	Value	Unit
Rover bus length	1.3	[m]	Surface roughness	0.4	[m]
Rover Bus height	0.25	[m]	Max C.G. offset from connection point	0.178	[m]
Slot width	1.2	[m]	Required pointing clearance	0.209	[m]
C.G. height middle of bus	0.2	[m]	Required total clearance	0.609	[m]
Rover mass (bus and mirror)	1110.8	[kg]	Maximum induced moment on the rocker bogie	198	[N m]

An actuation system needs to be present in order to perform these types of rotations and translations. As the rotation is not linear, a separated system from the translation system has been decided on. A linear motion actuator will be used for the translation: more specifically, one translating over a screw thread. This is done to avoid using a motor to translate along the length of the body, which would require room all along the side of the system, inside the bus. The rotating system will require a lot of torque, roughly $198 [Nm]$ as can be seen from Table 10.3. This will be dealt with by an engine on either side,

thus needing half that torque as a minimum. A planetary gearbox motor will be used for this, placed in the rocker bogie system. An overview of the system characteristics is given below.

Table 10.4: Required motors for the architecture¹²³.

Translating system	Value	Unit	Rotating system	Value	Unit
Peak power	400	[W]	Peak power	720	[W]
Average power	4	[W]	Average power	7.2	[W]
Mass (2 systems)	14.86	[kg]	Mass (2 motors)	20	[kg]
Slot dimensions (w x l)	40 x 1400	[mm]	Motor dimensions (w x h x l)	105 x 105 x 210	[mm]
Motor dimensions (w x h x l)	60 x 105.2 x 79.5	[mm]			

These values have been deduced from already existing machinery, and could potentially be optimised in a later phase of the design. Both systems are assumed to be operative only 1 percent of the time, hence the average power is 100 times lower than the peak power of the system.

10.3. Fine Pointing Mechanism

A final pointing system is required once the rough attitude has been set by the aforementioned architecture. A pointing accuracy of 0.5 [arcsec] is required to be reached by this system, as per requirement **SALT-SSYS-MECH-14**. The use of a compliant mechanism has been decided to be the best option when trading off the concepts in Figure A.4. It came out most preferable for its lightweight, accuracy and use of only a single part.

Compliant mechanisms are a group of mechanisms that depend upon the elastic body deformation of the component. Having a high precision as well as requiring only a handful of parts are the largest benefits of using such a mechanism. The most common type are the pseudo-rigid bodies, that partially consist of rigid members as well as flexible members. Flexible members allow for the most rotational freedom; this type of compliant mechanism is also the one taken into consideration in this subsystem for the sake of being widely researched and having a high TRL. More specifically a design that is already widely researched for its application is the space industry [32]. The type that is considered can be seen in Figure 10.4. A model is built analysing the kinematics of this structure in a simplified way in order to make sure that this system works as desired.

¹Siboni PGB, *Planetary Gearboxes*, URL: <https://f.hubspotusercontent00.net/hubfs/7023002/CATALOGHI/NUOVI%20CATALOGHI%202020/Siboni%20PGB%20catalogo%202020.pdf?hsCtaTracking=ee78eeca-9eb2-4216-8395-20db7ac48f87%7Ccd17dc90-0835-473f-b2c3-fa7f3aee5ee6>

²Tolomatic, *Screw driven actuators*, URL: <https://www.tolomatic.com/products/product-details/mxe-p-screw-driven-actuators>

³RS online, *Servo motor*, URL: <https://docs.rs-online.com/a6fc/0900766b815ad6fe.pdf>

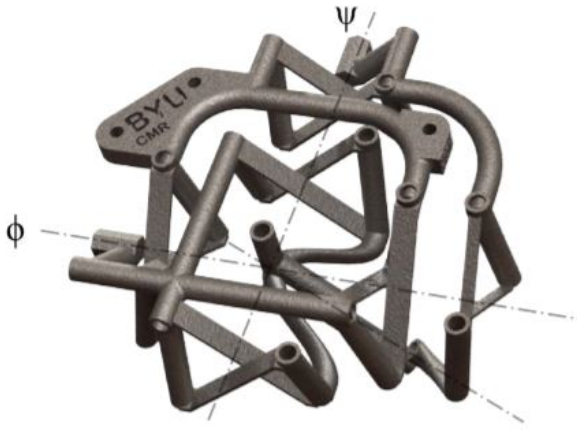


Figure 10.4: Selected compliant mechanism [32]

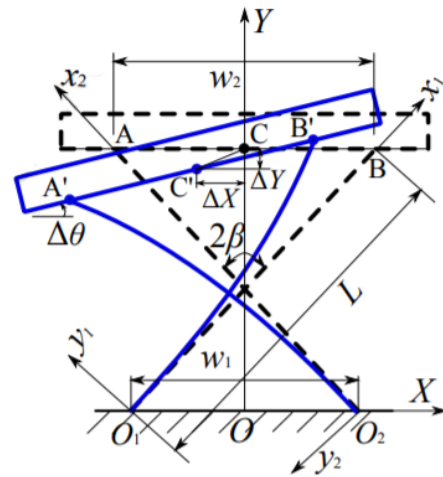


Figure 10.5: Geometry of a CAFD[33]

A torque motor is attached to both of the two free ends. A deflection is then created by applying a certain amount of torque to those ends, which results in the free tip in the middle rotating over two axes. Two types of flexible joints are largely responsible for this deflection, CAFD (cross-axis flexural pivot) and a STF (split-tube flexture). In six different locations the CAFD is placed, which is the most flexible joint of the two. Only one STF joint is present in this design. A translation as well as a rotation is induced by applying force on the CAFD, as can be seen in Figure 10.5.

For the purpose of modelling the displacement of this joint the following set of equations is used [33]:

$$\begin{bmatrix} \Delta X \\ \Delta Y \end{bmatrix} = \frac{1}{2} \begin{bmatrix} \cos(\beta) & \sin(\beta) \\ -\sin(\beta) & \cos(\beta) \end{bmatrix} \begin{bmatrix} -(Y_a + Y_b) & Y_a - Y_b \\ -(X_a - X_b) & X_a + X_b \end{bmatrix} \quad (10.1)$$

$$\begin{bmatrix} \sin(\beta) & -\cos(\beta) \\ \cos(\beta) & \sin(\beta) \end{bmatrix} \begin{bmatrix} X_b \\ Y_b \end{bmatrix} = \begin{bmatrix} -\sin(\beta) & -\cos(\beta) \\ \cos(\beta) & -\sin(\beta) \end{bmatrix} \begin{bmatrix} X_a \\ Y_a \end{bmatrix} + \begin{bmatrix} w_1 + w_2 \cos(\Delta\theta) \\ w_2 \sin(\Delta\theta) \end{bmatrix} \quad (10.2)$$

$$M = m_1 + m_2 + w_2 \begin{bmatrix} -\sin(\Delta\theta) & \cos(\Delta\theta) \end{bmatrix} \begin{bmatrix} \sin(\beta) & \cos(\beta) \\ -\cos(\beta) & \sin(\beta) \end{bmatrix} \begin{bmatrix} p_2 \\ f_2 \end{bmatrix} + \frac{1}{2} w_2 \begin{bmatrix} \sin(\Delta\theta) & -\cos(\Delta\theta) \end{bmatrix} \begin{bmatrix} F_x \\ F_y \end{bmatrix} \quad (10.3)$$

$$\begin{bmatrix} F_x \\ F_y \end{bmatrix} = \begin{bmatrix} -\sin(\beta) & \cos(\beta) \\ -\cos(\beta) & -\sin(\beta) \end{bmatrix} \begin{bmatrix} p_1 \\ f_1 \end{bmatrix} + \begin{bmatrix} \sin(\beta) & \cos(\beta) \\ -\cos(\beta) & \sin(\beta) \end{bmatrix} \begin{bmatrix} p_2 \\ f_2 \end{bmatrix} \quad (10.4)$$

The behaviour of the CAFD can be modelled using Equations (10.1) to (10.4). Very little research has been done on the STF joint, and for that reason a predetermined stiffness of 11.65 [Nm/rad] is for now considered [32].

A model was constructed using these joints as well as some connecting members in the same geometry as Figure 10.4. The connecting members were assumed to be rigid for the sake of simplicity, given that the validity can be checked by an existing model. As a last assumption, only rotations are considered and translation is neglected; this is done for the sake of keeping the model simple. As will be discussed in Section 10.5 the model corresponds to previous research, and can therefore be extended to fit our own case.

Since the process is already an iterative one, a few parameters are set from the start to keep the procedure within reasonable time. The material is first selected based on previous research on this

requirement to check, and realistically the risk can only be mitigated. For the fine positioning system this is mainly done by using a single component mechanism, meaning no dust can be trapped in any hinge or joint. Furthermore, all engine connecting points are shielded from dust by any covers. The same goes for those of the large range of motion architecture. For this reason, no permanent damage is expected and the requirement is also met.

10.5.1. Large Range of Motion Architecture

For the design of the large range of motion architecture a simple model was constructed, as is discussed in Section 10.2. For verification the model can be split up in units and the separate parts can be tested. The units considered in this case are: body geometry, body motion, body clearance and slide motion. Since the model is not very complicated, most units can also be tested by some quick hand calculations. Both methods showed no discrepancies and the model can therefore be assumed verified.

Lastly, there is the task of validating the system. Given that not a single assumptions has been made whilst constructing this model, validating the model is not of extreme importance. The model is a geometric representation of a moving block, such that very little surprises could occur. If desired, the model could be validated by building a small scale test, but for the current design phase this is not yet needed.

10.5.2. Fine Pointing Mechanism

Similar to the large range of motion architecture a model was constructed for the design of the compliant mechanism. First up there is the task of performing verification, which is largely done by performing unit tests on the system. Part of the code is isolated and tested separately in order to check its functioning. The large groups that have been tested are: motor model, CAFD joint model, STF model, geometric mechanism model. All units were tested with both common and uncommon inputs to see their reactions and all systems performed nominal in this. As a last part, some of the simpler parts were recalculated by hand, such as part of the geometry, given that some small discrepancies in trigonometry were detected. These have been resolved and after recalculation the system was determined to be verified.

The model is now to be validated, as the verification procedure is done. Since the model is based on an existing system which is tested in real life, validation can be done by comparing it to this test. The results of this can be found in the figure below.

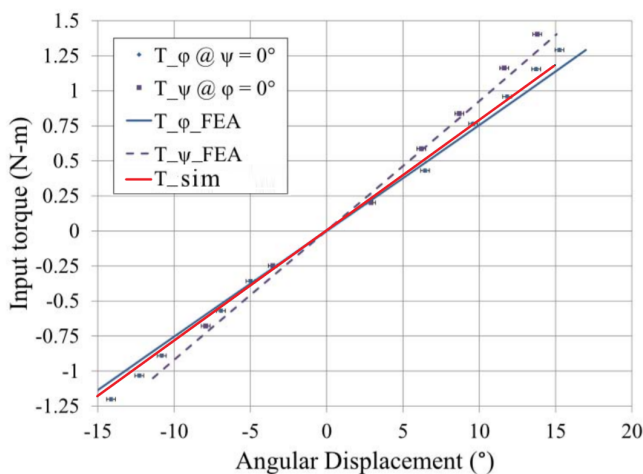


Figure 10.6: Modelled stiffness of the compliant mechanism.

The model constructed coincides with the data from both a finite element analysis and a real life test. The final element analysis is split up in two angles induced by either torque motor, labelled as T_{ϕ_FEA} and T_{ψ_FEA} in the Figure. A similar approach as taken for the real life test which takes the labels T_{ϕ} and T_{ψ} . This shows that the assumptions made on rigidity and deformations are valid and do not affect the model by a lot. Note that the figure also displays two lines of a finite element analysis; although these are not directly useful, they do provide assurance that the model is well-built. Now that both verification and validation have been performed, the model can be expanded towards the case of the SALT mission, and be applied as is done in Section 10.3.

11. Thermal Control System Design

The thermal control system maintains the optical elements of the telescope at temperatures of 40 [K] and 10 [K], and keeps all other subsystems in their desired temperature ranges. A design process was followed to establish possible components, which were then traded-off. These could then be combined to form the total thermal system. After that, possible configurations were tested in a Simulink model that simulated the temperature of the rover, mirrors and combiner individually. The simulation time was set to a full Moon-day, or 28 terrestrial days. The output of the model was a time series of the power imbalance [W] of each system, which need to be cancelled out through thermal control. This then gives an estimation on how many heating and cooling components are required and what their sizes are. The requirements that correspond to the thermal control system have been given in Table 11.1.

Table 11.1: Requirements of the thermal control system.

Requirement Code	Requirement
SALT-SYS-03	The system shall survive the thermal environment of the Moon.
SALT-SSYS-THM-01	All optical elements at the collectors shall have a temperature of no more than 40 [K] during observations.
SALT-SSYS-THM-02	All optical elements at the beam combiner shall have a temperature of no more than 40 [K] during observations.
SALT-SSYS-THM-03	The detector at the beam combiner shall have a temperature of no more than 10 [K] during observations.

This chapter presents how the thermal concepts were defined, how Simulink models are set up and how they are used to size the thermal subsystem. First, the design options and trade-off are given in Section 11.1. Second, the rover and mirror design process and results are presented in Section 11.2. Then, Section 11.3 explains the design process for the combiner, followed by the combiner bus design in Section 11.4. Finally, a verification and validation performed on the models is provided in Section 11.5.

11.1. Thermal Control Options

In Figure A.4, the two design option trees that correspond to thermal control are given. These are the design option trees for the heating and cooling subsystems, and they contain all possible instruments for thermal control. A trade-off was performed to define the usefulness of each instrument. Unlike other subsystems, the thermal subsystem required multiple trade-offs for each main payload system. This is because the thermal requirements vary per subsystem, which are given in Table 11.1.

The thermal system is split up into four systems: the rover and its subsystems, the mirror above the rover, the combiner optical elements and the combiner bus. The combiner bus is placed in a separate system away from the optical instruments in order to keep the radiative and conduction heating as low as possible. The rover has a lot of elements that need to be kept at a minimum of 258 [K] because of electrical components, and is therefore its own system. The mirror needs to be kept at 40 [K] and its cooling will be done by the rover's thermal subsystem. The following sections will detail the components that were selected for the thermal control systems and how well they performed in a Simulink model that represented the telescope on the Moon's surface.

11.2. Rover and Mirror Design

A Simulink model was created that took into account the connection between the radiative, conductive and internal energy present in the rover, mirror and Moon. A simple thermostat maintained the temperature of the systems, which were at 40 [K] for the mirror and 258 [K] for the rover subsystems. This 40 [K] followed from requirement *SALT-SSYS-THM-01*, while 258 [K] is to make sure electrical

components do not fail [35].

From early simulations it became clear that the system could not maintain equilibrium and that a large cooler and a gargantuan amount of power were required. The properties of the simulation elements were changed and new elements were added over the course of several design iterations. The final configuration of the rover and mirror system consists of the following elements:

- The rover is assumed to be a box encapsulated in Multi-Layer Insulation. The emissivity coefficient of this layer can be optimized for the system, which in turn determines the absorptivity coefficient, since they are equal for radiating in the IR spectrum [35]. The density of this layer is estimated to be $1.5 [kg/m^2]$ [36]. Heat conduction from the rover's wheels towards the Moon is small enough to be neglected.
- The mirror is assumed to be a circular plane of glass that is suspended above the rover through a metal structure. This structure enables the possibility of heat conduction from the warmer rover.
- The Moon is radiating heat at a varying temperature, which is represented by an average of $60 [K]$ and an amplitude of $25 [K]$, see Section 6.1.
- A Stirling type cryogenic cooler will keep the mirror's temperature below $40 [K]$. The hot side of this unit has been lowered to $80 [K]$ in order to increase the coefficient of performance (COP) to 0.11 [37] [38]. The mass will be calculated through a formula given in [37], which relates the mass to the temperature of the cold side and the required cooling power, Q_c .

$$Cryocooler\ Mass = 157 \exp(-0.0533 T_{cold}) \cdot Q_c^{(0.009 \cdot T_{cold} + 0.1275)} \quad (11.1)$$

- An $1 [cm]$ layer of Aerogel was added near the joints of the support structure and the rover body. Aerogel has a thermal conductivity of $0.004 [W/m/K]$ in vacuum, which is 3500 times lower than steel.¹ The heat conduction towards the mirror therefore decreases significantly.
- A heatshield with an effectiveness of 98% was installed between the rover and mirror to limit the radiative heating. Such values have been proven to be reachable in space engineering, with the JWST having a heatshield effectiveness of over 99.8%.² This value is reached with five heatshield layers, of which the first layer already blocks 90% of the radiation.
- A radiator can be installed onto the rover to get rid of left-over heat. This radiator has a specific power of $300 [W/m^2]$ and a specific weight of $10 [kg/m^2]$ [39].
- Patch heaters can be installed to provide additional heat when temperatures are getting too low for the rover.

Table 11.2: Simulink parameters corresponding to the rover.

Parameter	Value	Unit
Length	1.30	[m]
Width	1.50	[m]
Height	0.25	[m]
MLI emissivity	0.03	[-]
Dissipated power	80.24	[W]
Conductivity coefficient steel	14	$[W/(K \cdot m)]$
Support structure length	0.50	[m]
Support structure area	0.012	$[m^2]$

Table 11.3: Simulink parameters corresponding to the mirror.

Parameter	Value	Unit
Diameter	2.00	[m]
Emissivity front	0.03	[-]
Emissivity back	0.745	[-]
Heatshield effectiveness	0.98	[-]
Conductivity coefficient Aerogel	0.004	$[W/(K \cdot m)]$
Aerogel pathlength	0.010	[m]
Cryocooler COP	0.11	[-]

¹Thermtest Instruments, *Thermal Conductivity of Aerogel*, URL: <https://thermtest.com/applications/aerogel-thermal-conductivity-hfm>

²NASA - James Webb Space Telescope, *The Sunshield Webb/NASA*, URL: <https://jwst.nasa.gov/content/observatory/sunshield.html>

Table 11.2 and Table 11.3 show the parameters that were used in the Simulink models. With these values in place, it was shown that the mirror required an additional cooling of 1.43 [W], which needs to be done by the cryocooler. Meanwhile, the rover requires cooling of 39.34 [W] to maintain temperature. The COP of 0.11 makes the input heat for cooling 12.98 [W], and part of this power is used to heat the rover. An extremely small radiator is required to get rid to the remaining heat, which is 52.32 [W]. The total mass of the thermal system has been given in Table 11.4. Figure 11.1 shows the heat flow diagram of the rover, which helps in visualising the workings of the thermal subsystem.

Table 11.4: Mass of the rover's thermal control system.

Component	Mass [kg]
Multi-Layer Insulation	7.95
Heatshield	50
Cryocooler	22.15
Radiator	1.79
Total	81.89

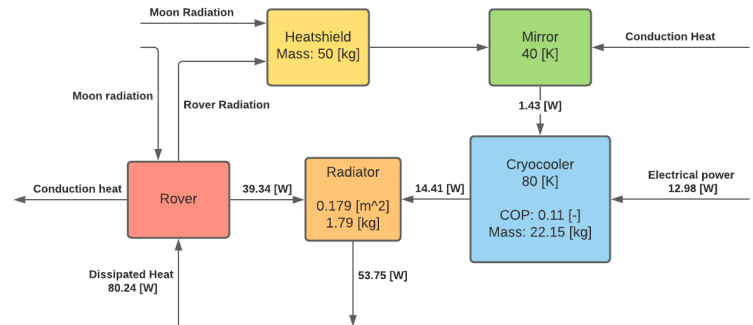


Figure 11.1: Heat flow diagram of the rover.

11.3. Combiner Optical Elements Design

Like the rover and mirror, a Simulink model was developed to give an indication on how much cooling and heating is required for the combiner. The combiner features optical instruments that need to be kept 10 [K] or 40 [K], as given in Table 11.1. During the trade-off it was decided to use stored cryogenics to cool the combiner, but early simulations showed that this would require excessive amounts of liquid helium. Thus, this option was discarded. The thermal system of the combiner will utilise many elements that are being used in the rover. However, with the lessons learnt during the thermal design of the rover and mirror, a slightly different approach was taken for the combiner:

- The combiner is assumed to be a cylinder that is positioned on the Moon with a support structure. Multi-Layer Insulation surrounds the structure and it has similar values for density as for the rover.
- Having all electrical components close to the detector would expose the detector to too much radiative heat. Therefore, the combiner-bus will be placed away from the detector and optical elements and will be discussed in Section 11.4.
- A heatshield was added between the combiner and the Moon to limit the incoming radiative heat. This heatshield has an effectiveness of 95%, which is lower compared to the rover's heatshield. The reason for this is that the Moon is the largest radiative heat source for the combiner and its maximum temperature is far below the rover's temperature. This also had the effect that its mass could be reduced slightly [40].
- A 2 [cm] layer of Aerogel was added to the joints of the support structure, lowering the conductive heat between the Moon and the combiner.
- It was decided to design a 2-stage cryocooler that would cool from 40 [K] to 10 [K] in the first stage and subsequently from 80 [K] to 40 [K] in the second stage. Cooling the detector to 10 [K] with a cryocooler hot side of 80 [K] would be too inefficient and caused an enormous increase in power consumption. The COP of the cryocoolers are 0.005 and 0.11 respectively.

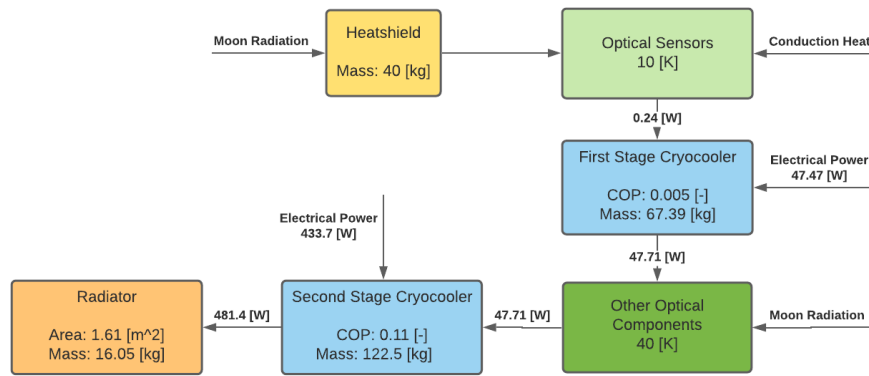


Figure 11.2: Heat diagram of the combiner.

Table 11.5: Simulink parameters corresponding to the combiner.

Parameter	Value	Unit
Diameter	1.50	[m]
Height	1.00	[m]
MLI emissivity	0.03	[-]
Dissipated power	0.03	[W]
Aerogel pathlength	0.020	[m]
Heatshield effectiveness	0.95	[-]
First stage COP	0.005	[-]
Second stage COP	0.11	[-]

Table 11.6: Mass of the combiner's thermal control system.

Component	Mass [kg]
Multi-Layer Insulation	12.37
Heatshield	40.0
Cryocooler 1st stage	67.39
Cryocooler 2nd stage	122.5
Radiator	16.05
Total	258.3

The parameters used to describe the combiner are presented in Table 11.5. For the support structure similar values were used as on the rover. These elements were able to keep the required cooling power very low at 0.24 [W]. However, the low COP value for the first stage caused the input power to be 47.47 [W]. These two powers combined need to be cooled down for by the second stage cryocooler, which operates at 80 [K]. The second stage power is 433.7 [W], which brings the total power to be removed through radiators on 481.4 [W]. With an power density of 300 [W/m²] the radiator panel area is then estimated to be 1.61 [m²]. The total input power for the thermal system of the combiner is then 481.2 [W]. The mass of the individual elements and total mass of the system are presented in Table 11.6 and also follow Equation 11.1. Similarly to the rover, a heat flow diagram for the combiner is given in Figure 11.2.

11.4. Combiner Bus Design

The combiner bus will contain the batteries that are used during peak power moments, power control units, communication equipment and computers. It was approximated as a box that has to be maintained at 258 [K], just as the rovers' electronics. To reduce the amount of radiated heat, the top of the box will be covered with a 5 [mm] layer of lunar regolith. There will be small fringes at the edge of the box so the astronauts know when the layer thickness is achieved. The conduction to the bottom of the box was neglected, as the lunar regolith layer is on average 5 meters deep [41] with thermal conductivity of $7.4 \cdot 10^{-4}$ [W K⁻¹ m⁻¹] [42] therefore acting as a very effective insulator. One of the small sides of the box will have the connections to the combiner, charge stations and solar panels. Therefore this side was considered to have the emissivity of steel. The other sides will be covered with louvers so the emissivity can be adjusted according to the temperature. The louvers can be designed such that they passively close at low temperatures and open to reveal a high emissivity panel at high temperatures. When charging the rovers, the dissipated power of the power control unit changes. Therefore,

the charging and non-charging scenarios were both considered.

Table 11.7: Parameters corresponding to the combiner bus.

Parameter	Value	Unit
Emissivity regolith [42]	0.95	-
Emissivity louver open [43]	0.8	-
Emissivity louver closed [43]	0.1	-
Emissivity connector panel ³	0.07	-
Thermal conduction regolith [42]	$7.4 \cdot 10^{-4}$	$[W K^{-1} m^{-1}]$
Thickness layer on top	0.0050	$[m]$
Length	1.78	$[m]$
Width	0.54	$[m]$
Height	0.21	$[m]$
Usual dissipated power	80.9	$[W]$
Charging dissipated power	132.8	$[W]$

Table 11.8: Results of combiner power control simulation.

Scenario	Heat difference $[W]$
Louvers closed normal	-27.71
Louvers open normal	174.93
Louvers closed charging	-93.05
Louvers open charging	109.59

Using the values in Table 11.7, a Python script was made that calculates the heat balance in the bus, using as a convention that heat going out is positive. If the heat balance is negative, the bus will heat up; if it is positive it will cool down. Since in the coldest condition the heat balance is negative and in the warmest condition the heat balance is positive; the louvers can control the temperature of the bus completely passive as can be seen in Table 11.8, as they open automatically when the temperature has risen to 290 $[K]$. In conclusion, no active heaters or coolers are necessary.

11.5. Verification and Validation

An Excel sheet was created in order to check the Simulink models for verification. The Excel sheet is essentially a less complex thermal model that only uses general formulas and is time-independent. It served as a check to confirm that the magnitude of the Simulink results is reasonable and within expectations. Complex interactions between multiple bodies were simplified and the Moon flux was put in as a non-variable number. This sheet was used throughout the development of the Simulink models and has helped in finding errors from the system, thereby verifying the Simulink models.

The outputs of the Simulink models were compared values of existing space missions. This is to check that no values for the mass or power consumption of the subsystem are unexpected outliers and are in-line with current thermal subsystems. This validation check was performed on the mass and size of the radiator, mass of the cryocoolers and power consumption of the systems.

In addition to that, the design was checked for compliance with the requirements mentioned in Table 11.1. SALT-SYS-03 demands the telescope to survive the thermal environment of the Moon and this has been achieved by sizing the thermal subsystem for keeping the other subsystems at 258 $[K]$. This is derived from the lowest operational temperatures of the batteries, which is 253 $[K]$. Thus, a safety margin of 5 $[K]$ has been added. The other requirements were also met by sizing the cryocoolers and radiators for the 40 $[K]$ and 10 $[K]$ temperature limits of the optical elements.

As a final note, the mass and sizes of thermal control components mentioned in this chapter are not the final values. These values presented here are based on maximum required power that followed from the power budget, and additional safety margins have been applied to for instance the temperature requirement of the batteries. Furthermore, because the telescope is accessible to astronauts, future additions to the system can be installed after launch. Therefore, in future stages of the design, the thermal control system will be updated to accommodate for the installation of extra instruments, which may also require cooling and heating.

12. Power System Design

Due to the restriction on nuclear energy, the design option space for the power system is limited to solar panels, which must be placed at the crater rim in order to receive sunlight. The crater rim panels will be connected to the combiner by cables, which will require a higher voltage to reduce losses, which in turn means that the system will require boost and buck converters. The rovers have batteries that can maintain them operational for 30 hours, such that even the longest measurements can be performed. The combiner will be powered directly by the solar panels, but will also have batteries to provide extra power during peak power moments. All the subsystem requirements can be found in Table 12.1, a complete overview of the power subsystem is presented in Section 16.4. The rover power system design is explained in Section 12.1, and the electrical architecture of the charging stations is presented in Section 12.2. The combiner power storage and consumption are explained in Section 12.5; this is followed by the transmission line in Section 12.4, and the solar arrays in Section 12.5. The models are verified and validated in Section 12.6. Finally, some extra remarks on the extensibility of the system and alternatives for the power subsystem are appended in Section 12.7.

Table 12.1: Requirements of the Power subsystem

Requirement Code	Description
SALT-SSYS-POW-01	The telescope shall use a renewable energy source.
SALT-SSYS-POW-02	The telescope shall not use nuclear power.
SALT-SSYS-POW-04	The power system shall be protected against solar flares up to a magnitude X1.
SALT-SSYS-POW-10	The power storage system shall support the power system under peak load.
SALT-SSYS-POW-11	The power storage system shall be capable of storing energy to support the equipment for one operational cycle.
SALT-SSYS-POW-12	The power subsystem shall be able to recharge during one operational cycle or less.

12.1. Rover

The rovers are designed to carry enough batteries to store sufficient energy for one operational cycle, as required by **SALT-SSYS-POW-11**. The batteries are selected according to their low-temperature performance, given that the higher the operational temperature of the batteries, the more power is required to keep them cool. The sizing of the rover batteries is further elaborated on in this chapter.

12.1.1. Required power

Table 12.2 shows the average power for each subsystem, which had to be determined before the batteries could be adequately sized. The average power accounts for peak power moments: for instance, the actuators have a peak power of 1200 [W], but since they do not operate constantly, the average is only 20.20 [w]. The power of the wheels calculated in Section 15.4 is divided by a typical electric engine efficiency of 85% [44]. The power distribution system loss is calculated to be 10% of the power used [35], and its mass is 0.07 [kg/W] [45] — given the power, the total mass is then 15.7 [kg] per rover. For all subsystems with power ranging from 0 to 500 [W] a contingency of 75% was added in the conceptual design phase, as is recommended by the AIAA.[45]. The layout of the rover power system is presented in Figure 12.1.

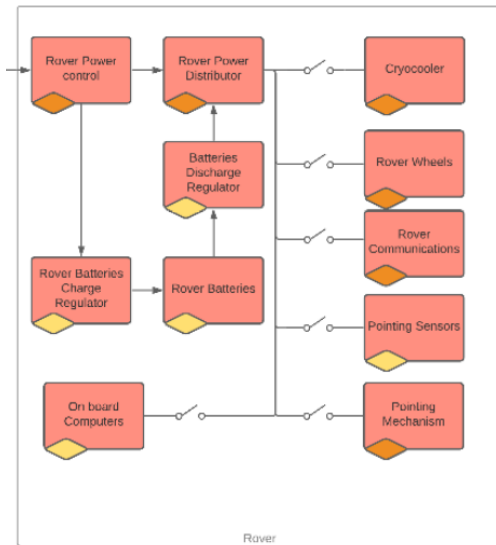


Figure 12.1: Snippet of the rover part of the electrical block diagram.

12.1.2. Battery sizing

Lithium-based batteries are employed in the rovers, given that they perform better than other battery types in terms of specific energy, despite their capacity loss at low temperatures, as Table 12.3 shows. It may be that future design iterations have access to all-solid-state lithium batteries, but these were not considered in this study, given that operating them at low temperatures can be a challenge. [46].

Table 12.3: Comparison between battery types, with their temperature ranges and specific energy.

Battery type	Temperature range [K]	Specific energy at 253[K] [Wh/kg]
Nickel-Hydrogen [47]	253 to 298	74
Nickel-Cadmium [48]	243 to 333	42
Lithium based	253 to 313	94

Data corresponding to a lithium-based battery from EaglePicher¹ is used to calculate the performance of the batteries. The batteries are designed to survive for 15 years, such that the rovers can continue to operate if the mission is extended.

Table 12.4: Values used for the calculation of the battery size.

Specification	Value	Unit
Operational time	30	hour
Maximum return time	1.4	hour
Life cycles (15 years)	3458	-
Depth of discharge(15 years)	0.8	-
Efficiency discharge and distribution	0.9	-
Charge efficiency	0.95	-

Table 12.2: Required average power per rover subsystem.

Subsystem	Avg power [W]
Thermal control	12.98
Rover wheels	35.15
Pointing sensors	12.00
Rough and fine pointing	20.20
Positioning sensors	30.50
Computers	5.00
Communications	0.05
Power distribution loss	12.52
Total	128.39
Total with Contingency	224.69

Table 12.5: Values specific to the battery cells at 253[K].

Specification	Value	Unit
Cell voltage	3.6	V
Cell capacity	48	Ah
Cell mass	1.6	kg
Peuker constant	1.03	-

The energy required by the rover is calculated to be the average power times the operational time. A margin is added to allow the rover to return to the charging station from the furthest distance. In total, the batteries have to provide 7053 [Wh] to the system. The energy stored in the batteries is calculated by dividing the required energy by the depth-of-discharge of the batteries and the discharge efficiency,

¹Eaglepicher - URL: <https://www.eaglepicher.com/sites/default/files/LP%20333037%2060Ah%20Space%20Cell%20%20040319.pdf>

presented in Table 12.4: this results in 9796 [Wh].

Each battery will be composed of 8 cells in series, summing up to 28.8 [V], which represents the bus voltage. The required total capacity is calculated by dividing the required energy stored in the batteries by the bus voltage, resulting in 362.63 [Ah]. The battery cell used as reference (Eaglepitcher) has a capacity of 60 [Ah] at room temperature, but it drops to 80% of that at 253 [K]; in order to account for this loss, the capacity value used is 48 [Ah]. The capacity changes with the discharge rate as well; Peukert's Law Equation 12.1 is used to compensate for this change and calculate the actual capacity. In Equation 12.1 k_p represents Peukert's constant, T_d is the discharge time, and I_{actual} is calculated by dividing the average power over the bus voltage. Once the formula is implemented, the actual cell capacity is 45.77 [Ah]. The number of required batteries is then simply the required capacity divided over the cell capacity, rounded up to the nearest integer. In conclusion, each rover needs eight batteries with eight cells each, which have a total mass of 102.4 [kg] each.

$$C_{actual} = C \left(\frac{C}{I_{actual}T} \right)^{k_p-1} \quad (12.1)$$

Charging the Eaglepitcher batteries at nominal speeds takes five hours. The required power is equal to the required stored energy divided over the charging efficiency and charging time; the rover, however, has to maintain its systems active while charging, such that the average power consumption must be added to this value. This results in a charging power of $9796/0.95/5 + 224.69 = 2286.91$ [W].

12.2. Charging station

The rover is designed to drive into a charging station to recharge its batteries: this station is composed of a connector that can slide vertically in order to compensate for any deviations in height. This movement is provided by a small motor that can wind or unwind a wire to move the connector. Any lateral deviations will be compensated for by adjusting the rover, given that it is equipped with precise and accurate positioning mechanisms. There will be four charging stati

One must determine the average power that a charging station requires in order to size its batteries. The rover operates for thirty hours, and takes five hours to charge; during these five charging hours, the rover still has to consume power to keep itself operational. It is therefore that the average power of each charging station is the rover charging power multiplied by the fraction of time it operates: $5/(30 + 5)$ [Hours]. The average power of a charging station is therefore 326.72 [W]

12.3. Combiner

The combiner is directly connected to the solar panels through a transmission line; it therefore only requires batteries to compensate for the power requirements in peak moments, e.g. when the rovers are charging. The layout of the combiner is presented in Figure 12.3.

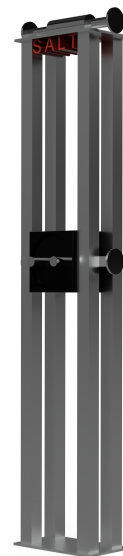


Figure 12.2: Rendering of the rover charge station.

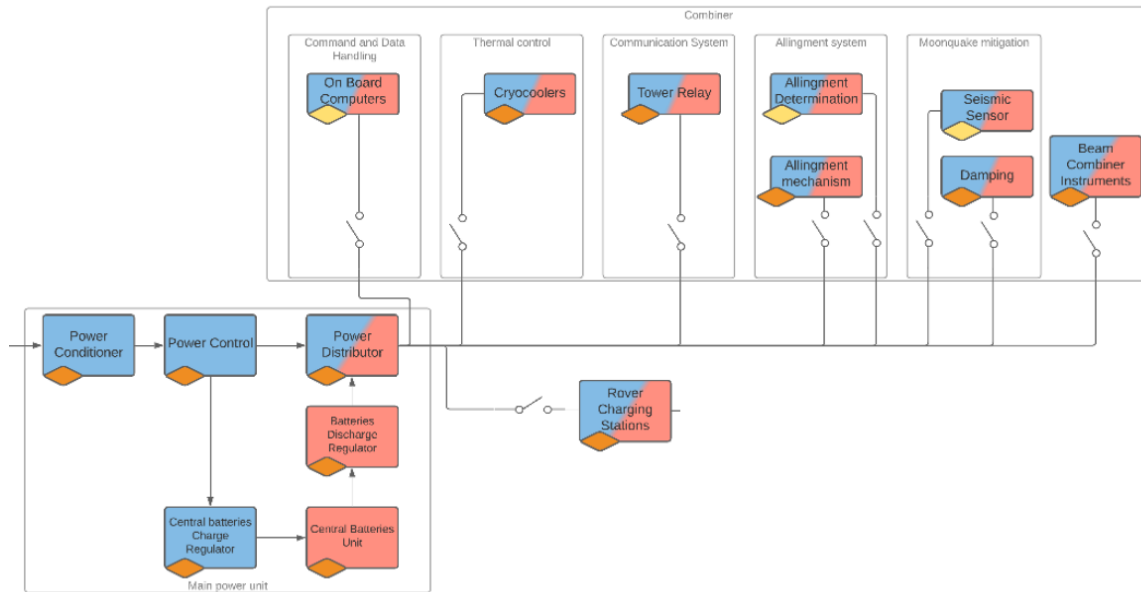


Figure 12.3: Electrical block diagram snippet of the elements under the combiner power system.

The required power by each subsystem can be seen in Table 12.6. Just as in the rover case they were derived by other subsystems, and a contingency margin was added. Since the power consumption is bigger the margin used was 60% [45], and it was not applied to the rover charging power since it has its own contingency already. The power distribution and control in the combiner is estimated to have a mass of 179.1 [kg]. [45].

Table 12.6: Required average power per element in the combiner region.

Subsystem	Avg power [W]	Max power [W]
Thermal control	481.2	481.2
Communications	15	65
Optical instruments	60	60
Alignment system	8.8	8.8
Computers	5	5
Charge Stations	1251.78	8762.44
Power distribution loss	202	1042
Total	2024.20	10424.94
Total with contingency	2558.5	11588.68

12.3.1. Batteries for Peak Power

In order to reduce the required transmission line size due to peak power levels, additional batteries are used that contain extra energy. As is shown in Table 12.6, the main contributors to peak power are the alignment subsystem and the charge stations. Storing the energy for the alignment and communications subsystems for a cycle requires 714 [Wh], and the charging station would require 45738 [Wh]. The batteries therefore need to provide 46452 [Wh] of energy; by dividing that by the depth of discharge and the discharge efficiency found in Table 12.4, the batteries need to store 60722 [Wh]. Using the same procedures as described in Section 12.1.2, the combiner shall have 48 batteries composed of 8 cells each, with a mass of 614.4 [kg].

12.4. Transmission Line

The distance from the combiner to the solar panels was estimated to be 20.5 [km]. Using a resistance of 6.4 [Ω/km] and linear density 68.5 [kg/km]², and considering that there must be two cables, one running in each direction, the total resistance of the cables is 262.4 [Ω], and the mass is 2808 [kg]. However, future iterations might make use of high temperature superconductors, due to the fact that the lunar surface may allow for it.

The transmission line connects the solar panels to the combiner, to reduce losses the voltage will be increased in this part. The required voltage was adjusted so that the losses on the cable would not surpass 10%. Therefore the average power of the combiner was divided by a typical efficiency of a DC to DC converter of 0.85³. Using Equation 12.2 where P_D is the power that arrives the buck converter, the resistance of the cable is R_C and the efficiency of the power line is $\eta_{PL} = 0.9$, the current through the power line is calculated. The power loss on the cable is then $P_l = I^2 R_C$, and the power provided by the solar panels will be the power loss plus P_D divided by the efficiency of the boost converter, also 0.85. Substituting in the values, the solar panels need to provide 3387 [W], while the losses on the cable and converters are 1185 [W]. To calculate the voltage, the power was divided by the current. The voltage after the boost converter needs to be 2748.7 [V] and the cables will have a voltage drop of 274.9 [V]. At the end of the power line, a buck converter will bring the voltage down to 28.8 [V], which is the voltage used in the batteries.

$$I = \sqrt{\frac{(1 - \eta_{PL})P_D}{\eta_{PL}R_C}} \quad (12.2)$$

12.5. Solar arrays

The solar arrays are placed on an elevated spot on the crater rim that always has sunlight. This light reaches the panels at very oblique angles, therefore the solar panels are rotated. This can be accomplished by using sun sensors and a rotation system, which combined can keep the incidence angle at less than 5°. Further design iterations may make use of more solar panels at different directions to remove the need of a moving mechanism.

The efficiency of solar cells changes with their temperature. Using a self-made model, one can calculate the number of cells that the solar array must have at the equilibrium temperature for a given required power. Azurespace cells are used as a reference⁴, which are assumed to operate at their maximum power point. The cells' degradation is already taken into account in the values in Table 12.7. The change in solar incidence due to the Earth's distance from the Sun was also considered. The change in incidence due to the Moon's own movement was neglected, however. The number of cells is given by Equation 12.4, where ΔT_s is the temperature difference between the actual temperature and the temperature given by the manufacturer. Using Equation 12.4 and Equation 12.3, one can numerically solve for the number of cells. The results for three different values of solar incidence are given in Table 12.8, where the efficiency is given by the electric power produced divided by the absorbed solar energy ($\alpha_s J_s A_c n(T_s) \cos(i)$).

²GORE cables - URL: https://www.gore.com/system/files/2019-10/GORE%20Space%20Cables%20-%20Catalog%2028Traditional%20Space%29_10-28-2019%20%28A4%20Electronic%29_0.pdf

³XP Power converters - URL: <https://www.xppower.com/products/high-voltage-dc-dc>

⁴Azurespace - URL: http://www.azurespace.com/images/0005979-01-01_DB_4G32C_Advanced.pdf

Table 12.7: Characteristics of Azurspaces's quadruple junction cells after 15 years of degradation in GEO.

Specification	Value	Unit
Emissivity ε_s	0.85	-
Absorptivity α_s	0.91	-
V_{mp0} at 298.15K	2.793	[V]
I_{mp0} at 298.15K	0.4238	[A]
$\frac{dI_{mp}}{dT}$	0.00007	[A/K]
$\frac{dV_{mp}}{dT}$	-0.009	[V/K]
Cell area A_c	$30.18 \cdot 10^{-4}$	[m ²]
Packing efficiency η_a	0.95	-

$$\alpha_s J_s \frac{A_c}{\eta_a} n(T_s) \cos(i) - \sigma \left(2 \frac{A_c}{\eta_a} n(T_s) \right) \varepsilon_s T_s^4 - P_{req} = 0 \quad (12.3)$$

$$n(T_s) = \frac{P_{req}}{(V_{mp0} + \Delta T_s \frac{dV_{mp}}{dT_s})(I_{mp0} + \Delta T_s \frac{dI_{mp}}{dT_s})} \quad (12.4)$$

Table 12.8: Results of the python script to size the solar panels, for three different solar incidences and an incidence angle i of 5°.

Solar incidence [W/m ²]	Number of cells	Equilibrium temperature [K]	Area [m ²]	Efficiency [-]
1321	2935	305.0	9.32	0.303
1367	2973	309.2	9.44	0.289
1412	3011	313.1	9.56	0.277

The solar cells have to be sized for the worst case scenario, which is when the solar incidence is the maximum. Therefore there should be 3011 solar cells. The array is also composed of interconnections, cabling and substrate. It is estimated that these elements will have a density of 4 [kg/m²] [45], while the moving mechanism is about 15 [kg] [45]. It is also considered that the structure that connects the panels to the ground will have a similar mass to spacecraft's panels connection to the bus, which increases the mass by 15% [45]. The total mass of the solar array is then 79.9 [kg].

12.6. Verification & Validation

The calculations and Excel spreadsheets are simple, and are therefore verified by hand calculations and unit checks. The solar cell efficiency is expected to decrease as these heat up, which was confirmed to happen.

The requirements **SALT-SSYS-POW-01** and **SALT-SSYS-POW-02** were both met by using solar panels; solar flares do not increase the decay of solar panels significantly, which in turn implies that **SALT-SSYS-POW-04** is also met. Batteries were put in place in the combiner to compensate for peak power moments, as specified in **SALT-SSYS-POW-10**. The rover's batteries were sized to maintain one full operational cycle and still have enough energy to return to their charging stations, meeting **SALT-SSYS-POW-11**. Finally, the battery charging time is smaller than an operation cycle, meeting **SALT-SSYS-POW-12**.

Validation was carried out by comparing the power requirements to those of Mars rovers, which have an average power of 110 [W] — similar to that of the SALT rovers.

Values of the operational time and battery specifications of the Hubble Space Telescope⁵ were added to the spreadsheet to validate the battery sizing calculations. The spreadsheet returned the same number of battery cells as used in Hubble when the Depth of Discharge was set to 100%, which validates the model.

The solar arrays were validated by using Hubble's required average power.⁶ The telescope employs

⁵NASA Hubble - URL: <https://www.nasa.gov/content/goddard/hubble-space-telescope-electrical-power-system>

⁶NASA Hubble solar arry - URL: http://www.esa.int/Enabling_Support/Space_Engineering_Technology/How_Hubble_got_its_wings

a solar array with an area of $18.8 [m^2]$, which is not comparable to the $5.92 [m^2]$ given by the model. However, the solar array on the telescope is from 2002, and only has an efficiency of 14%, which is half of that used for the solar cells. The solar array sizing is therefore considered validated.

12.7. Extensibility and Alternative

If **SALT-SSYS-POW-02** is dropped, nuclear power can be used instead. The rovers would then carry RTGs to provide energy. This would remove the need for solar panels at the crater rim, together with the transmission line; this in turn would reduce the total mass and installation complexity of the system. The RTG used in NASA's Perseverance rover would suffice: this reactor has a mass of $45 [kg]$ ⁷. Assuming each rover would have its own RTG, the combiner would need four similar reactors to maintain operation, but the mass of the power subsystem would be reduced to $360 [kg]$. This makes nuclear reactors worth considering in the future. The drawbacks of using RTGs would be the scarcity of plutonium and the increase in the generated heat. The excess heat generated by the RTG could be used to heat up the electronics, leading to a reduction in the necessary insulation of the rover electronics box. The scarcity of plutonium may not be an issue, given that recently the US has restarted the production as NASA plans to use it in its Moon missions.⁸

Should the mission be extended, and the number of rovers increased from four to eight, the power system would also need to be expanded. A new pack of batteries would be needed, effectively doubling the number of batteries in the combiner region. It would also require an additional solar array. Higher voltages in the transmission line would be required in order to keep the same loss levels.

⁷NASA science Mars - URL: <https://mars.nasa.gov/mars2020/spacecraft/rover/electrical-power/>

⁸NASA radioisotope power systems - URL: <https://rps.nasa.gov/about-rps/about-plutonium-238/%7D%7D>.

13. Communication System Design

This chapter will discuss the design of the communication system. The requirements for this system can be found in Table 13.1. First, the design options and trade-off for the communication system will be discussed in Section 13.1. Subsequently, a general overview of the system topology can be found in Section 13.2. This overview is followed by a data volume estimation in Section 13.3. The data volume estimation is combined with the selection of specific components and several analyses to establish link budgets in Sections 13.4 and 13.5. These link budgets show the feasibility of each link throughout the entire communications system. Finally, the design is verified and validated in Section 13.6.

Table 13.1: Requirements for the communication subsystem

Requirement code	Description
SALT-SYS-04	Communication with the lunar element and the ground station shall be establishable.
SALT-SSYS-COM-03	The system shall store commands and information in the event of a loss of communications.
SALT-SSYS-COM-04	The lunar segment shall have at least one two-way communication contact between the ground station and all mission elements per terrestrial day.

13.1. Design Options and Trade-off

Options overview

Several design options were considered to fulfil the aforementioned requirements. They can be found in the design option tree in Section A.4, and are also mentioned here:

- Existing lunar infrastructure: base station, NASA's LunaNet and/or Gateway, ESA's Moonlight
- Custom orbiter at Earth-Moon L2 point
- Single base station at Sverdrup
- Relay ground stations

From the options described above, the use of existing lunar infrastructure was eliminated. This is because the exact specifications of these facilities are unknown. It is therefore impossible to determine if these systems would fulfil the requirements for the communications subsystem. However, when the capabilities of these infrastructures becomes more clear, the use of these systems might become feasible. Should that be the case, the tools and specifications of SALT's communication design may be used to verify the fit of the existing infrastructure.

Options trade-off

The other options are traded off in Table 13.2 using the same trade-off procedure as described in Section 9.4.2. The most important criteria for this trade-off is the availability of a connection to Earth. Any communication blackouts will have a negative impact if a critical command needs to be sent to the telescope. Therefore, this criterion is deemed most important. The costs and power are the next most important parameters, since there are strict budgets that need to be adhered to. It is important to note that the mass criterion is focused on the mass that will be placed on the lunar surface. This is because the mass is an important factor for the rovers (and when landing on the Moon in general). The pieces of the system that will be placed in orbit will therefore not be taken into account when considering the mass of the different options. Finally, complexity has a relatively low weight, since this is a one of a kind mission, allowing for some complexity.

Table 13.2: Communication trade-off and the corresponding criteria.

	Availability	Complexity	Power consumption	Mass	Costs	Total
Criteria weight (%)	33.3	13.3	20	13.3	20	100
	Availability	Complexity	Power consumption	Weight	Costs	Normalised score
Custom relay orbiter L2	5	2	3	4	1	0.65
Ground relay	5	3	4	3	3	0.77
Ground station at Sverdrup	2	5	2	4	4	0.61

Both the custom orbiter and the ground relay system have an excellent score when it comes to availability. This is because both these options would have a permanent availability for a telescope-to-Earth connection. The orbiter at the Earth-Moon L2 Lagrange point would have a permanent view of both Earth and the lunar south pole, similar to the Queqiao relay satellite of China's Chang'e-4 mission ¹. This satellite would then communicate with the station on the rim of Sverdrup crater. A ground relay would consist of one ground station near the Sverdrup crater ridge, and one ground station at a location with a permanent line of sight to Earth. An example of such a location is the Malapert crater ridge. This relaying solution has also been considered by NASA [49] [50]. The last of the options, a single ground station at Sverdrup crater ridge, would provide poor availability as Earth is only visible for 50% of the time each month [51].

For the complexity criterion, the single ground station at Sverdrup crater ridge scores the best, since it requires only a single ground station. A ground relay system is more complicated as it requires the installation of a second ground station at Malapert. A custom satellite scores poorly on communication as they require the complete development of a satellite.

The power consumption criterion only focuses on the power consumption at the site of the telescope. A relay ground system scores the best as it only has to communicate with another site on the Moon. However, a second system needs to be present at that second site in order to enable communications with Earth. The custom satellite scores slightly worse, since the telescope needs enough power to communicate to a satellite in orbit. The single ground station at Sverdrup scores the worst, as it requires enough power to communicate with Earth directly.

A ground station at Sverdrup crater ridge scores the best for the costs criterion. Though the connection would only be available for two weeks each month, the ground station would have a direct to Earth (DTE) connection and would therefore only require one ground station. A ground relay system scores slightly lower in costs, since an additional ground station is required, and it needs to be installed at a separate location. The custom satellite scores poorly on costs, since it requires the development and deployment of a satellite.

Lastly, in the mass criterion the single ground station at Sverdrup and the satellite score the best, since they only require one ground station at the telescope site. The ground relay system scores slightly worse, as it requires a second ground station at another site. From this trade-off it is clear that a ground relay solution is the best option for SALT.

13.2. System Topology

This section describes the general topology and layout of the communications system. The position of the system inside and outside the Sverdrup crater can be seen in Figure 13.1. As has been mentioned before, the rovers will be situated in the crater while the power generation system will be located at the crater rim. The rovers will move around the crater and the combiner will be stationary. To ensure free movement of the rovers, it was decided to have the rovers communicate with the combiner, upon which

¹NASA, *Queqiao* - URL: <https://nssdc.gsfc.nasa.gov/nmc/spacecraft/display.action?id=QUEQIAO>

the combiner will communicate with the Sverdrup relay station. This ensures that only the combiner needs to have direct line of sight with the Sverdrup crater rim, which in turn is in the field of view of Malapert mountain. It is important to note that the crater rim is shared with the Shackleton crater, as can be seen in Figure 13.1. The Sverdrup relay station is also the location for data storage. Data will be stored here for a period of time, in case of a communication failure.

This location is easily accessible by astronauts so they can retrieve any valuable data in the unlikely case of a major communication breakdown. As can be seen in Figure 13.2, the data will be communicated from the Sverdrup crater rim to the relay station at Malapert mountain. Additionally, Figure 13.2 contains the Shackleton crater, where the astronauts from the Artemis mission program will probably be situated. The data will be buffered there until the communication window with Earth opens, after which both uplink and downlink to Earth will take place. The commands that are received from Earth will be sent back to the telescope via the Sverdrup station.

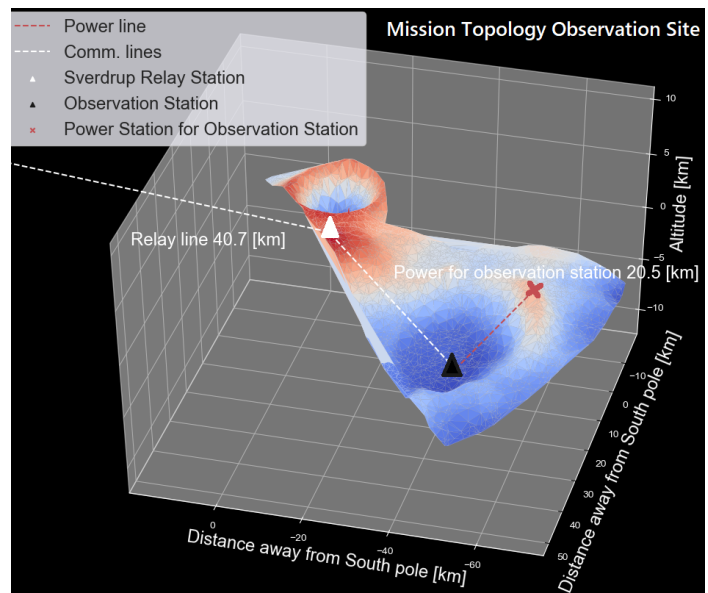


Figure 13.1: Mission topology of the rover operation site.¹

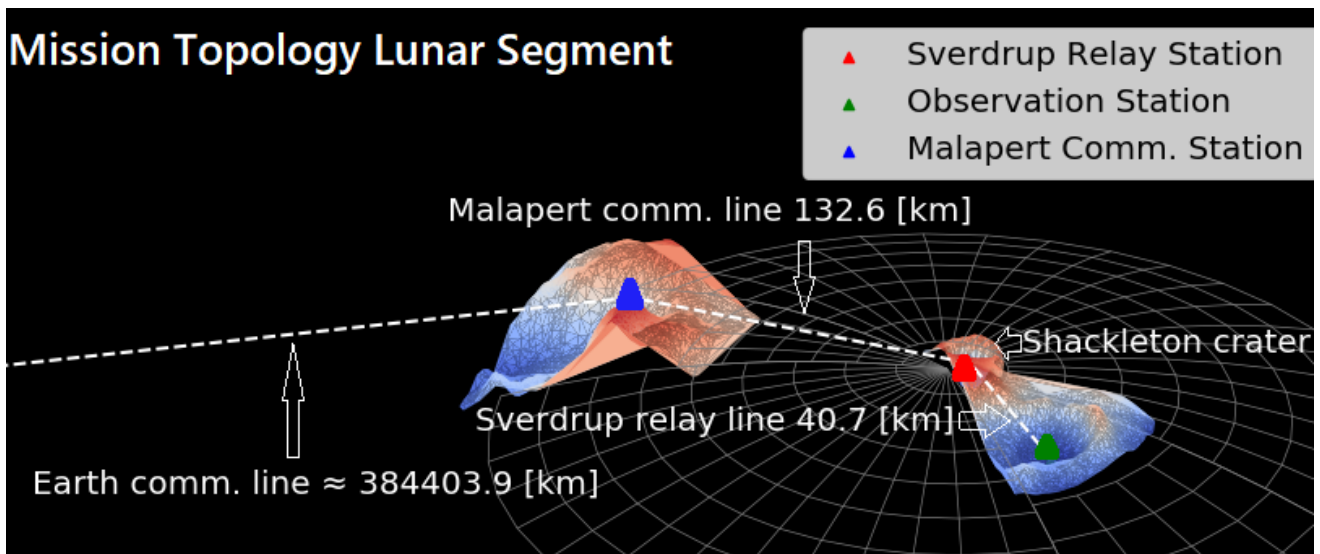


Figure 13.2: Mission topology of the main communication line.¹

13.3. Data Volumes

First, the data volume will be discussed. The determination of the data volume leads to a required data rate that can be used in a link budget. The main data sources include observational data, telemetry from a variety of sensors, point cloud data from the Lidar system, and images from other cameras on the rover. An overview of the estimated data sizes can be seen in Table 13.3 and 13.4. These data sizes are based on one 24 hour day. It is important to note that only the total bitrates are shown in the table. Telemetry is needed by the operators to ensure the health of the rover and all other mission

¹Maps generated from LOLA data: URL=[//oderest.rsl.wustl.edu/GDSWeb/GDSL0LARDR.html](http://oderest.rsl.wustl.edu/GDSWeb/GDSL0LARDR.html)

elements. Scientists also have a need for this data, since they can use it to determine exactly how the system was calibrated during the observation. The data size of the telemetry is difficult to determine without knowing the detailed design of all components. For this stage of the design, it is estimated to be 1 [Mb] for each individual system element.

Operators on Earth can employ navigational data from the Lidar for simulation and control, or for emergency procedures — the rover getting stuck, for example. The estimated data rate of the Lidar has been derived from its point rate in combination its point size of 12 [bits] [52] and 60 seconds of footage transmitted per Earth day. The images from the cameras can be used to monitor the physical state of the rover. The image size is based on Perseverance’s Hazcams and assumes 10 images per 24 hours [53]. A PNG compression reduces the data by a factor of 2.7 [54].

Out of all the data that the system generates, the observation data is the most important one. As has been described in Chapter 9, the exact design of the detector is outside the scope of this report. A 2048x2048 sensor with a 16-bit pixel-depth[55] has been used in lieu of more detailed information. The estimation assumes 10 frames of observation data sent back to Earth every 24 hours; this means that some onboard processing is needed to create 10 frames out of all the data gathered during the integration time (however, the exact description of this processing is outside the scope of the report). It is important to note that this number of frames depends on the circumstances of the observation. For example, more observation data could be sent if Lidar data and images from the rover are not needed.

The only data source for the uplink to the system are commands. Commands consist of data such as required position, movement and integration time. It is difficult to estimate the exact size of the commands. For this stage of the design, it is assumed to be 1 Mbit.

The communication windows were chosen in such a way that the bitrates were attainable by the chosen hardware. The chosen hardware will be elaborated upon with the link budgets in the next section. Furthermore, a coding margin was added to allow for the addition of error detection and correction bits. For the Moon-to-Moon communication, a 32-bit CRC checksum was added ². A Reed-Solomon (255,223) + convolutional coding scheme was added For the Malapert to Earth connection [56].

Table 13.3: Data volume estimate for downlink.

Equipment	Bits [Mb]	Bitrate [Mb/s]
Rover Downlink 250 Sec. communication window		
Telemetry	1	-
Lidar	936.00	-
Hazcams	42.67	-
Total data	979.7	3.92
Coding margin	981.6	3.94
Combiner downlink 208 sec. communication window		
Observational data	671.09	-
Combiner telemetry	1	-
Charging station telemetry	1	-
Total data	1655.76	7.96
Coding margin	1659	7.98
Sverdrup relay station downlink 660 sec. communication window		
Sverdrup relay station telemetry	1	-
Sverdrup power station telemetry	1	-
Total data	1657.76	2.51
Coding margin	1661	2.52
Malapert communication station downlink 35 minutes communication window		
Malapert relay station telemetry	1	-
Malapert power telemetry	1	-
Total data	1659.76	0.8
Coding margin and coding rate (RS+convolutional)	2323.7	1.1

Table 13.4: Data volume estimate for uplink.

Equipment	Bits [Mb]	Bitrate [kb/s]
Rover Uplink 125 Sec. communication window		
Commands	1	-
Total data	1	8
Coding margin	1	8
Combiner Uplink 0.8 Sec. communication window		
Rover commands [x4]	4	-
Combiner commands	1	-
Power station commands	1	-
Total data	6	7.5
Coding margin	6.01	7.51
Sverdrup relay station Uplink 4 Sec. communication window		
Sverdrup relay station commands	1	-
Sverdrup relay power station commands	1	-
Total data	10	2500
Coding margin	10.02	2505
Malapert communication station Uplink 2100 Sec. communication window		
Malapert comm. station commands	1	-
Malapert comm. power station commands	1	-
Total data	12	5.7
Coding margin	16.8	8

²CCSDS, Proximity-1 Space Link Protocol - URL: <https://public.ccsds.org/Pubs/210x0g2.pdf>

13.4. Malapert and Earth Link Budget

The general architecture of a communications system can be found in Figure 13.3. The goal of this section is to design this architecture by combining components and other aspects relevant to the design. This design is done through the use of the link budget, which can be found in Table 13.5.

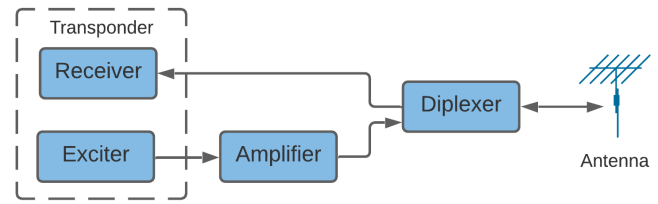


Figure 13.3: General architecture of communications components.

The worst case scenario was used to calculate the Slant range to the Moon. This includes a distance of 405696 [km] and an elevation angle of 10 degrees³ [57]. The Slant range was subsequently calculated using $S = R_E \left(\sqrt{\left(\frac{r^2}{R_E^2} \right) - \cos^2 \delta} - \sin \delta \right)$. The X-band was selected for the transmission frequency — specifically 8475 [MHz], given that is in the middle of the assigned band for data downlink [58]. OQPSK was chosen as a modulation scheme, given that is supported by NASA's Deep Space Network [59] and provides high spectral efficiency. The spectral efficiency was calculated using $\rho = \frac{\log_2(M)}{2} [\text{bits/s} \cdot \text{Hz}]$, where $M = 4$ in the case of OQPSK [60]. For this link, it resulted in a bandwidth of 2.2 [MHz] including a 0.5 roll-off factor [61], which is within acceptable range of 50 [MHz] [58]. It should be noted that 50 [MHz] is the total allocated bandwidth for X-band downlink. Therefore, it is desirable to use significantly less bandwidth so that other missions can also use this band for communication. A Reed-Solomon (255,223) + convolutional coding scheme was selected to detect and correct bit errors. This specific coding scheme was chosen because of its efficiency and support from DSN [59]. This coding scheme also adds 8 [dB] of coding gain [56].

The choice for transponder and antenna design is a balance between power and size. A more powerful transponder can use a smaller antenna to send the signal; a smaller antenna, however, has a beam that is less concentrated, such that a large portion of the Earth will be covered with the signal. Having a powerful signal covering the entire Earth is undesirable, given that every antenna pointed at the Moon will be saturated with that signal. A larger antenna can create a more concentrated beam and provides more gain to the signal. However, large antennas might be difficult or impossible to be installed by the astronauts. For this design, an existing transponder with internal power amplifier is chosen, to provide 3.8 [W] of output power⁴. A parabolic antenna with a diameter of 0.3 [m] is proposed to close the link budget. An efficiency of 0.5 is assumed [62] and the gain is calculated using $G_A = \frac{4\pi A_{\text{eff}}}{\lambda^2}$. The 3 dB beamwidth of this antenna is given by $\text{beamwidth} = \frac{66\lambda}{D}$, where λ is the wavelength of the signal and D is the diameter of the antenna. The coverage of the Earth is calculated using $\text{coverage} = 2 \cdot \tan\left(\frac{\text{beamwidth}}{2}\right) \cdot 405696$, which is based on Figure 13.4. The beam that this antenna sends out will still cover the entire Earth. However, since the emitted power is low, this is not expected to be a problem.

The free space attenuation⁵ was calculated using $L_p = -20 \log\left(4\pi \frac{S}{\lambda}\right)$. The zenith total atmospheric attenuation is assumed to be 0.5 [dB]. The DSN ground station properties are based on the specifications of the 34 [m] antennas [63]. It is important to note that the antenna noise temperature will be higher than the value found in the specifications, since the antenna is pointing at the Moon instead of Deep Space. A noise temperature of 200 [K] is assumed as a consequence [64].

³NASA, Moon Fact Sheet - URL: <https://nssdc.gsfc.nasa.gov/planetary/factsheet/moonfact.html>

⁴NASA, Iris V2.1 CubeSat Deep Space Transponder - URL: https://www.jpl.nasa.gov/cubesat/pdf/Brochure_IrisV2.1_201611-URS_Approved_CL16-5469.pdf

⁵ITU-R, Calculation of free space attenuation - URL: https://www.itu.int/dms_pubrec/itu-r/rec/p/R-REC-P.525-4-201908-I!!PDF-E.pdf

Certain losses, such as line and connector losses, are difficult to determine at this stage. The values of these losses depend on the specific cables and components that are used, and that specific selection is outside the scope of this report. For now, these losses are assumed to be -1 [dB]. The required signal-to-noise ratio was based on the modulation scheme in combination with a bit error rate (BER) of 10^{-5} . This BER provides a balance between design complexity and error probability. Any errors that do occur will be detected by the coding scheme. Those erroneous packets can be requested again via the uplink.

The last component, the diplexer, filters and combines the incoming and outgoing signal. It has to be designed carefully to prevent a phenomenon called multipactor discharge. This is a phenomenon where secondary electron emissions may lead to an exponential increase in electrons, which can damage the RF equipment [65]. It can happen at any point where high RF power exists. Because of the complexity of this problem, the exact design and selection of this component is left for the next stage of the design.

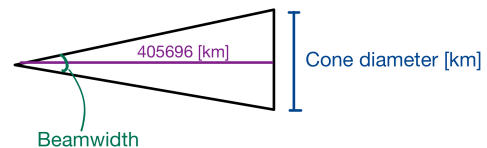


Figure 13.4: Diagram to calculate coverage of the signal.

13.5. Lunar Segment Link Budget

The architecture that was described in Figure 13.3 also applies to the lunar segment. All link budgets are similar and are designed to use identical components, apart from a less powerful transceiver on the rover due to energy constraints. Therefore, only the rover downlink budget will be discussed in this section. The additional link budgets with the more powerful transponder⁶ can be found in the Appendix.

The link budget for the downlink of the rover can be found in Table 13.6. A maximum distance of 500 [m] is used, since that is the most extreme baseline configuration of the telescope. The connection with the combiner will use a 400 [MHz] transmission frequency, which is similar to the UHF rover-to-orbiter system on NASA's Mars rovers⁷. The BPSK modulation scheme is employed for this design because of its simplicity to implement and ease of modulation/demodulation. Furthermore, spectral efficiency is not expected to be a concern on Moon-to-Moon communication at low power outputs. A more sophisticated modulation scheme is therefore deemed unnecessary.

A 32-bit CRC checksum has been selected to allow for error detection during communication. This checksum is easy to implement, adding only a small number of extra bits and protecting against 99.99% of all errors⁸. A transponder with low power usage is made use of, as it is beneficial to the battery-powered rover [66]. An omnidirectional antenna was chosen because a lack of pointing simplifies the design. It is important to note that an omnidirectional antenna at this frequency has a negative gain. A gain of -5 [dBi] is assumed for the time being⁹. The same antenna is used at the combiner, and as a consequence the gain is estimated to be -5 [dBi] there as well. The noise temperature of a receiving antenna on the Moon is estimated to be 200 [K] [67]. It should be noted that this is probably an overestimate, given that the antenna will see a lot of Deep Space.

⁶L3Harris, Mars UHF transceiver - URL: https://www.l3harris.com/sites/default/files/2020-07/ims_eo_datasheet_UHF_Mars_Transmitter.pdf

⁷L3HARRIS, L3HARRIS PERSEVERANCE ROVER MISSION SUPPORT - URL: <https://www.l3harris.com/sites/default/files/2021-02/L3Harris-IMS-E0-Sellsheet-Rover.pdf>

⁸BARR group, CRC math theory - URL: <https://barrgroup.com/embedded-systems/how-to/crc-math-theory>

⁹Steatite, Vertically polarised omnidirectional antenna 10 MHz to 1 GHz - URL: <https://www.steatite-antennas.co.uk/wp-content/uploads/2019/01/QOM-SL-0.01-1-N-SG-R.pdf>

Table 13.5: Downlink budget for Malapert to Earth communication

Malapert downlink budget			
Orbit & Tracking			
R_E	Earth radius	6378	km
h	Orbital altitude (circular orbit)	405696	km
r	Orbit radius (circular orbit)	412074	km
δ	Min. elevation angle	10	°
S	Slant Range	410919	km
Malapert Downlink Properties			
f	Transmission frequency	8475	MHz
λ	Wavelength	0.035	m
D	Data rate	1.1	Mbit/s
	Modulation scheme	OQPSK	-
G_{coding}	Coding gain	8	dB
Malapert Transmission Power			
P_{RF}	Transponder output	3.8	W
		5.8	dBW
		35.8	dBm
L_{line}	Line & connector losses	-1	dB
L_{point}	Pointing loss	-5	dB
D	Diameter of transmitting antenna	0.30	m
e	Efficiency of transmitting antenna	0.50	-
$G_{\text{ant.}}$	Antenna directivity (minimum)	25.50	dBi
P_{EIRP}	Transmitted EIRP	25.30	dBW
Communication channel			
L_{path}	Path loss (free space, normalised to λ)	-223.29	dB
$L_{\text{atm.90}^\circ}$	Zenith total atmospheric attenuation	-0.50	dB
$L_{\text{atm.}}$	Atmospheric loss	-2.88	dB
L_{channel}	Total channel loss	-226.17	dB
Ground Station Reception			
$L_{\text{G.s.},i}$	Isotropic signal level at ground station	-200.87	dBW
$L_{\text{G.s.},\text{ant.}}$	Antenna directivity (minimum)	68.00	dBi
$L_{\text{pol.}}$	Polarization mismatch	-3.00	dB
L_{line}	Line, connector & surge protector losses	-1.00	dB
T_{noise}	Reception noise temperature	200	K
		23	dBK
k	Boltzmann constant	-228.6	$\frac{\text{dBW}}{\text{KHz}}$
S/N_0	Signal-to-noise power density	76.7	dBHz
E_b/N_0	Signal-to-noise	16.3	dB
$(E_b/N_0)_{\text{req}}$	Required signal-to-noise ratio	9.6	dB
$(E_b/N_0)_{\text{margin}}$	Total link margin	6.7	dB
SE	Spectral efficiency	1	bit/s/Hz
B_{est}	Bandwidth	2.2	MHz
w	3 db beamwidth	7.78	deg
Cov	Coverage of Earth (diameter cone)	55188.70	km

Table 13.6: Downlink budget of the rover to combiner communication

Rover downlink budget			
Distance			
d	Distance	0.5	km
Rover Downlink Properties			
f	Transmission frequency	400	MHz
λ	Wavelength	0.749	m
D	Data rate	4	Mbit/s
	Modulation scheme	BPSK	-
G_{coding}	Coding gain	1	dB
Rover Transmission Power			
P_{RF}	Power amplifier output	0.01	W
		-20	dBW
		10	dBm
L_{line}	Line & connector losses	-1.00	dB
$G_{\text{sat.ant.}}$	Antenna directivity (minimum)	-5.00	dBi
P_{EIRP}	Transmitted EIRP	-26	dBW
Communication Channel			
L_{path}	Path loss (free space, normalised to λ)	-78.47	dB
L_{channel}	Total channel loss	-78.47	dB
Combiner Station Reception			
$S_{\text{G.s.},i}$	Isotropic signal level at combiner	-104.47	dBW
L_{line}	Line and connector losses	-1.00	dB
$G_{\text{G.s.},\text{ant.}}$	Antenna directivity (minimum)	-5.00	dBi
T_{noise}	Reception noise temperature	200	K
		23.0	dBK
k	Boltzmann constant	-228.6	$\frac{\text{dBW}}{\text{KHz}}$
S/N_0	Signal-to-noise power density	96.1	dBHz
E_b/N_0	Signal-to-noise	30.1	dB
$(E_b/N_0)_{\text{req}}$	Required signal-to-noise ratio	9.6	dB
$(E_b/N_0)_{\text{margin}}$	Total link margin	20.5	dB
SE	Spectral efficiency	0.5	bit/s/Hz
B_{est}	Bandwidth	16	MHz

13.6. Verification and Validation

The calculations for the link budget were done using separate Excel sheets for the different downlink and uplink connections. These Excel sheets were verified by the use of hand calculations, since the equations were simple enough to solve by hand. The sheets have also been verified using the data from the BIRD satellite [62].

The capabilities of existing hardware were taken into account to validate the design. These capabilities include the RF power and data rate of the transceiver^{10 11} [66]. The choices for modulation and coding scheme were validated by a comparison with existing hardware and the capabilities of the DSN ground stations [68]. As has been noted in the previous sections, there are still a few uncertainties regarding the line losses, pointing losses and noise temperature on the Moon. To increase the accuracy of the link budget, these uncertainties have to be investigated in the next stage of the design.

It can be determined that this subsystem complies with the requirements. The presented link budgets ensure that communication between the lunar element and Earth can be established, which satisfies requirement **SALT-SYS-04**. Also, the design ensures a one hour contact per terrestrial day, which satisfies requirement **SALT-SSYS-COM-04**. It is important to note that this is dependent on the availability of the DSN. This design was optimised to limit the amount of required contact time. However, the availability of the DSN is still very limited [69]. As described in the previous section, the commands and data will be stored at the Sverdrup relay station to have a backup in case of a loss of communications. This satisfies requirement **SALT-SSYS-COM-03**.

It is important to reiterate that the use of existing communications infrastructure has not been considered for this design. This choice was made because it was impossible to generate a design when there are no known specifications. However, this option can be reconsidered once these do become available. Due to the low data rates the odds are high that, for instance, the Artemis communication systems will be capable of handling such an addition. Nevertheless, until specifications are published this remains uncertain. In the case that this becomes available, the tools and specifications presented in this chapter can be used to determine the fit of the design.

¹⁰NASA, Iris V2.1 CubeSat Deep Space Transponder - URL: https://www.jpl.nasa.gov/cubesat/pdf/Brochure_IrisV2.1_201611-URS_Approved_CL16-5469.pdf

¹¹L3Harris, Mars UHF transceiver - URL: https://www.l3harris.com/sites/default/files/2020-07/ims_eo_datasheet_UHF_Mars_Transmitter.pdf

14. Remote Sensing

This chapter will discuss the sensing systems that will form part of and complement the SALT mission. Section 14.1 discusses seismic sensing aspects and the necessity of such a system, complete with a model and a proposed sensor design. Section 14.2 describes the sensors that are equipped on the collectors and combiner of the SALT system.

14.1. Seismic Sensing

Moonquakes were investigated by the Apollo missions between 1969 and 1978. The magnitude of the moonquakes vary — deep moonquakes have magnitudes of up-to 2 on the Richter scale at a depth between 700-1200 km . They are frequent and correlated to thermal tides. Shallow moonquakes can be as close as 100 km to the surface, and are significantly more energetic. Estimates show that magnitude 4, 5 and 6 moonquakes could occur on the Moon every 9, 32 and 112 years, respectively [70]. For the extended mission, this amounts to an 11.8% probability of occurrence for a single magnitude 6 moonquake, and a 30% probability of a magnitude 5. The chance that a magnitude 6 moonquake would occur close enough to hinder the mission is even lower. As such, only magnitude 5 moonquakes are taken into account, which is also reflected in Table 14.1.

Table 14.1: Relevant requirement for seismic sensing

Code	Requirement
SALT-SSYS-MECH-13	The system shall survive moonquakes of magnitude 5

Shallow moonquakes appear to occur in random locations with a surface frequency between 0.21 [Hz] and 21 [Hz] [71]. Magnitude 5 earthquakes tend to cause reasonable damage on Earth. Considering that the mission's extended lifetime is 15 years, it is crucial that the SALT system to be designed to mitigate the effects of such quakes.

The fundamental principles behind moonquakes are similar to those of earthquakes. Seismic waves originating from the hypocenter (or focus) of a quake consist of body waves and surface waves. Body waves travel through the interior of the Moon, and are of two types: pressure (or primary), P-waves which propagate quickly and are non-damaging, and shear (or secondary), S-waves which are slower but result in ground displacement. Surface waves follow body waves, and these are generally the most damaging forms of seismic waves. They propagate from the epicenter, which is the point on the lunar surface directly above the quake's hypocenter. The major ones are: Love waves and Rayleigh waves, which propagate as shown in Figure 14.1¹.

¹Retrieved from Encyclopædia Britannica at: britannica.com/science/seismograph/Applications-of-the-seismograph

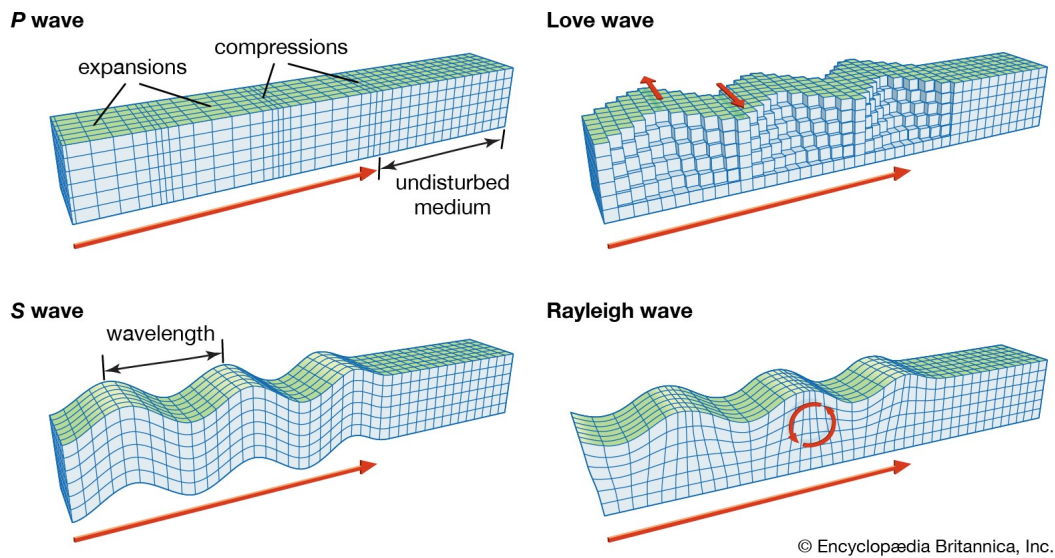


Figure 14.1: An image showing the main types of seismic waves

To allow for timely activation of a mitigation system, the implementation of an early warning system which detects P-waves is necessitated. Furthermore, this proposed system would partially contribute to the requirement stated in Table 14.1, as a robust network of seismic sensors will eventually provide enough of a response time to safe the SALT system.

14.1.1. Seismic Sensing Model

To determine the placement of these sensors, and to determine an estimate for amount of time that can be provided to protect the SALT system, a simplified early warning model was developed. Due to the limited resources available to characterise moonquake propagation, the following assumptions were made:

1. Only surface waves from shallow moonquakes will affect the SALT system
2. The surface of the moon is uniform and homogeneous
3. The speed of sound in lunar regolith is constant
4. Both Love and Rayleigh waves travel at the same velocity
5. The waves propagate instantaneously from a point source
6. The waves propagate outward and uniformly
7. The quake intensity remains the same during propagation, i.e. wave energy is constant
8. Asteroid impacts cause P-waves and surface waves
9. The sensors detect the first wavefront accurately and instantaneously
10. The sensors provide feedback to the SALT system instantaneously
11. Sverdrup crater's rim is perfectly round

The model flow can be summarised as follows:

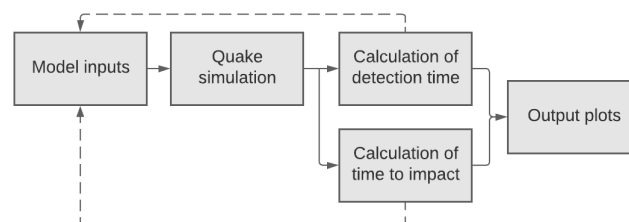


Figure 14.2: Seismic sensing model flow

As an input the model takes the location of the SALT system within the Sverdrup crater, the number of seismic sensors and their locations. The reference frame for this model is the centre of Sverdrup within the Euclidian plane. The propagation of a moonquake's seismic wave can be simulated to begin from a randomly generated location within a $50km^2$ frame. As a part of the seismic wave, the sensors detect the first occurring, low impact P-waves, and the model calculates the time between detection of this wave and a surface wave striking the SALT system. The model uses Euclidian distances between the SALT system and the sensors to calculate the the difference between the aforementioned times — thus providing the available preparation time to safe the SALT system. The output plots show the results of the simulations and how each result varies by changing the inputs.

The effects of each assumption are addressed in the order of their listing, and are as follow:

1. The seismic waves caused by deeper quakes will have a negligible effect as their intensity is greatly reduced towards the surface [72], and will have a marginal impact on the SALT system. They are therefore not considered in the model. In actuality, the sensors may pick these readings up, and still send a warning out depending on their calibration.
2. The terrain of the lunar surface is hardly uniform, and its composition is inconsistent. It is expected that this would vary the detection times as propagation of the P-waves would largely depend on the speed of sound through the composition. This is due to the longitudinal nature of the wave, and as an average, an upper estimate is chosen for this speed within lunar regolith. Its impact on the model is marginal due to the conservative estimate chosen, and due to the corresponding changes in the velocity of surface waves. However, the terrain changes may disperse surface waves ², leading to a reduced impact on the SALT system.
3. $7.7km/s$ is an upper estimate of the velocity of sound in lunar regolith [73], and is chosen in conjunction with the previous assumption. In actuality, the velocity of a P-wave is given by the following relation:

$$v_p = \sqrt{\frac{K + \frac{4}{3}\mu}{\rho}} \quad (14.1)$$

where K , ρ and μ are material properties of the medium, which are not always consistent and the chosen average velocity partially mitigates the effects of these inconsistencies.

4. Love waves travel slightly faster than Rayleigh waves, and in actuality, are slower than S-waves. Although due to the loose upper layer of the lunar surface, the wave velocities will be quite low. For the purpose of this model, a very conservative velocity estimate is chosen for the surface waves, and is determined to be the same as S-waves caused by shallow quakes, which is $4km/s$ [73]. The effect this has on the model is that impact times will be longer than in actuality.
5. This assumption partially holds true as the strain energy during a quake is released instantaneously. The epicenter of a quake is treated as a point source although there may be a small area of influence from where the quake propagates, which is determined via triangulation. The effect this has on the model is that the detection times will be very slightly shorter than expected.
6. Wave propagation in actuality is not perfectly uniform. This is due to the varying wave intensity which arises once again due to variations in the composition of the lunar regolith.
7. Seismic waves decay and their intensity reduces over time, whilst also varying due to composition changes. In actuality, the P-waves may possibly decay slightly and remain undetected [74], which make it harder for the network to detect quakes. This may result in moonquakes not being detected if their origin is significantly further away from the sensor network.
8. Asteroid impacts can be treated as a very shallow quakes as they only impact the surface, and thus only have a wave velocity of $1km/s$ [75]. However, this greatly varies depending on the size of the asteroid [76] and these effects need to be further investigated once asteroid impacts have

²British Geological Survey www.bgs.ac.uk/discovering-geology/earth-hazards/earthquakes/how-are-earthquakes-detected/

improve characterisation. The effect this has on the model is that the seismic waves caused by asteroid impacts can travel much faster in actuality and thus lead to shorter time for both detection and impact on the SALT system.

9. The sensor calibration in actuality will be imperfect, and will have an inherent delay in detecting and processing the P-wave. This will notably lengthen the detection time.
10. Relaying live signals from a coordinated sensor network will further induce delays, shortening the available preparation time. However, the model does not take this delay into account.
11. Sverdrup's rim has in actuality has some eccentricity, and may slightly change the sensor positioning on the rims, should this be the chosen configuration for sensor placement. The effect this has on the detection times is negligible.

14.1.2. Model Results

From the output of this model, it can be determined the potential response time is dependent on factors such as number of active sensors, sensor placement and placement configuration. If not prepared for, the moonquakes can prove to be hazardous during operation of the SALT system. The steps taken to mitigate the effects of moonquakes are described in Section 15.3.

In simulations of up-to 10000 quakes, it was determined that the ideal configuration for sensor placement is a ring format, as concentric rings detected P-waves faster on average than linear arrays of sensors. Additionally, to account for false positives, the model is extended to ensure that two of the closest sensors detect the quake, and only then is a signal sent to the SALT system. This reduces the preparation time, but the built in redundancy will prevent repeated seizing of operations. For this reason, a 2-ring configuration was deemed to be suitable for the purpose of the SALT mission. Furthermore, in comparison with the 1-ring configuration, the 2-ring configuration detects quakes on average, 0.9s faster.

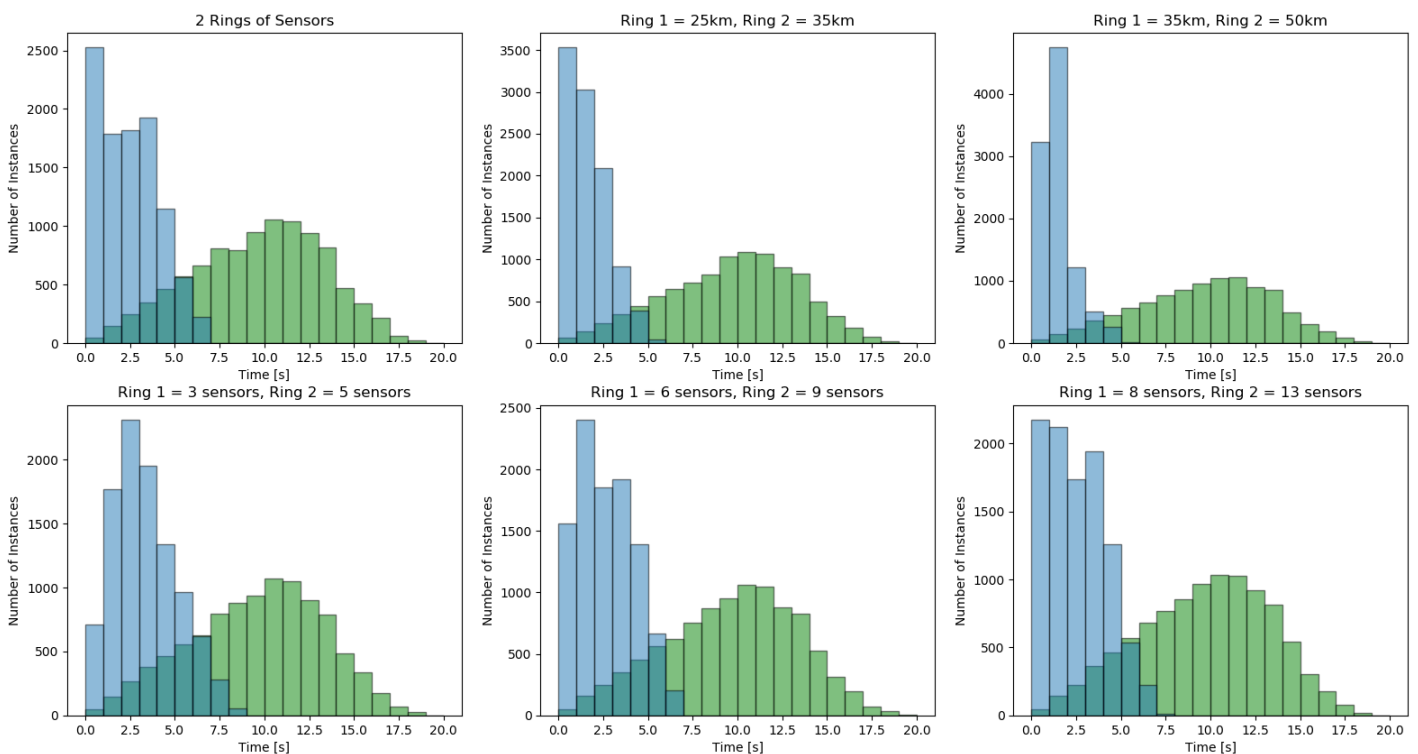


Figure 14.3: Histograms of simulation data showing the distribution of the time taken to detect quakes in blue and the time taken to impact SALT in green

Figure 14.3 shows that with a constant number of sensors, the instances of shorter detection times

increases as the sensors are placed further outwards. The first plot is the reference, with the sensor rings placed at 18km and 25 out from the centre of Sverdrup crater. Finally, it can be seen that when using a 2-ring configuration, the number of sensors used in each ring can be minimised with negligible effect of the time taken to detect quakes.

As part of the SALT mission, it is unfeasible for astronauts to place these sensors at such distances, and thus, an initial 1-ring configuration with 7 sensors around the Sverdrup crater rim is proposed, with extensions made as required. With this current configuration, the SALT system will receive an average of 6.09s of preparation time before impact. The proposed network of sensors is also expected to evolve with the number of active lunar missions within the region, and data from the network will be available to the scientific community. Moonquake detection on arrival may prove to be infeasible due to the lack of preparation time available to brace the system for impact. However, it may still serve as a contingency system in case the primary early warning system fails — by making use of the rovers' onboard sensors.

14.1.3. Model Verification and Validation

Using the V&V framework laid out in Chapter 8, the model was verified by completing hand tests with simulated moonquakes, and simulated placements of exemplar sensors. The model is largely dependent on the correct calculation of Euclidian distances and the hand tests as well as manual inspection ensure that this is the case. Additionally, the plotted outputs were inspected to ensure that the data is represented correctly.

Validation of such a model is challenging at this time as there are currently no active deployed seismic sensors of the envisioned nature on the lunar surface. It is expected that the rough order of magnitude for detection times that can be achieved is realistic, with the chosen wave velocities.

14.1.4. Sensor Design Considerations

The seismic sensors will have to be designed in order to withstand the lunar environment, and will have a power system decoupled from that of the SALT system. Ease of deployment, and thus extensibility, is a major factor in the design as it can facilitate the possibility of the sensor network expanding rapidly. Additionally, if a sensor is faulty or damaged, it can quickly be replaced.

Sensor Architecture

Unlike on Earth, the sensors do not have to be placed in boreholes to minimise noise³. This allows the simplified design of such a sensor as it can remain close to the surface — adopting a probe-like architecture.

It has been identified that each probe must be equipped with 3-component accelerometers in order to measure accelerations in 3-axes. The accelerometers used will be MEMS based, similar to those of the Mars Insight mission's SEIS experiment [77], and will be housed with their electronics board and cabling. Finally, the probe's base must be equipped with pins in order to remain firmly positioned on the lunar surface.

Sensor Communications

The probe must be calibrated to send signals when they detect accelerations beyond a certain threshold, in order to minimise potential sources of background noise, if any. These signals will be communicated back to a central station, which observes seismic activity within the region and will further relay it to the SALT system in case of a quake. For this purpose, each probe will be equipped with a transmitter and an antenna. The data volumes expected from each of the accelerometers during one Sol ($24\text{h } 39\text{m } 35\text{s}^4$) is 213061 kBits [78]. As a result, an uncompressed data rate of 7.2 kbps is expected during

³Berkely Borehole Network seismo.berkeley.edu/bdsn/bb_overview.html

⁴Technical Notes on Mars Solar Time: giss.nasa.gov/tools/mars24/help/notes.html

measurements.

A low-power UHF-band radio transmitter and antenna are mounted on the probe to transmit the measurements to the central station — which will be equipped with an adequate receiver.

Sensor Electrical and Thermal Properties

In order to save power, the transmitter will remain idle until the aforementioned threshold is crossed. Once the threshold is crossed, the transmitter will remain active for the duration of the reading. For this case, the duration under maximum power usage is assumed to be that of the average moonquake duration — which is known to be more than 10 minutes long⁵.

Each probe will be connected to its own solar panel, which will generate the required power to operate it as they are to be placed on the crater rim. The access to the PEL makes this an optimum configuration, but it must withstand temperatures of 175K, as shown in Section 6.1. Active temperature control increases the complexity of a probe system. However, with an operational window between 193.15K and 333.15K for the MEMS accelerometers and an effective lithium based battery operation window between 253K and 313K as shown in Table 12.3, an active temperature control system is warranted.

This active temperature control is a combination of patch heaters and passive insulation, the operation of which will be determined by an internal temperature sensor. Passive temperature control can be achieved by covering the sensors in lunar regolith, as is done for the electrical box of the SALT system.

Sensor Deployment and Operations

The probes will be deployed manually by astronauts once their locations have been finalised. Additional considerations for deployment include penetrators from lunar orbit, but have failed to deploy as intended [79]. Furthermore, precise probe placement using such a system will prove to be challenging and therefore manual deployment is deemed feasible. The lunar soil can be compacted by the astronauts to some extent, thus allowing the pins to secure the probe into the surface.

Once deployed, the sensor calibrations must be validated to correctly account for background noise. The probe will operate as shown in Figure 14.4.

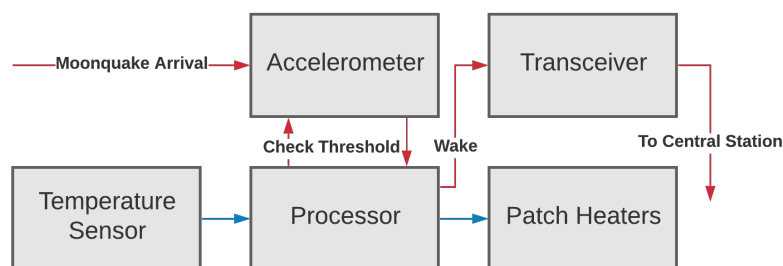


Figure 14.4: Operation and components of the seismic probe

Recommendations for the future development of these sensors include material considerations to withstand the PEL as well as optimising the communication system for a response with minimum delay.

14.2. Autonomous Vehicle Sensing

Due to the nature of the mission, it is expected that the SALT system will carry out numerous tasks in partial, or complete autonomy with minimal input from ground stations once observation parameters have been set. In order to do this, the rovers will be equipped with sensors and have subroutines in place for expected scenarios. Each of the sensors described in the following subsections fulfils a

⁵NASA Moonquakes: nasa.gov/exploration/home/15mar_moonquakes.html

specific purpose, that stems from one of the subsystem requirements shown in Table 14.2. Although not immediately apparent from the current requirements, it is expected that the rovers cannot operate and fulfil these requirements without such sensors. The use of sensor technologies on extraterrestrial vehicles has been well established and components with comparable performance will be used.

Table 14.2: Relevant requirement for autonomous sensing.

Origin	Code	Requirement
VLMT-PER-01	SALT-SYS-01	The telescope shall characterise the thermal infrared signature of exoplanets.
Investors	SALT-SYS-11	The mission shall have a probability of success of 0.920 [8] or higher
VLMT-PER-10	SALT-SSYS-SENS-12	The optical path length shall be able to be corrected
VLMT-SR-01	SALT-SSYS-MECH-13	The system shall survive moon quakes of magnitude 5
Risk Assessment	SALT-SSYS-OPE-09	A repair strategy shall be established

14.2.1. Light Detection and Ranging (LiDAR)

A major challenge that the SALT rovers face is to operate safely and navigate accurately within the dark environment of the Sverdrup crater. Failure to do this successfully can severely compromise the primary mission objective **SALT-SYS-01**, or result in complete mission failure. Additional challenges with regards to navigation is the possibility of damage to the rovers by elements on the lunar surface, such as boulders. In order to overcome these challenges, and as a result increase the operational reliability of the system as a whole to meet **SALT-SYS-11**, LiDAR sensors are necessitated on each of the SALT rovers.

LiDAR sensing operates on the principles of time of flight, by targeting a laser at an object and measuring the time taken to reflect back to the receiver. Each of these measurements results in a 360-degree point-cloud image being generated, which can aid in hazard avoidance, as well as provide accurate and simultaneous terrain mapping as the rovers traverse through the lunar surface. Accurate terrain mapping does not fall within the scope of the SALT mission. However, if the Sverdrup crater is accurately mapped by predecessor or cartography missions in the region, the point cloud generated by the LiDAR sensors can be compared with the terrain maps produced by these missions for absolute positioning. For the SALT system, the Quanergy M8 Ultra LiDAR sensor [80] will be used and its specifications are listed in Table 14.4.

Alternative considerations for hazard avoidance included a combination of floodlights and cameras to illuminate the area surrounding the rover. However this was deemed to be unfeasible due to the relatively higher power draw and increased system complexity. Furthermore, the shadows cast by the floodlights would increase the difficulty in distinguishing terrain features via the use of conventional cameras such as those mounted on the Mars rovers.

Finally, due to the long baselines of upto 500m away from the combiner, each rover must accurately align itself with the combiner during the discrete rotation steps, with an accuracy in the order of millimetres. This allows **SALT-SSYS-SENS-12** to be met, as the optical delay line relies on the accurate positioning between the rovers and the combiner. Due to the poor range of the M8 Ultra LiDAR sensors, a separate dedicated laser measurement or guidance system must be implemented for this purpose, as part of the laser metrology system described in Section 9.4. The Acuity AR2000 rangefinder [81] from Schmitt Industries matches these requirements and its specifications are summarised in Table 14.3, and 4 of these can be installed on the beam combiner to guide the collector rovers.

Table 14.3: Specifications of the AR2000 rangefinder [81]

Parameter	Specification
Measuring Range	500 [m]
Measuring Accuracy	1 [mm]
Measuring Frequency	100 [Hz]
Mass	0.7 [kg]
Power Consumption	5 [W]

Table 14.4: Specifications of the M8 Ultra LiDAR sensor [80]

Parameter	Specification
Measuring Range	0.5-200 [m]
Measuring Accuracy	<3 [cm]
Update Frequency	100 [Hz]
Mass	0.9 [kg]
Power Consumption	15 [W]

14.2.2. Inertial Navigation System (INS)

The INS can act as a standalone navigation system and can accurately determine the relative position of each rover once provided with a known starting reference. This is enabled by using readings from the accelerometers and gyroscopes during movement, to accurately determine headings and orientations. It is this system that will be used to orient the rovers to the combiner in order to send the beams of light towards it.

Furthermore, despite the implementation of a seismic sensing network, there remains the probability of moonquakes occurring within the Sverdrup crater, or the probability of the sensing network failing to warn the SALT system about an impending quake, which compromises **SALT-SSYS-MECH-13**.

Thus, each rover will be equipped with an INS which will comprise of accelerometers and gyroscopes, which act as motion and rotation sensors, respectively. The Perseverance rover's ⁶ system, consisting of 3-axis MEMS accelerometers as well as 3-axis fiber-optic gyroscopes will be used. The data from the INS will be monitored during static measurements for abnormally large disturbances and will be used to unlock the damping system. Vibrations during operation are inherent to any system, and these will be filtered out with certain thresholds to accurately detect quake arrival.

Table 14.5: Specifications of the Northrop Grumman INS

Parameter	Specification
Motion Sensor Type	3-directional Solid-state fiber-optic gyros
Rotation Sensor Type	3-dimensional Solid-state MEMS accelerometers
Mass	0.748 [kg]
Power Consumption	12 [W]

14.2.3. Radio Detection and Ranging (RADAR)

An imaging RADAR can be used to complement LiDAR systems to generate a 3-dimensional image [82], or serve as a backup in case of their failure. Additionally, they can aid in relative positioning between rovers and the combiner, by the use of a omni-directional radar beacon at the combiner, such as the Kratos 25X-X C band tracking beacon [83], and TYCO RADAR transceivers onboard each rover [84]. Due to the lower power usage of such a system, it can be used a backup relative positioning system.

Table 14.6: Specifications of the Kratos 25X-X C-band RADAR tracking beacon [83]

Parameter	Specification
Frequency	C-Band
Mass	0.51 [kg]
Power Consumption	9 [W]

Table 14.7: Specifications of the Tyco RADAR Detection [84]

Parameter	Specification
Frequency	C-Band
Range	1000 [m]
Mass	3 [kg]
Power Consumption	3.5 [W]

⁶Northrop Grumman's INS for Perseverance: news.northropgrumman.com/news/releases/northrop-grumman-provides-navigation-system-for-nasas-perseverance-mars-rover-mission

14.2.4. Cameras

Despite the limited use of conventional cameras in the dark environment of the Sverdrup crater, they can prove to be useful in improving the reliability of the system as well aid in satisfying **SALT-SSYS-OPE-09**. Thus, only a camera with a 360° mount and a flash will be implemented for undercarriage imaging, and will only be activated if a rover is stuck or stranded in an attempt to diagnose the fault. Once the fault is diagnosed, astronauts can attempt to recover and repair the rover if the rover cannot be recovered by commands from the ground station. The camera sensor will be the comparable to that of the Hazcam on the Perseverance rover [53].

Table 14.8: Specifications of the Perseverance Hazcam [53]

Parameter	Specification
Horizontal FOV	136°
Vertical FOV	102°
Focal Ratio	f/12
Focal Length	14 [mm]
Mass	0.498 [kg]
Power Consumption	1-3 [W]

14.2.5. Sensor Fusion

In order for the sensors to maximise their effectiveness in mapping surrounding terrain for accurate positioning, as well as provide orientation and hazard detection, inputs from multiple sensors will be processed by the OBC to stitch together a complete image. Due to these systems working in conjunction with one another and their emphasis on absolute positioning, positioning via triangulation has not been considered, and is a recommendation to be considered for future development. This can be achieved by placing omni-directional RADAR transceivers on every rover. Finally, the beam combiner can be used as a datum for the absolute positioning methods, and this data can further be relayed between rovers to determine their positioning relative to one another.

15. Structural Design

This chapter will discuss the design of the most important mechanical systems of the rover. The requirements pertaining to these mechanical systems can be found in Table 15.1. Firstly, the design process for the suspension of the rover is explained, with stress and vibrational analysis being carried out. With the results obtained from this vibrational analysis, the design of the support structure of the primary mirror is discussed. The mirror segments themselves were designed in Section 15.3.3. The rover must traverse over the lunar surface, and to enable this, Section 15.4 covers the wheel and drive train design. The effects of lunar dust are discussed in Section 15.5.

Table 15.1: Requirement overview for all mechanical systems.

Code	Requirement
SALT-SSYS-MECH-01	The beam collectors shall be able to reposition between 50 and 500 meter from the beam combiner.
SALT-SSYS-MECH-02	The telescope shall be extendable to 8 beam collectors (in * configuration).
SALT-SSYS-MECH-06	The system shall survive moonquakes.
SALT-SSYS-MECH-08	Lunar dust shall not permanently damage mechanisms.

15.1. Rover Suspension Design

”Over the past decade, the rocker-bogie suspension design has become a proven mobility application known for its superior vehicle stability and obstacle-climbing capability” - Harrington [85]. Considering this statement, as well as numerous other rover suspension models, the rocker-bogie system was deemed to be the obvious choice for a large and heavy lunar-rover with strict stability requirements and a low probability of failure. The objective of this section is to design and verify a lightweight and robust rocker-bogie suspension to provide the optical system with sufficient stability and manoeuvrability during a measuring period.

15.1.1. Suspension Geometry

A rocker-bogie suspension consists of three wheel supports that eventually meet at one main connection point located at the rover bus. The rover bus carries all major subsystems of the rover except the optical systems. Fundamentally, it consists of two main structural components: the upper and lower link, i.e. the rocker and bogie. The rocker has its pivot point located on the bus and allows the bus to maintain stability while moving. The smaller link pivots around the most aft end of the upper link, and has two wheels connected to it. This allows all six wheels to stay in contact with the ground whilst moving over obstacles, thus improving traction and overall stability of the rover.

To come up with a suitable configuration for this specific rover, a closer investigation was performed on the driving requirements that will define the geometry of the rover. Firstly, the rover has to be able to move over the rough surface of the Sverdrup crater whilst maintaining sufficient ground clearance in order to avoid damage. Next, the geometry has to allow the bus to point at most 85° , as was discussed in Chapter 10. Lastly, the rover shall not tip over during pointing, thus preventing the center of mass to move out of the contact area with the ground.

Geometrical relations were derived to size the rover’s legs, as presented in Figure 15.1, where links and bearings are indicated by letters. The lengths of the links are numbered accordingly, and the angle between the links (θ) has to remain constant. The coordinates in Table 15.2 govern the positions of all points and were derived using basic geometry. The three design parameters are the wheelbase w , the required height h and the wheel radius r_{wheel} that were derived from the aforementioned requirements. It was decided to set the wheelbase at $1.8m$ to ensure a sufficiently large contact area within which the center of gravity can translate during pointing manoeuvres. h was decided to be $0.8m$, which is larger

than required from an operations standpoint. Originally constrained to be $0.4m$ for obstacle clearance within the crater plus $0.2032m$ for pointing clearance, the uncertainty of the actual texture mappings inside the lunar crater are high. Thus, the total clearance was raised by $0.2m$ as a measure of safety. The wheel radius is derived in Section 15.4 and equals $0.25m$.

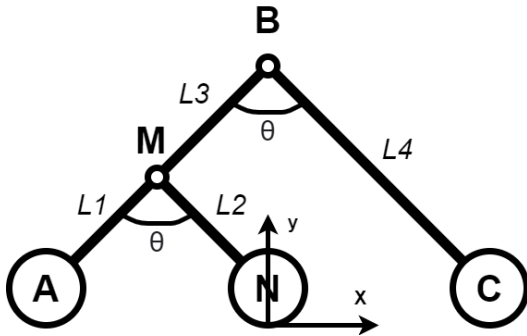


Figure 15.1: General geometry breakdown of the rocker-bogie suspension.

Table 15.2: Rocker-bogie coordinates making up the suspension geometry.

Coordinate	x-general	y-general	x [m]	y [m]
A	$-w/2$	r_{wheel}	-0.9	0.252
B	0	h	0	0.8
C	$w/2$	r_{wheel}	0.9	0.252
M	$-w/4$	$\frac{h+r_{wheel}}{2}$	-0.45	0.526
N	0	r_{wheel}	0	0.252
Section center	-	-	-0.169	0.492

15.2. Stress Analysis

With the geometry of the rocker-bogie suspension having been set, the beam-like structure that makes up the rocker and bogie has to be further designed. The focus of this subsection is to design a simple cross-section for each beam member as well as deciding the material of which the elements will be made. A preliminary stress analysis was performed on paper after which a simple program was written to compute the Von Mises stress for each point in the cross-section according to Equation 15.1. Both normal and torsional stresses are functions of the x and y distance from the center of the cross-section, the forces applied to the system and the moment of inertia of the cross-section. It should be noted that the cross-section of all beams was modelled as a hollow square with outer dimension T and thickness t . The loading is represented as a point load of $800[N]$ (from $m_{estimate}g_{moon}/2$) acting $0.5m$ behind the cross-section. This is in the reader's perspective $-0.5m$ in the direction perpendicular to the cross-section. This loading represents half the mass of the bus and optical systems acting in the middle of the bus, therefore creating an inward bending moment on the suspension.

$$\sigma_{VonMises} = \sqrt{\frac{1}{2} \left[(\sigma_{xx} - \sigma_{yy})^2 + (\sigma_{yy} - \sigma_{zz})^2 + (\sigma_{zz} - \sigma_{xx})^2 \right] + 3(\tau_{xy}^2 + \tau_{yz}^2 + \tau_{zx}^2)} \quad (15.1)$$

The result of this simplified, discretised element model is shown in Figure 15.2, where the arrow visualises the effect of a shift in center of gravity (c.g.) on the load paths during pointing. The maximum stress of $56.71MPa$ is obtained when the c.g. is positioned $0.75m$ to the right of the y -axis (see coordinate system in Figure 15.1 for reference).

This stress will drive the material and cross-section choice of the members. Since the modelled stresses are fairly low for most metal choices, titanium was selected as the most reliable and lightweight option. Re-running the discretised model again for a tubular cross-section deemed the best option due to the better torsional stiffness properties it provides. A outer diameter of 5.5 cm was chosen with a thickness of 0.65 cm. The discretised model was verified using numerous manual checks of the code as well as a unit test on the moments of inertia and the individual stresses. Linking the logical increase in Von Mises stress when the point of application moves further away from the cross-section center also verifies that the model is correct. The model was validated by using a simple, single supported horizontal beam as cross-section of which the maximum stresses are commonly known. The average error of the discretised model was 6.72% compared to the standard solution. Although it is a relatively large error, the model was deemed validated for such a preliminary design phase.

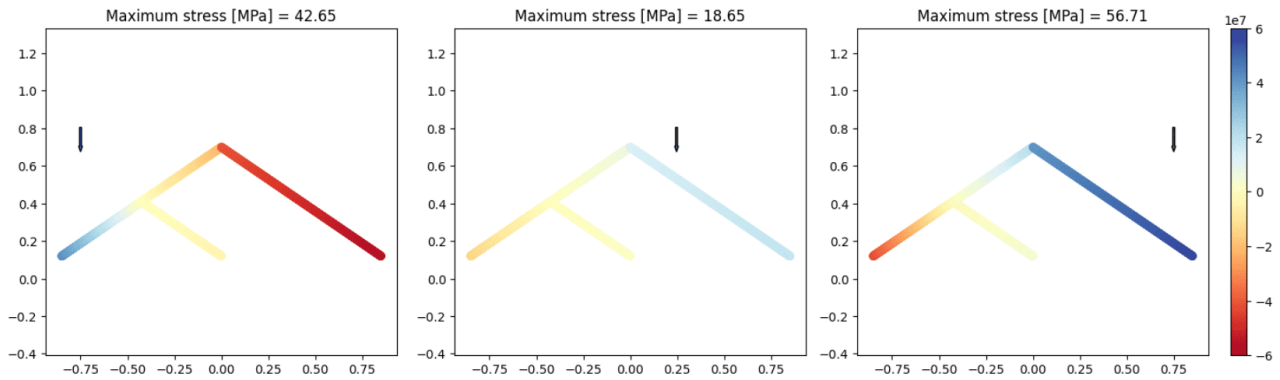


Figure 15.2: Von Mises stress distributions in the rocker-bogie legs during centre of mass shift (arrow) due to pointing, excluding torsional stresses

15.3. Vibrational Analysis

The surface of the Moon is host to moonquakes; as such, it is important to investigate vibrations induced by these moonquakes and, if necessary, introduce methods to mitigate these vibrations. Using a nomogram, it was determined that a magnitude 5 moonquake at 300km distance is equivalent to a magnitude 4 moonquake at 100km distance, having an amplitude of 20mm . The most extreme case of a magnitude 5 moonquake at 100km induces an amplitude of 100mm . A moonquake occurring at this distance (right below the mission), however, seems unlikely. Following from, Section 14.1, the moonquake is conservatively modelled as a simple sine-wave with an amplitude of 20mm and a frequency between 0.21 and 21 [[Hz]]. The frequency does not vary with time. The format of the sine wave can be seen in Equation 15.6

15.3.1. The Vibrational Model

A vibrational model of the rover was created to measure the effects of the moonquake. The rover contains sensitive instruments on both the mirror mounting and the rover body. Therefore, it was deemed necessary to mitigate vibrations from the bottom up, adding springs and dampeners to each of the wheels. The following assumptions were made for the model:

1. The joints of the rocker bogie suspension are locked and can be assumed rigid. In reality only the top joint, connecting the body to the suspension would be locked. It is expected that the 'bogie' joint would move freely and aid in mitigation of the vibrations.
2. The rover suspension, body and telescope mount are rigid.
3. The rover is symmetric along its movement axis.
4. The rover is modelled as a single point mass at its centre of mass.
5. The rover is free to roll. This means the body will not have vibrations in its movement axis.
6. Surface plane vibrations can be ignored. In reality, this is completely false as moonquakes also have a lateral component. However, because the Moon's surface is not flat, it is assumed that there will be a lateral motion with the two sides of the rocker-bogie swaying side to side, mitigating the vibrations.
7. The surface of the Moon is perfectly rigid, and transfers vibration directly and completely to the rover's wheels. In reality, the lunar regolith serves as an additional dampener. This only results in making the analysis more conservative.
8. Angle of rotation around the centre of mass is small enough to use the small angle approximation.

The system is modelled with 2 degrees of freedom. An upwards motion and a rotation around the centre of mass. Each wheel is modelled as a spring and damper in parallel. To get a general solution, each spring and damper as well as the movement axis of the wheels are set to be unique. The resulting

system is shown in Figure 15.3 with the associated equations of motion shown in Equation 15.2 and Equation 15.3.

The vibrational model was also designed to analyse lateral movement. This analysis would have involved adding a phase or bump difference between the wheels in Equation 15.6. Due to time constraints, these analyses were not performed.

As previously mentioned, moonquakes have a maximum frequency of 21 [Hz]; as a consequence, a rover natural frequency of at least 5 times higher is desired: 105 [Hz] or higher.

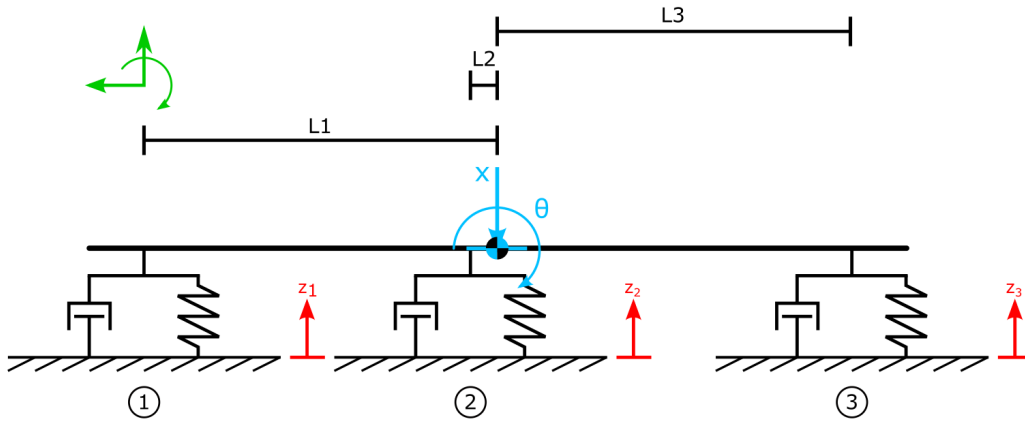


Figure 15.3: Schematic of vibrational model

$$\dot{x}_2 = -\frac{c_1 + c_2 + c_3}{m}x_2 - \frac{k_1 + k_2 + k_3}{m}x_1 + \frac{c_1l_1 + c_2l_2 + c_3l_3}{m}\theta_2 + \frac{k_1l_1 + k_2l_2 + k_3l_3}{m}\theta_1 + \frac{c_1}{m}\dot{z}_1 + \frac{c_2}{m}\dot{z}_2 + \frac{c_3}{m}\dot{z}_3 + \frac{k_1}{m}z_1 + \frac{k_2}{m}z_2 + \frac{k_3}{m}z_3 \quad (15.2)$$

$$\dot{\theta}_2 = \frac{c_1l_1 + c_2l_2 + c_3l_3}{J}x_2 + \frac{k_1l_1 + k_2l_2 + k_3l_3}{J}x_1 - \frac{c_1l_1^2 + c_2l_2^2 + c_3l_3^2}{J}\theta_2 + \frac{k_1l_1^2 + k_2l_2^2 + k_3l_3^2}{J}\theta_1 - \frac{c_1l_1}{J}\dot{z}_1 - \frac{c_2l_2}{J}\dot{z}_2 - \frac{c_3l_3}{J}\dot{z}_3 - \frac{k_1l_1}{J}z_1 - \frac{k_2l_2}{J}z_2 - \frac{k_3l_3}{J}z_3 \quad (15.3)$$

Here $x = x_1$, $\ddot{x} = \dot{x}_2$ and $\dot{x} = \dot{x}_1 = x_2$. The equations are converted to a state space model with state vector $\vec{x}(t) = [x_1 x_2 \theta_1 \theta_2]^T$ and input vector $\vec{u}(t) = [\dot{z}_1 \dot{z}_2 \dot{z}_3 z_1 z_2 z_3]^T$.

15.3.2. Verification of the Vibrational Model

The following steps were taken to verify the model:

- The model's configuration is based on a simpler exercise from the course material of AE2135-II and adapted to include an extra wheel. Where possible, the equations of motion were checked to match this exercise.
- The equations were derived independently twice, and thoroughly hand-checked.
- A simpler one wheel model acting straight into the centre of mass was created to verify the motion in the x direction. Equivalent spring and damping coefficients were derived and θ was fixed to 0. The motion of the two models was found to match.
- For rotation, the contribution of one wheel was checked to match the aforementioned exercise. The contribution of the middle wheel was then removed and the state-space was simulated with an initial rotation. An equal but opposite initial rotation was then simulated and the motions were compared for symmetry.

Validation was not performed, as data on a spring and damper rocker bogie system could not be found. In further stages of development, a prototype could be made along with a more advanced vibrational model. The prototype and model could be tested on a flat surface first to match horizontal and vertical motion independently. More validation can then be performed by using a rough surface. Since this model only serves as a first estimation, such detailed validation was deemed unnecessary.

15.3.3. Design Constraints: Mirror segments

Some constraints must be found to obtain values for a configuration of the dampers and springs. The segments of the mirror were deemed the most fragile components; to quantify this fragility, the natural frequency of the mirrors was determined. The mirror segment design of the LUVOIR mirrors was taken as a reference for the structural design of the segments, as they utilise the same ULE-glass chosen by the optics team. The mirror segments are sandwich structures made of a honeycomb or isogrid core and thin ULE-glass end-plates. [86]. The material of the LUVOIR segment core has not yet been determined, but a common material is silicon carbide (SiC) used in the GAIA and the proposed ORIGINS missions [87] [88].

The hexagonal segments were first approximated as a solid circular disk; their natural frequency was then calculated using methods described in "Vibration of Plates" (1969) by A. Leissa [89]. This method proved to be inaccurate, deviating with a factor 2, attributed to the solid disk assumption. Instead, the natural frequency was approximated using the studies on the LUVOIR mirror segments. LUVOIR's segments have three connection points in triangle configuration where the actuators are connected. This design is also used for JWST. The same configuration can be used by SALT. The LUVOIR segments have a first natural frequency of 180 [Hz]. "The Design and Construction of Large Optical Telescopes" by P. Y. Bely describes the relationship of natural frequency as proportional to $\frac{h}{D^2}$ [22]. The natural frequency is then calculated in Equation 15.4. The values used and the resultant mass and natural frequency are shown in Table 15.3.

$$\frac{f_{luv}}{f_{salt}} = \frac{\frac{h_{luv}}{D_{luv}^2}}{\frac{h_{salt}}{D_{salt}^2}} \quad f_{salt} = \frac{D_{luv}^2}{D_{salt}^2} \quad (15.4)$$

Table 15.3: Properties of LUVOIR and SALT mirror segments.

Property	LUVOIR	SALT	Unit
Diameter (point to point)	1.35	0.462	[m]
Total thickness	36.4	36.4	[mm]
Areal Density	10	10	[kg/m ²]
Area	1.184	0.139	[m ²]
Segment mass	11.837	1.386	[kg]
First frequency	180	1537.734	[Hz]

The natural frequency of the mirror segments is many times higher than the surface frequencies of 21 [Hz]. This means that this investigation does not produce a constraint for the vibrational analysis.

Thermal properties of the segments were considered briefly: SiC and ULE both offer very low thermal expansion. The radius of curvature is most affected by difference in thermal expansion ratios. The relation is given by Equation 15.5. For the thermal studies on LUVOIR, the difference in CTE varies between $\Delta\alpha = 0$ and $\Delta\alpha = 5e^{-9}$ [86]. The temperature variation expected in the mirrors during operation is less than 10K. The radius of curvature is 72.37 [m] as elaborated in Section 9.4.2. The resulting change in radius of curvature of 7.2 [mm] can be mitigated by the segment's actuators. The compatibility of the material configuration itself has already been investigated extensively by NASA for their space telescopes in comparable thermal environments [86] [87] [90].

$$\Delta R = \frac{R^2 \Delta T \Delta \alpha}{h} \quad (15.5)$$

15.3.4. Results of Vibrational Analysis

The model can now be run to design the springs and dampers. Table 15.4 lists the properties of the model, derived from Section 15.1.1 and Table 20.2. To ease in design, the following simplifications have been made to the model:

1. Equivalent damping coefficient has been set to 0.95 of the mass of the system. Close to, but not exactly critical. This is to compensate for accumulation of lunar dust. Since all dampers are equal, the damping coefficient of a single set of wheels can be calculated by: $c = (0.95m) \cdot 3$.
2. Initial displacement of the wheels has been set to 0.
3. The motion of the wheels $U(t)$ is the same for all wheels. The phase for the motion is a constant 0. The motion is described by Equation 15.6.
4. The spring coefficient is a free variable, but the same across all wheels.
5. The initial displacement and rotation of the COM is zero.

Table 15.4: Properties used in the state space model.

Property		
Rover Mass (m)	1750	[kg]
Polar moment of inertia (J)	125	[m ⁴]
Damping Coeff (c_1, c_2, c_3)	4987.5	[Ns/m]
Equivalent Damping Coeff	1662.5	[Ns/m]
Front wheel (l_1)	-0.9	[m]
Middle wheel (l_2)	0.0	[m]
Back wheel (l_3)	0.9	[m]

$$U_{1,2,3}(t) = 0.02 \cdot \sin((2\pi f)t + phase_{1,2,3}) + bump_{1,2,3} \quad phase_{1,2,3} = bump_{1,2,3} = 0 \quad (15.6)$$

Figure 15.4 shows the maximum acceleration, displacement and velocity, as well as the recovery time for multiple frequencies in the expected range. The graphs show the spring coefficient for a singular wheel in the horizontal axis, which would equal values $k_1/2$, $k_2/2$ and $k_3/2$. The recovery time is represented as time to first 0 from a 0.02 initial displacement without the moonquake in effect. Any spring coefficient higher than $2000[N/m]$ recovers within 10 seconds. A 10-second recovery time, although not required, is already more than acceptable. $2000[N/m]$ is therefore set as a lower limit for the spring coefficient. An upper limit proved more difficult to find. For a frequency of 21 [Hz] the surface acceleration is $350[m/s^2]$. A spring coefficient of $56000[N/m]$ or higher would exceed this surface acceleration. This value is already many times lower than the spring coefficient of a beam the system replaces. As a comparison, launcher payloads usually have to be designed for shock loads of around $10g$ ($98.1[m/s^2]$) at 21 [Hz][91]. Using a slightly lower shock load of $9g$ as another constraint, the upper limit becomes $13500[N/m]$. The springs should thus have a spring coefficient between $2000[N/m]$ and $13500[N/m]$.

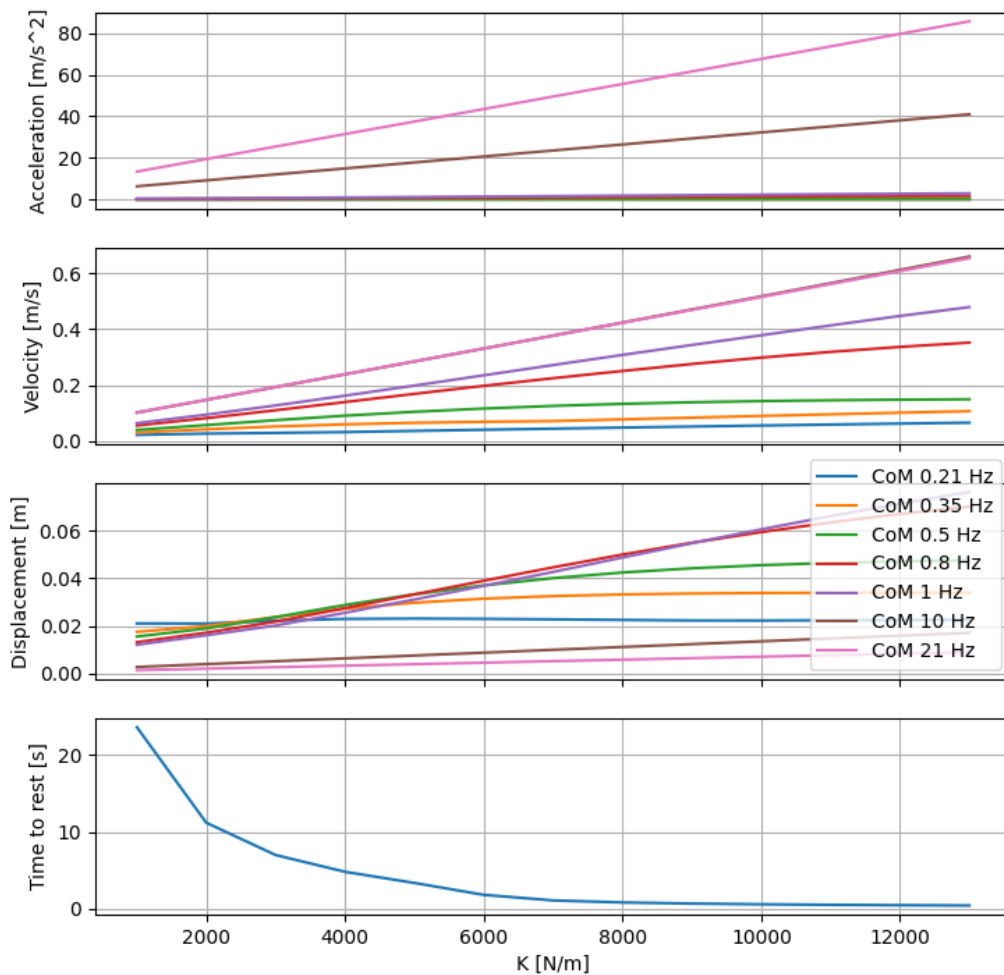


Figure 15.4: Plots for acceleration, velocity and displacement for different spring coefficients and frequencies. Value K is the spring coefficient for a single wheel

From there, the springs could further be optimised for weight or cost. This was not done for this report and should be investigated in the future. For now, it is clear that compression springs are more commonly sized at the upper limit. Nevertheless, a lower spring displacement is preferred to reduce the height of the springs and their encasing. It was therefore decided to design for a total displacement of $8[cm]$ (positive displacement times 2) resulting in a final spring stiffness of $6000[N/m]$. Such springs can be built to order. For the dampers, linear dashpot dampers will be used. The spring and dampers are to be configured in a concentric configuration to minimise space used.

Figure 15.3.4 show the displacement, velocity and acceleration response of the system with $k_{1,2,3} = 6000 \cdot 2$ for $0.7 [[Hz]]$ (maximum displacement) and $21 [[Hz]]$ (maximum acceleration). The $21 [[Hz]]$ acceleration response shows the significance of adding a spring damper system at the wheels.

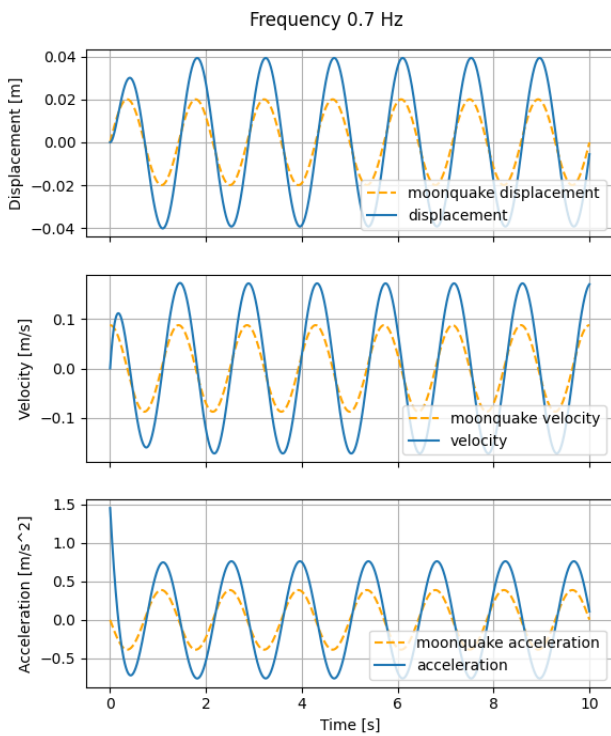


Figure 15.5: Frequency response at frequency 0.7 [Hz] (Max displacement).

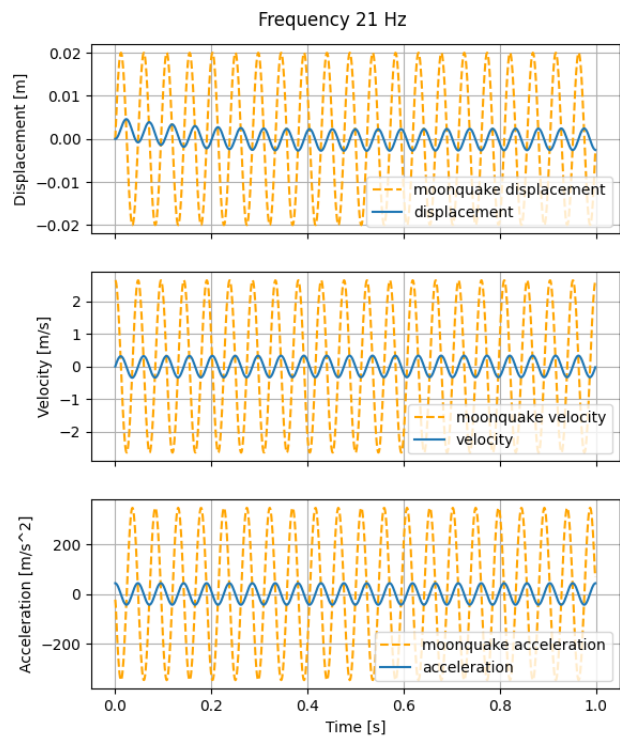


Figure 15.6: Frequency response at frequency 21 [Hz] (Max acceleration).

The addition of a spring damper system is not ideal for measurements, as the springs would wobble when rotating the mirrors. Instead, a locking system should be present to hold the spring and damper in a neutral position during normal operation. This lock would release upon detection of a moonquake. The detection of moonquakes is described in Section 14.1.1. Since the mechanical activation of such a lock could be made instantly, the warning time is instead limited by the time it takes to save the mirrors.

15.4. Wheel Design

The fundamental function of the wheels is to provide rolling motion by maximising the traction on the lunar surface. The wheel design and soil composition are the main factors that determine both traction and friction. The design approach and equations leverage the theory of terramechanics and motor vehicle design principles. This section will conclude by showcasing the final wheel design and the power required per wheel.

15.4.1. Wheel Configuration and Driving Modes

To reiterate, the purpose of locomotion is to generate traction and propel the rover forward. Forward thrust is the result of traction between both the wheel contact patch and the ground, which introduces forces working against the direction of motion. The forces associated with uphill driving are rolling resistance and a gravitational component. However, when driving over loose sand or lunar regolith, other impediments are introduced which slows down the vehicle. Most significant contributions would come from the bulldozing effect and the resistance introduced by the compaction of the soil in front of the wheel. A metric commonly known as the drawbar-pull, is the vector sum of traction and all opposing forces acting on the wheel. It is an important metric that will be used throughout this section and determines whether a wheel is able to let the rover translate over the lunar surface. The objective of the rover wheel design is to maximise traction and minimise all opposing forces as much as possible. The power budget will eventually benefit from this optimisation since it will optimise the power required to move the vehicle. The following subsections will go over all forces acting on one wheel, with numerous references made to the free-body diagram of the wheel, shown in Figure 15.7.

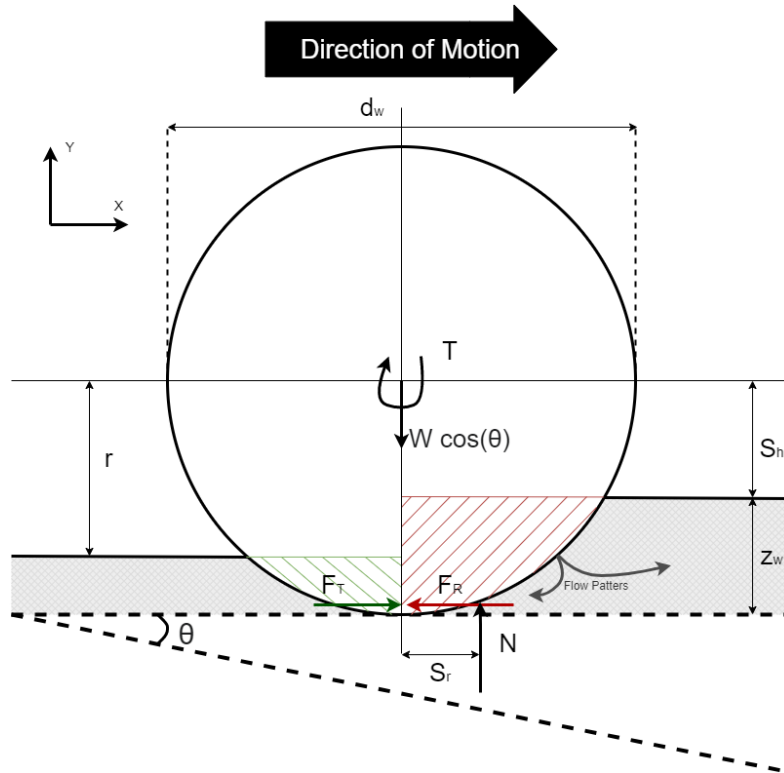


Figure 15.7: Free body diagram of a *driving* wheel moving through loose regolith

15.4.2. Sinkage

Since the rover moves on very loose regolith, it will inevitably sink into the ground whilst moving. To maintain the attitude of the rover body, the rocker bogie suspension system will compensate for this issue. The amount of sinkage is dependant on the soil properties, loading conditions, shape, stiffness and dimensions of the wheel. For a complete analysis, flexible wheels should be considered, but will not be covered as few lunar rovers have had flexible wheels in the past. Rigid wheels retain their shape and therefore their rolling diameter stays constant. The relation between contact pressure, p , and sinkage, z_w , is given Equation 15.7. All other parameters describe the soil or wheel characteristics and can be found in the nomenclature. Wheel diameter (d_w) and wheel width (b_w) are shown in Figure 15.7. Most characteristics were taken from lunar regolith [92], and missing parameters were filled up by the properties of sand with 0% moisture content [93]. The source describes the derivation, arriving at the sinkage formula, shown in Equation 15.8.

$$p = \left(\frac{k_c}{b_w} + k_\phi \right) z_w^n \quad (15.7) \quad z_w = \left(\frac{3W \cos \theta}{(3-n)(k_c + b_w k_\phi) \sqrt{d_w}} \right)^{\frac{2}{(2n+1)}} \quad (15.8)$$

15.4.3. Traction

Motion is obtained by a combination of traction and rolling motion. For wheels that are not powered, there is no traction by definition since there is no longitudinal force acting on the contact patch. The maximum force a wheel can exert onto loose soil without slipping is denoted to be the maximum soil thrust H . The expression is shown in Equation 15.9 [93] and is in Newtons. It is represented as F_t in Figure 15.7. All parameters can be found in the nomenclature.

$$H = \left(c \left(\frac{\pi}{4} \right) \left(2\sqrt{(d_w - \delta_w) \delta_w} + \sqrt{(\delta_w + z_w)(d_w - \delta_w(1 - z_w))} \right) b_w + W_w \cos \theta \tan \phi \right) \left(1 - e^{-\frac{J}{K}} \right) \quad (15.9)$$

15.4.4. Soil Compaction Resistance

Soil thrust can be lost on irregular terrain due to the compaction of the soil in front of the wheel. It can best be visualised by treating the soil as a fluid rather than a solid, which is reasonable approximation for lunar regolith. The flow patterns of the dust particles that make up the regolith are shown in Figure 15.7 by grey arrows. A portion of the dust is pushed and compressed in front of the wheel, instead of being pushed backwards to provide soil thrust. Intuitively, it can be determined that the higher the sinkage, the higher the soil compaction resistance becomes. A simplified model assumes that the normal pressure on the submerged part of the wheel is equal to the normal pressure that would act on a rigid plate of the same area. This was validated by physical testing to be a trustworthy model for wheels up to 0.5 meters in diameter [94]. The relation is shown in Equation 15.10 and is a component of the F_r vector in Figure 15.7.

$$R_c = b_w \int_0^{z_w} \left(\frac{k_c}{b_w} + k_\phi \right) z^n dz \quad (15.10)$$

15.4.5. Bulldozing Resistance

The bulldoze effect becomes relevant once a substantial amount of soil is moved by the wheel itself, and should be taken into account when designing a lunar rover wheel. This effect becomes clear when referring to Figure 15.8 and is both a function of sinkage and wheel width, therefore making it important to optimise the wheel design to reduce the bulldozing effect. This can be reduced by inserting slots along the circumference of the wheel, similar to the groves on a car tire to mitigate the effects of aquaplaning. No mathematical model exists for these slots, but one slot is included in the final design as can be seen in Figure 15.10 on the most right image. The bulldozing resistance force is shown in Equation 15.11 to 15.15.

$$R_b = \left(\frac{b_w \sin(\alpha + \phi)}{2 \sin \alpha \cos \phi} \right) (2cK_c z_w + \gamma K_\gamma z_w^2) + \frac{\pi \gamma l_r^2 (90 - \phi)}{540} + \frac{\pi c l_r^2}{180} + c l_r^2 \tan \left(45 + \frac{\phi}{2} \right) \quad (15.11)$$

$$K_c = (N_c - \tan \phi) \cos^2 \phi \quad (15.12) \quad \alpha = a \cos \left(1 - \frac{2z_w}{d_w} \right) \quad (15.14)$$

$$K_\gamma = \left(\frac{2N_\gamma}{\tan \phi} + 1 \right) \cos^2 \phi \quad (15.13) \quad l_r = z_w \tan^2 \left(45 - \frac{\phi}{2} \right) \quad (15.15)$$

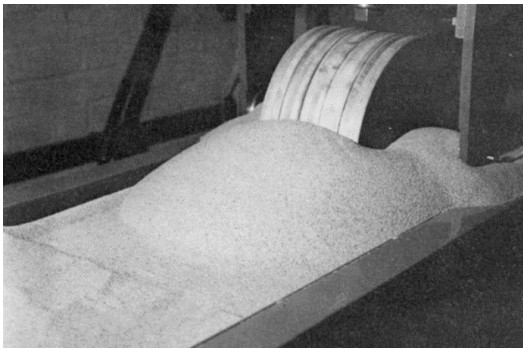


Figure 15.8: Bulldozing effect shown for a wide wheel with high sinkage and loose soil [94].



Figure 15.9: Small rover prototype testing in the lunar environment test bed at the University of Luxembourg [95].

15.4.6. Rolling Resistance

Rolling resistance is the effect of hysteresis on compliant wheels. Hysteresis is a phenomena which dissipates kinetic energy into heat due to the compliance of the wheel shape during a rolling motion. Generating an accurate estimate of rolling resistance is an involved process and should be tested to validate the estimate. It contains a lot of free variables such as slippage, material, speed, temperature and loading conditions. Wheel diameter and width also play an important role in computing f_r . It is however known that rolling resistance decreases for stiffer tires and increases for higher travelling

speeds [96]. Given that the rover will travel at velocities in order of a few centimeters per second and a metal wheel has a very high stiffness compared to any rubber tire, it can safely be assumed that the rolling resistance is negligible. Note that there are general misconceptions in rolling resistance, since it is commonly mistaken as the only resistance counteracting the motion of a wheel. In reality, this is not the case: it is the effect of hysteresis on compliant rolling wheels.

15.4.7. Gravitational Resistance

Letting the rover drive on an incline requires the motor to provide additional torque to overcome the gravitational force component. The terrain slope in the Sverdrup crater varies between 0° and 5° as shown in Figure 6.4. It was chosen to design based on the maximum slope instead of the mean, to guarantee that the motor is designed for this peak torque over a substantial time period. A layer of safety was placed in the design of the required power since more accurate mappings of Sverdrup are needed to design up to the limit. Therefore, the gravitational component of F_r is $mg \sin(5^\circ)$.

15.4.8. Wheel and Drive-train Design

To maintain a constant velocity, torque delivered by the motor should compensate for all impediments summed into F_r . That is, the free body diagram in Figure 15.7 has to be in force equilibrium to move at a constant velocity. One should note that the normal force does not apply at the symmetry axis of the wheel but slightly in front of it. This is due to the fact that more contact area is in front on the symmetry axis than behind, this is visualised by the red and green shaded area's. Since the assumption was made the normal force acts in the middle of the contact patch, it is therefore drawn by S_r in front of the symmetry line. This also slows down the wheel by creating a counteracting moments. Taking moment equilibrium around the center of the wheel, the torque required by the motor is $T = F_R \cdot (d_w/2) + N \cdot S_r$. To compensate for unforeseen obstacle that could be present in the crater, it is recommended to take a contingency on peak power and peak torque of at least 50%. The required torque is therefore 15.46 [Nm] per wheel. This is with the assumption of having all six wheels as *driving* wheels, i.e. all wheels provide traction and propel the rover forward.

The required battery power to move the rover can be calculated using the relation given in Equation 15.16. Taking an average measurement time of 10 hours and requiring a full rotation around the combiner per rover per measurement at the maximum baseline of 1 km, the average speed at which the rover will need to travel is approximately 0.1 meters per second. With a contingency of 50% too, this results in a required power of 10 Watts per wheel, a total of 60 Watts per rover.

$$P_{avg} = T \frac{2V_{avg}}{d_w} \quad (15.16)$$

Selecting the right drive-train configuration is one of the last steps. As mentioned before, all wheels should provide traction in order to limit the possibility of the rover getting stuck. To maximise the efficiency, torque motors shall be placed directly on the drive axle to limit mechanical transmission losses. The system characteristics of the chosen electromotors are shown in Table 15.5.

Table 15.5: DC electromotors for rover drivetrain¹²³.

Drivetrain electromotor	Value	Unit
Peak power	400	[W]
Average power	4	[W]
Mass (6 motors)	44.04	[kg]
Slot dimensions (w x l)	40 x 1400	[mm]
Motor dimensions (w x h x l)	60 x 105.2 x 79.5	[mm]

Table 15.6: Soil and wheel characteristics

Parameter	Value	Unit	Parameter	Value	Unit
m	166.7	kg	J/K	3	[-]
g	1.62	m/s^2	γ	1500	kg/m^3
θ	3	$^\circ$	z_w	4.82	cm
n	1.1	[-]	d_w	503.4	mm
k_c	0.1	[-]	b_w	278.8	mm
k_ϕ	3.9	[-]	δ_ϕ	0	mm
c	0.15	[-]			

These values have been deduced from already existing machinery and so could potentially be more optimised in a later phase of the design. Both systems are assumed to be operative only 1 percent of the time, hence the average power is 100 times lower than the peak power of the system.

Finally, this section is concluded by showcasing the final wheel design in Figure 15.10. The dimensions and regolith characteristics used for the calculations are summarised in Table 15.6. The wheels have small fins that have proven to increase soil thrust, but was not taken into account during the calculations since no mathematical models exist.

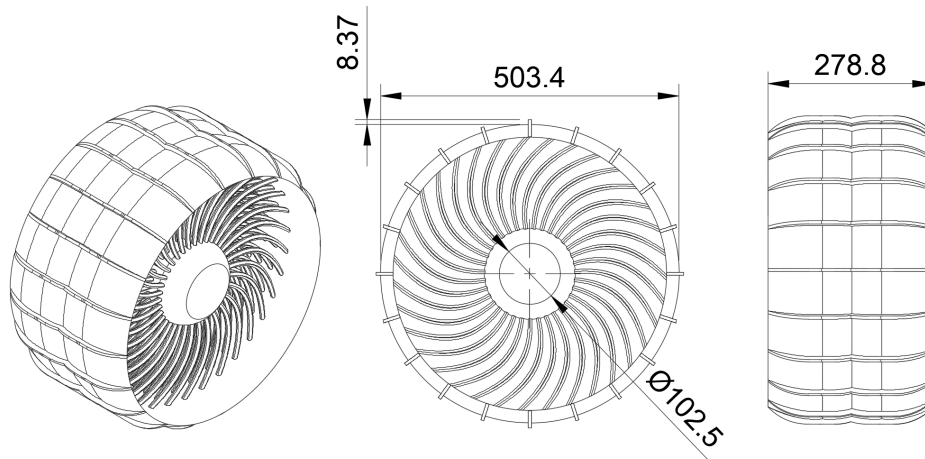


Figure 15.10: Technical drawing of one *driving* rover wheel with dimensions [mm]

15.4.9. Verification and Validation

After the complete analysis, the dimensions of the rover wheel were optimised for the lunar surface and are showcased in Figure 15.10. All the aforementioned formula's were integrated in a Python program after which the values for width and wheel diameter could be optimised. Rigorous inspection of the code was first performed as a first verification test. This procedure was followed up by performing unit tests and order of magnitude tests to see whether the output values made sense. Since the actual model of a wheel driving through very loose regolith would require a similar test setup as in Figure 15.8, a more complete validation test would be necessary to build a prototype of the undercarriage to validate its overall performance. The prototype could be analysed on an artificial lunar testing environment like the one of the University of Luxembourg. A figure of this test environment can be seen in Figure 15.9.

15.5. Dust-proofing

This section outlines a set of measures against the Lunar regolith dust. The top layer of Lunar regolith is a fine dust that can get kicked up when rovers drive over the surface or when a moonquake occurs. For this reason, a ballistic flight analysis was performed on the dust particles. Two causes that may kick up dust are the driving wheels or a moonquake occurrence. The results of the analysis are shown in Figure 15.11. It can be seen that for both cases, the dust does not travel higher than 0.26 meters above the surface. This means that critical areas such as the rover body and the telescope won't be affected.

¹Siboni PGB, *Planetary Gearboxes*, URL: <https://f.hubspotusercontent00.net/hubfs/7023002/CATALOGHI/NUOVI%20CATALOGHI%202020/Siboni%20PGB%20catalogo%202020.pdf?hsCtaTracking=ee78eeca-9eb2-4216-8395-20db7ac48f87%7Ccd17dc90-0835-473f-b2c3-fa7f3aee5ee6>

²Tolomatic, *Screw driven actuators*, URL: <https://www.tolomatic.com/products/product-details/mxe-p-screw-driven-actuators>

³RS online, *Servo motor*, URL: <https://docs.rs-online.com/a6fc/0900766b815ad6fe.pdf>

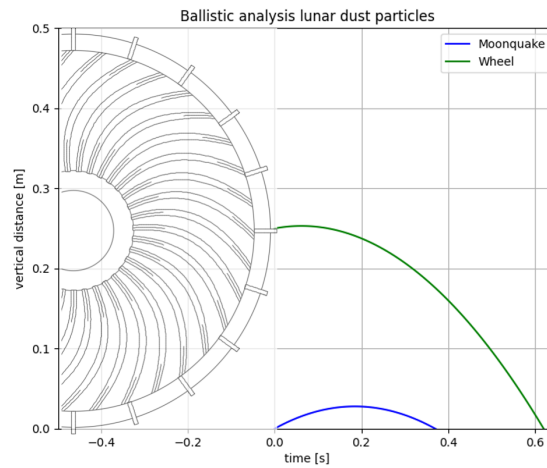


Figure 15.11: Ballistic analysis of lunar dust, wheel travelling at $0.1 [m/s]$, moonquake frequency of $21 [Hz]$

Two more lunar dust properties should be considered, micro-asteroid impacts and a perpetual surface dust cloud. Dust clouds are caused by electrostatic phenomena [97]. Estimates give the dust cloud a depth of about $30 [cm]$, found by measuring the Moon's horizon glow [98][97]. The cloud consists of nanometre particles. The cloud is low enough to not affect the mirrors or combiner, but could still stick to exterior surfaces like the body and heatshield due to the dust's electrostatic properties. During further developments, some form of coating could be investigated to prevent this. Although it is not deemed necessary.

Micro-asteroids range between $10 [nm]$ to $1 [mm]$ in size and impact the lunar surface at 10 to $72 [km/s]$, kicking up a 1000 times their mass in dust [98]. Assuming a random distribution in impact location, Sverdrup would be hit with about 1400 micro-asteroids over a five year period. The probability of a direct hit is negligible, estimated to be less than a hundredth of a percent over the extended mission. Still, the dust kicked up could reach the mirrors. Neither the dust coverage on the mirrors over time nor the decrease in optical performance with increased dust coverage were investigated for this report. As such, the frequency of mirror cleaning has not been determined. Pending further investigation on this, three solutions to clean the mirrors are presented:

- Low frequency: astronaut cleaning. As astronauts would be able to visit the site to perform maintenance. Cleaning the mirrors could form part of this maintenance.
- High frequency: automated cleaning mechanism. An electromagnetic device [99] could be mounted on a 2d linear actuator above the mirrors. The device would then pass over the mirror and remove the dust.
- Passive: mirror surface treatment. If compatible and not damaging to the system's performance, a layer could be added to the top of the mirror that reduces stiction [99]. The mirror could then be rotated, allowing the dust to fall off.

For the remainder of the system, the following dust proofing methods should be used:

- In general, the rover and combiner encasings should be sealed. Where necessary this can be done with sealed or closed bearings.
- External components such as the bottom facing cameras on the rover should include a mechanism to clean them independently.
- The heatshield and baffle have a secondary purpose of protecting the mirror from kicked up dust. The heatshield extends out wider than the mirror diameter.
- The rover should be held static for a time between stopping and pointing to allow the dust to settle. This serves to minimise dust on the mirrors.
- Combiner inlets will contain covers which only open during measurements.

16. System Characteristics

This chapter describes the characteristics of the SALT system. The communication flow diagram is shown first, followed by the electrical characteristics; these can be visualised in the accompanying hardware diagram. The section is closed with a data flow and software diagram, representing the data flow through the system.

16.1. Communication Flow Diagram

Successful communication is vital to any long distance mission. The communication diagram shown in Figure 16.1 presents the communication lines of this mission. As can be seen, the operation site and the scientists are connected by a relay system.

The graph shows that observation requests from scientists must first be proposed to the internal scientists. If the proposal is accepted it is sent to the operators, who command the system to perform the operation. The command is transmitted via the relay system and reaches the core computer, which autonomously sends the different instructions to the correct subsystems.

If a signal is to be transmitted to Earth, it crosses the relay in the opposite order and reaches the operators. The signal is then separated into observation data and telemetry. The former is redirected to a database, where it is accessible to scientists, and where it will be processed and added to the FITS file database. The latter is sent to the telemetry database, which is accessible to SALT operators only. If the telemetry reveals a failure, the astronauts might be deployed to perform maintenance, which requires notifying the relevant space agencies, such as NASA.

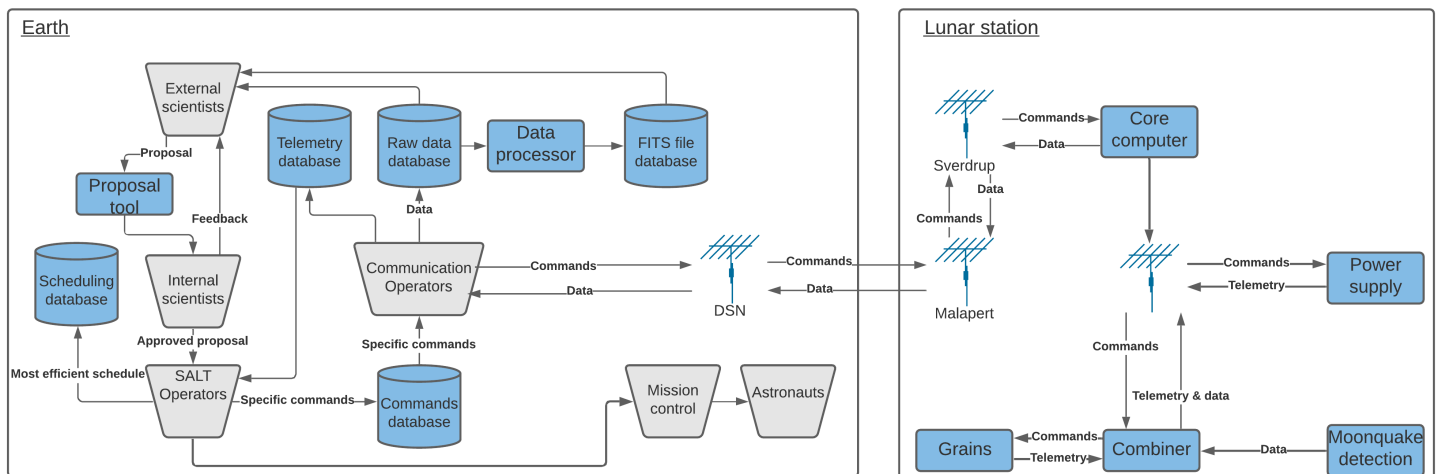


Figure 16.1: Communication flow diagram of the SALT mission.

16.2. Hardware Diagram

A diagram is presented in order to simplify the relations between different elements of the system. The hardware diagram shown in Figure A.1 presents the internal structure related to the communication

and electrical subsystems of the mission elements (the rovers, charging stations, combiner, etc.). It displays the relationships between the main elements of the system, such as the communications lines, powerlines and optical lines. The communication network is subdivided into an inbound and outbound flow as a means to improve clarity. These also include wireless connections.

16.3. Data Flow and Software Diagram

Figure 16.2 describes the data flow through the different components of the system. The figure is useful in that it can also be used to determine what software needs to be developed for the mission.

Scientists can interact with the observation data through a web server, similar to the existing VLTI systems [100]. Observation data that is not frequently used is stored in the archival database. All commands and the data returning from the telescope is sent using RF 4. RF-[X] refers to an antenna and its surrounding equipment, and RF 4 specifically refers to a Deep Space Network antenna.

The Malapert communication station on the Moon is used to relay data from Sverdrup to Earth and the other way around. Observational data that has to be sent to Earth will be buffered on Sverdrup so that all the data can be sent from this location directly. As previously mentioned in Chapter 13, the observational data size will be in the order of hundreds of megabytes, depending on the detailed configuration of the detector. Telemetry data is expected to be of a smaller size and can be sent more often at a lower data rate depending on ground station availability. Any commands from Earth will be sent from Malapert to the Sverdrup ground station, at the crater rim, which in turn relays the commands to the combiner. Here, commands are processed and prioritised before being sent to the rovers and power supply station. Astronauts can also interface with this ground station should any complications or emergencies arise.

Once the rover has received the commands it will store them in a queue. These tasks can then be performed once the rover has completed its current operation. The nominal tasks will consist of driving to location and pointing the mirror at a certain location. These tasks will be accomplished through a control loop using location sensors and drive electronics. This is elaborated upon in Section 14.2. The rover will also read out the telemetry of all its own systems and send the relevant data back to the Sverdrup ground station via the combiner.

Lastly, the collector and its subsystems will receive commands from the Sverdrup ground station and put these in a tasks queue. These tasks will include tasks such as readout patterns of the detector, integration time and instructions for the thermal subsystem of the collector. The observational tasks will command an ASIC similar to the SIDECAR on the JWST [101]. Any pre-processing will also be done in this subsystem before the data is sent back to Earth via the Sverdrup ground station. There will also be an algorithm in place to put the system in hibernation mode when lunar quakes occur.

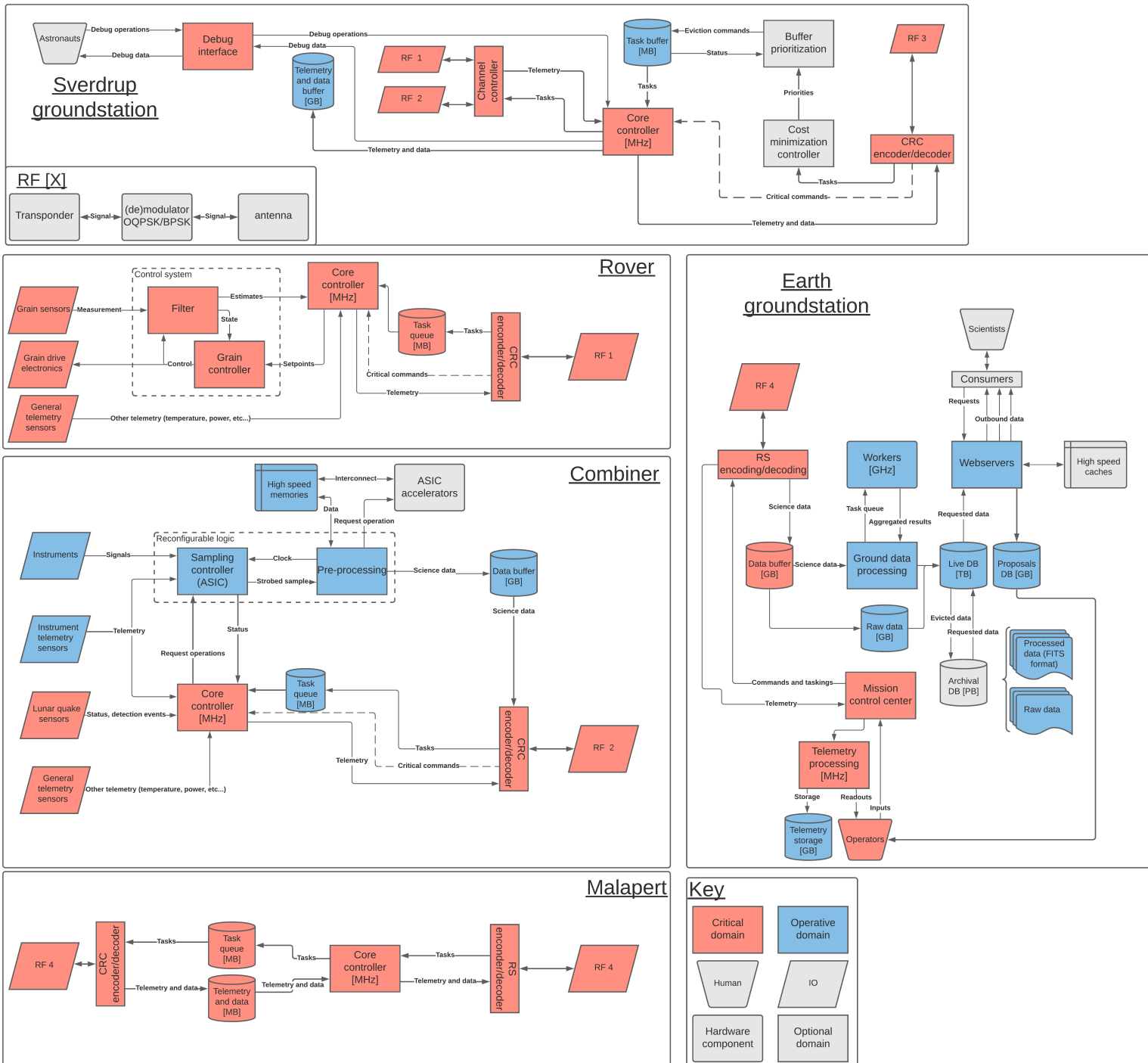


Figure 16.2: Data flow and software diagram of the SALT mission.

16.4. Electrical Characteristics

The electrical subsystem has many elements with interconnecting relationships. The electric diagram in Figure 16.3 presents these relationships in a clear and intuitive way. It shows whether each element uses low or high voltage, and whether they are powered by batteries or solar power — with the possibility of them being powered by both. The low voltage blocks require a voltage converter, but this is not reflected in the diagram. The high voltage will be 28.8[V] while the low voltage will be any system that require less than that. Lastly the very high voltage will be around 3[kV].

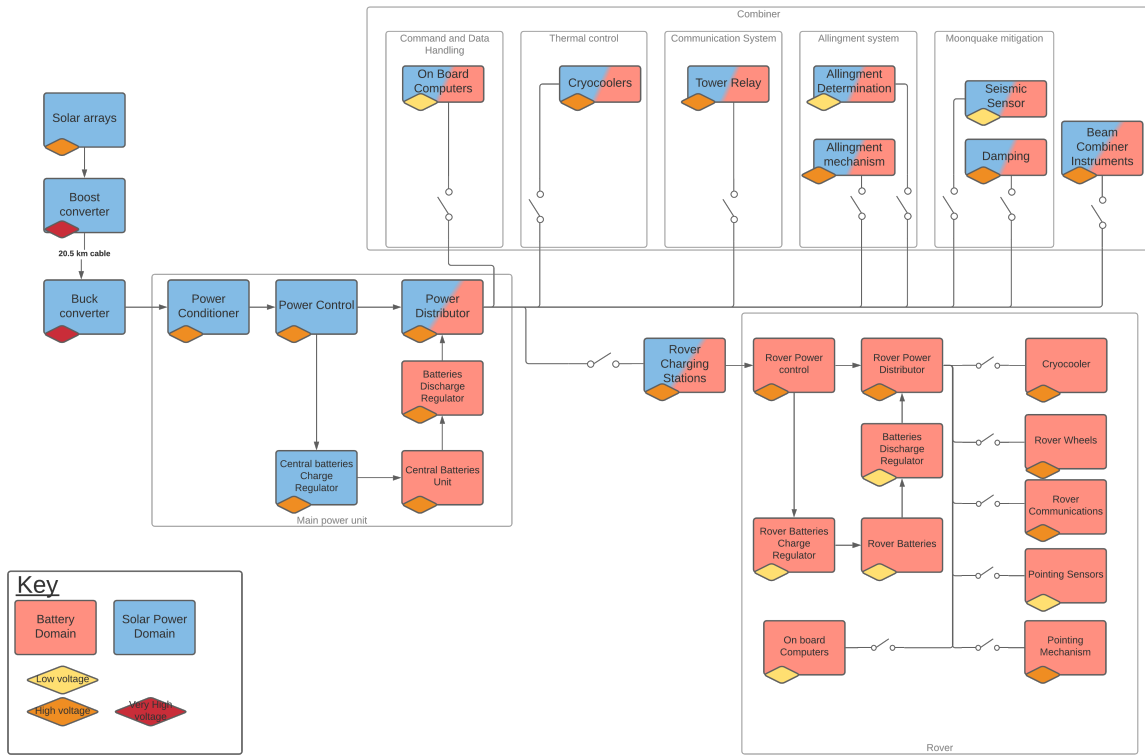


Figure 16.3: Electrical block diagram of SALT on Rovers

17. Project Characteristics

This chapter describes the characteristics of the project as a whole. Section 17.1 describes the plan for manufacturing, assembly, integration and testing. Section 17.2 describes the characteristics of the operations site. The installation plan is discussed in Section 17.3. The operations and logistics are discussed with the use of a diagram in Section 17.4. An N2 chart is presented in Section 17.5 to show the interaction between subsystems. The next steps of the SALT mission are discussed in Sections 17.6 and 17.7 with a diagram and a Gantt chart. Environmental sustainability is discussed in Section 18.1. Followed by economic and social sustainability, which are presented in Section 18.2 and Section 18.3, respectively.

17.1. Manufacturing, Assembly, Integration and Testing plan

The manufacturing, assembly, integration and testing plan of SALT is summarised in Figure 17.1. As shown, the subsystem parts can either be manufactured or bought from a provider; the details of how each part will be produced will be decided on during the detailed design phase. Each part will be checked and tested to see if they meet their requirements. After that, the subsystems will be assembled and tested to validate that they meet their requirements. Once the subsystems are validated, the complete system elements can be assembled into the final product, which can be tested as part of its launch certification process. If any of the tests fail up to this point, either some parts will have to be remade or design changes will be performed.

Once the system is launched, it will be transported to the Moon and assembled. The installation of the system on the lunar surface is further explained in Section 17.3. Three tests will be performed during the assembly on the surface. The first one will be performing visual checks of the system elements, to see if they were damaged during transportation. The second one will be testing the communication channel once it is assembled. And the last one is testing if the system as a whole is functioning. Failing any of this tests will require a repair mission.

17.2. Operations Site Characteristics

The Sverdrup crater landing site was chosen for a number of reasons, but primarily for its moderate slope, the constant darkness within the crater, and the constant sunlight and ease of communication from the crater's rim.

Unfortunately, not many details are known about the terrain inside the crater, given that LOLA's data does not possess enough resolution to draw conclusions about the density and size of potential boulders. What is known, however, is the slope of the terrain within the crater. Figure 17.2 shows the slope of the crater as derived from the LOLA measurements. The figure clearly shows that the slope throughout the crater is manageable, even allowing for navigation in and out of the crater with a slope of less than 15°. This is suitable for operations, as the assembly of the whole system shall require transporting material from the inside of the crater to the outside. Not shown by the figure is Malapert mountain, the mountain on which the main communications antenna is

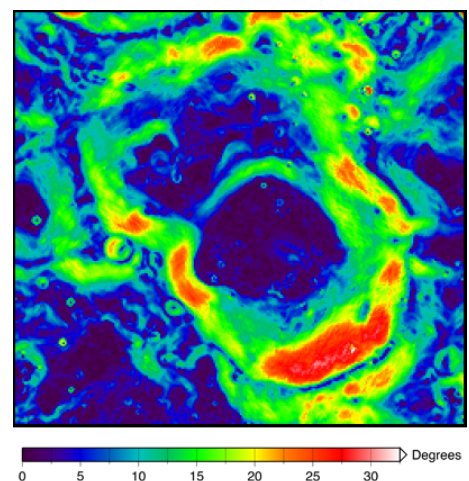


Figure 17.2: Slope map of the Sverdrup Crater¹.

¹Lunar Orbiter Laser Altimeter - URL:
<https://lola.gsfc.nasa.gov/feature-20110705.html>

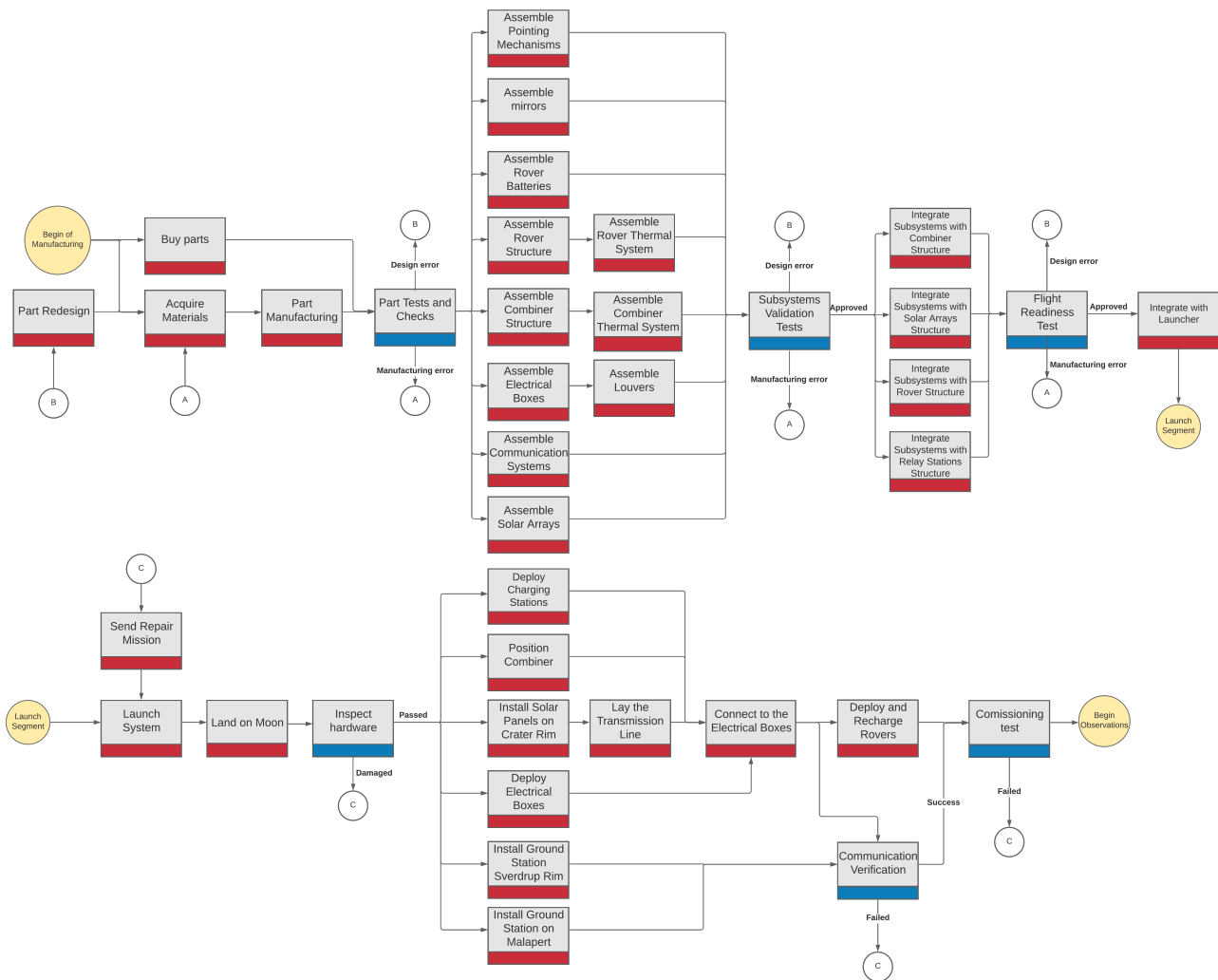


Figure 17.1: Diagram of the Manufacturing, Assembling, Integration and Testing plan.

to be located. This specific location presents a challenge in that its pronounced slope of 25° makes it hard to navigate. However, due to the presence of other missions in the operations area, facilities may be in place on the mountain that would allow for communication before SALT is even deployed.

17.3. Surface Installation Plan

Once the landing has been complete, the operation can proceed to the installation phase. This phase depends heavily on the labour of astronauts from nearby bases, which shall have to rendezvous with the lander in the crater, collect the communications relays, solar panels and cable, and install them.

The solar panels shall be installed on the rim of the crater, such that they are located on a PEL. Their installation will follow these steps:

- The star trackers shall be installed on the rovers; these do not come installed beforehand due to launch constraints. This should not require more than putting them in place and plugging them in.
- The cryocooler for the combiner shall be deployed on the ground near the combiner itself, at a distance of a few meters.
- The rover charging stations shall be deployed near the combiner. These will require no assembly

to operate and will only require plugging into the power system.

- The solar panel shall be ferried over to the Peak of Eternal Light on the rim of the crater — three routes leading in and out of the crater are provided in Figure 17.3 — and installed there; the cable connecting the solar panel and the rest of the system shall be deployed over the edge of the peak and connected to the solar panel.
- The astronauts shall return to the operation site and plug in the solar power cable into the electric box, then cover the box in regolith in order to reduce its emissions. They shall then get the antennas.
- The antennas will be installed outside the crater. The first shall be installed on the rim of the crater and act as a relay. The second shall be installed on the peak of Malapert mountain, and will have constant contact with the Earth.

One thing worth noting is that there is a distinct possibility of one of the existing missions making use of an antenna on Malapert mountain. If that were the case, the installation of the last antenna might be unnecessary, depending on the relationship between SALT and the potential mission. Figure 17.3 illustrates all the steps involved in the installation process and shows their respective position in and around the crater.

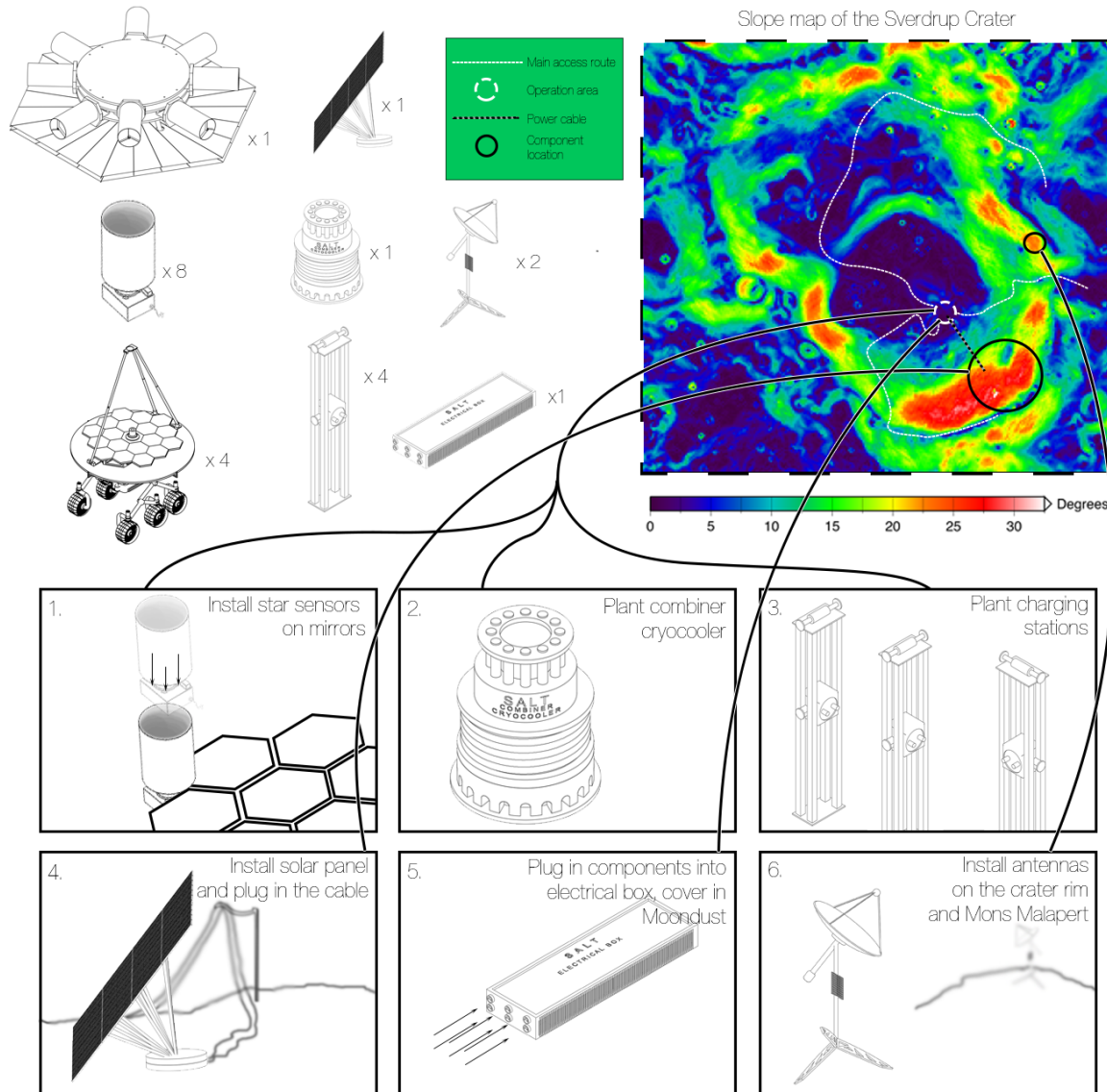


Figure 17.3: Installation plan step-by-step manual

17.4. Operations and Logistics Diagram

The operation logistics of the mission are presented in Figure 17.4. The purpose of this diagram is to show the interactions between different mission elements and external parties, and their influence on the SALT mission. The operation space has been separated into operations on Earth, Space, the Moon, and cooperating companies — the latter mainly being a collection of external parties on which the mission depends.

Starting at the initial design proposal, on the left-side of the diagram, components will be manufactured and tested. If the design proves to be unable to perform the mission, then it has to be iterated until a satisfactory product is delivered. This product will then be launched via SpaceX's Starship and transported to the Moon's surface. From there, the relay station will have to be installed on Malapert mountain and the observation station on the Sverdrup crater, both with the use of astronauts. If the setup is completed, the start-up procedure can begin and the mission can start switching on the equipment and establishing communication with Earth. Once this has been finished, the scientific payload is ready to begin its operation cycles. The lunar operations team will determine whether or not the system is properly functioning and if the system has to endure special environmental conditions. In the case of failure the astronauts will have to visit the equipment again for repairs. If none of these are the case, the system can perform the nominal operations, such as generating power, performing observations and communications, as well as scheduled maintenance and moonquake detection. After this, the system will loop back to normal operation. If the operation cycle is concluded the end-of-life phase begins: the lunar elements will be disassembled and separated into reusable components and components for storage. These will be used by the astronauts or will be moved to the lunar base of the Artemis mission, respectively. Lastly, the diagram includes the communication system. This system interacts with the mission elements by allowing contact with the observation equipment as well as requiring maintenance from astronauts.

It can be concluded from the figure that the astronauts perform a crucial part in the mission operations and logistics. This is seen from their central position accompanied by numerous arrows relating them to different mission elements. Therefore, the cooperation with the Artemis mission and NASA as a whole must not be underestimated.

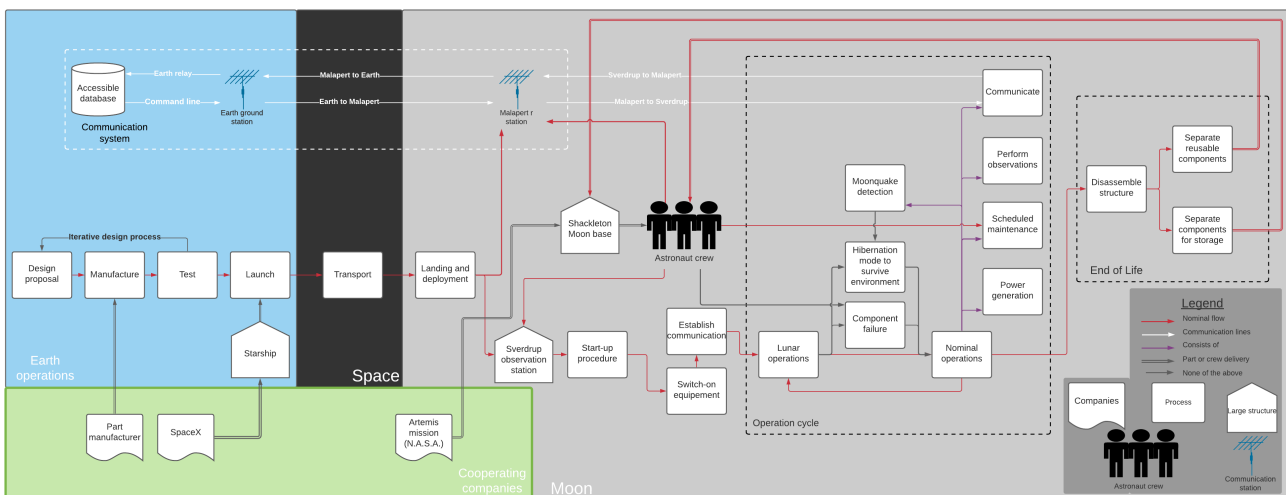


Figure 17.4: Operations and logistic flow diagram.

17.4.1. Maintenance

During the span of the mission astronauts will have to perform both scheduled and unscheduled maintenance. Points of access to the Sverdrup crater and Malapert mountain need to be found, for either type of maintenance to be possible.

A study of the VIPER mission by NASA proposes a direct journey to the Sverdrup crater from the Shackleton crater[102], shown in Figure 17.6. Note that this map shows the slope of the terrain, not the altitude. An altitude graph of the local topology is shown on the left. It can be seen that the proposed route covers the Sverdrup communication station on the way to Sverdrup crater (near Site 004) in Figure 17.6, and once on the crater floor proceeds to stay close to the rim due to its mission objective. Naturally, the astronauts will move towards the observation location to perform the necessary tasks. The maintenance tasks will mostly involve the mechanical parts of the system, such as the wheels or damping system, given that much of the equipment of is designed not to fail during the life of the mission and requires special tools/material to restore.

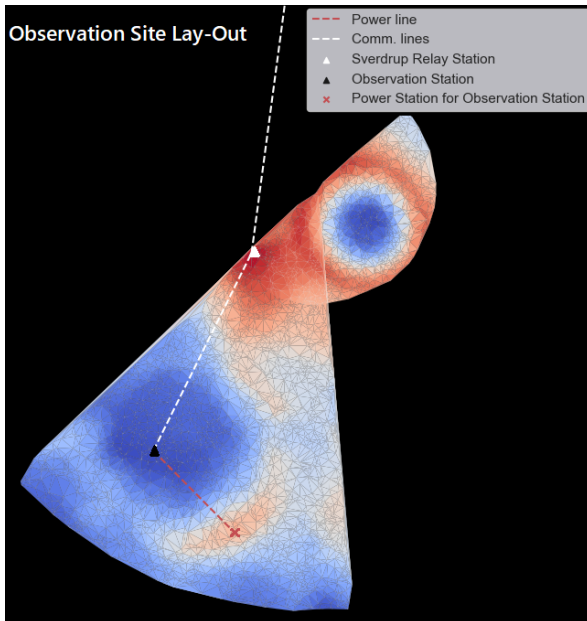


Figure 17.5: Lay-out of the observation site.

The astronauts will need access to the power station. This achievable by meeting the VIPER journey at 432, climbing out of the crater and moving to the station from there. Alternatively, it can be done by moving further down and going around the elevated part of the crater rim to enter the power station. Both options are illustrated in Figure 17.7.

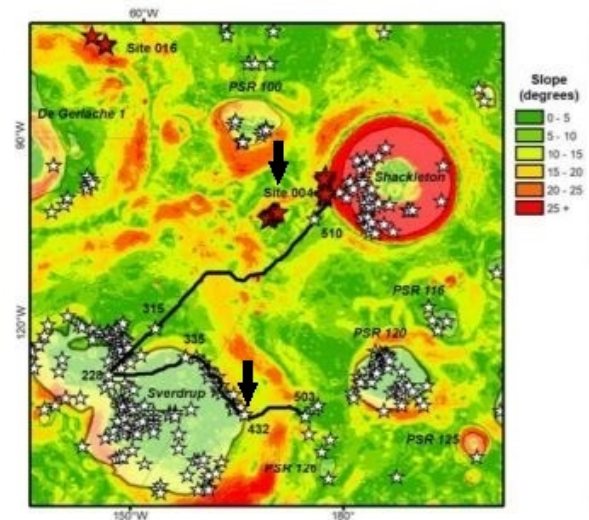


Figure 17.6: Proposed journey for the VIPER rover.[102]

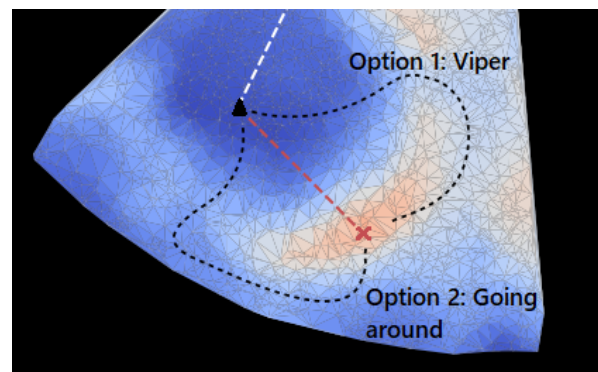


Figure 17.7: Traverse options to the power station.

The last consideration is the antenna on Malapert mountain: this is the farthest journey the astronauts will have to embark on, and will therefore be avoided when possible through clever design. The setup is designed to be as simple as possible, in order to avoid unexpected failures. The system consists of two small antennas, a light pointing system, a computer, solar panels and a beam structure. Due to the absence of complex systems it could be designed not to require any scheduled maintenance throughout the life time of the rovers, especially with well-placed redundancy. Since Malapert mountain is already being studied for communication systems with the Shackleton crater, the Artemis mission might utilize a relay system such as SALT's. The astronauts might thus already be familiar with the journey and have their own routes and procedures.

Unscheduled Maintenance Procedures

Apart from the unknown frequency of unscheduled maintenance events, the cause of failure may also vary from case to case. Fast repair procedures have to be established, in order to limit the impact of an unexpected component or system failure. The most complex system of the mission is the rover, and is therefore the most likely candidate for failure. Events such as a mechanical failure, being stuck due to lunar dust, or rough terrain and equipment failure can all bring the mission to a halt. Because of this, the rover is equipped with various tools to autonomously investigate any issues. The most useful tools for the scientist and operators are the Lidar and Hazcams, the latter also used by the Perseverance rover [53]. The Hazcams are located at the bottom of the rover bus, and are able to capture images of the wheels and terrain and send them back to the scientist on Earth for investigation. The Lidar is used mainly for autonomous navigation. Both the hazcams and Lidar store information up to the failure event, and are able to transmit data back to Earth in order to simulate the situation to determine the origin of recurring problems². The rovers transmit telemetry for internal components as well, so that scientist on Earth have various ways to investigate the problem and set up a plan accordingly. The operation plan is then communicated with the astronauts and executed. The procedures for other components, such as the combiner and relay station, are similar in nature but do not employ the additional camera equipment.

17.5. Subsystem Relations in N² Chart

Concurrent design allows for multiple subsystems to be designed at the same time. To facilitate the next steps in the design process, the subsystem design interactions must be well-defined. The N2-chart helps visualise a subsystem's required inputs and its produced outputs. This reveals where iterative processes will be required in the design. Each yellow box is a function on the lines there are the outputs of that function and the columns show the inputs for that function.

The interfaces between subsystems is shown in Figure 17.8. Most of the subsystems only require information to flow down from other subsystems design. The only two cases that require an iterative process are thermal with power, and structures with motion. Thermal outputs its average power consumption, which influences the size of the solar panels and batteries, which in turn increases the demand on the thermal control to keep these elements warm, thereby increasing the average power; clearly, an iterative process is required to size these subsystems. The system's structure depends on the size of the motion mechanisms, while the motion mechanisms depend on the system's mass and total moment of inertia; once more, an iterative process takes place between these two.

17.6. Project Design and Development Logic

The project will follow similar design phases as defined by ESA.³ This report corresponds to Phase A of the project, and aims to show that building this telescope on the Moon is not only feasible, but also facilitated by different space agencies' renewed interest in the exploration of the Moon.

Since the study was not conducted by a space agency, an extra phase was added in the project plan, during which the project is pitched to space agencies in hopes of a signing a contract. Phase B is initiated afterwards, during which the preliminary design takes place and the necessary technology is developed. It is followed by Phase C, during which the detailed design takes place, building on the preliminary design. The testing of the system begins during Phase C, and carries on into the next phase. Phase D encapsulates the production of the system, during which more testing is carried out to validate the system, such that all requirements are met. Once the certification for launch is granted, the system will be mounted on the launcher and transported to the Sverdrup crater. Phase E corresponds to nominal operations, and Phase F to the end-of-life. The whole project design and development logic is summarised in Figure 17.9.

²The technical data of these cameras is described in Chapter 13

³ESA - How a mission is chosen - URL: http://www.esa.int/Science_Exploration/Space_Science/How_a_mission_is_chosen

Input ↓ Output ←	Optical instruments	Generated data	Required pointing precision	Survival temperature range Operational temperature range Generated heat	Average power Peak power Minimum battery time (exposure time)	Allowed oscillations Subsystem dimensions Moment of inertia		
	Command, Control and Communications	Interest area to point	Survival temperature range Operational temperature range Generated heat	Average power Peak Power	Subsystem dimensions Elements moment of inertia			
	Telescope pointing	Attitude Control and Determination	Survival temperature range Operational temperature range Generated heat	Average power Peak power	Subsystem dimensions Elements moment of inertia			
			Thermal control	Average power	Subsystem dimensions Elements moment of inertia			
			Survival temperature range Operational temperature range Generated heat	Power subsystem	Subsystem dimensions Elements moment of inertia			
					Structures & Mechanisms	System mass Total moment of inertia		
			Survival temperature range Operational temperature range Generated heat	Average power Peak power	Subsystem dimensions Elements moment of inertia	Translation mechanism		
	Observable space	Communication window Distance to permanent line of sight location	Maximum visible angle	Surface temperature Solar incidence	Distance to location with sunlight		Surface roughness	Location

Figure 17.8: N² chart of the subsystem interface.

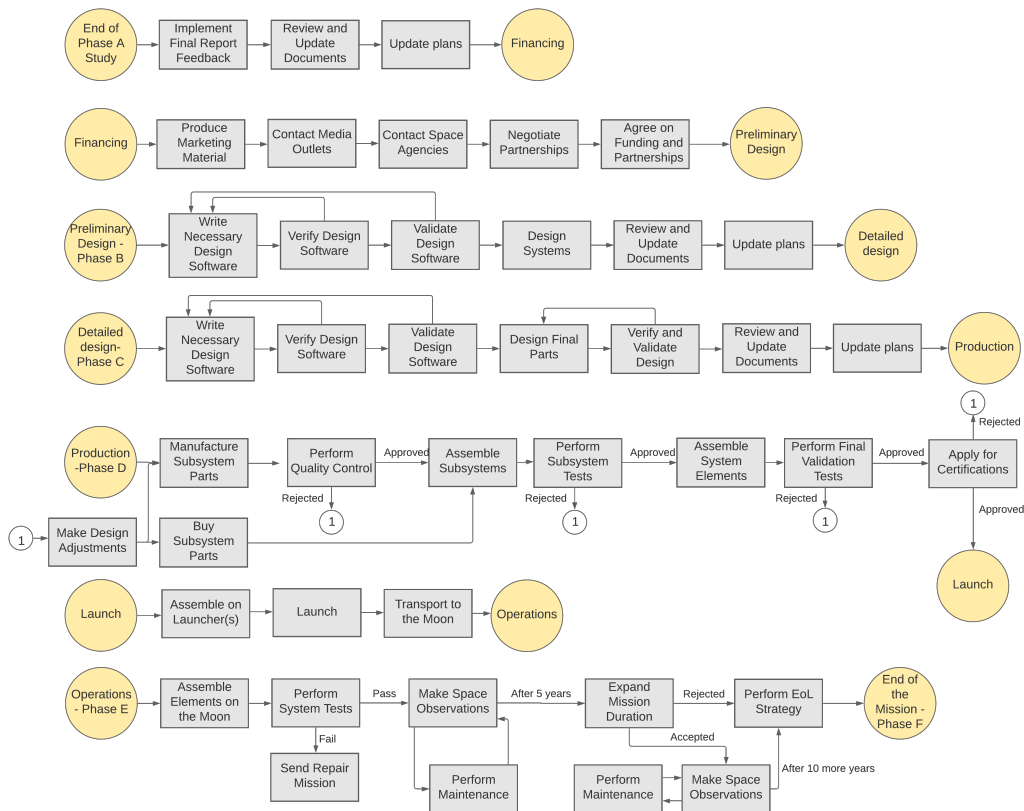


Figure 17.9: Project Design and Development logic diagram.

17.7. Project Gantt Chart

Figure 17.10 shows the complete Gantt chart for the project: the blue stripes represent individual tasks, and the burgundy stripes represent project phases. Note that the End-of-life section is yet to be determined; this is due to the possibility of the mission being extended for ten years, as per requirement **SALT-SSYS-SCH-01**: *The extended mission, including potential upgrades and repairs for less than 20 [%] of the total launch mass, should last for another 10 years.*

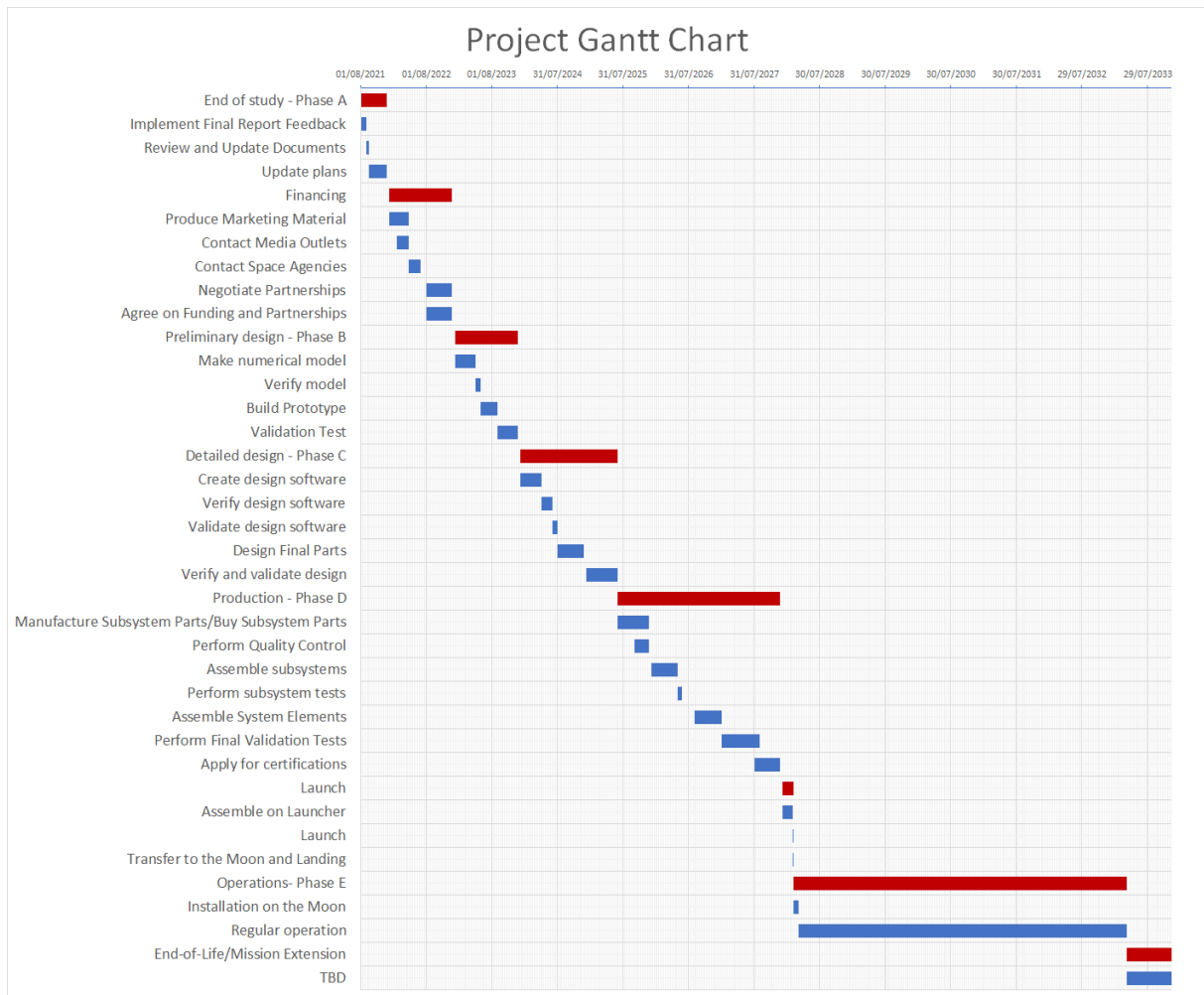


Figure 17.10: Project Gantt Chart. The major gridlines represent a year, while the minor ones represent a week.

18. Sustainable development strategy

The implementation of a sustainable development strategy is a vital necessity for well-being of the design group and the stakeholders, as well as present and future generations. Sustainability stands on three pillars: environmental, economical and social. In this section, these three pillars are addressed from the perspective of the SALT mission. First, environmental sustainability is discussed in Section 18.1. Followed by economic and social sustainability, which are presented in Section 18.2 and Section 18.3, respectively.

18.1. Environmental Sustainability

Integrating environmental sustainability into a space mission is a challenging task. The SALT mission takes a completely different approach to implementing environmental sustainability. It is through the philosophy of 'lean manufacturing'. This philosophy essentially aims to deliver value to the customer at minimal waste. Given that in a space mission most of the resources are devoted to the design phase, it stands to reason that this method would be preferred over an alternative, such as using sustainable materials. After all, the spaceflight industry is always pushing boundaries in product optimisation. Although the SALT mission values sustainability, implementing different manufacturing techniques and materials that are deemed more sustainable is counter-intuitive. The SALT mission did not consider environmental sustainability in the concept trade-off for this very reason; it was simply not worth incurring penalties on criteria such as precision and weight for a structure using as little material as it does — after all, only one telescope will be built, and the material consumption is negligible as a consequence, especially when compared with some mass-produced products. The environmental aspects of the mission, negligible as they might be, have been foregone for the benefit of social sustainability: the potential discovery of life on other worlds, and all the social ramifications that come with it, outweighs any potential damage to the environment that could be caused by this mission.

18.1.1. Lean Manufacturing

The main principles of lean manufacturing are [103]:

- Eliminate waste
- Identify value
- Generate flow

The process of waste elimination involves way more than that of material waste. It also stands for waste of time, knowledge, resources and more. Value is equally broad in its definition: it refers to the use the final product has to society, and if a production step does not add value it is considered waste. Where value identification focuses on detecting the valuable parts, waste elimination focuses on reducing the valueless parts. These form the first two principles on the list. The last principle is flow generation, which revolves around the design and development process. It tries to keep the process 'flowing' by having as many simultaneous processes going on as possible, instead of sequential ones.

The implementation of this philosophy can be done by a group of consultants that are part of the team. This ensures that the implementation remains flexible and is not forced onto the team. Any further details on the breakdown will be investigated in further research.

18.2. Economic Sustainability

The second out of three pillars of sustainability is that of the economy. A mission like this is only valued if it can contribute to the economy. SALT does so in two ways: the first is the fact that a large portion of the budget goes into R&D, meaning that not much value is gone to waste into material, and is instead put into society by creating jobs.¹ In this way the economy is stimulated both in mission planning and execution, where human support is necessary. Additionally, the project output generates value as well. Not only will the results stimulate new scientific research, but the results themselves carry value. Improving our knowledge on exoplanets could also advance new technologies, which is also economically sustainable. Given all of the above, this mission can easily be recognised as economically sustainable.

18.3. Social Sustainability

Social sustainability measures to what extent this mission provides value to society. The mission affects society in both tangible and intangible ways. The space industry has been known for creating spin-off technologies that are now used in society and can support social sustainability in this way². Additional benefits manifest as the advancement of workforce development and industrial capabilities.

The SALT mission has many beneficial effects: out of these, the hardest to quantify are those that affect the nature of our lives. The SALT mission can inspire young people to pursue careers that advance the forefront of technology and push the boundaries of our knowledge. Additionally, the mission might help in building international trust and relationships through cooperation in the shared exploration of new frontiers [104]. The excitement for the journey to worlds beyond can be dated back to the sixties when over 600 million people watched the Apollo 11 landing, which back then was over one fifth of the global population³. Clearly, space exploration stirs the imagination, and brings out the best in Man. After all, *"Imagination will carry us to worlds that never were, but without it we go nowhere."*⁴

¹ESA, *Job creation and growth with space* - URL: http://www.esa.int/Applications/Observing_the_Earth/Job_creation_and_growth_with_space

²Jet Propulsion Laboratory, *20 Inventions We Wouldn't Have Without Space Travel* - URL: <https://www.jpl.nasa.gov/infographics/20-inventions-we-wouldnt-have-without-space-travel>

³NY Times, *The Apollo 11 Mission Was Also a Global Media Sensation*, URL: <https://www.nytimes.com/2019/07/15/business/media/apollo-11-television-media.html>

⁴Carl Sagan, *Cosmos*, 1980

19. Sensitivity Analysis

A sensitivity analysis was conducted to quantify the robustness of the feasibility of the final design, i.e. how feasible the rover design is once design parameters are changed. Since SALT is a first-of-its-kind project, some of the design parameters can change by large amounts due to unforeseen problems that might arise at a later stage. Therefore it is important to quantify what these effects are.

Per subsystem, the feasibility of the design due to hypothetical changes is quantified. Furthermore this chapter will investigate whether any changes might cause the design to not fulfil the requirements presented in Section 5.3.

19.1. Operation Location

The operation location is dependent on many factors, but only one of them stands out as one that could influence the mission: the terrain. Currently, not much is known about the terrain in and around the Sverdrup crater. The data that is available is limited to little more than altimeter data and temperature measurements. While this does provide some idea of what challenges one may face, the resolution of these data does not allow one to determine the challenges to navigation that the terrain could pose. Boulders, lunar dust and ice could all prove to be a major challenge to the rovers and the astronauts installing the system. These problems have also been identified as risks in Section 4.3. If it were found that the terrain in the area is still too rough, or that there is too much dust to navigate, the entire rover structure might have to be redesigned in order to cope with these new challenges.

19.2. Optics

The set optical system parameters such as mirror diameter are relatively sensitive to requirement changes, but are also very flexible. An increase in the maximum SNR requirement (currently **SALT-SSYS-SENS-04**) would lead to a larger mirror design, but would not invalidate the current work. The lower SNR requirements do not have an impact at this stage, as the optical model evaluates the lowest SNR band of each planet to remain conservative in the face of incompletely characterised planets. As the optical model is refined it may also be found that significant SNR increases can be supported within the current design. **SALT-SSYS-SENS-11** was easily satisfied with the existing design. A change in this requirement will have little impact on the design of SALT from the perspective of the mirror sizing or optical architecture. **SALT-SSYS-SENS-01** is directly correlated to the baseline. With current baseline requirements this requirement is easily satisfied, however an increase of this resolution by more than factor 2 will require a revision of **SALT-SSYS-MECH-01**.

The optical subsystems performance is also tied to the performance of the pointing subsystem. The number of planets that can be observed is largely a function of how many planets are in SALT's field of regard. If this is reduced significantly, so will SALT's performance. However, the optical model was evaluated with a 60° pointing angle, whereas the pointing system should provide (90°) of pointing (Chapter 10). This should provide sufficient isolating margin for the optical subsystem.

19.3. Pointing

The pointing system is dependant on a number of variables, which all all prone to change. In order to detect any possible hinder from these changes on the pointing system a sensitivity analysis is performed.

The compliant mechanisms solely depends on the weight of the mirror and therefore is not very sensitive to change. Current estimates take into account a 20% safety margin on the mass of the structure

that is carried and would allow a weight increase of 47 [kg]. Any larger increase would require recalculation of the mechanisms characteristics, but would not be detrimental to the design solution. A say on the limitations of a compliant mechanism is difficult as no studies have yet been conducted on this.

The rough pointing system is already more dependent on other subsystems than the compliant mechanism. The actuation system does not only depend on the mass of the system, but also the size of the mirror, radiation shield, bus and wheel base. The mirror and radiation shield limit the system in rotation. Any mirror diameter over 3 [m], under current bus and wheelbase size, would not be capable of rotating 60 [degrees] as the mirror would hit the wheel dampers. Increasing the bus width or wheel layout could resolve these issues, but in order to quantify this increase one would have to resolve a multi variable problem. Overall the rough pointing design is not a very robust one, but is one that is specifically designed for the current design solution. It is therefore a very efficient solution.

19.4. Thermal

A Monte Carlo simulation for sensitivity analysis was performed on both Simulink thermal models. Parameters whose values are not fixed in these stages of the design were given a uniform distribution of a range of possible values. Then, random samples of these parameters were combined and used on the simulations to create M different scenarios for thermal control. The average required power of all scenarios is the expected value. The standard error was calculated as the square root of the sample variance, divided by the numbers of scenarios. The bias was calculated as the difference of the average when increasing M by a factor 10.

Table 19.1: Required cooling or heating power 99.9% confidence intervals, calculated using Monte Carlo simulation and fluctuating Moon temperatures. Bias is the difference between the expected value of $M=10^5$ and $M=10^4$.

Name	Power difference $M=10^3$		Power difference $M=10^4$		Power difference $M=10^5$		Bias
	Lower bound	Higher bound	Lower bound	Higher bound	Lower bound	Higher bound	
Combiner cooling	0.40	0.43	0.41	0.42	0.41	0.42	0
Mirror cooling	1.27	1.37	1.29	1.33	1.31	1.32	0.005
Rover bus cooling	37.68	41.25	38.60	39.80	39.18	39.54	0.16

As can be seen from Table 19.1, the confidence bounds of the combiner and mirror cooling powers are very narrow. This shows that the sensitivity of the model is low, which means that small changes to input parameters do not change the output drastically. As the number of scenarios increases to $M = 10^5$, the confidence bound decreases. Even more simulations would narrow the interval even more, which again shows that the model has a low sensitivity, which is desirable. However, when analysing the required mirror cooling values, it can be seen that this falls just outside of the confidence interval. The reason for this is not known and needs to be further inspected in future design phases. Luckily, the other cooling powers do exist in the confidence interval.

19.5. Power

The power system is very sensitive to the required power consumption. Therefore, contingency margins were added to the required power. This allows for power consumption growth during later phases of the design and compensates for this sensitivity. The other variables that this subsystem depends on are specifications of batteries, specifications of solar cells and efficiencies. The values used for efficiencies are conservative, so changes in them will most likely reduce the size of the power system. The values used for batteries and solar cells specifications are realistic and come directly from products available in the market. Similar products can be found in case those cannot be used. So those values are not prone to big changes.

19.6. Communication

From a link margin perspective there are a few parameters that have only been estimated for this design stage. These parameters include component specific losses and the noise temperature on the Moon. These were estimated to be 1 [dB] and 200 [K] respectively. However, even a significant change in these parameters is not expected to endanger the feasibility of the design. The only connections that are limited in link margin are the Malapert-Earth downlink and the Sverdrup-Malapert up/downlink. For the Sverdrup-Malapert connection the data rate can simply be decreased should the connection become unfeasible. This decrease in data rate would increase the link margin. For the Malapert-Earth connection a decreased data rate is more difficult since that would increase connection time. This additional time would have to be scheduled with the DSN. A solution for this connection would be an increased antenna size or a different transponder that provides more power. Therefore, the requirements are feasible even if certain estimated parameters change.

A larger challenge arises in the operational domain. The installation of an antenna on Malapert mountain is a challenging endeavour. Even though NASA itself has been researching this option, the feasibility of such a mission remains questionable at this design stage [49]. Should this mission prove impossible, the telescope will have a communication blackout for two weeks per month. This would violate requirement SALT-SSYS-COM-04 which states that there should be one contact per terrestrial day. In this case the other options for the communications system should be reconsidered. As has been stated before, the use of existing lunar infrastructure is a very viable option. For this design stage it has not been considered because of its unknown specifications. If a mission to Malapert mountain proves too difficult or too costly, the existing infrastructure can be reexamined. If that proves impossible as well, a custom orbiter solution can be considered.

19.7. Structures

Failure of structural components often lead to a total mission failure. An analysis on the sensitivity was therefore conducted on all some of the structural components discussed in Chapter 15. Considering the structural analysis of the rover legs, the c.g. range during pointing was first increased by 10% to see what the effect would be on the design. The maximum increase in moment of inertia (MOI) required to sustain the new loading was around the z-axis (Figure 15.1) and should be increased by 1.5%. Since this increase is very small, it would not effect the feasibility of the design. Next, the original gravity load was increased by 25% as discussed in the contingency section of Chapter 20. This would again affect the MOI around z-axis the most and required an increase of 7.8%. This will also not affect the feasibility of the design. Sinkage due to the loose consistency of lunar regolith proved to be a real impediment for the heavy rover. To see how the design would be affected in a worst case scenario, the rover mass was increased by 25% (Chapter 20). Next to that, it is unclear how much the regolith properties differ inside the crater compared to the samples taken from the Apollo mission. Therefore the density of lunar regolith, γ , was decreased by 10%. The numerical wheel design models required the wheel width to increase by 75%, limiting the manoeuvrability of rover significantly while increasing the required power since the bulldozing effect becomes more apparent. Although the manoeuvrability is hard to quantify, it can be said that the wheel design should be reconsidered and might be replaced by tracks to increase the contact area of the rover. This effect might threaten the feasibility of the repositioning requirement SALT-SSYS-MECH-01.

For the vibrational analysis, it should be noted that the moonquake properties used are already very conservative. In the theoretical case where a moonquake's epicentre is right at the crater, the surface displacement would increase to about 100 [mm]. This would in turn increase the displacement, velocity and acceleration of the rover. The springs coefficient could be reduced to give equal performance as is achieved currently. The displacement would however still be higher. The springs and their encasings would be significantly larger, but still manageable at 30 to 40 [cm] in height.

20. Resource Allocation, Contingencies and Budgets Analysis

Resources need to be allocated efficiently in order to successfully carry the mission to term. This section analyses the mission's cost and mass. The cost budget is presented in Section 20.1, and is accompanied by a cost breakdown structure, presented in Section 20.2. A few cost contingencies are proposed in Section 20.3, and Section 20.4 presents a breakdown of the mass of the system.

20.1. Cost Budget

The most immediate concern of any possible mission partner or investor is the cost budget. With this in mind, a careful deconstruction of every mission element has been carried out, giving a price to every phase and every element of the project.

The budget has been divided in different phases, following the plan laid out in Section 17.6 and the times presented in the project Gantt chart in Section 17.7. The first of these is Phase A, the budget of which is shown in Table 20.1.

All other phases in this table present the budget in the same format. These make use of a hypothetical design crew, numbering up to 469 members. All prices are estimated using current job market data and the times laid out in the Gantt chart. All work days are treated as eight hours long, and staff members are paid by the hour.

Using a margin of 25%, the total budget adds up to € 2,480,654,788.74 . This does not meet the required one billion stated in **VLMT-COST-01**, violating the top-level requirement. This budget is, however, comparable to the Perseverance rover's 2.7 billion¹, and much inferior to the James Webb Space Telescope's "nearly ten billion"². It is for this reason that a change in the allowed budget was recommended, and that the original requirement was renegotiated, allowing for a total budget of € 2.5 billion.

¹The Planetary Society - The cost of Perseverance - URL: <https://www.planetary.org/space-policy/cost-of-perseverance>

²Business Insider - NASA's launch of the \$10 billion James Webb Space Telescope has been delayed 7 months to Halloween 2021 - URL: <https://www.businessinsider.nl/nasa-james-webb-space-telescope-jwst-launch-date-october-2021-2020-7?international=true&r=US>

Table 20.1: SALT Cost Budget

End of study - Phase A			Production - Phase D		
Category	Cost	Notes	Category	Cost	Notes
Mission management			PM & SE		
Project manager salary	€ 135,200.00	Manager extra + overtime (Includes design time)	Management	€ 12,308,000.00	123080 Man-hours
Secretary salary	€ 125,200.00	Overtime (Includes design time)	Systems engineers	€ 14,480,000.00	144800 Man-hours
Rest of the team			Manufacturing		
Implement Final Report Feedback	€ 192,000.00	Eight team members' salary	Material costs	€ 25,000.00	50 tons of steel
Review and update documents	€ 91,100.00	Eight team members' salary + editor's extra	Parts costs (production)	€ 755,600,000.00	Engineers' salary + part machining costs
Update plans	€ 627,200.00	Eight team members' salary	Spare parts costs	€ 188,900,000.00	25% of parts get made twice
Miscellaneous			Inspection & Testing	€ 13,904,000.00	Testing engineers from R&D
Coffee for design team	€ 1,440.00	For the ten design team members, for the next year	Assembly		
Face masks for design team	€ 240.00	Hopefully just for another year	Assembly team salary	€ 7,176,000.00	71760 Man-hours
Office & Computer costs	€ 20,000.00		Quality Control		
Software licenses	€ 15,796.41		Quality control salary	€ 124,500.00	9960 Man-hours
Total	€ 1,208,176.41		Logistics		
Financing			Transport fees (Incl. import)	€ 5,000,000.00	
Category			Equipment renting	€ 20,000,000.00	
Mission management			Testing facilities fees	€ 50,000,000.00	Cryo chamber, vacuum chamber, etc
Management and original team salary	€ 2,800,000.00	All ten, for the whole phase (includes contacting space agencies)	PR		
PR Team salary			PR team	€ 3,840,000.00	38400 Man-hours
Produce Marketing Material	€ 678,400.00		Budget for talks and travel	€ 200,000.00	
Contact Media outlets	€ 409,600.00		Miscellaneous		
Legal Team salary			Coffee for design team	€ 374,112.00	For the design team members, for the next three years
Negotiate Partnerships	€ 483,840.00		Total	€ 1,071,931,612.00	
Agree on Funding and Partnerships	€ 483,840.00		Launch		
Total	€ 4,855,680.00		Category		
Research & Development - Phases B & C			Launch		
Category			Category	Cost	Notes
Mission management			Launch		
Project manager salary	€ 855,360.00	7128 Man-hours	Launcher price	€ 200,000,000.00	Estimate, based on Falcon Heavy's 150 million
Secretary salary	€ 784,080.00	7128 Man-hours	Flying the team to Florida and back	€ 50,000.00	Estimate
Management team salary	€ 10,692,000.00	14656 Man-hours	Insurance	€ 40,000,000.00	10% of launch cost
Mission planning			Total	€ 240,050,000.00	
Systems engineers	€ 14,256,000.00	142560 Man-hours	Operation - Phase E		
Electrical team	€ 14,256,000.00	142560 Man-hours	Category		
Structures team	€ 28,512,000.00	285120 Man-hours	System Operation		
Optics team	€ 21,384,000.00	213840 Man-hours	Management	€ 25,214,400.00	252144 Man-hours
Thermal team	€ 10,692,000.00	106920 Man-hours	Operators	€ 44,496,000.00	444960 Man-hours
Software team	€ 28,512,000.00	285120 Man-hours	Operator training	€ 8,400,000.00	Trained for a year
Test engineers	€ 14,256,000.00	142560 Man-hours	Operation equipment	€ 5,000,000.00	
Communications team	€ 14,256,000.00	142560 Man-hours	Astronauts	€ 13,824,000.00	
Pointing team	€ 17,820,000.00	178200 Man-hours	Astronaut training	€ 4,608,000.00	
Mobility team	€ 17,820,000.00	178200 Man-hours	Sustainability officers	€ 17,280,000.00	172800 Man-hours
Research scientists	€ 14,256,000.00	142560 Man-hours	DSN Usage price	€ 9,812,994.33	Based on http://deepspace.jpl.nasa.gov/admiss .
Legal costs			Maintenance & Replacement Costs		
Lawyers	€ 5,987,520.00	85536 Man-hours	New replacement rover	€ 267,982,903.00	
Other legal fees	€ 898,128.00		Additional maintenance components	€ 40,197,435.45	
Hardware, software licenses			PR		
Asana	€ 45,792.00		PR team	€ 3,840,000.00	
Microsoft Office	€ 162,943.20		Budget for talks and travel	€ 1,000,000.00	
Lucidchart	€ 9,311.04		Total	€ 441,655,732.78	
Fusion 360	€ 134,622.12		End-of-life		
Matlab & Simulink	€ 176,231.44		Category		
Office & Computer costs	€ 636,000.00		Moon segment decommission		
PR			Astronauts	€ 8,000.00	
PR team	€ 5,702,400.00	17820 Man-hours	SALT Memorial Plaque setup	€ 1,000.00	
Budget for talks and travel	€ 200,000.00		Earth segment decommission		
Miscellaneous			Sustainability engineers	€ 1,440,000.00	14400 Man-hours
Coffee for design team	€ 45,792.00	For the design team members, for the next year	Logistics budget	€ 1,000,000.00	
Total	€ 222,350,179.80		Send-off gift for team	€ 23,450.00	
			Total	€ 2,472,450.00	

20.2. Cost Breakdown Structure

The figures given in Section 20.1 are summarised in this section in the form of a Cost Breakdown Structure, shown in Figure 20.1.

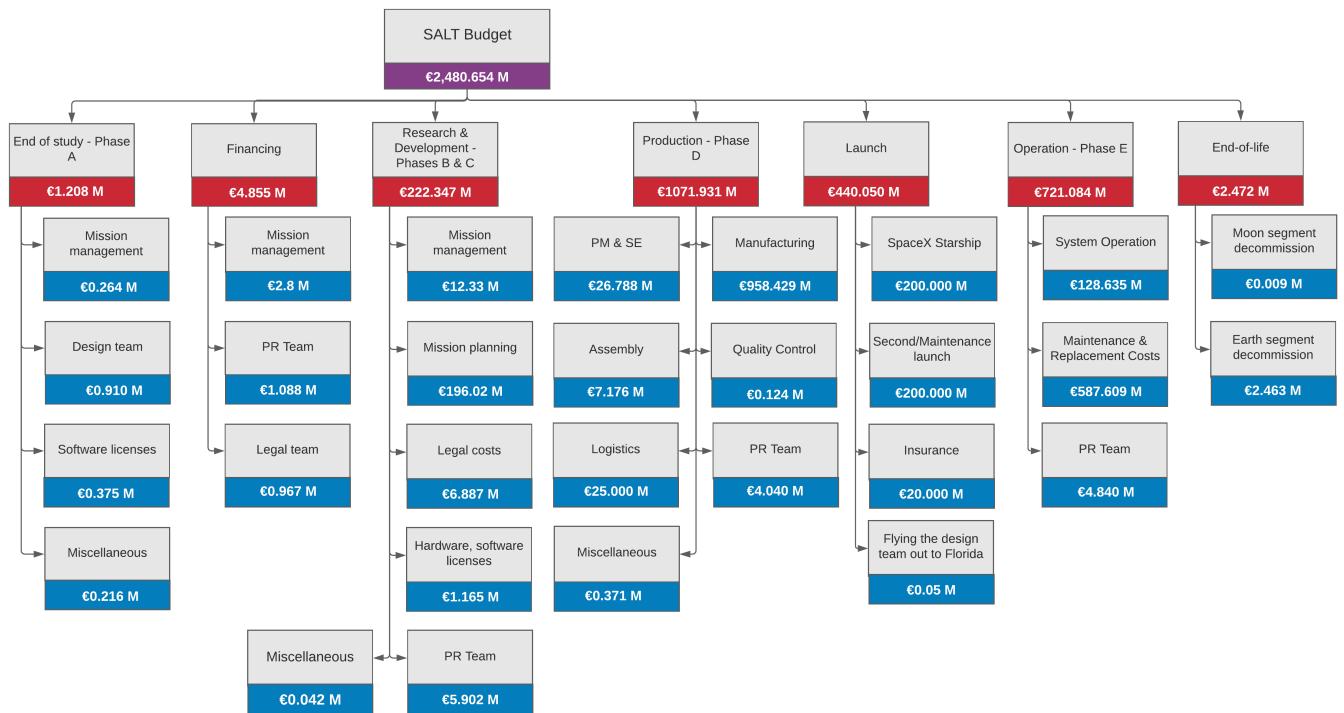


Figure 20.1: Cost Breakdown Structure

20.3. Cost Contingency

Space missions have a tendency to exceed their allotted budget; missions with a similar profile to SALT are no exception — the James Webb Telescope, with its ten billion dollars in budget, being the prime example.³ It is therefore vital for the SALT mission to be prepared for that event. Given the uncertain nature of cost estimation, however, it is hard to create contingencies for the likely event of a lack of funding. Risks **PL01** and **PL02** listed under Chapter 4 suggest the use of multiple different partners and a promotion of the mission in the public sphere, which will generate interest and guarantee its funding is increased if necessary.

20.4. Mass Breakdown

Having a breakdown of all contributing parts towards the final mass that shall be launched to the Moon is of great importance to the client and the company providing the launch vehicle. It is not only useful to distinguish the large contributors to the total mass, it also offers a sanity check on the masses of all components. A detailed mass breakdown was made for each main component, namely the rovers, the combiner and all other peripheral equipment. The breakdown is shown in Table 20.2. Some notes regarding the approach of the mass breakdown are listed below:

1. The main structural components described in the mass breakdown were first designed as described in Chapter 15. These components were later modelled using Computer Aided Design (CAD). Since the rover bus, rover suspension, telescope support structure and combiner are fully custom designed, the mass estimates were derived from the digital model. It was verified by hand if densities were correctly imported into the model. It was also checked if the values seemed realistic.
2. Since electronic systems, batteries, optical equipment and thermal systems were selected before being modelled, the mass was derived from the available mass figures instead of derived from

³Business Insider - NASA's launch of the \$10 billion James Webb Space Telescope has been delayed 7 months to Halloween 2021 - URL: <https://www.businessinsider.nl/nasa-james-webb-space-telescope-jwst-launch-date-october-2021-2020-7?international=true&r=US>

CAD.

3. Bulk pieces such as nuts and bolts are included in the contingency section unless otherwise stated in the breakdown table.
4. The optical systems turned out to be very difficult to estimate due to the early stages of the optical architecture. A preliminary estimate of 100 [kg] was chosen. This same estimate was used for the optical components inside the beam-combiner. It is based on the comparable architecture of the MIRI telescope which weighs 100 [kg]⁴
5. The mass breakdown of the beam-combiner does not include battery weight. Power is provided from the electrical box as described in Chapter 12.
6. CF indicates that the component shall be made out of carbon fibre.

20.4.1. Mass Contingencies

Although the mass breakdown contains an already fairly detailed overview, it only breaks it down into the main components and subsystems. A more detailed level of the mass breakdown can only be generated during the detailed design phase. Some of the missing and difficult to estimate components are bolts and nuts, fixation brackets inside the launcher, assembly tools for the astronauts and boxes containing the mirrors before they are installed, only to name a few. Therefore, a contingency of 25% was chosen as a layer of safety. In this way, the contingency's can be lowered during the later stages of the design instead of being increased.

20.4.2. Total Mass

As shown at the bottom of Table 20.2, the total estimated mass equals 12,289.47 [kg]. Taking the aforementioned contingency of 25% on top of that results in a total system mass of 15,361.84 [kg].

⁴The Mid Infrared Instrument - URL: <https://www2.le.ac.uk/departments/physics/research/xroa/astrophysical-facilities-1/the-mid-infrared-instrument-miri>

Table 20.2: Mass Breakdown

System/component	single part mass [kg]	number of parts	cumulative mass [kg]	Source derived from
Rover			1798.00	
Structural components			1326.1	
Wheel	47.2	6	283.2	CAD
Rocker bogie suspension	202	2	404	CAD
Bus	389	1	389	CAD
Bus fixing brackets	12	1	12	CAD
Primary mirror backbone structure (CF)	60	1	60	CAD
Secondary mirror support structure	12	1	12	CAD
Tertiary mirror support structure	24	1	24	CAD
Secondary mirror support arm (CF)	3.5	3	10.5	CAD
Single hexagon mirror	1.5	18	27	[105]
Single mirror actuator	4.6	18	82.8	[105]
Mirror attachments	1.2	18	21.6	CAD
Drivetrain			56.64	
Electric motor	7.34	6	44.04	Chapter 15
Fixed gearbox	2.1	6	12.6	Chapter 15
Pointing mechanisms			53.21	
Compliant mechanism	0.79	1	0.79	Chapter 10
Small RoM actuators	4.7	2	9.4	Chapter 10
Star tracker	4.08	2	8.16	Chapter 10
Large RoM actuators (rotation)	10	2	20	Chapter 10
Large RoM actuators (translation)	7.43	2	14.86	Chapter 10
Thermal systems			81.89	
Cryocooler	22.15	1	22.15	Chapter 11
Radiator	1.79	1	1.79	Chapter 11
Heatshield	50	1	50	Chapter 11
Multi Layer Insulation	7.95	1	7.95	Chapter 11
Power systems			231.19	
Batteries	12.82	8	102.58	Chapter 12
Power distribution unit	17.4	1	17.4	Chapter 12
Electrical cabling	111.22	1	111.22	[45]: page 367, section 6.6.4.
Communication systems			3.57	
Onboard computer system	3	1	3	Chapter 13
Transceiver	0.01	1	0.01	Chapter 13
Antenna	0.56	1	0.56	Chapter 13
Sensing			5.15	
LiDAR sensor	0.9	1	0.9	Section 14.2
Inertial navigation system	0.75	1	0.75	Section 14.2
Radar transceiver	3	1	3	Section 14.2
Hazcam	0.5	1	0.5	Section 14.2
Optical systems			100	
Beam Combiner			1562.93	
Structural components			1074.75	
Assembly stage (CF)	213.2	3	639.6	CAD
Fixation brackets for support poles	2.5	16	40	CAD
Support poles	8.81	8	70.48	CAD
Fixation bolt + nut (M30)	0.67	16	10.67	⁵⁶
Single beam collector	78.5	4	314	CAD
Pointing mechanisms			1.32	
Large RoM actuators (rotation)	1.32	1	1.32	Chapter 10
Thermal systems			258.31	
Multi-Layer Insulation	12.37	1	12.37	Chapter 11
Heatshield	40	1	40	Chapter 11
Cryocooler 1st stage	67.39	1	67.39	Chapter 11
Cryocooler 2nd stage	122.5	1	122.5	Chapter 11
Radiator	16.05	1	16.05	Chapter 11
Power systems			119.65	
Power distribution unit	17.4	1	17.4	Chapter 12
Electrical cabling	102.25	1	102.25	[45]: page 367, section 6.6.4.
Communication systems			5.56	
Onboard computer system	3	1	3	Chapter 13
Transceiver	2	1	2	Chapter 13
Antenna	0.56	1	0.56	Chapter 13
Sensing			3.34	
Laser rangefinders on combiner	0.7	4	2.8	Section 14.2
Combiner radar beacon	0.54	1	0.54	Section 14.2
Optical systems			100	
Peripheral Equipment			3462.02	
Transmission line cable (solar array to site)	2800	1	2800	Chapter 12
Batteries of the electrical box	12.82	48	615.46	Chapter 12
Sverdrup transceiver	2	1	2	Chapter 13
Sverdrup antenna	0.56	1	0.56	Chapter 13
Sverdrup battery power station + solar array	15.8	1	15.8	Chapter 13
Malapert transceiver	2	1	2	Chapter 13
Malapert antenna	10	1	10	Chapter 13
Malapert battery power station + solar array	16.2	1	16.2	Chapter 13
Solar Array	79.9	1	79.9	Chapter 12
Total system mass			12296.88	

21. Reliability, Availability, Maintainability, Safety Analysis and Compliance Matrix

This chapter covers the product's capabilities and whether or not it meets the system requirements, through the use of a RAMS analysis – which improves upon the system's efficiency — and a compliance matrix, used to check if the telescope meets the requirements.

21.1. Reliability, Availability, Maintainability and Safety Analysis

A RAMS analysis is a decision tool that helps optimise the availability and reduce the life cycle cost by improving the efficiency of the use of equipment and labour, while maintaining safe usage of the system.¹ Through an analysis of the mission's internal interaction between subsystems and external interactions with cooperating parties, multiple optimisation options have been identified, and are presented in the following sections.

21.1.1. Component Contribution to System Downtime

A useful tool to determine the reliability of a system is a fault tree analysis, or FTA¹. It delivers a clear representation of the failure points of a system and allows engineers to determine which components might fail or require the most maintenance. While these are usually produced in a later design stage, an initial version can be generated through estimations by following the guidelines presented in NASA's technical support server [106],[107].

The SALT mission's FTA is shown in Figure A.3. A coding scheme is employed in order to determine the relative downtime of each failure. Different colours have been assigned based on complexity and statistical data [108]. Nevertheless, the values remain rough estimates.

A pie chart can be constructed in the same manner as the risk pie chart in NASA's Architecture Study [108] by weighing the different failures. The result is shown in Figure 21.1. The highest contribution to the downtime is related to the mechanical subsystem; this is an unsurprising result, given that it is the easiest subsystem for astronauts to access and manage. The optical system, on the other hand, is rather complex and difficult to repair, and is therefore designed not to fail. Due to the availability of astronauts, nearly every system can experience downtime without causing a mission failure. Because of this, the reliability estimate is based on downtime instead, which can occur due to malfunctions in the optical system. A readability estimate of the rovers can be obtained using statistical data for component failure rates [109]. The uniformly distributed downtime expectancy allows for the component failure probability to be equally weighted into a rover system failure probability, found to be 0.881 or 88.1%. However, this estimate can be improved, due to the system being capable of operating in a two-rover inoperative mode, by making use of a two-element Bracewell interferometer setup [17]. Although an equivalent performance would require a greater operational time than using a four rover constellation, the system will not experience downtime. Using the binomial probability distribution, the reliability increases to 0.994 or 99.4%.

21.1.2. Redundancy Philosophy

Redundancy is an effective and intuitive method of improving the reliability of the system, but can introduce complications: the main complication being that a system's weight increases rapidly with increasing redundancy, but it increases complexity and cost too. The SALT system has several points

¹Functional Safety Engineering Service: <https://www.fses.global/service/ram-analysis/>

COMPONENT CONTRIBUTION TO SYSTEM DOWNTIME

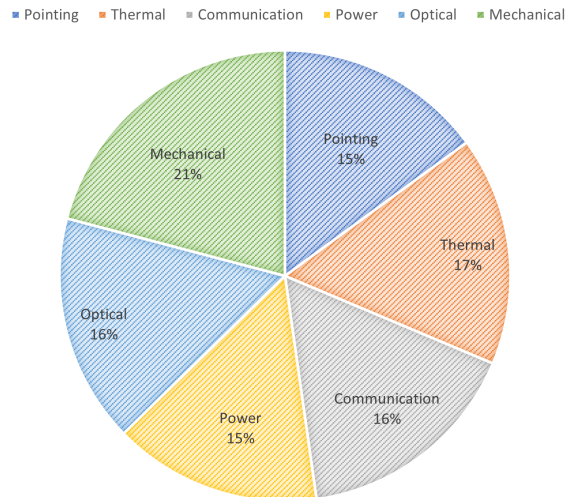


Figure 21.1: Pie chart displaying components relative downtime expectancy.

of redundancy as well as graceful degradation, an example of these being the number of rovers — given that two rovers can still operate, albeit with limited performance. Another example is the amount of on-board navigation cameras.

21.1.3. Optimisation of Maintenance Procedures

Quick maintenance capabilities are a key to reducing the downtime of the system. Commonly, maintenance procedures can be separated into four distinct phases [110]:

- Failure warning notification
- Problem analysis & solution production
- Communication & operations²
- System test run

The first entry in the list, the failure warning system, consists of the identification of failures in the system and notifying the operators on Earth. This step in the procedure will be the shortest of the list, due to the limited involvement of personnel. Nevertheless, options to improve potential points of failure can be examined, such as the identification process of a malfunction. If the system is not capable of identifying a malfunction, the risk exists of the issue propagating and permanently damaging components. As a means to combat this, the system transmits all of its telemetry and most of its camera footage to Earth on a daily basis, which minimises the autonomy of the system. This procedure is mostly constrained by the communications window of the DSN, and cannot be improved easily because of this. A possible solution would be to transmit information to the astronauts of the Artemis mission as well, and have them supervise the system.

The latter three items on the list allow for large improvements due to the low pressure on the uplink data budget presented in Table 13.4. The table shows that all commands can be received in much less time than the total communications window. Furthermore, telemetry is merely a small fraction of the downlink data volume, and can be given priority over observation data during transmission, in case there are any system failures. This allows for multiple two-way communications between equipment, astronauts and scientists in half an hour of DSN usage, which in turn allows the three phases to be performed concurrently. In the ideal scenario, astronauts would be on the way to Sverdrup as soon as

²Operations include repairs as well as cleaning of excessive lunar dust on equipment

a problem's origin has been identified — provided it is not software-related. Once they arrive, they can start repairs and receive new status updates from the ground station. The repairs make use of similar components as the ISS, LRU's³, these will allow safe and easy access to the interior of the rover and replacement of components. Once finished, a test run can be performed, such that the astronauts can verify whether it is operating correctly. If this is not the case, a new maintenance cycle can be started right away because of the close communication with the ground. Scheduled maintenance operations are already well-established, however, and initial communication with Earth-based scientists might not be necessary.⁴.

21.1.4. Safety

The main application of safety measures during the mission is related to astronaut maintenance operations and the journeys over the lunar surface. The complete darkness inside the crater and surroundings poses a risk to these operations. The vehicle and space suits will likely be provided of light sources due to the Artemis mission being located in the Shackleton Crater, which is also a perpetually shadowed region. The problem of safely locating the rovers and performing maintenance remains an issue, however. The way SALT approaches it is by utilising the lights used for the Hazcams. With these lights, rovers can be easily located. Additionally, lights of different colours can be added to simulate position lights, similar to those found on aircraft. Other stations located in shadowed areas, such as the combiner, could be equipped with a similar system.

21.2. Compliance Matrix

The compliance matrix revisits all requirements and checks if the design has met them. The requirements that have been met were assigned a check mark, the requirements that cannot be determined yet were assigned a question mark. As stated in Section 20.1, the increase in the budget provided during the final review is enough, so that most requirements are met, as shown in Table 21.2 and Table 21.3. Some requirements could not be confirmed yet, those are presented in Table 21.1 :

Table 21.1: Explanations for requirements that were assigned a question mark.

Code	Reason of uncertainty
SALT-SSYS-SENS-09	The particle radiation survival will have to be looked into in the detailed design.
SALT-SSYS-MECH-08	It was checked that lunar dust will not damage mechanisms, but in the detailed design this should be looked further into.
SALT-SSYS-MECH-10	The materials shall be further looked into in the detailed design.
SALT-SSYS-MECH-11	There is not enough information on the lunar lander to determine if this requirement is met.
SALT-SSYS-MECH-12	There is not enough information on the launcher to determine if this requirement is met.
SALT-SSYS-11	The estimations of reliability are rough in this stage of the design. Currently they are met, but will need to be revisited in the next stages.

³LRU: Lunar Replacement Unit, inspired by ISS's ORU's: Orbital Replacement Units

⁴More information about maintenance procedures can be found in Section 17.4.1

Table 21.2: Compliance matrix of SALT requirements (1/2).

Code	Requirement	Check	Reference
Sensing Subsystem			
SALT-SYS-01	The telescope shall characterise the thermal infrared signature of exoplanets.	✓	Chapter 9
SALT-SSYS-SENS-01	The angular resolution of the telescope shall be less than 5 milliarcsec at a wavelength of 10 μm .	✓	Chapter 9
SALT-SSYS-SENS-02	The spectral resolution shall be at least 300 [-].	✓	Chapter 9
SALT-SSYS-SENS-03	The spectral range shall cover wavelets of 6 to 20 μm .	✓	Chapter 9
SALT-SSYS-SENS-04	The signal-to-noise ratio shall be equal or greater than 10 for H ₂ O.	✓	Chapter 9
SALT-SSYS-SENS-05	The signal-to-noise ratio shall be equal or greater than 5 for CO ₂ .	✓	Chapter 9
SALT-SSYS-SENS-06	The signal-to-noise ratio shall be equal or greater than 5 for O ₃ .	✓	Chapter 9
SALT-SSYS-SENS-09	The system shall survive the particle radiation environment.	?	
SALT-SSYS-SENS-10	Lunar dust shall not permanently damage the sensing equipment.	✓	Chapter 9
SALT-SSYS-SENS-11	The optical system shall be able to observe exo-planets with a 5.0E-20 [W/m ²] brightness or higher with an SNR of 10 [-] during 10 hours of observation	✓	Chapter 9
SALT-SSYS-SENS-12	The optical path length shall be able to be corrected.	✓	Chapter 9
SALT-SSYS-SENS-13	The optical path length shall be kept stable with an accuracy of less than 1.5 [nm] w.r.t. the beam combiner.	✓	Chapter 9
SALT-SSYS-SENS-14	The optical path length shall be controllable with a range of 10 μm	✓	Chapter 9
Mechanical Subsystem			
SALT-SYS-02	The telescope shall comprise of 4 beam collectors and 1 beam combiner in an X-configuration.	✓	Chapter 15
SALT-SSYS-MECH-01	The beam collectors shall be able to reposition between 50 and 500 meter from the beam combiner.	✓	Chapter 15
SALT-SSYS-MECH-02	The telescope shall be extendable to 8 beam collectors (in X-configuration).	✓	Chapter 15
SALT-SSYS-MECH-08	Lunar dust shall not permanently damage mechanisms.	?	
SALT-SSYS-MECH-10	The system shall make use of renewable materials.	?	
SALT-SSYS-MECH-11	The system shall survive the landing phase onto the Moon.	?	
SALT-SSYS-MECH-12	The payload shall not damage the launch vehicle.	?	
SALT-SSYS-MECH-13	The system shall survive moon quakes of magnitude 5.	✓	Chapter 15
SALT-SSYS-MECH-14	The pointing system shall have a pointing accuracy of 0.5 [arcsec] or less.	✓	Chapter 15
SALT-SSYS-MECH-15	The telescope shall be able to point within an angle of 90 [deg] from the local surface normal vector.	✓	Chapter 15
Thermal Subsystem			
SALT-SYS-03	The system shall survive the thermal environment of the Moon.	✓	Chapter 11
SALT-SSYS-THM-01	All optical elements at the collectors shall have a temperature of no more than 40 [K] during observations.	✓	Chapter 11
SALT-SSYS-THM-02	All optical elements at the beam combiner shall have a temperature of no more than 40 [K] during observations.	✓	Chapter 11
SALT-SSYS-THM-03	The detector at the beam combiner shall have a temperature of no more than 10 [K] during observations.	✓	Chapter 11
Communication Subsystem			
SALT-SYS-04	Communication with the lunar element and the ground station shall be establishable.	✓	Chapter 13
SALT-SSYS-COM-03	The system shall store commands and information in the event of a loss of communications.	✓	Chapter 13
SALT-SSYS-COM-04	The lunar segment shall have at least one two-way communication contact between the ground station and all mission elements per terrestrial day.	✓	Chapter 13

Table 21.3: Compliance matrix of SALT requirements (2/2).

Code	Requirement	Check	Reference
Operations			
SALT-SYS-05	The mission fits within the scope of foreseen (human) spaceflight plans of organisations with experience of launching humans to space.	✓	Chapter 17
SALT-SSYS-OPE-02	The telescope shall not interfere with other missions.	✓	Chapter 17
SALT-SYS-06	The system shall be deployed and maintained by astronauts and the ground element.	✓	Chapter 17
SALT-SSYS-OPE-03	The telescope shall not pollute the surface of the Moon after decommissioning.	✓	Chapter 17
SALT-SSYS-OPE-04	The telescope shall be operational within 3 years from the next Moon landing by humans.	✓	Chapter 17
SALT-SSYS-OPE-05	The telescope shall be safe to maintain.	✓	Chapter 17
SALT-SSYS-OPE-06	The system's software must be update-able.	✓	Chapter 17
SALT-SSYS-OPE-07	The lunar element shall be assembled on the Moon surface.	✓	Chapter 17
SALT-SSYS-OPE-09	A repair strategy shall be established.	✓	Chapter 17
SALT-SSYS-OPE-10	The operations shall not be halted because of the presence of lunar dust.	✓	Chapter 17
SALT-SSYS-OPE-11	The equipment shall be able to perform 30 [h] operational cycles.	✓	Chapter 17
SALT-SSYS-OPE-12	The telescope shall be operational for at least 70 [%] of each Moon night period.	✓	Chapter 17
Power Subsystem			
SALT-SYS-07	The power subsystem shall supply continuous power for operation.	✓	Chapter 12
SALT-SSYS-POW-01	The telescope shall use a renewable energy source.	✓	Chapter 12
SALT-SSYS-POW-02	The telescope shall not use nuclear power.	✓	Chapter 12
SALT-SSYS-POW-04	The power system shall be protected against solar flares up to a magnitude X1.	✓	Chapter 12
SALT-SSYS-POW-10	The power storage system shall support the power system under peak load.	✓	Chapter 12
SALT-SSYS-POW-11	The power storage system shall be capable of storing energy to support the equipment for one operational cycle or more.	✓	Chapter 12
SALT-SSYS-POW-12	The power subsystem shall be able to recharge during one operational cycle or less.	✓	Chapter 12
Cost			
SALT-SYS-08	The total cost of the mission for the first five years shall be less than 2500 [M€], excluding cost for already foreseen human Moon exploration missions.	✓	Chapter 20
SALT-SSYS-BUDG-01	The cost from failure of the mission shall be mitigated.	✓	Chapter 20
SALT-SSYS-BUDG-03	An extra reflector and beam collector shall be manufactured to be sent as replacements if needed.	✓	Chapter 20
Schedule			
SALT-SYS-09	The nominal mission shall be 5 years.	✓	Chapter 17
SALT-SSYS-SCH-01	The extended mission, including potential upgrades and repairs for less than 20 [%] of the total launch mass, should last for another 10 years.	✓	Chapter 17
Reliability			
SALT-SYS-11	The mission shall have a probability of success of 0.920 [8] or higher.	?	
SALT-SSYS-REL-03	The end of life strategy shall not have single points of failure.	✓	Section 21.1
SALT-SSYS-REL-06	No single part failure shall cause complete loss of a function.	✓	Section 21.1

22. Conclusion

The stated goal of the SALT mission is *“to improve the characterisation of exoplanet atmospheres, within 3 years of the next manned lunar landing”*. The SALT design team has completed a detailed phase-A design of a system that will accomplish that goal.

In the preliminary design phase a number of concepts were identified. Three of these progressed to the final design trade off: a rail concept, maglev concept, and rover concept. The benefits and drawbacks of each option were weighed in an AHP process. The rover concept won this initial design trade and was advanced to the detailed design phase because it enabled rotational noise reduction, simplified installation, and is easy expansion of the system.

The current SALT design is based on independent unit telescopes installed on freely moving rovers. These independent rovers allow the system to optimise its configuration to observe any target system. SALT will be located at the lunar south pole, in the permanent shadow of Sverdrup crater. This provides the system with an unobstructed view, suitable terrain, and an appropriate thermal environment. It is also proximal to planned human activities in Shackleton crater, providing the human support required for the activities detailed in Sections 17.3 and 17.4.1. The crater rim provides the ideal location for solar installation that will almost continuously supply the system with energy, and seismic sensors that provide warnings against incoming moonquakes. Communication relays will maintain contact between the installation, lunar astronauts, and Earth.

This design provides a very high performance alternative to the suspended Darwin mission and other planned space telescopes (2.06[mas] resolution for SALT vs 5[mas] for Darwin). Preliminary optical modelling detailed in Section 9.3.2 show that the current design can observe at least 838 planets at a signal-to-noise ratio of 10[–] or better across all bands. For comparison, Darwin was only expected to screen 218 planets over the course of its mission [2]. SALT is also capable of revisiting observed planets for additional measurements, within the planned mission time frame.

Current estimates place the total mission cost at approximately 2.4 billion EUR. This represents a major cost saving compared to other planned space telescopes (\$6.7 billion for HABEX, \$8-\$35 billion for LUVOIR), while providing much better angular resolution (equivalent to 1[km] diameter, whereas LUNAR is < 15[m] and HABEX is 4[m]). SALT is also inherently upgradeable. Rovers allow for easy expansion and proximity to the Shackleton crater eases transportation and human support. Also, the optical design is based on a series of tables. Swapping or stacking new tables could enable new capabilities such as visual band imaging. This makes the system by far the most modular and adaptable space instrument ever constructed. Furthermore, the ongoing maintenance and improvement of this system intimately involves astronauts, further justifying the importance of human lunar habitation.

This report includes a detailed system level design, but does not finalise the specifics of most subsystems. Further general design stages were detailed in the report. However, there are a few design categories that require special attention. These are: optics, location, and verification & validation.

The SALT optical subsystem is still at a very early design stage and has not been tested in any way. Before designs proceed, demonstrators from Darwin (such as the nulling breadboard) should be adapted, or new demonstrators should be built to validate the design and expected performance.

There is also limited topographical information for SALT’s operating location. Because the design and function of the SALT rovers is dependent on surface roughness, additional characterisation of the crater

surface must be completed. This data may be collected by the VIPER rover, if it is tasked to visit Sverdrup (by 2023).

Finally, many of the models used in SALT's design have undergone suitable verification where possible. This involved hand testing, comparison with existing models, or sanity checking where appropriate. However, due to the early nature of the SALT design and time limitations associated with this design phase, detailed validation of these models is considered a priority area.

If SALT is constructed it will represent a revolutionary change in humanity's ability to understand other worlds. We will be able to image planets at resolutions never before possible, while achieving state of the art (or better) sensitivity. SALT will also help prove out a number of capabilities, including lunar assembly, maintenance, and retirement. Its modular and highly upgradeable nature is a first for a space based telescope. SALT will prove that we can build things on other bodies, that we should build them, and that humans can play an important role in their construction and operation.

References

- [1] Scott Gaudi et al. *Habitable Exoplanet Observatory*. Aug. 2019.
- [2] Alain Leger and Tom Herbst. "DARWIN A Proposal for the Cosmic Vision". In: *arXiv preprint arXiv:0707.3385* (2007).
- [3] Space Studies Board, Engineering National Academies of Sciences, Medicine, et al. *Powering Science: NASA's Large Strategic Science Missions*. National Academies Press, 2017.
- [4] LUVVOIR Team et al. "The LUVVOIR mission concept study final report". In: *arXiv preprint arXiv:1912.06219* (2019).
- [5] M Meixner et al. "Origins space telescope mission concept study report". In: *arXiv preprint arXiv:1912.06213* (2019).
- [6] DSE Group 4. *Project Plan Report*. Kluuyverweg 1, 2629 HS Delft: Delft University of Technology, Apr. 2021.
- [7] DSE Group 4. *SALT - Synthetic Aperture Lunar Telescope Baseline Report*. Kluuyverweg 1, 2629 HS Delft, The Netherlands: Delft university of Technology, 2021.
- [8] Brienne Bogenberger. *James Webb Space Telescope Project Mission Requirements Document*. Tech. rep. Goddard Space Flight Center, Nov. 2007.
- [9] Jasper Bouwmeester. *Project Guide Design Synthesis Exercise: Very Large Moon Telescope*. Kluuyverweg 1, 2629 HS Delft: Delft University of Technology, Apr. 2021.
- [10] Julie Stopar and Heather Meyer. *Topography and Permanently Shaded Regions (PSRs) of the Moon's South Pole (80°S to Pole)*. 2021.
- [11] Cheryl Warner. *NASA's Plan for Sustained Lunar Exploration and Development*. Apr. 2020.
- [12] Lonnie Shekhtman. *NASA's Artemis Base Camp on the Moon Will Need Light, Water, Elevation*. Jan. 2021. URL: <https://www.nasa.gov/feature/goddard/2021/nasa-s-artemis-base-camp-on-the-moon-will-need-light-water-elevation>.
- [13] Bradley W. Carroll and Dale A. Ostlie. *An introduction to modern astrophysics*. Cambridge University Press, 2018.
- [14] S. R. Deitrick, A. T. Russell, and S. B. Loza. *LANDING SITE ANALYSIS FOR A LUNAR POLAR WATER ICE GROUND TRUTH MISSION*. 2020.
- [15] Klaus D. Goepel. "Implementing the Analytic Hierarchy Process as a Standard Method for Multi-Criteria Decision Making In Corporate Enterprises - A New AHP Excel Template with Multiple Inputs". In: (2013).
- [16] DSE Group 4. *SALT - Synthetic Aperture Lunar Telescope Midterm Report*. Kluuyverweg 1, 2629 HS Delft, The Netherlands: Delft university of Technology, 2021.
- [17] C. Dandumont et al. "Exoplanet detection yield of a space-based Bracewell interferometer from small to medium satellites". In: *Journal of Astronomical Telescopes, Instruments, and Systems* 6(3) (2020).
- [18] Marat Khairoutdinov. *ATM348-Rad_Blackbody*. URL: <http://rossby.msrc.sunysb.edu/~marat/MAR542/ATM542-Chapter2.pdf>.
- [19] Michael Shao et al. "Visible nulling interferometer". In: *Proceedings of SPIE - The International Society for Optical Engineering* (Oct. 2004). DOI: 10.1117/12.552527.
- [20] O. Wallner. *DARWIN System Assessment Study*. 2006.
- [21] S. Dubovitsky and O. P. Lay. "Architecture Selection and Optimization for Planet-Finding Interferometers". In: *Proceedings of SPIE* 5491 (2004), pp. 284–295.
- [22] Pierre Y. Bely. *The design and construction of large optical telescopes*. Vol. 530. Springer-Verlag, 2003.
- [23] A. Nanjangud et al. "Towards Robotic On-Orbit Assembly of Large Space Telescopes: Mission Architectures, Concepts, and Analyses". In: *70th International Astronautical Congress (IAC)* (2019).
- [24] David M. Chaney, James B. Hadaway, and Jakes Lewis. "Cryogenic radius of curvature matching for the JWST primary mirror segments". In: *Proceedings of SPIE - The International Society for Optical Engineering* (2009).
- [25] Mario Gai et al. "The VLTI fringe sensors: FINITO and PRIMA FSU". In: *New Frontiers in Stellar Interferometry*. Ed. by Wesley A. Traub. Vol. 5491. International Society for Optics and Photonics. SPIE, 2004, pp. 528–539. URL: <https://doi.org/10.1117/12.551495>.
- [26] Choquet E., Cassaing F., and Perrin G. et al. "GRAVITY: Design and performances of the fringe tracker". In: (2010).
- [27] T.C. van den Dool et al. "The DARWIN Breadboard Optical Delay Line Verification Programme". In: *SPIE Astronomical Telescopes + Instrumentation* (2006).
- [28] Valeri I. Karlov et al. "High-precision fringe tracking invariant to systematic model errors". In: *J. Opt. Soc. Am. A* 18.10 (Oct. 2001), pp. 2565–2576. DOI: 10.1364/JOSAA.18.002565. URL: <http://josaa.osa.org/abstract.cfm?URI=josaa-18-10-2565>.

- [29] Ron P. H. Haaksman et al. "A Combined Nulling and Imaging Pupil-Plane Beam-Combiner for DARWIN". In: (2006).
- [30] Stefanie N. Milam et al. "The James Webb Space Telescope's Plan for Operations and Instrument Capabilities for Observations in the Solar System". In: *Publications of the Astronomical Society of the Pacific* 128.959 (Jan. 2016), p. 018001. DOI: 10.1088/1538-3873/128/959/018001. URL: <https://doi.org/10.1088/1538-3873/128/959/018001>.
- [31] Marcio A.A. Fialho and Daniele Mortari. "Theoretical limits of star sensor accuracy". In: (2019).
- [32] E.G. Merriam¹ et al. "Monolithic 2 DOF fully compliant space pointing mechanism". In: *Mechanical Sciences* (2013).
- [33] F. Ma and G. Chen. "Modeling Large Planar Deflections of Flexible Beams in Compliant Mechanisms Using Chained Beam-Constraint-Model". In: *Journal of Mechanisms and Robotics* (2015).
- [34] R. M. Fowler, L. L. Howell, and S. P. Magleby. *Compliant space mechanisms: a new frontier for compliant mechanisms*. Oct. 2011. URL: <https://ms.copernicus.org/articles/2/205/2011/ms-2-205-2011.pdf>.
- [35] B.T.C. Zandbergen. *Aerospace Design & Systems Engineering Elements I Part: Spacecraft (bus) design and sizing*. TU Delft, 2017.
- [36] S. Dye, A. Kopelove, and G.L. Mills. "Integrated and Load Responsive Multilayer Insulation". In: *AIP Conference Proceedings* 1218.946 (2010). <https://aip.scitation.org/doi/pdf/10.1063/1.3422464>.
- [37] H.J.M. ter Brake and G.F.M. Wiegerinck. "Low-power cryocooler survey". In: *Elsevier* (2002).
- [38] B. Collaudin and E. Gavila. *Cryogenic Integration in Satellites*. https://indico.cern.ch/event/792215/contributions/3558254/attachments/1918508/3172791/Cryogenic_integration_in_satellites_-_ThalesAleniaSpace.pdf: Thales Alenia Space, Oct. 2019.
- [39] D. Gilmore. *Spacecraft Thermal Control Handbook, Volume 1: Fundamental Technologies*. Vol. 1. Aerospace Press, 2002.
- [40] J. Carey et al. "Inflatable Sunshield in Space (ISIS) versus next generation space telescope (NGST) sunshield - A mass properties comparison." In: *AIAA* (2000).
- [41] Yuriy G Shkuratov and Nataliya V Bondarenko. "Regolith layer thickness mapping of the Moon by radar and optical data". In: *Icarus* 149.2 (2001), pp. 329–338.
- [42] Paul O Hayne et al. "Global regolith thermophysical properties of the Moon from the Diviner Lunar Radiometer Experiment". In: *Journal of Geophysical Research: Planets* 122.12 (2017), pp. 2371–2400.
- [43] Issamu Muraoka et al. "Numerical and experimental investigation of thermal louvers for space applications". In: *Journal of the Brazilian Society of Mechanical Sciences* 23.2 (2001), pp. 147–153.
- [44] Giulio Avanzini, Emanuele L de Angelis, and Fabrizio Giuliotti. "Performance analysis and sizing guidelines of electrically-powered extraterrestrial rovers". In: *Acta Astronautica* 178 (2021), pp. 349–359.
- [45] Charles D Brown. *Elements of spacecraft design*. American Institute of Aeronautics and Astronautics, 2002.
- [46] Zehua Lin and Jin Liu. "Low-temperature all-solid-state lithium-ion batteries based on a di-cross-linked starch solid electrolyte". In: *RSC advances* 9.59 (2019), pp. 34601–34606.
- [47] James D Dunlop. *NASA handbook for nickel-hydrogen batteries*. Vol. 1314. National Aeronautics, Space Administration, Scientific, and Technical ..., 1993.
- [48] Patrick Bernard and Michael Lippert. "Nickel-cadmium and nickel-metal hydride battery energy storage". In: *Electrochemical energy storage for renewable sources and grid balancing*. Elsevier, 2015, pp. 223–251.
- [49] Leslie J Deutsch, Joseph I Statman, and Gary K Noreen. "Low cost communication support of Lunar Missions". In: (2005).
- [50] Burton L. Sharpe and David G. Schrank. "Malapert mountain: Gateway to the moon". In: *Advances in Space Research* 31.11 (2003). The Moon: Science, Exploration and Utilisation, pp. 2467–2472. ISSN: 0273-1177. DOI: [https://doi.org/10.1016/S0273-1177\(03\)00535-0](https://doi.org/10.1016/S0273-1177(03)00535-0). URL: <https://www.sciencedirect.com/science/article/pii/S0273117703005350>.
- [51] Scott Bryant. *Lunar Pole Illumination and Communications Maps Computed from Goldstone Solar System Radar Elevation Data*. Feb. 2009.
- [52] Demetrios Gatzliolis and Hans-Erik Andersen. *A Guide to LIDAR Data Acquisition and Processing for the Forests of the Pacific Northwest*. Tech. rep. USDA, July 2008.
- [53] Justin Maki et al. "The Mars 2020 Engineering Cameras and Microphone on the Perseverance Rover: A Next-Generation Imaging System for Mars Exploration". In: *Space Science Reviews* 216 (Dec. 2020). DOI: 10.1007/s11214-020-00765-9.
- [54] BP Patel and R Patel. "An analytical study on comparison of different image compression formats". In: *International Journal for Innovative Research in Science & Technology (IJRST)* 1.7 (2014), pp. 24–31.
- [55] Bruno Lopez et al. "An overview of the MATISSE instrument—science, concept and current status". In: *The Messenger* 157 (2014), pp. 5–12.

- [56] Yasuo Hirata and Osamu Yamada. "6 - Applications to Communication Systems". In: *Essentials of Error-Control Coding Techniques*. Ed. by Hideki Imai. Academic Press, 1990, pp. 103–169. ISBN: 978-0-12-370720-8. DOI: <https://doi.org/10.1016/B978-0-12-370720-8.50010-6>. URL: <https://www.sciencedirect.com/science/article/pii/B9780123707208500106>.
- [57] David D Morabito and David Heckman. "Lunar Reconnaissance Orbiter K-Band (26 GHz) Signal Analysis: Initial Study Results". In: *The Interplanetary Network Progress Report 42* (2017), p. 211.
- [58] Dong K Shin. "Frequency and channel assignments". In: *JPL DSN Deep Space Network Series* (2014), pp. 810–005.
- [59] Deep Space Network. *Deep Space Network Services Catalog*. Tech. rep. Tech. Rep. DSN, 2015.
- [60] Simon Haykin. *Communication systems*. John Wiley & Sons, 2008.
- [61] Huanzhen Yang, Lidong Zhu, and Tingyong Wu. "The effects of mismatched roll-off factor on the receiving performance of QAM signals". In: *2009 International Conference on Communications, Circuits and Systems*. IEEE, 2009, pp. 86–90.
- [62] Wilfried Ley, Klaus Wittmann, and Willi Hallmann. *Handbook of space technology*. Vol. 22. John Wiley & Sons, 2009.
- [63] Stephen D Slobin and T Pham. "34-m BWG Stations Telecommunications Interfaces," in: *DSN Telecommunications Link Design Handbook* (2015).
- [64] DD Morabito. "Lunar noise-temperature increase measurements at S-Band, X-Band, and Ka-band using a 34-meter-diameter beam-waveguide antenna". In: *The Interplanetary Network Progress Report 42* (2006), p. 166.
- [65] James R Wertz, David F Everett, and Jeffery J Puschell. *Space mission engineering: the new SMAD*. Microcosm Press, 2011.
- [66] W. Kuhn, N. Lay, and E. Grigorian. "A UHF proximity micro-transceiver for Mars exploration". In: *2006 IEEE Aerospace Conference*. 2006. DOI: 10.1109/AERO.2006.1655779.
- [67] Robert C. Moore. "Satellite RF Communications and Onboard Processing". In: *Encyclopedia of Physical Science and Technology (Third Edition)*. Ed. by Robert A. Meyers. Third Edition. New York: Academic Press, 2003, pp. 439–455. ISBN: 978-0-12-227410-7. DOI: <https://doi.org/10.1016/B0-12-227410-5/00884-X>. URL: <https://www.sciencedirect.com/science/article/pii/B01227410500884X>.
- [68] Deep Space Network. "DSN Telecommunications Link Design Handbook". In: *Pasadena, CA: JPL* (2010).
- [69] Stephen M. Lichten et al. "Allocation of Deep Space Network Ground System Tracking and Communications Assets During the 2020-2021 Timeframe of the "Mars Armada"". In: *2018 SpaceOps Conference*. DOI: 10.2514/6.2018-2502. eprint: <https://arc.aiaa.org/doi/pdf/10.2514/6.2018-2502>. URL: <https://arc.aiaa.org/doi/abs/10.2514/6.2018-2502>.
- [70] Yosio Nakamura. "Shallow moonquakes-How they compare with earthquakes". In: *Lunar and Planetary Science Conference Proceedings*. Vol. 11. 1980, pp. 1847–1853.
- [71] Yohei Nishitsuji et al. "Reflection imaging of the Moon's interior using deep-moonquake seismic interferometry". In: *Journal of Geophysical Research: Planets* 121.4 (2016), pp. 695–713.
- [72] Y. Nishitsuji et al. "Reflection imaging of the Moon's interior using deep-moonquake seismic interferometry". In: *Journal of Geophysical Research: Planets* 121 (2016).
- [73] F. Sohl and G. Schubert. "Interior Structure, Composition, and Mineralogy of the Terrestrial Planets". In: *Treatise on Geophysics* (2007), pp. 27–68.
- [74] S. Takemura, M. Kobayashi, and K. Yoshimoto. "Prediction of maximum P- and S-wave amplitude distributions incorporating frequency- and distance-dependent characteristics of the observed apparent radiation patterns". In: *Earth, Planets and Space* 68 (2016).
- [75] V. Adushkin, I. Nemchinov, et al. *Catastrophic Events Caused by Cosmic Objects*. 2nd ed. Springer, 2008.
- [76] E. Grün, M. Horanyi, and Z. Sternovsky. "The lunar dust environment". In: *Planetary and Space Science* 59 (2011), pp. 1672–1680.
- [77] C. Nunn et al. "Standing on Apollo's Shoulders: A Microseismometer for the Moon". In: *The Planetary Science Journal* (2021).
- [78] P. Lognonné et al. "SEIS: Insight's Seismic Experiment for Internal Structure of Mars". In: *Space Sci Rev* (2019).
- [79] R. Yamada et al. "Frequency band enlargement of the penetrator seismometer and its application to moonquake observation". In: *Advances in Space Research* 56 (2015), pp. 341–354.
- [80] *M8™ LiDAR Sensor Data Sheet*. 2020.
- [81] *Acuity AR2000 Series Laser Distance Meters Data Sheet*. 2015.
- [82] S. Campbell et al. "Sensor Technology in Autonomous Vehicles". In: (2018).
- [83] *Model 25X-X C-Band RADAR Transponder Data Sheet & Technical Specifications*. 2021.
- [84] *Tyco Radar Detection for Enhanced Perimeter Security Data Sheet*. 2019.

- [85] Brian D Harrington and Chris Voorhees. "The challenges of designing the rocker-bogie suspension for the mars exploration rover". In: (2004).
- [86] Michael J Eisenhower et al. "ATLAST ULE mirror segment performance analytical predictions based on thermally induced distortions". In: *UV/Optical/IR Space Telescopes and Instruments: Innovative Technologies and Concepts VII*. Vol. 9602. International Society for Optics and Photonics. 2015, 96020A.
- [87] Mariëlle van Veggel et al. "Experimental set-up for testing alignment and measurement stability of a metrology system in Silicon Carbide for GAIA". In: *Optomechanics 2005*. Vol. 5877. International Society for Optics and Photonics. 2005, p. 587701.
- [88] William A Goodman. "3D Printed and Additively Manufactured RoboSiC™ for Space, Cryogenic, Laser and Nuclear Environments". In: *International Symposium on Microelectronics*. Vol. 2018. 1. International Microelectronics Assembly and Packaging Society. 2018, pp. 000099–000103.
- [89] Arthur W Leissa. *Vibration of plates*. Vol. 160. Scientific and Technical Information Division, National Aeronautics and ..., 1969.
- [90] H Philip Stahl. "JWST mirror technology development results". In: *Optical Manufacturing and Testing VII*. Vol. 6671. International Society for Optics and Photonics. 2007.
- [91] J Jaap Wijker. *Spacecraft structures*. Springer Science & Business Media, 2008.
- [92] David S McKay et al. "The lunar regolith". In: *Lunar sourcebook*. Vol. 7. Citeseer, 1991, pp. 285–356.
- [93] J Wong. "Theory of Ground Vehicles John Wiley & Sons Inc". In: (1993).
- [94] Mieczyslaw Gregory Bekker. *Introduction to terrain-vehicle systems. part i: The terrain. part ii: The vehicle*. Tech. rep. Michigan Univ Ann Arbor, 1969.
- [95] Philippe Ludivig et al. "TESTING ENVIRONMENTS FOR LUNAR SURFACE PERCEPTION SYSTEMS; COMBINING INDOOR FACILITIES, VIRTUAL ENVIRONMENTS AND ANALOGUE FIELD TESTS." In: (2020).
- [96] RG Pope. "The effect of wheel speed on rolling resistance". In: *Journal of terramechanics* 8.1 (1971), pp. 51–58.
- [97] Timothy J Stubbs, Richard R Vondrak, and William M Farrell. "A dynamic fountain model for lunar dust". In: *Advances in Space Research* 37.1 (2006), pp. 59–66.
- [98] Eberhard Grün, Mihaly Horanyi, and Zoltan Sternovsky. "The lunar dust environment". In: *Planetary and Space Science* 59.14 (2011), pp. 1672–1680.
- [99] R Kruzelecky et al. "Moondust lunar dust simulation and mitigation". In: *40th International Conference on Environmental Systems*. 2010, p. 6023.
- [100] European Southern Observatory. *Very Large Telescope Paranal Science Operations VLTI User Manual*. Feb. 2021.
- [101] Markus Loose et al. "High-performance focal plane arrays based on the HAWAII-2RG/4RG and the SIDECAR ASIC". In: *Focal Plane Arrays for Space Telescopes III*. Vol. 6690. International Society for Optics and Photonics. 2007, p. 66900C.
- [102] Myriam Lemelin et al. "Framework for Coordinated Efforts in the Exploration of Volatiles in the South Polar Region of the Moon". In: *The Planetary Science Journal* 2.103 (June 2021).
- [103] KaziM. Saidul Huq and Konstantinos Mitrogogos. "Impact of Lean Manufacturing on Process Industries". In: (2019).
- [104] ISECG. "Benefits stemming from space exploration". In: (2013).
- [105] Robert M Warden. "Cryogenic nano-actuator for JWST". In: *Proceedings of the 38th Aerospace Mechanisms Symposium, Langley Research Center*. 2006.
- [106] Glenn C. Klein and Jr. Donald E. Rash. *FAULT TREE ANALYSIS NiH2 AEROSPACE CELLS FOR LEO MISSION*. Tech. rep. N92-22 777. Gates Aerospace Batteries and Reliability Analysis Center, 1991.
- [107] Felix Bidner. *Fault Tree Analysis of the HERMES CubeSat*. Tech. rep. University of Colorado at Boulder, Mar. 2010.
- [108] *NASA's Exploration Systems Architecture Study*. Tech. rep. 214062. NASA, Nov. 2005.
- [109] J. Dolan S. Stancliff and A. Trebi-Ollennu. *Planning to Fail - Reliability as a Design Parameter for Planetary Rover Missions*. Tech. rep. The Robotics Institute and Jet Propulsion Laboratory.
- [110] Silvano Colombano et al. "A system for fault management and fault consequences analysis for NASA's Deep Space Habitat". In: *ResearchGate* (Sept. 2013).

A.1. Hardware Diagram

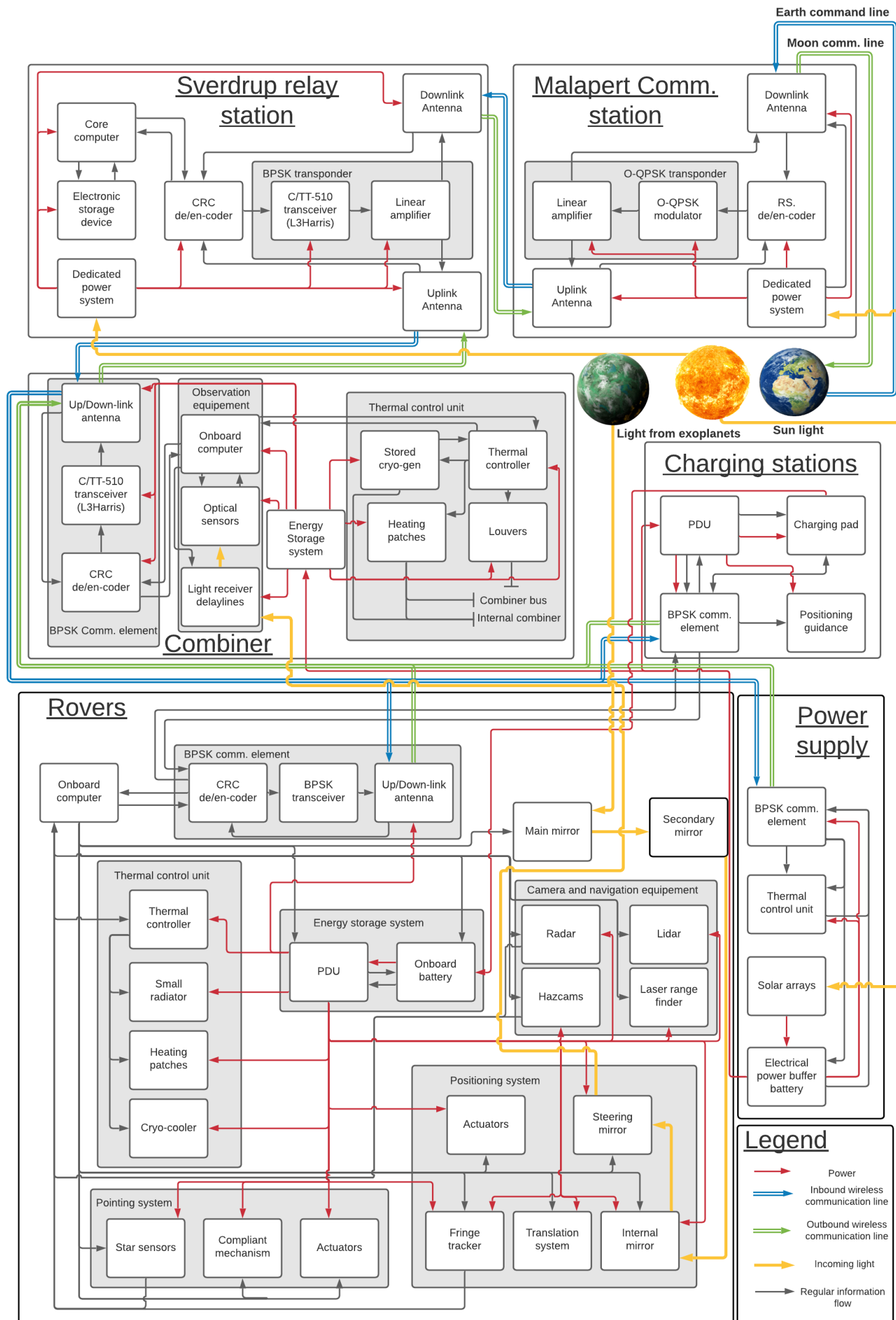


Figure A.1: Hardware diagram of the SALT mission¹

¹Sun image: https://toppng.com/sun-transparent-background-PNG-free-PNG-Images_87016
 Earth image: https://www.pngfind.com/mpng/ihJboJT_real-world-clipart-earth-transparent-background-planet-earth/
 Exoplanet image: <https://pnghut.com/png/W7eVKz7JRL/earth-exoplanet-clip-art-nasa-archive-transparent-png>

A.2. Requirements Discovery Tree

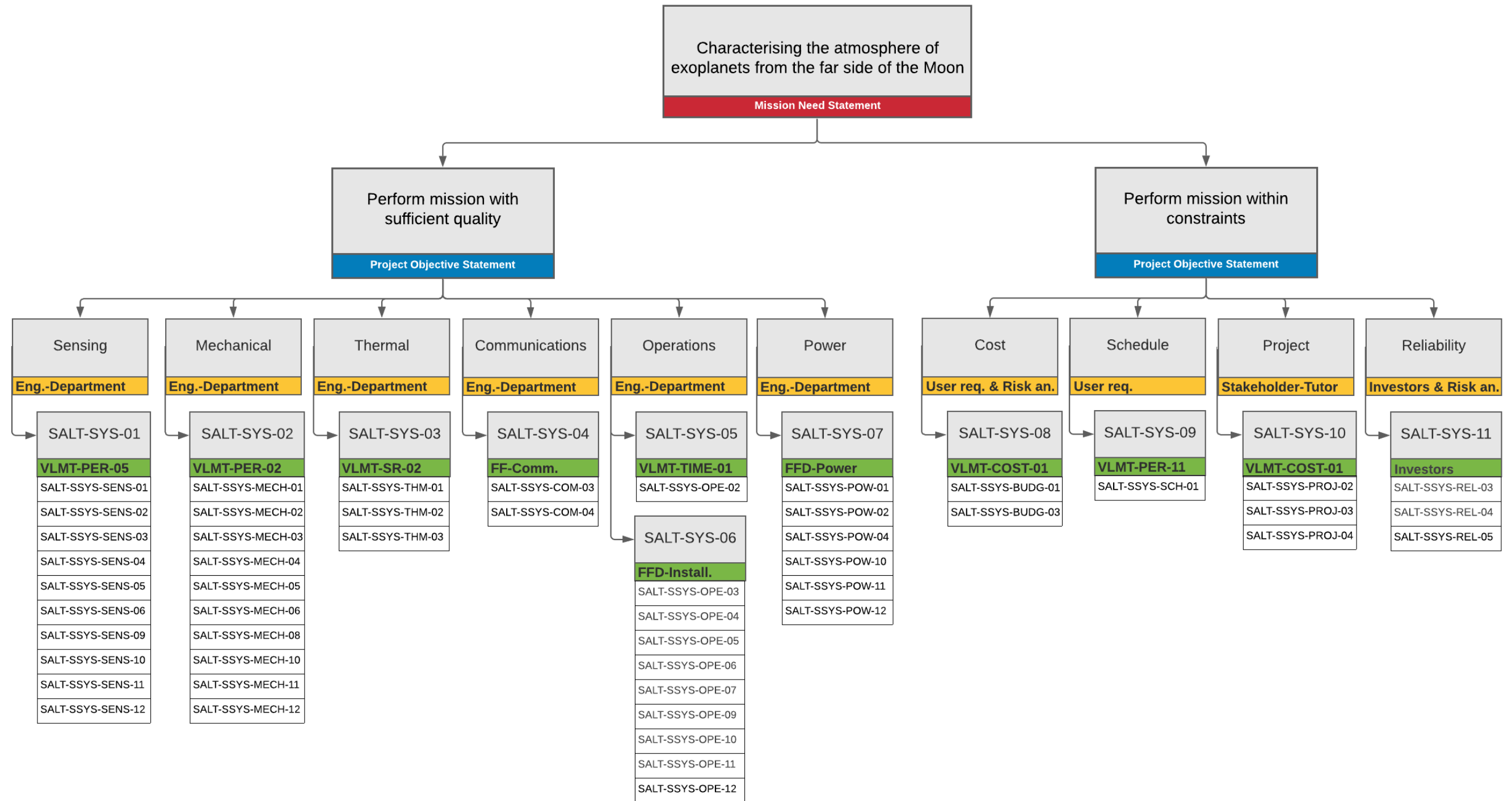


Figure A.2: Requirement discovery tree - RDT

A.3. Fault tree analysis

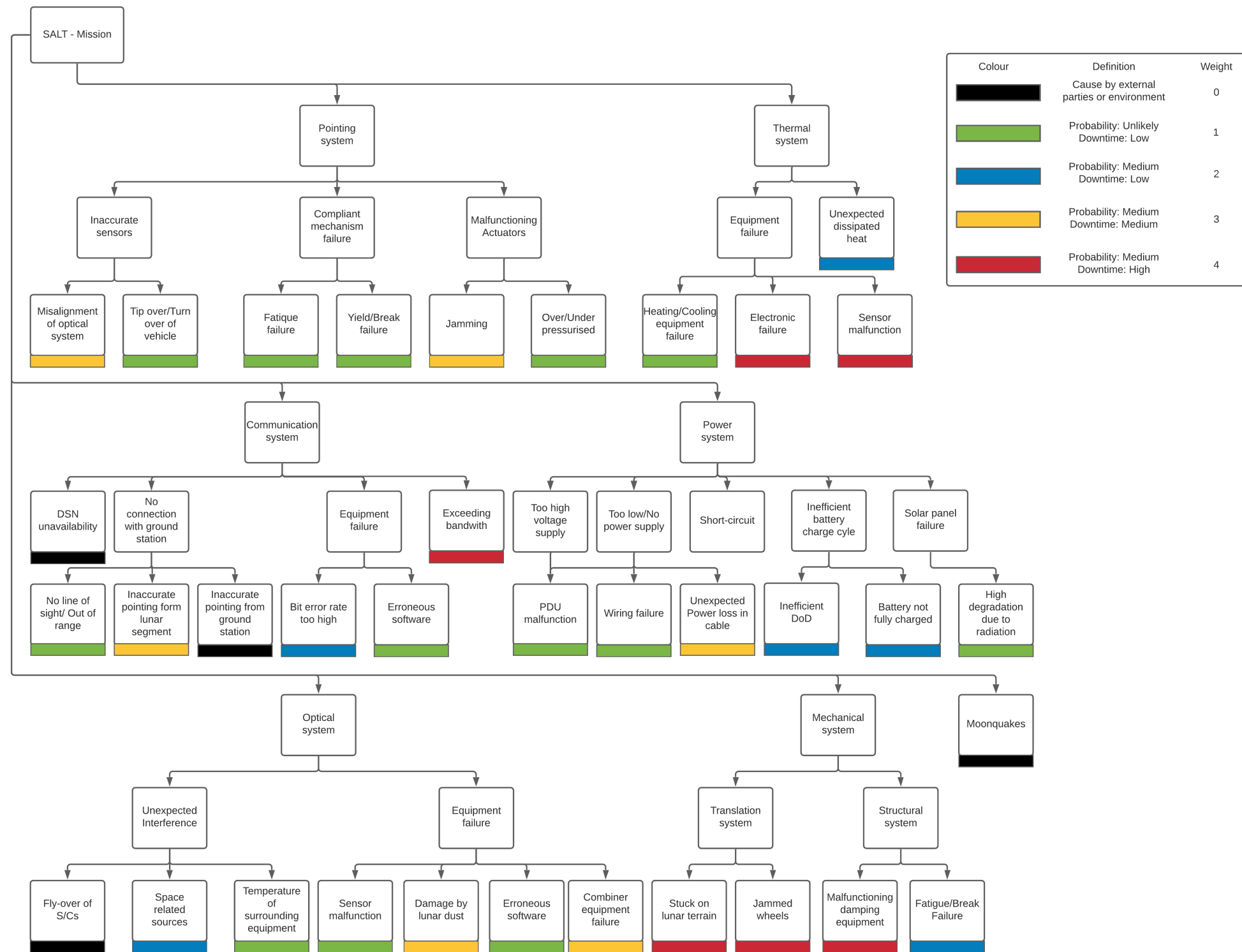


Figure A.3: Fault Tree Analysis - FTA

A.4. Design Option Trees

This appendix shows the design option trees for all the different subsystems of SALT. The goal of these trees was to generate all possible design options for the subsystems. Some of these options were clearly unfeasible and were immediately eliminated. The remaining options were taken as input for design trade-offs and have been discussed in each relevant chapter.



Figure A.4: Design option trees for the subsystems.

A.5. Link Budgets

Table A.1: Uplink budget for Earth to Malapert communication

Malapert uplink budget			
Orbit & Tracking			
R_E	Earth radius	6378	km
h	Orbital altitude (circular orbit)	405696	km
r	Orbit radius (circular orbit)	412074	km
δ	Min. elevation angle	10	°
S	Slant Range	410919	km
Earth station Properties			
f	Transmission frequency	7160	MHz
λ	Wavelength	0.042	m
D	Data rate	8	kbit/s
	Modulation scheme	OQPSK	-
G_{coding}	Coding gain	8	dB
DSN Transmission Power			
P_{RF}	Transponder output	5	kW
		37	dBW
		67	dBm
L_{line}	Line & connector losses	-1	dB
L_{point}	Pointing loss	-5	dB
L_{filter}	Pointing loss	-1.5	dB
$G_{\text{ant.}}$	Antenna directivity (minimum)	56	dBi
P_{EIRP}	Transmitted EIRP	85.49	dBW
Communication channel			
L_{path}	Path loss (free space, normalised to λ)	-221.82	dB
$L_{\text{atm.90}^\circ}$	Zenith total atmospheric attenuation	-0.50	dB
$L_{\text{atm.}}$	Atmospheric loss	-2.88	dB
L_{channel}	Total channel loss	-224.70	dB
Malapert Station Reception			
$L_{G.s.i}$	Isotropic signal level at ground station	-139.21	dBW
D	Diameter of receiving antenna	0.15	m
e	Efficiency of receiving antenna	0.50	m
$G_{S., \text{ant.}}$	Antenna directivity (minimum)	18.02	dBi
$L_{\text{pol.}}$	Polarization mismatch	-3.00	dB
L_{line}	Line, connector & surge protector losses	-1.00	dB
T_{noise}	Reception noise temperature	200	K
		23	dBK
k	Boltzmann constant	-228.6	dBW/KHz
S/N_0	Signal-to-noise power density	88.4	dBHz
E_b/N_0	Signal-to-noise	49.4	dB
$(E_b/N_0)_{\text{req}}$	Required signal-to-noise ratio	9.6	dB
$(E_b/N_0)_{\text{margin}}$	Total link margin	39.8	dB
SE	Spectral efficiency	1	bit/s/Hz
B_{est}	Bandwidth	16	kHz

Table A.2: Uplink budget of the combiner to rover communication

Rover uplink budget			
Distance			
d	Distance	0.5	km
Rover Properties			
f	Transmission frequency	400	MHz
λ	Wavelength	0.749	m
D	Data rate	8	kbit/s
	Modulation scheme	BPSK	-
G_{coding}	Coding gain	1	dB
Combiner Transmission Power			
P_{RF}	Power amplifier output	0.01	W
		-20	dBW
		10	dBm
L_{line}	Line & connector losses	-1.00	dB
$G_{\text{sat. ant.}}$	Antenna directivity (minimum)	-5.00	dBi
P_{EIRP}	Transmitted EIRP	-26	dBW
Communication Channel			
L_{path}	Path loss (free space, normalised to λ)	-78.47	dB
L_{channel}	Total channel loss	-78.47	dB
Rover Reception			
$S_{G.s.i}$	Isotropic signal level at combiner	-104.47	dBW
L_{line}	Line and connector losses	-1.00	dB
$G_{G.s. \text{ant.}}$	Antenna directivity (minimum)	-5.00	dBi
T_{noise}	Reception noise temperature	200	K
		23.0	dBK
k	Boltzmann constant	-228.6	dBW/KHz
S/N_0	Signal-to-noise power density	96.1	dBHz
E_b/N_0	Signal-to-noise	57.1	dB
$(E_b/N_0)_{\text{req}}$	Required signal-to-noise ratio	9.6	dB
$(E_b/N_0)_{\text{margin}}$	Total link margin	47.5	dB
SE	Spectral efficiency	0.5	bit/s/Hz
B_{est}	Bandwidth	32	kHz

Table A.3: Downlink budget of the combiner to Sverdrup station communication

Combiner downlink budget			
Distance			
d	Distance	40.7	km
Combiner Properties			
f	Transmission frequency	400	MHz
λ	Wavelength	0.749	m
D	Data rate	8	Mbit/s
	Modulation scheme	QPSK	-
G_{coding}	Coding gain	1	dB
Combiner Transmission Power			
P_{RF}	Power amplifier output	8.50	W
		9.29	dBW
		39.29	dBm
L_{line}	Line & connector losses	-1.00	dB
G_{sat.ant.}	Antenna directivity (minimum)	-5.00	dBi
P_{EIRP}	Transmitted EIRP	3.29	dBW
Communication Channel			
L_{path}	Path loss (free space, normalised to λ)	-116.68	dB
L_{channel}	Total channel loss	-116.68	dB
Sverdrup Station Reception			
S_{G.S.,i}	Isotropic signal level at combiner	-113.39	dBW
L_{line}	Line and connector losses	-1.00	dB
G_{G.S.ant.}	Antenna directivity (minimum)	-5.00	dBi
T_{noise}	Reception noise temperature	200	K
		23.0	dBK
k	Boltzmann constant	-228.6	dBW/KHz
S/N₀	Signal-to-noise power density	87.2	dBHz
E_b/N₀	Signal-to-noise	18.2	dB
(E_b/N₀)_{req}	Required signal-to-noise ratio	9.6	dB
(E_b/N₀)_{margin}	Total link margin	8.6	dB
SE	Spectral efficiency	1	bit/s/Hz
B_{est}	Bandwidth	16	MHz

Table A.4: Uplink budget of the Sverdrup station to combiner communication

Combiner uplink budget			
Distance			
d	Distance	40.7	km
Sverdrup station Properties			
f	Transmission frequency	400	MHz
λ	Wavelength	0.749	m
D	Data rate	7.5	Mbit/s
	Modulation scheme	QPSK	-
G_{coding}	Coding gain	1	dB
Sverdrup Transmission Power			
P_{RF}	Power amplifier output	8.50	W
		9.29	dBW
		39.29	dBm
L_{line}	Line & connector losses	-1.00	dB
G_{sat.ant.}	Antenna directivity (minimum)	-5.00	dBi
P_{EIRP}	Transmitted EIRP	3.29	dBW
Communication Channel			
L_{path}	Path loss (free space, normalised to λ)	-116.68	dB
L_{channel}	Total channel loss	-116.68	dB
Combiner Reception			
S_{G.S.,i}	Isotropic signal level at combiner	-113.39	dBW
L_{line}	Line and connector losses	-1.00	dB
G_{G.S.ant.}	Antenna directivity (minimum)	-5.00	dBi
T_{noise}	Reception noise temperature	200	K
		23.0	dBK
k	Boltzmann constant	-228.6	dBW/KHz
S/N₀	Signal-to-noise power density	87.2	dBHz
E_b/N₀	Signal-to-noise	18.5	dB
(E_b/N₀)_{req}	Required signal-to-noise ratio	9.6	dB
(E_b/N₀)_{margin}	Total link margin	8.9	dB
SE	Spectral efficiency	1	bit/s/Hz
B_{est}	Bandwidth	15	MHz

Table A.5: Downlink budget of the Sverdrup station to Malapert station communication

Sverdrup station downlink budget			
Distance			
d	Distance	132.6	km
Sverdrup Properties			
f	Transmission frequency	400	MHz
λ	Wavelength	0.749	m
D	Data rate	2.5	Mbit/s
	Modulation scheme	QPSK	-
G_{coding}	Coding gain	1	dB
Sverdrup Transmission Power			
P_{RF}	Power amplifier output	8.50	W
		9.29	dBW
		39.29	dBm
L_{line}	Line & connector losses	-1.00	dB
G_{sat.ant.}	Antenna directivity (minimum)	-5.00	dBi
P_{EIRP}	Transmitted EIRP	3.29	dBW
Communication Channel			
L_{path}	Path loss (free space. normalised to λ)	-126.94	dB
L_{channel}	Total channel loss	-126.94	dB
Malapert Station Reception			
S_{G.s.,i}	Isotropic signal level at combiner	-123.65	dBW
L_{line}	Line and connector losses	-1.00	dB
G_{G.s.ant.}	Antenna directivity (minimum)	-5.00	dBi
T_{noise}	Reception noise temperature	200	K
		23.0	dBK
k	Boltzmann constant	-228.6	$\frac{\text{dBW}}{\text{KHz}}$
S/N₀	Signal-to-noise power density	76.9	dBHz
E_b/N₀	Signal-to-noise	13	dB
(E_b/N₀)_{req}	Required signal-to-noise ratio	9.6	dB
(E_b/N₀)_{margin}	Total link margin	3.4	dB
SE	Spectral efficiency	1	bit/s/Hz
B_{est}	Bandwidth	5	MHz

Table A.6: Uplink budget of the Malapert station to Sverdrup station communication

Sverdrup uplink budget			
Distance			
d	Distance	132.6	km
Malapert Downlink Properties			
f	Transmission frequency	400	MHz
λ	Wavelength	0.749	m
D	Data rate	2.5	Mbit/s
	Modulation scheme	QPSK	-
G_{coding}	Coding gain	1	dB
Malapert Transmission Power			
P_{RF}	Power amplifier output	8.5	W
		9.29	dBW
		39.29	dBm
L_{line}	Line & connector losses	-1.00	dB
G_{sat.ant.}	Antenna directivity (minimum)	-5.00	dBi
P_{EIRP}	Transmitted EIRP	3.29	dBW
Communication Channel			
L_{path}	Path loss (free space. normalised to λ)	-126.94	dB
L_{channel}	Total channel loss	-126.94	dB
Sverdrup Station Reception			
S_{G.s.,i}	Isotropic signal level at combiner	-123.65	dBW
L_{line}	Line and connector losses	-1.00	dB
G_{G.s.ant.}	Antenna directivity (minimum)	-5.00	dBi
T_{noise}	Reception noise temperature	200	K
		23.0	dBK
k	Boltzmann constant	-228.6	$\frac{\text{dBW}}{\text{KHz}}$
S/N₀	Signal-to-noise power density	76.9	dBHz
E_b/N₀	Signal-to-noise	13	dB
(E_b/N₀)_{req}	Required signal-to-noise ratio	9.6	dB
(E_b/N₀)_{margin}	Total link margin	3.4	dB
SE	Spectral efficiency	1	bit/s/Hz
B_{est}	Bandwidth	5	kHz

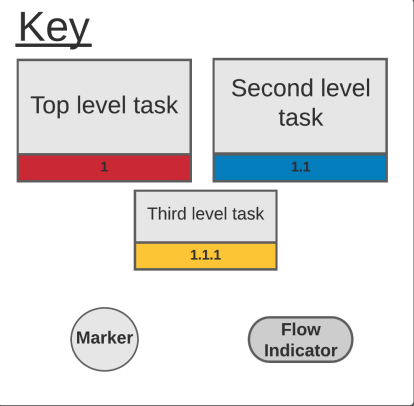
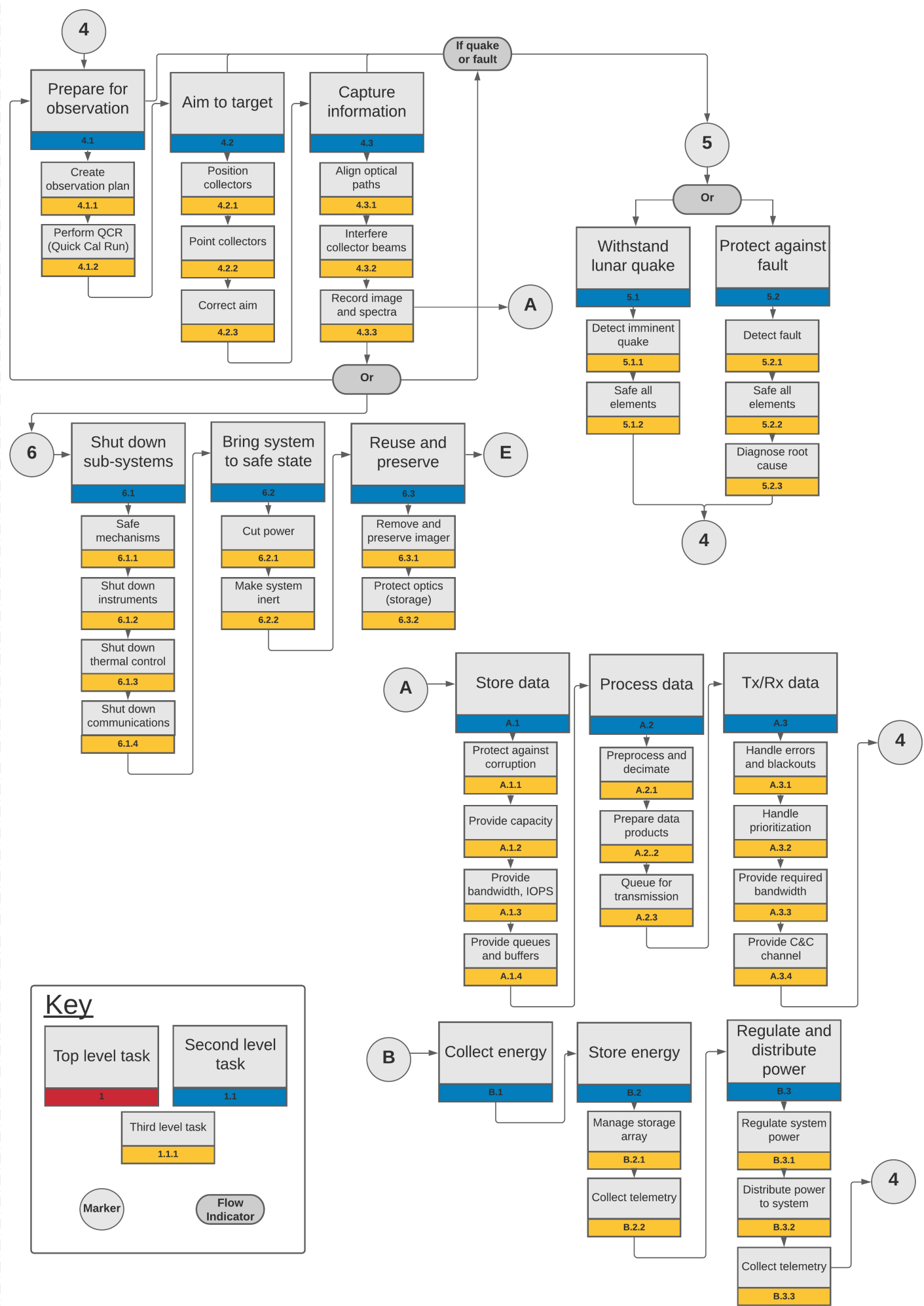
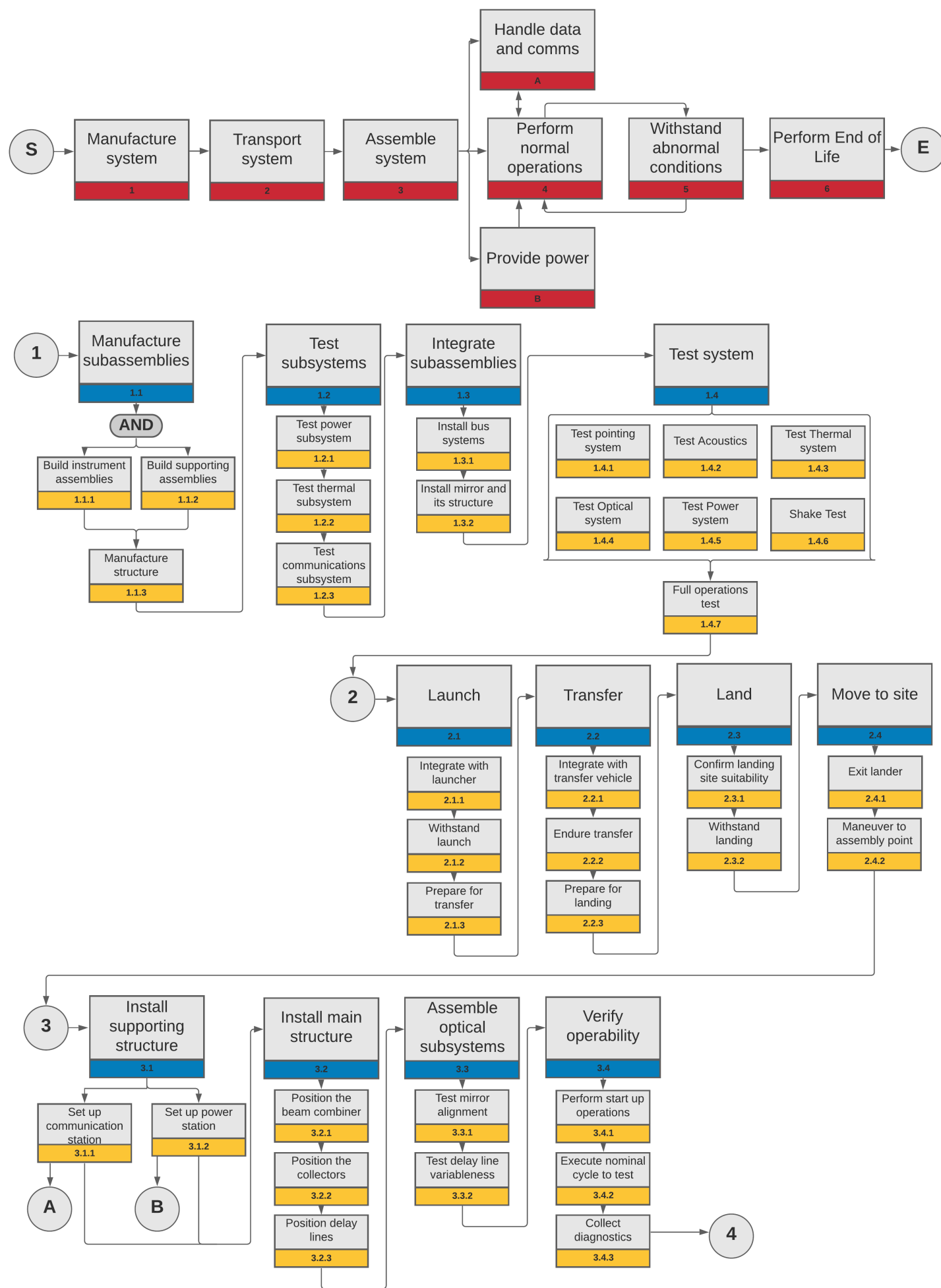


Figure A.5: Functional flow diagram

